Strontium Stable Isotope Behaviour Accompanying Melting and Magmatism in the Earth - Moon System

Nadine Chelsea Sutcliffe

St Anne's College, Oxford

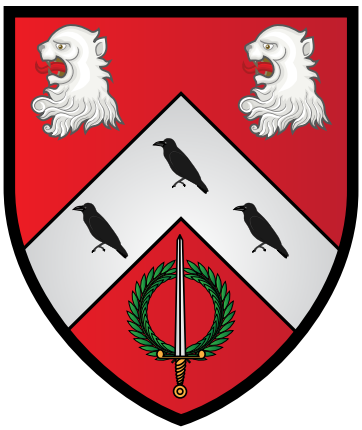

Thesis submitted for the Degree of Doctor of Philosophy, University of Oxford

Trinity Term 2013

Supervised by K. W. Burton, A. N. Halliday and D. Porcelli

Strontium Stable Isotope Behaviour Accompanying Melting and Magmatism in the Earth - Moon System

Nadine Chelsea Sutcliffe
St Anne's College, Oxford
Trinity Term 2013

Abstract

This thesis concerns the application of a new technique for measuring the stable isotopes of Sr, specifically pertaining to mass dependent fractionation in high temperature processes on the Earth and Moon. Processes such as mantle melting and differentiation on Earth and the formation of the Lunar Magma Ocean are investigated by the application of a double-spike TIMS method to terrestrial and lunar material to obtain high-precision $^{87}Sr/^{86}Sr$, $^{88}Sr/^{86}Sr$ and $^{84}Sr/^{86}Sr$ data. Measurements of mantle-derived mafic material provide insights into the $^{88}Sr/^{86}Sr$ composition of the silicate mantle. Ocean Island Basalts possess restricted $\delta^{88}Sr$ compositions, whilst Mid-Ocean Ridge Basalts from the Pacific, Atlantic and Indian ridges reveal variations in $\delta^{88}Sr$, the majority of which is seen within the FAMOUS section of the Mid-Atlantic Ridge. These variations are attributed partly due to the effects of plagioclase crystallisation and partly due to mantle source heterogeneity. Analyses of mineral separates from three different igneous systems provide an understanding of $\delta^{88}Sr$ fractionation at a mineral-scale. The possibility of $\delta^{88}Sr$ fractionation as a result of magmatic differentiation has also been assessed, and found to occur between the basalt and rhyolitic end-members of the Icelandic Hekla suite. Variations in the $^{87}Sr/^{86}Sr$ ratios of these rocks are also found, and considered most likely to be due to contamination. Analyses of lunar rocks indicate that the highland suite appears to be relatively uniform in $\delta^{88}Sr$, whilst significant fractionation to light $\delta^{88}Sr$ compositions occurs in the mare basalts. Such variations are thought to be associated with the crystallisation of plagioclase during the differentiation of the lunar magma ocean. Lastly, precise $^{87}Rb/^{86}Sr$ and $^{87}Sr/^{86}Sr$ data yield a model age for the Moon of 4.523 ± 0.019 Ga.

Strontium Stable Isotope Behaviour Accompanying Melting and Magmatism in the Earth - Moon System

Nadine Chelsea Sutcliffe
St Anne's College, Oxford
Trinity Term 2013

Extended abstract

This thesis details the application of a new geochemical tracer, stable strontium (Sr) isotopes, to investigate whether this isotope system can be used to provide new information on key geological processes in the terrestrial and lunar environment. Comparing the isotopic compositions of silicates from the Earth and the Moon can shed light on processes such as the differentiation, mantle melting, and terrestrial moon formation. Geochemically, Sr has primarily been of interest in the past due largely for its radiogenic isotope composition, $^{87}Sr/^{86}Sr$. It is only recently that interest in the mass dependent fractionation of Sr isotopes, $^{88}Sr/^{86}Sr$, has been rekindled following the pioneering work of Patchett (1980), and the focal point of such work has centred on the isotope behaviour in the low temperature environment. At higher temperatures the degree of isotope fractionation is smaller, making the precise measurement of variations in $^{88}Sr/^{86}Sr$ exceedingly difficult. Nevertheless, several investigations in recent years, focusing primarily on planetesimals and meteoric material, have renewed interest in the behaviour of stable Sr in high temperature environments. In these studies, the major terrestrial silicate reservoirs have been largely overlooked, and much of the data is based on limited sample selections. Additionally, these data were measured by Multi-Collector Inductively-Coupled Plasma-Mass-Spectrometry (MC-ICP-MS) to an external precision on $^{88}Sr/^{86}Sr$ of no better than ~±50 ppm. Variations in high temperature material in the stable isotopes of an element as heavy as Sr are relatively small

compared to such analytical resolution and are often not resolved. In this study, a double-spike Thermal-Ionisation-Mass-Spectrometry (TIMS) technique was employed that allowed such small variations to be resolved. This thesis builds on these initial studies, but includes a more comprehensive range of samples (both lunar and terrestrial) and the measurements are made to a higher precision. Several key questions are addressed concerning the behaviour of this novel stable isotope system in the terrestrial environment, such as whether variations exist in the composition of mantle melts due to mantle processes and the effects of igneous differentiation. An analogous situation is investigated on the Moon by constraining the lunar mantle composition and examining the effects of differentiation during crystallisation of the lunar magma ocean. Although the main focus of this thesis concerns the stable isotope ratio $^{88}Sr/^{86}Sr$, information gained by the application of the $^{87}Sr/^{86}Sr$ and $^{84}Sr/^{86}Sr$ ratios was also obtained adding further context and understanding to the overall behaviour of the Sr isotope system.

The first case study is centred on constraining an estimate of the Sr stable isotope composition of the terrestrial mantle based on examining mantle melts (oceanic basalts) and understanding the processes of mantle melting, given the dearth of existing terrestrial data for $^{88}Sr/^{86}Sr$. An extensive suite of oceanic basalts was analysed so as to explore the composition of the mantle. Analyses of Mid-Ocean Ridge Basalts (MORB) from the Pacific, Atlantic and Indian Oceans revealed variations in $\delta^{88}Sr$ of +0.106 ± 0.011 to +0.312 ± 0.006‰ (~0.21‰). The majority of this variation is seen within a single sample area, the FAMOUS section of the Mid-Atlantic Ridge. Correlations with Eu/Eu* suggest this variation is, in part, due to fractional crystallisation of plagioclase. However, this correlation is weak and variations in the radiogenic $^{87}Sr/^{86}Sr$ ratio the basalts, from 0.702468 (±2) to 0.703105 (±3), suggest that mantle heterogeneity plays an additional role.

The $\delta^{88}Sr$ compositions of Ocean Island Basalts (OIB) range from $\delta^{88}Sr = +0.280 \pm 0.008$ to $+0.224 \pm 0.018$‰. Whilst the averages of OIB and MORB are identical, the former posses a restricted range of $\delta^{88}Sr$ compositions compared to the latter (OIB variance ~0.0003; MORB variance ~0.0013). The relatively uniform compositions of OIB are surprising when compared to the large variations seen for MORB. As OIB represent a number of mantle end-members, reflected in the wide range of $^{87}Sr/^{86}Sr$ compositions from 0.702779 (±3) to 0.704708 (±3), it would appear that global recycling plays a minimal role in the outcome of the stable Sr composition of mantle melts, or else, mantle melting acts to homogenise these variations. Preliminary investigations into the composition of subducted crustal material recycled into the mantle suggest it possesses a lighter Sr stable isotope composition ($\delta^{88}Sr = \sim 0.20$‰) than the average oceanic basalt ($\delta^{88}Sr = +0.25 \pm 0.01$). The discrepancy between the two may provide evidence for a process that is responsible for "re-setting" the values of this input to that of the oceanic basalts.

The Sr isotope composition of minerals (clinopyroxene and plagioclase) separated from basalt and gabbro from several tectonic settings (the Skaergaard intrusion, Mt Silvestri, and FAMOUS MORB) were analysed in order to further examine differentiation processes. The $\delta^{88}Sr$ compositions of the minerals varies widely and is inconsistent with mineral type relative to other coexisting minerals and to the melt, but clinopyroxene is consistently heavier than plagioclase in the Skaergaard and Silvestri samples. However, the Silvestri system is most likely contaminated and the melt composition of the Skaergaard cumulate is unknown, so such values may be unrepresentative. The plagioclase separates of MORB were found to be consistently heavier in $\delta^{88}Sr$ than the corresponding glasses, in agreement with a previous suggestion

that the heavy isotopes of Sr preferentially partition into plagioclase (Charlier et al., 2012).

Analyses of a differentiation sequence from the volcano of Hekla, Iceland, is used to explore the processes causing stable isotope fractionation in the absence of potential continental crustal contamination. Variations in $\delta^{88}Sr$ from +0.287 ± 0.01‰ for basalt to +0.146 ± 0.01‰ for rhyolite correlate strongly with indices of magmatic differentiation. This suggests that magmatic differentiation does indeed cause fractionation through the removal of mineral phases into which the lighter isotopes of Sr preferentially partition (likely plagioclase +/- clinopyroxene). However, variations from $^{87}Sr/^{86}Sr$ = 0.703161 (±2) for basalt to $^{87}Sr/^{86}Sr$ = 0.703220 (±5) for rhyolite suggest contamination, for which the most likely assimilant material is either an altered basalt with secondary carbonate present, or an older, unaltered, basalt.

A variety of lunar rock types, from highland to mare basalt, were analysed to allow an accurate comparison of processes responsible for stable Sr isotope fractionation in the terrestrial and lunar environment. Variations in the $\delta^{88}Sr$ composition of ~0.3‰ were found, from $\delta^{88}Sr$ = +0.129 ± 0.011‰ for a high-Ti mare basalt to +0.448 ± 0.007‰ for a ferroan anorthosite (FAN). With the exception of this FAN, the highland rocks appear to possess relatively uniform $\delta^{88}Sr$ compositions. In contrast, significant fractionation to light $\delta^{88}Sr$ compositions occurs in the mare basalts. These variations are thought to be linked to the crystallisation of plagioclase, preferentially incorporating the heavy Sr isotopes, during the differentiation of the lunar magma ocean. This is consistent with previous data (Charlier et al., 2012). A comparison of high precision $\delta^{84/86}Sr$ and $\delta^{88/86}Sr$ terrestrial and lunar data in three-isotope space reveals no offset between the respective mass dependent fractionation lines. The absence of any nucleosynthetic anomalies in ^{84}Sr is in agreement with previous data for the Earth and

the Moon (Clayton et al., 1984; Dauphas et al., 2002; Trinquier et al., 2007, 2009). Finally, high precision $^{87}Rb/^{86}Sr$ and $^{87}Sr/^{86}Sr$ data yield a precise Rb-Sr model age for the Moon, based on FAN 60015, of 4.523 ± 0.019 Ga. When combined with Hf-W data (Touboul et al., 2007), this constrains the formation of the Moon to 45-57 Ma after the start of the solar system, suggesting an early Moon-forming Giant Impact. However, more recent FAN dating data suggests the age of the Moon is much younger (~200 Myr; Borg et al., 2011), which implies that the assumptions made in the Rb-Sr calculations are incorrect. Using this young age of the Moon constrains the Rb/Sr ratio of the precursor material to a considerably lower value (0.018) than previously thought.

Acknowledgments

First and foremost I would like to thank my supervisors Kevin, Alex and Don, those who have supervised me in the past (Sune, Dave and Fatima), and everyone who helped in Durham and the OU (Ian, Chris, Helen and Geoff). Without your support, encouragement, and advice none of this would have been possible. Kevin, I enjoyed our scientific discussions as much as I enjoyed our three-hour chats in the Durham café, and I can't thank you enough for both. Ian, you were never my supervisor, but you took the time to teach me the ways of the TIMS as if you were- thank you. Chris, you always made me feel so welcome at the OU, thank you for taking the time to do so. Helen, Kevin, and Tamsine- thanks for the all the cheese and the martinis, and for making every trip to Durham something to look forward to!

Secondly, I would like to extend my thanks to all past and present members of TOILET for their advice, companionship and dedicated beer-time. I would especially like to thank Julie for not laughing at my questions in the lab in my first year, Pogge for always having time to bounce ideas around and showing me how to distinguish between endless shades of green down a microscope, and Paul for the Hekla samples and discussions. Emily- I cannot express what an inspiration you have been over the years, and just such a pleasure to be around! I couldn't have asked for a better strontium buddy, thanks for your patience. Jane, your enthusiasm and encouragement in the group have been a tremendous help and a welcome change, and Fee, those impromptu hugs went a long way. I would especially like to thank Julia for the countless coffee breaks, chats, and rants through eight years of education together: the write up would have been a lot more painful if it weren't for you. Thanks also to Elaine, who always has a smile and a word of encouragement, and all the technical and support staff at Oxford, especially Phil Holdship for all his help with the Element. I am extremely grateful to my

examiners, Mark Rehkämper and David Pyle for their constructive feedback and discussion.

I am forever grateful to the amazing people I've met along the way here in Oxford. Owen, Maria, Becky, Johnny, Pam, AJ, Si, Chloe, Kaye, Nick, Brandon, and many more: your friendship and company made all the work and stress worthwhile. Keian and Aled, Juxon HQ felt more of a home than I've ever had away from Spain thanks to you two, and I put that down to your sparkling conversation. I am hugely grateful to Micaela and Colin for letting me intrude upon their home these last few months and for providing stellar company, thank you. Colin - I will never forget the understanding, love, and patience you've shown this year, from supplying me with food, chocolate, and gin, to letting me rant about trivial matters to de-stress. I hope, when the time comes, that I can show you the same depth of love and support. I promise to stop being a hermit now. Last but not least, I cannot even begin to express my appreciation and gratitude to my family, Mum, Dad, and Richard, without whom none of this would have happened. I have always had the freedom and the privilege to choose in life, and that is all down to the knowledge that your faith, love, and support in me are unconditional.

I would like to acknowledge the many coffee beans that died for the cause.

This work has been supported by the Science and Technologies Facilities Council and the Burdett Coutts Fund.

To my mother, for teaching me the significance of things.

To my father, for showing me how little they can matter.

"…That place is Earth, the seat of Man; that light
His day, which else, as the other hemisphere,
Night would invade; but there the neighbouring moon
(So call that opposite fair star) her aid
Timely interposes, and her monthly round
Still ending, still renewing, through mid Heaven,
With borrowed light her countenance triform
Hence fills and empties to enlighten the Earth,
And in her pale dominion checks the night.
That spot, to which I point, is Paradise… "

John Milton- *A Paradise Lost, Book III,* 1667.

Table of Contents

List of Figures

List of Tables

CHAPTER ONE

Introduction

Summary

Recent studies have shown that fractionation of the stable isotopes of the element strontium (Sr) occurs at high temperature in terrestrial planets and asteroids. This thesis is primarily concerned with the application of new techniques to measure isotope variations between two of the stable isotopes of Sr, ^{88}Sr and ^{86}Sr, in high temperature environments to a higher resolvable precision, but also involves the study of the remaining stable isotopes: the radiogenic $^{87}Sr/^{86}Sr$ ratio and nucleosynthetic $^{84}Sr/^{86}Sr$ ratio. All three isotope ratios are measured in terrestrial and extra-terrestrial samples to investigate mass dependent variations in $^{88}Sr/^{86}Sr$, mass independent variations in $^{84}Sr/^{86}Sr$, and radiogenic variations in $^{87}Sr/^{86}Sr$. A novel technique, the addition of a double spike in combination with thermal ionisation mass spectrometry, offers the possibility of measurement of all three ratios to a very high precision. The following chapter outlines the principles of isotope theory and the processes by which isotopic fractionation can occur. The theory and development behind the approach chosen, as well as its application are explained. Lastly the aims of the study and the thesis structure are outlined.

1.1. Isotope fractionation

Isotopes are atoms of the same element with an identical number of protons and electrons, but varying numbers of neutrons. This results in a relative mass difference between isotopes, which is often measureable using modern day mass spectrometry. Isotope geochemistry measures the relative abundances of these in cycles and systems in the terrestrial planets and their Solar System. Isotopes can exhibit nucleosynthetic anomalies resulting from stellar sources, and, are often classed as radiogenic or stable according to whether they are affected by radioactive decay or not.

1.1.1. Nucleosynthetic anomalies

Nucleosynthesis is the process that creates new atomic nuclei from pre-existing nucleons, primarily protons and neutrons. The first nuclei, H and He, were created during Big Bang nucleosynthesis, and the heavier elements by later stellar nucleosynthesis in stars and supernova nucleosynthesis during explosions of stars, both of which are on-going processes. There are several processes and pathways responsible for nucleosynthesis including neutron capture (*s*-process), rapid neutron capture (*r*-process), and the photodisintegration of existing nuclei (*p*-process). *p*-, *s*- and *r*-processes occur in different stellar environments: *s*-process in Asymptotic Giant Branch stars and *p*- and *r*-processes in Supernovae. *s*- and *r*-process nuclides can be formed in common stellar environments such as asymptotic giant branch stars and Type II super-novae, respectively, whilst *p*-process nuclides form in extreme conditions that can generate either proton-capture or photodisintegration, which can occur in Type I and Type II supernovae (Rauscher et al., 2002; Travaglio et al., 2011). Nucleosynthetic

anomalies result from distinct inputs of materials produced as a result of these various processes (*s, r* and *p*-processes) and can be identified by deviations from mass-dependent isotopic variations, for example by displacement of mass-fractionation line of three-isotope plots. This approach forms the basis of the identification of planetary bodies based on mass-independent variations in stable oxygen (O) isotopes (Clayton et al., 1976).

1.1.2. Radiogenic isotopes

Radiogenic isotopes are daughter isotopes that form from decay of radioactive isotopes. During radioactive decay, the nuclei of unstable atoms undergo spontaneous transformations that give rise to the emission of particles and energy. Radiogenic isotopes have two principal uses in geochemistry. First, the decay of long-lived radioactive isotopes can be used in the determination of the ages of rocks and minerals for the measurement of geologic time, as geochronometers. Second, these isotopes can be used as geochemical tracers to identify geological processes and sources.

a) Radiogenic isotopes in geochronology

The rate of decay of an unstable parent nuclide is proportional to the number of atoms (N) remaining at any time (t), in the relationship depicted by Equation 1.1:

$$\frac{-dN}{dt}dt \propto N \qquad \textit{Equation 1.1}$$

where $-dN/dt$ is the nuclear decay rate. Introducing a decay constant, λ, and integrating this mathematically transforms this into Equation 1.2:

$$-lnN = \lambda t + C \qquad \textit{Equation 1.2}$$

and the classic first order decay equation upon substitution:

$$N = N_0 e^{-\lambda t} \qquad \textit{Equation 1.3}$$

where N_0 is the decay constant for the nuclide.

Given this relationship and rearranging these equations derives Equation 1.4.

$$D = D_0 + N(e^{\lambda t} - 1) \qquad \textit{Equation 1.4}$$

This equation is the underlying principle that allows age determinations of rocks and minerals based of the decay of a radioactive parent to a stable daughter, *D*. Where *D* and *N* are measureable quantities, the former being the number of atoms of the daughter nuclide and D_0 is the number of daughter atoms present initially (when $t = 0$), either assumed or calculated from co-genetic sample suites of the same age. However, this relationship is only applicable and true under the following circumstances, as outlined by Faure (1986):

1. The system is closed, with no addition or removal of either the parent or daughter nuclides, or both are affected so that D^*/N is modified only as a result of radioactive decay.
2. The value of D_0 must be known or accurately calculated.
3. The decay constant, λ, must be known accurately and precisely.
4. The measurements of *D* and *N* must be accurate and representative.

b) Radiogenic isotopes as geochemical tracers

The use of Sr and other radiogenic isotopes as tracers is based on the concept that distinct isotopic signatures of reservoirs develop when separated from one another for

significant periods of time. This results from fractionation of the parent/daughter element ratios due to chemical fractionation as a consequence of differences in incompatibility between the parent and daughter elements. In this way, different terrestrial reservoirs can develop diverging isotopic signatures over different timescales, from contrasting or similar initial compositions. The field was developed in the early 1960s, stemming from the distinction between crustal magma sources and mantle sources on the basis of their initial Sr isotopic compositions (Hurley et al., 1962). Since this incipient work, several long-lived parent-daughter systems have been applied to oceanic basalts as well as crustal rocks. The isotopic composition of oceanic basalts are taken to be representative of their mantle source isotopic compositions based on the assumption that basalts are in equilibrium with their mantle source and that any mass dependent isotopic fractionation during partial melting of the mantle is negligible or correctable. Thus, they serve as powerful tracers of the time-integrated parent/daughter ratios of mantle sources of igneous rocks. This prompted the discovery of considerable degrees of isotopic heterogeneity in the mantle composition of long-lived radiogenic systems such as Sr, Nd and Pb (Hedge and Walthall, 1963; Gast et al., 1964; Tatsumoto, et al., 1965; Hart, 1971). Using these isotope systematics, Zindler and Hart (1986) and Hart (1988) defined different mantle reservoirs and identified the existence of several mantle components. These end-members, termed DMM (low $^{87}Sr/^{86}Sr$ and $^{206}Pb/^{204}Pb$), EM1, EM2 (low $^{143}Nd/^{144}Nd$ and high $^{87}Sr/^{86}Sr$ with relatively low and high $^{206}Pb/^{204}Pb$, respectively), and HIMU (low $^{87}Sr/^{86}Sr$ and high $^{206}Pb/^{204}Pb$) result from varying extents of crust–mantle interaction during recycling and are thought to represent the depleted, enriched, and high- μ ($^{238}U/^{204}Pb$) mantle. A fifth end-member, named PHEM/FOZO/C, which is thought by some to be common to many or all plumes, has intermediate or depleted Sr, Nd, and Pb isotopic compositions and un-radiogenic He

(Farley and Craig, 1992; Hart et al., 1992; Hanan and Graham, 1996) and has been defined as the point of convergence of linear data arrays from which OIB trends arise (Hart et al., 1992).

1.1.3. Stable isotopes

Stable isotopes are those that do not undergo radioactive decay. Although in principle they could be radiogenic and the product of radioactive decay, these are discussed in the above Section (1.1.2.), and the following applies to isotopes whose abundance is not affected by radioactive decay at all. During stable isotopic fractionation, heavy and light isotopes partition differently between two compounds or phases as a result of a mass difference between isotopes during chemical or physical processes. Variations in stable isotopes are typically expressed in delta (δ) notation as the relative deviation permil (‰) of a sample's isotopic ratio to that of a recognised standard, denoted in Equation 1.5, below.

$$\delta^{i}D_{X} = \left(\frac{R_{X}^{i/j}}{R_{STD}^{i/j}} - 1\right) \times 1000 \qquad \textit{Equation 1.5}$$

where R represents the ratio of isotopes i and j, of element D, in the sample (X) and standard (STD). The heaviest isotope is usually expressed as the numerator so as to generate positive values when a sample is enriched in the heavier isotope i relative to the standard and thus has a heavier composition.

1.1.3.1. Mass-dependent stable isotope fractionation

Stable isotopes are chemically identical and partake in the same reactions, but physicochemical processes can cause measurable variances in the atomic abundances of isotopes in different phases, collectively termed mass dependent isotopic fractionation. There are two types of isotope fractionation: equilibrium fractionation and kinetic fractionation.

Kinetic isotope fractionation arises from unidirectional processes occurring as a result of incomplete isotopic exchange between reactants (Schauble, 2004). In these reactions, equilibrium in the system is not attained due to the removal of a reactant or excessively fast rates of reactions. Kinetic fractionation results from differences in the velocities of the isotopes and largely favours the lighter isotopes of an element as these are lighter and can move at a faster speed. Examples of processes that result in kinetic fractionation include diffusion, biological reactions, and evaporation.

Equilibrium fractionation on the other hand, requires that isotopic equilibrium between the reactants is reached and maintained throughout the reaction and is driven by differences in the vibrational energies of isotopes with different masses (Urey, 1947). This is further affected by the reduction in the vibrational energy (zero-point energy) when a heavier isotope is substituted for a lighter one, and is dependent on temperature. As a result, heavier isotopes favour short stiff bonds in lower energy states (Schauble, 2004). A consequence of this is that more energy is required to break the bond of a heavy isotope compared to a lighter isotope, and at high temperatures this temperature dependence can be approximated by the relationship:

$$ln\alpha \propto \frac{1}{T^2} \qquad \textit{Equation 1.6}$$

As a result the degree of isotopic fractionation is greater at low temperatures. The degree of isotopic fractionation between two phases is also governed by a number of other physical properties, which include reaction rate, mass, the relative mass difference between the isotopes, bonding environment and oxidation state (O'Neil, 1986; Schauble, 2004). The degree of isotopic fractionation is expressed by the fractionation factor α, which is the ratio between the isotopic proportions of the two phases, A and B, of a system:

$$\alpha_B^A = \frac{R_A}{R_B} = \frac{\delta_A + 10^3}{\delta_B + 10^3} \qquad \textit{Equation 1.7}$$

The exact difference between two phases is given as the difference in their delta values, as a Δ. This is related to the fractionation factor as below:

$$\Delta_{A-B} = \delta_A - \delta_B \approx 10^3 ln\alpha_{A-B} \qquad \textit{Equation 1.8}$$

For mass dependent fractionation, the magnitude of the effect varies proportionally with the difference in mass between the two isotopes considered. This mass dependence of isotopic fractionation can be described by Equation 1.9, after Young et al. (2002), if m_i, m_j, and m_k are the masses of isotopes i, j, and k respectively, of element D:

$$^{k/j}D \propto \left(^{i/j}D\right)^{\beta} \qquad \textit{Equation 1.9}$$

where β is later defined as:

$$\beta = \frac{m_i - m_k}{m_j - m_k} \qquad \textit{Equation 1.10}$$

As long as both isotope ratios are expressed using a common denominator, the difference between isotope ratios of an element is only dependent on the mass differences between the isotopes. This results in a straight line on a three-isotope plot, called a mass-dependent fractionation line. Equilibrium and kinetic fractionation follow slightly different mass dependence rules, and can therefore theoretically be identified on a three-isotope plot. The two possess mass fractionation lines with different slopes (the exponent β relating to the fractionation factor) as described by Young et al. (2002) in Equations 1.11 and 1.12 for equilibrium and kinetic fractionation respectively.

$$\beta_E = \frac{\left[\frac{1}{m_k} - \frac{1}{m_i}\right]}{\left[\frac{1}{m_k} - \frac{1}{m_j}\right]} = \frac{\left[\frac{1}{m_1} - \frac{1}{m_2}\right]}{\left[\frac{1}{m_1} - \frac{1}{m_3}\right]} \qquad \textit{Equation 1.11}$$

$$\beta_K = \frac{ln\left[\frac{m_{k_{XR}}}{m_{i_{XR}}}\right]}{ln\left[\frac{m_{k_{XR}}}{m_{j_{XR}}}\right]} = \frac{ln\left[\frac{m_1}{m_2}\right]}{ln\left[\frac{m_1}{m_3}\right]} \qquad \textit{Equation 1.12}$$

where $m_{k_{XR}}$, etc. are the masses of isotopically substituted molecules and $m_1 < m_2 < m_3$.

1.2. Geochemistry of strontium

Strontium (Sr) is a Group 2 alkaline earth metal, with an atomic number of 38 and an atomic mass of 87.62 amu, named upon its recognition in 1790 in mines near the Scottish village of Strontian. Like other Group 2 elements it forms divalent cations and is classified as lithophile in the Goldschmidt classification. Thus, it typically bonds to oxygen in silicates and oxides and is concentrated in the mantle and the crust. These lithophile elements have closed (filled) outer electron shell ionic configurations, and tend to form ionic bonds. Along with K, Rb, Cs and Ba, its large ionic radius gives it the attributes of the large-ion lithophile elements (LILE). Chemically it behaves similarly to other Group 2 alkaline elements, Ba and Ca, and is refractory with a 50% condensation temperature (T_C) of 1464K (Lodders, 2003). Minerals of Sr are relatively rare, and the two principal minerals celestine (strontium sulphate, $SrSO_4$) and strontianite (strontium carbonate, $SrCO_3$) are mainly found in association with hydrothermal deposits or pegmatite. The size of Sr cations (Sr^{2+} ion -118 pm) is intermediate between those of Ca^{2+} (100 pm) and K^{+} (138 pm), for which it may substitute in a number of rock-forming minerals including K-feldspar, gypsum, plagioclase and, especially, calcite and dolomite. Although its smaller radius allows it to replace Ca in Ca-bearing minerals such as plagioclase and apatite, the size difference in ionic radii does restrict such replacement as Sr ions favour 8-fold co-ordination sites, whereas Ca ions are suitably small to fit, in addition, into 6-fold sites. Additionally, substitution for K^{+} in K-feldspar must be associated with Si^{4+} replacement by Al^{3+} in order to maintain electrical neutrality (Attendorn and Bowen, 1997).

1.2.1. Isotopes of strontium

Strontium has four naturally occurring stable isotopes ^{84}Sr, ^{86}Sr, ^{87}Sr and ^{88}Sr, listed with their exact atomic masses and natural abundance in Table 1.1 below.

Isotope	Atomic mass (m_a/u)	Natural abundance (%)
^{84}Sr	83.913430	0.56
^{86}Sr	85.9092672	9.86
^{87}Sr	86.9088841	7.00
^{88}Sr	87.905618	82.58

Table 1.1: Naturally occurring stable isotopes of Sr given with their atomic mass and natural abundance (Faure, 1986).

1.2.1.1. Radiogenic Sr isotopes

Radioactive ^{87}Rb decays via beta emission to stable ^{87}Sr as shown in Equation 1.13 with a half-life of 48.8 billion years (Steiger and Jäger, 1977), which results in the accumulation of radiogenic ^{87}Sr over time.

$$^{87}_{37}Rb \rightarrow {}^{87}_{38}Sr + \beta^- + \nu^- + Q \qquad \textit{Equation 1.13}$$

where β^- is the beta particle, ν^- is an antineutrino, and Q is the decay energy.

Thus, there are two sources of ^{87}Sr in any Rb- containing material: that which formed by nucleosynthesis and that which accumulated from radioactive decay of ^{87}Rb. Since both Rb and Sr are lithophile and are found in a variety of rock-forming minerals, this parent daughter relationship forms a useful geochronometer for the measurement of time in any Rb and Sr bearing rock or mineral. The growth of radiogenic ^{87}Sr in a Rb-containing mineral can be illustrated by substitution into the derivative from the law of radioactivity, Equation 1.14, to give the number of ^{87}Sr daughter atoms produced by the decay of ^{87}Rb in a rock or mineral since its formation *t*:

$$^{87}Sr = {}^{87}Sr_i + {}^{87}Rb\left(e^{\lambda t} - 1\right) \qquad \textit{Equation 1.14}$$

where ^{87}Sr is the total number of atoms at the present time; $^{87}Sr_i$ is the number of atoms initially; ^{87}Rb is the number of atoms at the present time; and λ is the decay constant of ^{87}Rb in units of inverse time.

Accurate and precise determinations of the relative abundances of isotopes is possible by mass spectrometry rather than the abundances of individual isotopes, thus dividing Equation 1.14 by the stable isotope ^{86}Sr gives Equation 1.15:

$$\frac{^{87}Sr}{^{86}Sr} = \left(\frac{^{87}Sr}{^{86}Sr}\right)_i + \left(\frac{^{87}Rb}{^{86}Sr}\right)\left(e^{\lambda t} - 1\right) \qquad \textit{Equation 1.15}$$

To solve Equation 1.15 for *t* to determine the age of a sample, the present-day isotope ratio $^{87}Sr/^{86}Sr$ is measured by mass spectrometry, and the $^{87}Rb/^{86}Sr$ ratio is calculated from the measured concentrations of Rb and Sr. However, the initial ratio $(^{87}Sr/^{86}Sr)_i$ must be known or accurately estimated and the age determination is only applicable if the conditions outlined by Faure (1986) are satisfied. An important condition is that the system has been closed from the time *t* to the present and there has been no gain or loss

of Rb and Sr, otherwise the value of *t* is compromised. The Subcommission on Geochronology of the International Union of Geological Sciences recommend the adoption of the following values of isotope ratios (Faure, 1986):

$$^{86}Sr/^{88}Sr = 0.1194$$

$$^{84}Sr/^{86}Sr = 0.056584$$

$$^{85}Rb/^{87}Rb = 2.59265$$

1.2.1.2. Stable Sr isotopes

Strontium lacks several of the qualitative chemical characteristics outlined by O'Neil (1986) in that it is relatively heavy, exists in a single predominant oxidation state in nature, and forms ionic bonds, and does not have large mass differences between the measured stable isotopes. As the atomic number of an element increases the degree of isotopic variation decreases as the relative mass difference between the isotopes diminishes. The mass differences between ^{88}Sr and ^{86}Sr (2.3%) and ^{84}Sr and ^{86}Sr (4.7%) are small, requiring very precise measurements. However, new developments in mass spectrometry have enabled the measurement of many "non traditional stable isotopes" of elements such as calcium, magnesium and iron (Johnson et al., 2004).

The three isotopes aside from ^{87}Sr are non-radiogenic and thus are not affected by radioactive decay. The ^{84}Sr isotope is nucleosynthetic so can vary due to mass dependent and mass independent processes. The isotopes ^{86}Sr and ^{88}Sr are produced by

the same nucleosynthetic process, and so provide information relating solely to mass dependent processes. Stable strontium isotopes are given in the defined delta notation relative to the standard reference material SRM 987, a purified Sr carbonate, in parts per million distributed by the National Institute of Standards and Technology or NIST (formerly known as the National Bureau of Standards or NBS) given in Equations 1.16 and 1.17 for $^{88}Sr/^{86}Sr$ and $^{84}Sr/^{86}Sr$ respectively. Isotope anomalies in $^{84}Sr/^{86}Sr$ can also be expressed in ε units, which is the variation relative to NBS in parts per 10^{-4} (Equation 1.18) after internal normalization to an $^{88}Sr/^{86}Sr$ ratio of 8.375209 (Nier, 1938).

$$\delta^{88}Sr = \left(\frac{^{88/86}Sr-sample}{^{88/86}Sr-NBS-987} - 1\right) \times 1000 \qquad \textit{Equation 1.16}$$

$$\delta^{84}Sr = \left(\frac{^{84/86}Sr-sample}{^{84/86}Sr-NBS-987} - 1\right) \times 1000 \qquad \textit{Equation 1.17}$$

$$\varepsilon^{84}Sr = \left(\frac{^{84/86}Sr-sample}{^{84/86}Sr-NBS-987} - 1\right) \times 10000 \qquad \textit{Equation 1.17}$$

1.2.1.2.1. Nucleosynthetic Sr isotopes

The isotope ^{84}Sr is a proton rich *p*-only nuclide, ^{86}Sr and ^{87}Sr are *s*-only nuclides, and ^{88}Sr is predominantly *s*-process with some *r*-process contribution. The *s*- and *r*-processes involve neutron addition in combination with β decay, and produce isotopes that fall on the neutron-rich side of the valley of stability. Thus, ^{86}Sr, ^{87}Sr, and ^{88}Sr are the most abundant isotopes of Sr, whilst ^{84}Sr falls on the neutron-poor side of the valley of stability and is the least abundant. As the only rare *p*-process isotope, which is formed in extreme conditions in Type I and Type II supernovae, ^{84}Sr is an interesting potential tracer of nucleosynthetic contributions. As such, any isotopic anomalies found in the ^{84}Sr composition of planetary materials could provide insights into both early solar nebular heterogeneity inherited from presolar stellar sources and the processes that caused non-mass-dependent variations. As the radiogenic $^{87}Sr/^{86}Sr$ ratio varies due to decay from ^{87}Rb, and the data are mass fractionation corrected to a fixed value of $^{88}Sr/^{86}Sr$, this leaves the detection of non-mass dependent nucleosynthetic effects in the $^{84}Sr/^{86}Sr$ ratio only.

The first nucleosynthetic Sr isotope variations were identified in calcium and aluminium rich inclusions (CAIs) and chondrules from the carbonaceous chondrite meteorite Allende CV3, most likely due to a deficit in the *p*-process ^{84}Sr nuclide (Papanastassiou and Wasserburg, 1978). Since this pioneering study, it has only been in recent years that interest in the $^{84}Sr/^{86}Sr$ isotopic compositions of planetary bodies has re-ignited, primarily due to advances in mass spectrometry techniques, and precise $^{84}Sr/^{86}Sr$ isotopic compositions of chondrites, carbonaceous chondrites, basaltic achondrites, CAIs, ordinary chondrites, HED meteorites, angrites, eucrites, and other meteoritic bodies have been determined (e.g. Podosek et al., 2004; Andreasen and

Sharma, 2007) Moynier et al., 2012; Paton et al., 2013; Hans et al., 2013). Podosek et al. (2004) analysed the Sr isotopic compositions of individual SiC fractions from the Murchison (CM) chondrite and found Sr isotopic anomalies inferred to be an enrichment of *s*-process nucleosynthetic products. Andreasen and Sharma (2007) measured the $^{84}Sr/^{86}Sr$ isotopic compositions of bulk meteorites (carbonaceous chondrites, an ordinary chondrite, and a eucrite) to a high precision and found them to be uniform and identical to the terrestrial composition (BCR-2). In contrast to this, deviations from terrestrial Sr were reported for ^{84}Sr values in CAIs of Allende (Hans et al., 2011). Moynier et al. (2012) later repeated the measurements made by Podosek et al. (2004) as well as measuring terrestrial samples, CAIs, lunar samples, martian samples and bulk meteorites. The lunar and martian samples were found to be indistinguishable from terrestrial values, whilst chondrites and CAIs exhibit variations in $\varepsilon^{84}Sr$, and CAIs being the most enriched in ^{84}Sr. Paton et al. (2013) measured the isotopic composition of CAIs, bulk chondrites, and differentiated meteorites asteroids and also found that CAIs exhibit the largest anomalies in $\mu^{84}Sr$ (in agreement with Moynier et al., 2012). Angrites, ordinary chondrites, enstatite chondrites, and a eucrite had isotopic compositions indistinguishable from the average $\mu^{84}Sr$ terrestrial value, determined to be −22 ppm. More recently, Hans et al. (2013) report high precision $^{87}Sr/^{86}Sr$ and $^{84}Sr/^{86}Sr$ data for eucrites, angrites and CAI, and again find ^{84}Sr excesses in CAIs, whilst determining that the $^{84}Sr/^{86}Sr$ ratios of all the eucrites and angrites are indistinguishable from those of the terrestrial samples.

1.2.1.2.2. Mass dependent Sr isotopes

Radioactive decay does not affect the stable isotopes ^{86}Sr and ^{88}Sr. Nucleosynthetic processes can affect both, but careful monitoring of this in extra-terrestrial material allows variations in the $^{88}Sr/^{86}Sr$ ratio due to mass dependent fractionation to be investigated. As the magnitude of mass dependent fractionation varies proportionally with the difference in mass between the two isotopes, the difference between equilibrium and kinetic fractionation can be calculated. For Sr, substituting the exact atomic masses given in Table 1.1 into Equations 1.11 and 1.12 equates to exponents of β_K=0.505744918 and β_E=0.511553128, where m_1=84 m_2=86 and m_3=88, the exact masses of which are given in Table 1.1. in m_a/u.

$$\beta_K = \frac{ln\left[\frac{m_1}{m_2}\right]}{ln\left[\frac{m_1}{m_3}\right]} = \frac{ln\left[\frac{m_{84}}{m_{86}}\right]}{ln\left[\frac{m_{84}}{m_{88}}\right]} = 0.505744918 \quad \beta_E = \frac{\left[\frac{1}{m_1} - \frac{1}{m_2}\right]}{\left[\frac{1}{m_1} - \frac{1}{m_3}\right]} = \frac{\left[\frac{1}{m_{84}} - \frac{1}{m_{86}}\right]}{\left[\frac{1}{m_{84}} - \frac{1}{m_{88}}\right]} = 0.511553128$$

This is illustrated graphically on a three-isotope plot between $\delta^{88}Sr$ and $\delta^{84}Sr$ in Figure 1.1. The offset between the two is below the limits of precision or current mass-spectrometry techniques, and thus distinguishing between the two is difficult.

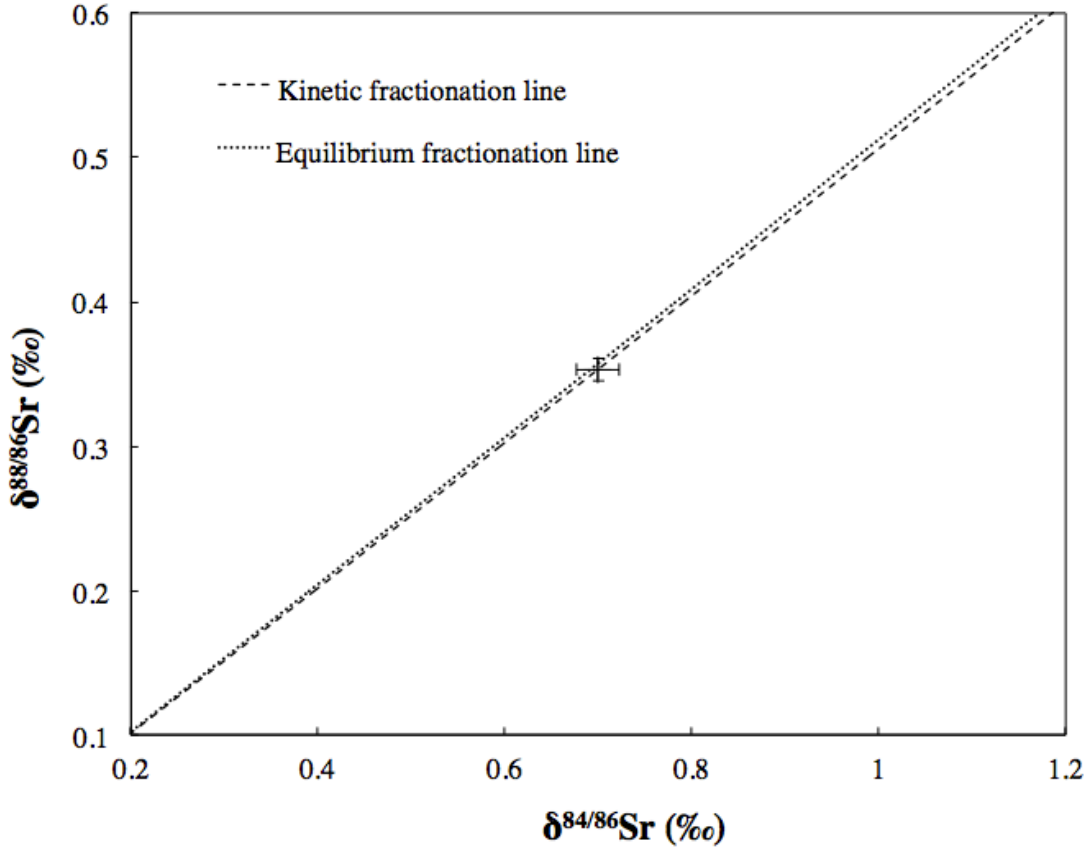

Figure 1.1: Comparison of the equilibrium and kinetic mass-dependent fractionation lines. Typical error bars (2 s.e.) of a measurement are shown to illustrate the difficulty in separating the two fractionation processes with current measurement precision.

The first investigation into stable Sr isotope fractionation involved extra-terrestrial material, and showed that some refractory calcium-aluminium rich inclusions (CAIs) in carbonaceous chondrite meteorites preserve anomalous Sr isotope compositions (Papanastassiou and Wasserburg, 1978). However, these variations were attributed to non-mass dependent processes and are most-likely due to a deficit in the least abundant isotope ^{84}Sr, a *p*-process nuclide, attributed to production in distinct nucleosynthetic sites (Papanastassiou and Wasserburg, 1978; Birck, 2004). Mass-dependent Sr variations were discovered in chondrules and CAIs from Allende using a novel double-spike technique in combination with Thermal-Ionisation Mass Spectrometry (TIMS),

which corrected for instrumental mass fractionation (Patchett, 1980a,b). Co-variations were found between the $^{88}Sr/^{86}Sr$ and $^{84}Sr/^{86}Sr$ ratios consistent with the expected effects of mass-dependent fractionation, and the $^{88}Sr/^{86}Sr$ ratio of CAIs and chondrules were found to be up to ~3‰ lighter than bulk chondrites and terrestrial samples. Since this pioneering work in the field of stable Sr it has only been over the last decade that the development and application of this technique have continued, mainly due to advances in the field of mass spectrometry. Using Multi Collector – Inductively Coupled Plasma – Mass Spectrometry (MC-ICP-MS) in combination with standard bracketing (SSB), Fietzke and Eisenhauer (2006) found a significant temperature dependent fractionation of $\delta^{88/86}Sr$ associated with precipitation of aragonitic $CaCO_3$ from seawater. This sparked considerable interest in using the stable $\delta^{88/86}Sr$ system in combination with the radiogenic Sr ratio as tracer of processes in low-temperature marine and terrestrial environments (Ruggeberg et al., 2008; Halicz et al., 2008; Krabbenhöft et al., 2009; Krabbenhöft et al., 2010; Bohm et al., 2012; Ohno et al., 2008; Ohno and Hirata, 2007; Wei et al., 2013). In these studies, the variable $^{88}Sr/^{86}Sr$ composition of various reservoirs has been characterised. Seawater has been determined to be homogeneous with heavy $\delta^{88}Sr$ values of ~ 0.38‰ to 0.39‰ (Fietzke and Eisenhauer, 2006; Halicz et al., 2008; Ohno et al., 2008; Krabbenhöft et al., 2010); marine biogenic carbonates show values from 0.1‰ to 0.3‰ (Halicz et al., 2008; Ohno et al., 2008; Krabbenhöft et al., 2010); and terrestrial carbonates show very light values of ~− 0.1‰ to − 0.3‰ (Halicz et al., 2008; Ohno et al., 2008). Chemical weathering, pedogenesis, and carbonate deposition are likely the main processes that cause the fractionation of stable Sr isotopes (Halicz et al., 2008). Large seasonal $\delta^{88}Sr$ variations in river water range from 0.147‰ to 0.661‰, with low $\delta^{88}Sr$ values (< 0.3‰)

interpreted to be due to a dominant contribution from the weathering of carbonate rocks, and the high $\delta^{88}Sr$ values from weathering of silicates (Wei et al., 2013).

There has been considerably less interest in the development of the stable Sr isotope system in the high-temperature environment. This may primarily be because the degree of isotopic fractionation is comparatively small at the high temperatures associated with this environment (following the relationship given in Equation 1.6, the degree of isotopic fractionation decreases as temperature increases) making the accurate measurement of any fractionation difficult. In spite of this, the pioneering investigations into mass independent and dependent Sr isotope variations were in high temperature environments, yet it has been only in the last few years that in-depth investigations into solar system and terrestrial materials has continued. In 2010, Moynier et al. (2010) determined the $\delta^{88}Sr$ values of a variety of terrestrial samples, martian meteorites, a lunar meteorite, HED, undifferentiated primitive meteorites, chondrules and refractory inclusions. For this, MC-ICP-MS was used in combination with SSB and a correction for instrumental mass bias 'externally' by using admixed zirconium isotopes ($^{90}Zr/^{91}Zr$) yielding a ±50 parts per million (ppm) level of precision at which almost all whole-rock samples aside from chondrites were found to be isotopically indistinguishable. The CV and CO chondrites were found to be isotopically light. The range of fractionation observed extended from isotopically light chondrules from Allende ($\delta^{88}Sr = -1.73‰ \pm 0.09‰$) to the heavy Allende matrix ($\delta^{88}Sr = + 0.66‰ \pm 0.09‰$). Individual members of the following group averages were inferred to have homogenous compositions: $\delta^{88}Sr_{\text{ordinary chondrites}} = +0.28 \pm 0.16‰$ (n=4); $\delta^{88}Sr_{BSE} = +0.27 \pm 0.05‰$ (n=8); $\delta^{88}Sr_{moon} = +0.33 \pm 0.09‰$ (n=1); $\delta^{88}Sr_{Mars} = +0.25 \pm 0.07‰$ (n=4); $\delta^{88}Sr_{\text{carbonaceous chondrites}} = +0.19 \pm 0.20‰$ (n=6); $\delta^{88}Sr_{HED} = +0.33 \pm 0.04‰$ (n=2); and $\delta^{88}Sr_{\text{enstatite chondrites}} = + 0.31 \pm 0.13‰$ (n=4). A later more comprehensive analysis, also by MC-ICP-MS, confirmed the variations in

CAIs and chondrules reported previously, spanning a range of $\delta^{88}Sr$= -0.35 ±0.10‰ to + 0.65 ±0.08‰ (Charlier et al., 2012). This study incorporated a diverse range of samples from the Moon, Mars and Earth, in addition to carbonaceous chondrites and differentiated meteorites. The variation in $\delta^{88}Sr$ between the bulk compositions of each of these groups is limited and difficult to resolve at analytical uncertainty. However, statistically Mars, angrites, eucrites and bulk carbonaceous chondrites are indistinguishable, but lighter than mantle-derived terrestrial igneous rocks. On average there is a hint that lunar samples may be lighter than the terrestrial rocks (Figure 1.2). Evolved rhyolites and lunar basalts were found to possess far lighter $\delta^{88}Sr$ compositions that co-vary with the europium anomaly, an index of plagioclase fractionation (Figure 1.3). As such, the fractionation of $\delta^{88}Sr$ during magmatic evolution could be modelled by the heavy isotopes of Sr being preferentially partitioned into plagioclase with a fractionation factor of ~1.0002 for $^{88}Sr/^{86}Sr$, illustrated in Figure 1.3 for terrestrial and lunar samples.

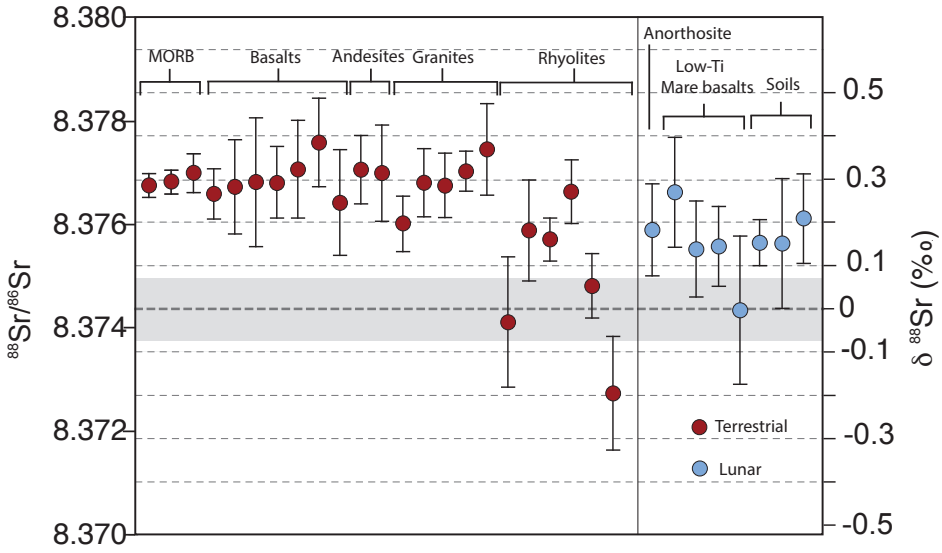

Figure 1.2: Plot of $\delta^{88}Sr$ compositions of terrestrial and lunar silicates (after Charlier et al., 2012).

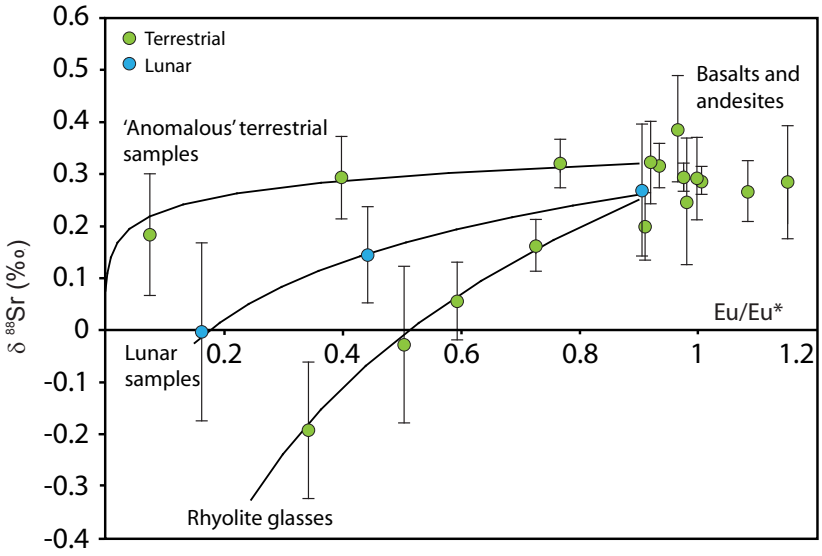

Figure 1.3: Plot of $\delta^{88}Sr$ versus Eu/Eu* in terrestrial magmas and lunar basalts. Sr fractionation is modelled using *f* values of 1.000598 and 1.000823 for rhyolites and lunar basalts respectively (after Charlier et al., 2012).

The authors concluded that such modelling demonstrates that extensive fractionation of a phase in which Sr is compatible, in this case plagioclase, can profoundly change the stable isotope composition of Sr in the evolving melt fraction. Importantly, this indicates that mass-dependent magmatic processes alone are capable of generating measurable variations in Sr stable isotopes in high-temperature environments.

In addition to these two primary studies, a number of geological rock standards (BHVO-1, BHVO-2, BCR-2, DNC-1, BIR-1, JB-1, JB-2, JB-3, JA-2, AGV-2, G-2 and JG-2) have been analysed by others (Ohno and Hirata, 2007; de Souza et al., 2010; Shalev et al., 2013; Ma et al., 2013). A summary of all available $^{88}Sr/^{86}Sr$ data for high temperature materials, both terrestrial and extra terrestrial, measured to date is presented in Figure 1.4.

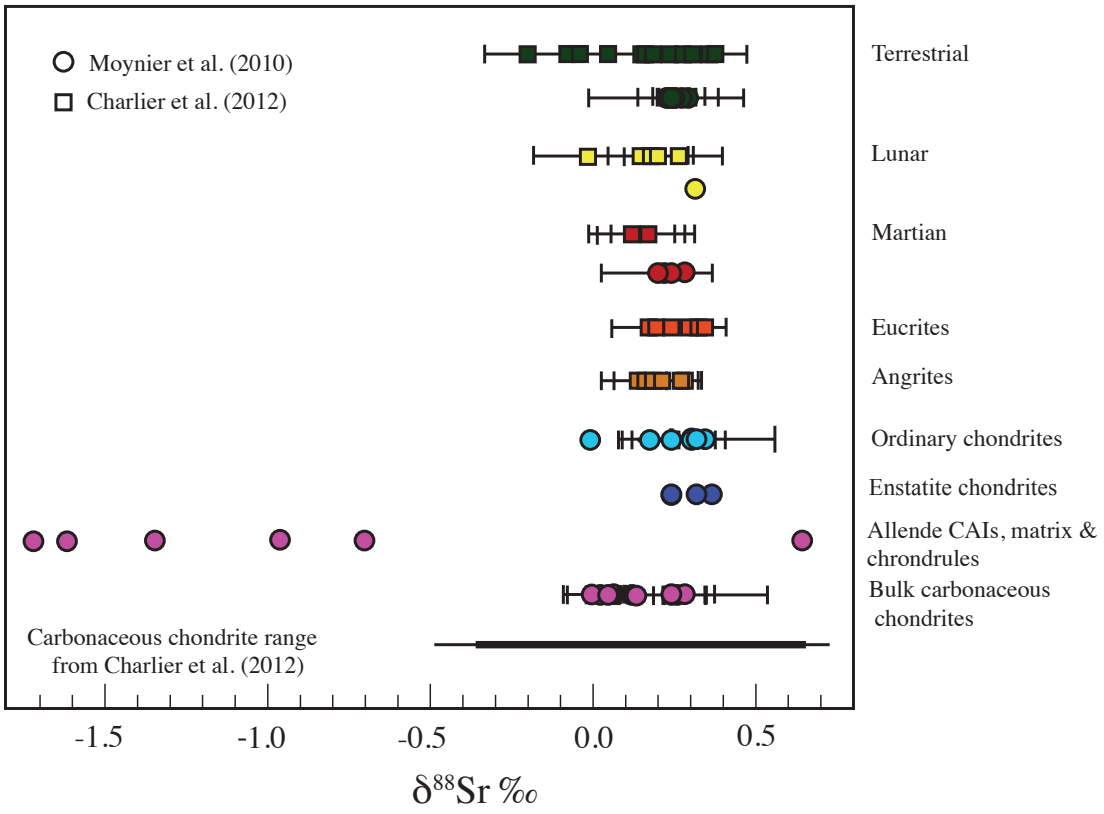

Figure 1.4: Summary of all $\delta^{88}Sr$ data available to date (Charlier et al., 2012; Moynier et al., 2010). Geostandard data from Ohno and Hirata (2007), de Souza et al. (2010), Shalev et al. (2013) and Ma et al. (2013) lie within the terrestrial range shown, and are obscured by the data from Moynier et al. (2010) and Charlier et al. (2012).

1.3. Measurement of Sr isotopes

To determine differences in Sr isotope abundances and the $^{87}Sr/^{86}Sr$, $^{88}Sr/^{86}Sr$, and $^{84}Sr/^{86}Sr$ ratios of samples requires a precise measurement by mass spectrometry. There are a variety of mass spectrometry techniques, but the two commonly used for Sr isotopes are TIMS and MC-ICP- MS. Multi Collector ICP-MS generates an ion beam by the introduction of a purified sample into a plasma, whilst for TIMS a sample is heated up and ionized on a metal filament. Whether one is used over the other depends on which ratios are to be measured and for what purpose:

1.3.1. $^{87}Sr/^{86}Sr$

Initial interest in Sr isotopes largely concerned the radiogenic $^{87}Sr/^{86}Sr$ ratio. For this, the ^{88}Sr and ^{86}Sr isotopes were traditionally used to correct for the instrumental mass fractionation that occurs during TIMS analysis. Following the recent development of MC-ICP-MS as a technique to precisely measure multiple samples in shorter time periods, this method also became a viable common option in the measurement of radiogenic Sr. Both techniques yield a typical external precision of 10-15ppm and correct for any variation in the $^{87}Sr/^{86}Sr$ ratio due to mass or temperature dependent equilibrium or kinetic fractionation (e.g. instrumental mass fractionation) by normalization to the commonly accepted $^{86}Sr/^{88}Sr$ ratio of 0.1194 (Nier, 1938).

1.3.2. $^{88}Sr/^{86}Sr$

Using a fixed $^{88}Sr/^{86}Sr$ value allows the measurement of $^{87}Sr/^{86}Sr$ ratios to a very high precision but prohibits the detection of any mass-dependent variation in this ratio amongst samples. Since the pioneering work made to measure the stable $^{88}Sr/^{86}Sr$ isotope composition (Patchett, 1980a,b), there has been recent renewed interest in determining the mass dependent variations in the stable $^{88}Sr/^{86}Sr$ isotope composition (e.g. Fietzke and Eisenhauer, 2006) and a number of techniques have been used for the precise measurement of stable Sr isotopes. Many stable Sr isotope measurements have been undertaken by MC-ICP-MS using either Sample-Standard-Bracketing (SSB, e.g. Fietzke and Eisenhauer, 2006) or element doping with Zr (e.g. Nowell et al., 2007; Yang et al., 2008; Liu et al., 2012; Ohno and Hirata, 2007; Ohno and Hirata, 2008; Moynier et al., 2010; Charlier et al., 2012) yielding an external precision of 0.05 to

0.07‰ (2SD). Alternatively, a precision 2-3 times better is achieved by analysis by Double-Spike Thermal Ionisation Mass Spectrometry (DS-TIMS), which has also been employed in a number of studies (Krabbenhöft et al., 2009; Krabbenhöft et al., 2011; Böhm et al., 2012; Shalev et al., 2013).

1.3.3. $^{84}Sr/^{86}Sr$

The primary use of the $^{84}Sr/^{86}Sr$ ratio is as an investigative tool into mass independent (nucleosynthetic) variations in extra-terrestrial materials. As ^{84}Sr is the least abundant isotope, very accurate measurements are required. During MC-ICP-MS analyses, significant ^{84}Kr interferences on ^{84}Sr can lead to inaccurate or imprecise $^{84}Sr/^{86}Sr$ ratios. This drawback can limit MC-ICP-MS studies to terrestrial samples, as well as the precision of double-spike measurements by this technique. In contrast, the precise measurement of $^{84}Sr/^{86}Sr$ can be achieved by TIMS (Patchett, 1980a,b; Andreasen and Sharma, 2007; Moynier et al., 2012; Paton et al., 2013; Hans et al., 2013). However, for all of these studies the $^{84}Sr/^{86}Sr$ ratio is normalised to $^{88}Sr/^{86}Sr$ to correct for instrumental fractionation and thus variations in $^{84}Sr/^{86}Sr$ could be due to enrichment or depletion of ^{84}Sr, ^{86}Sr, or ^{88}Sr. For example, an apparent positive $^{84}Sr/^{86}Sr$ anomaly could either be attributed to a *p*-process excess on ^{84}Sr or to an *r*-process excess on ^{88}Sr. The magnitude of mass dependent fractionation varies proportionally with the difference in mass between the two isotopes considered (Equation 1.9) and any deviation from this behaviour is considered to be mass-independent fractionation. For Sr, distinguishing between mass dependent and nucleosynthetic anomalies requires a comparison of $^{84}Sr/^{86}Sr$ and $^{88}Sr/^{86}Sr$ on a three-isotope plot to identify any such deviations from mass-dependent fractionation lines and to assign the cause of variation

to either nucleosynthetic ^{84}Sr or mass dependent ^{86}Sr. For this, both the $^{84}Sr/^{86}Sr$ and $^{88}Sr/^{86}Sr$ ratio must be measured precisely. This can be achieved by analysis by TIMS combined with the application of a Sr double spike.

1.4. DS-TIMS (Double-spike)

Instead of normalisation to a fixed ratio by comparison with isotopic analyses of standards, double spiking can be used to correct for mass bias if the element in interest has four or more isotopes, as is the case for Sr (Rudge et al., 2009). Double spiking prior to separation by column chemistry also corrects for any fractionation during ion chromatographic Sr separation, which alleviates the requirement of 100% column yields. For Sr, ^{84}Sr, ^{85}Rb, ^{86}Sr, ^{87}Sr and ^{88}Sr are measured. Measurement of ^{85}Rb allows for the correction for interferences arising from ^{87}Rb in the sample, assuming an $^{87}Rb/^{85}Rb$ ratio of 0.385041. Both a spiked and un-spiked measurement is required if an isotope ratio varies due a non-mass dependent process (e.g. Galer, 1999; Albarède and Beard, 2004). The isotopic composition of the sample is calculated from measurements of the isotope abundances of four isotopes in two aliquots of the same sample: the unspiked sample (Nat) and the sample spiked (Mix) with an estimated amount of the element having a pre-determined and distinctly different isotopic composition. From these, the instrumental mass fractionation is obtained, which is assumed to follow the commonly used exponential law (Rudge et al., 2009; Albarde and Beard, 2004). This allows the "true "isotopic composition of the sample to be calculated. This dynamic is illustrated for Sr in Figure 1.5.

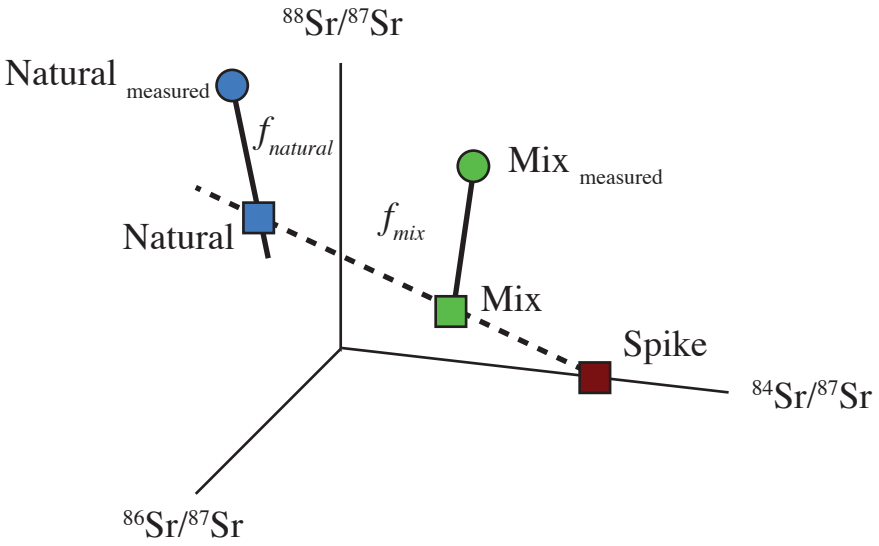

Figure 1.5: Illustration of the mechanics and concept behind the DS technique. The composition of the natural sample and spike are known, and the spike-sample mixture lies on the dashed mass fractionation trend line. As the $^{88}Sr/^{86}Sr$ varies due to radiogenic ingrowth in addition to mass fractionation, an unspiked run is necessary.

The double spike technique is commonly used in combination with TIMS analysis for the precise measurement of stable isotopes whilst correcting for instrumental fractionation by distinguishing between natural and instrumental mass fractionation (e.g. Galer, 1999; Johnson and Beard, 1999; Siebert et al., 2001). The DS-TIMS technique was first applied to Sr by Patchett (1980a,b) and is now increasingly employed for high-precision $^{88}Sr/^{86}Sr$ measurement (Krabbenhöft et al., 2009; Krabbenhöft et al., 2011; Böhm et al., 2012; Shalev et al., 2013). As the $^{87}Sr/^{86}Sr$ ratio can vary as a result of radiogenic in-growth, a separate spiked and un-spiked measurement is required for Sr analysis, in turn allowing an evaluation of coupled mass dependent variations in $^{84}Sr/^{86}Sr$ and $^{88}Sr/^{86}Sr$ ratios along with radiogenic $^{87}Sr/^{86}Sr$ ratios in terrestrial samples. Furthermore, this approach has the advantage of enabling the detection of any nucleosynthetic variations in $^{84}Sr/^{86}Sr$ ratios in extra-terrestrial samples. All three Sr

isotope ratios can be measured to a high precision: $^{87}Sr/^{86}Sr$ ratios to ~±7 ppm, $^{88}Sr/^{86}Sr$ to better than ±10 ppm external precision, and $^{84}Sr/^{86}Sr$ to better than ±20ppm (all 2SD). This is a considerable improvement in precision for the measurement of $^{88}Sr/^{86}Sr$ over MC-ICP-MS with SSB or Zr-empirical-external-normalization (EEN), both of which are also burdened with the requirement of ~100% column yields and sensitivity to matrix effects (Krabbenhöft et al., 2009; Krabbenhöft et al., 2010), and is highlighted in Figure 1.6. Double spiking by MC-ICP-MS is possible, and can improve the precision of analyses compared to SSB or EEN techniques (Shalev et al., 2013). However, this is still considerably inferior than that achieved by DS-TIMS, where the SSB or EEN is typically less than <0.01‰ for $^{88}Sr/^{86}Sr$ and DS-MC-ICP-MS is greater than 0.02‰, illustrated in Figure 1.7 (Shavel et al., 2013; Krabbenhöft et al., 2009).

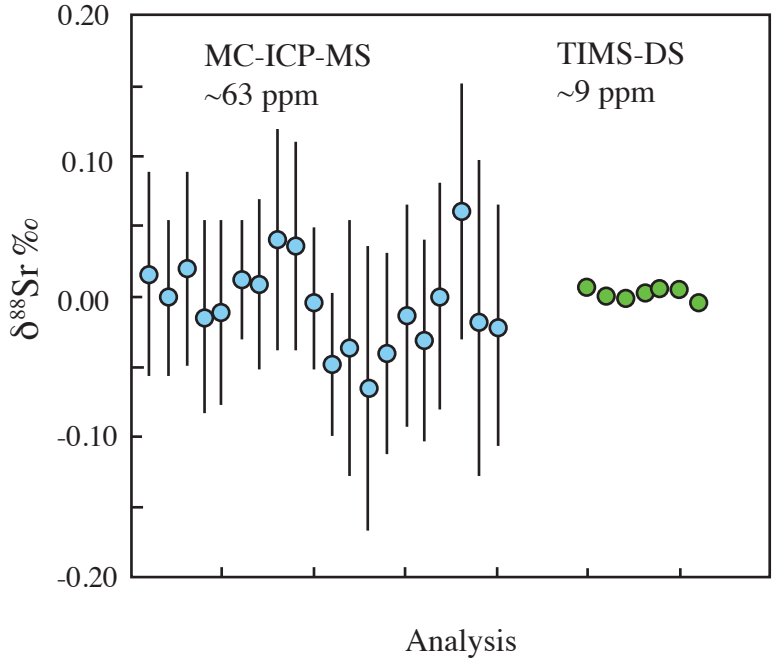

Figure 1.6: Comparison of precision of $\delta^{88}Sr$ data collected from MC-ICP-MS-SSB and TIMS-DS by I.J. Parkinson. The error bars for the DS-TIMS data are obscured by their symbols.

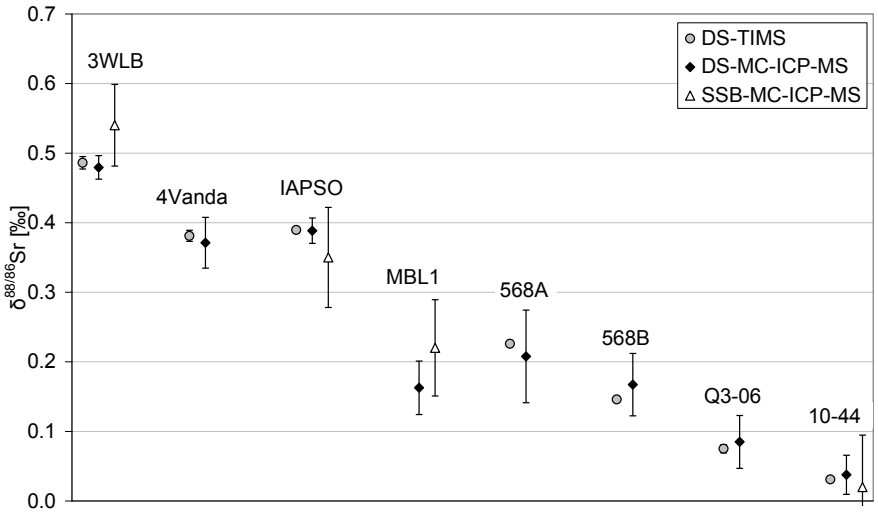

Figure 1.7: Comparison of external 2SEM errors (‰) obtained by the MC-ICP-MS-SSB, MC-ICP-MS-DS, and TIMS-DS methods for various samples (Shalev et al., 2013).

In summary, double spiking in combination with TIMS enables the measurement of all $^{87}Sr/^{86}Sr$, $^{88}Sr/^{86}Sr$ and $^{84}Sr/^{86}Sr$ ratios to a precision far better than any alternative technique currently being used, as well as enabling the investigation of both mass dependent variation in $^{88}Sr/^{86}Sr$ and mass independent fractionation in $^{84}Sr/^{86}Sr$.

1.5. Motivation for study

The Earth's moon is often studied to allow insights into ancient processes on Earth, which have been eliminated by processing that has occurred in its geological history. Together, the Earth-Moon system provides a depth of understanding in the field of cosmochemistry rarely attained from other solar system bodies due to limited sampling. This has been greatly enhanced by retrieval of lunar rock specimens from the American and Soviet lunar missions in the 1960's and 1970's. Whilst the studies that exist on stable Sr cover a wide range of Solar System materials, the sample selections regarding

the Earth and its Moon are limited (Charlier et al., 2012; Moynier et al., 2010). Aside from these, stable Sr isotopes have only been measured for a limited range of terrestrial silicate rocks, and these are predominantly geostandards. Fractionation of stable Sr isotopes clearly occurs at high temperatures on the Earth and its Moon due to magmatic processes alone (Charlier et al., 2012). However, all existing high temperature $\delta^{88}Sr$ data has been determined by MC-ICP-MS techniques, which, whilst being sufficiently precise to resolve variations in the $^{88}Sr/^{86}Sr$ in low temperature samples, lack the precision to detect variations for which the degree of fractionation is significantly smaller (Equation 1.6). This is summarised in one of the main conclusions of Charlier et al. (2012):

> "Higher-precision determinations of $\delta^{88}Sr$ by MC–ICP-MS would certainly help to further resolve and explain some of the differences between planetary bodies that we have identified in this paper. However, measurement of all three Sr isotope ratios (i.e., $^{88}Sr/^{86}Sr$, $^{87}Sr/^{86}Sr$ and $^{84}Sr/^{86}Sr$) by high-precision double-spike TIMS methods is necessary to resolve the timing and contribution of nucleosynthetic and mass dependent inputs into the evolution of Sr in the early solar system."

The primary focus of this thesis is to further the application of the stable isotopes of Sr in high temperature environments, focussed on the Earth-Moon system, whilst also using information provided by $^{87}Sr/^{86}Sr$ and $^{84}Sr/^{86}Sr$ to unravel processes occurring and to add a depth of understanding of the overall behaviour of the Sr isotope system. The DS-TIMS methodology is the perfect tool for a three-pronged approach to investigating all three isotope ratios of Sr to a high precision, as well as mass dependent and mass independent fractionation in the Earth and its moon.

1.6. Thesis structure

First, an overview of the methodology and analytical techniques used in the collection of Sr isotope data in this thesis is given in Chapter 2. The main research objective is then practically addressed by a number of studies that comprise the subsequent chapters 3-6. In Chapters 3, 4 and 5, a groundwork of understanding in the terrestrial high temperature environment is established. For this, a thorough investigation into the stable Sr compositions of the basalt products of mantle melts was carried out in Chapter 3 in combination with the radiogenic $^{87}Sr/^{86}Sr$ ratio as a tracer tool, to provide insights into terrestrial mantle processes. In Chapter 4 a series of magmatic minerals were studied in order to further pinpoint the causes of stable isotope fractionation at a mineral level. In Chapter 5 a detailed study of the effects of magmatic differentiation on the stable isotopes of Sr was conducted in the terrestrial setting of the volcano of Hekla in Iceland. In this, the radiogenic $^{87}Sr/^{86}Sr$ ratio is used as a means of assessing contribution from contaminants. Knowledge gained from these terrestrial studies is then applied to an extensive suite of lunar silicates, from anorthosites to mare basalts, to unravel processes occurring on the Moon, their effect on the stable isotopes of Sr, and further investigate differences between the two neighbouring bodies in Chapter 6. Early solar system processes are investigated by searching for nucleosynthetic anomalies in $^{84}Sr/^{86}Sr$ and using high-precision Rb-Sr isotope data to provide an accurate age of the Moon. Chapter 7 brings together the conclusions made in previous chapters to present an overall discussion of stable Sr isotope fractionation in the Earth-Moon system.

CHAPTER TWO

Analytical methods

Summary

The following chapter presents the details and applications of the chemical and analytical techniques used in the collection of data for this thesis. All laboratory work and chemical techniques were carried out at the University of Oxford. However, due to unforeseen circumstances at the start of this project, mass spectrometry analyses were made at two institutions other than Oxford, the Open University and Durham University.

Firstly, a short introduction gives an overview of the historical development of Sr isotope techniques along with the advantages, applications and the reasons behind the choice of the technique used here; double spiking in combination with Thermal Ionisation Mass Spectrometry (TIMS). In the first half of this chapter, the chemical procedures used for the chemical separation of Sr are disclosed. This includes the chemical techniques used to process and digest the samples, the double spike technique and its practical application, and lastly the technique for the chemical separation of Sr. The second half of the chapter gives an overview of the procedures and techniques used in the running of the TIMS and the acquisition of isotopic data. Lastly, details are given on data processing, including deconvolution of the spiked and un-spiked measurements, as well as on means of assessing the quality of the data, such as standards, precision and blanks.

2.1. Introduction to Sr isotope techniques

Historically, Sr has been of interest principally for its radiogenic isotope ratio $^{87}Sr/^{86}Sr$, which can be used as a tracer for weathering processes as well as for chronology by radioactive decay of ^{87}Rb to ^{87}Sr. Measurements of radiogenic Sr are conventionally made by thermal ionisation mass spectrometry (TIMS) and more recently multiple-collector inductively coupled plasma mass spectrometry (MC-ICP-MS), by using a fixed $^{88}Sr/^{86}Sr$ ratio of 0.1194 as a normalization ratio to correct for instrumental mass-dependent effects. Using a fixed $^{88}Sr/^{86}Sr$ value allows the measurement of $^{87}Sr/^{86}Sr$ ratios to a very high precision but assumes the $^{88}Sr/^{86}Sr$ ratio is constant between samples and prohibits the detection of any mass-dependent variation in this ratio amongst samples. Since the pioneering work made to measure the stable $^{88}Sr/^{86}Sr$ isotope composition (Patchett, 1980a,b) there has been recent renewed interest in determining the mass dependent variations in the stable $^{88}Sr/^{86}Sr$ isotope composition (e.g. Fietzke and Eisenhauer, 2006) and a number of techniques have been used for the precise measurement of stable Sr isotopes. Many stable Sr isotope measurements have been undertaken by MC-ICP-MS using either standard-sample bracketing (e.g. Fietzke and Eisenhauer, 2006) or element doping with Zr (e.g. Nowell et al., 2007) yielding an external precision of 0.05 to 0.07 ‰. However, significant ^{84}Kr interference on ^{84}Sr and a variable interference that also sits on ^{84}Sr can lead to inaccurate or imprecise $^{84}Sr/^{86}Sr$ ratios. This drawback can limit MC-ICP-MS studies to terrestrial samples, as well as the precision of double-spike measurements by this technique. Thus, for the measurement of $^{88}Sr/^{86}Sr$ ratios to the high precision required (for example, in this study), or for the precise measurement of $^{84}Sr/^{86}Sr$ ratios to investigate non-mass dependent processes in extra terrestrial samples, MC-ICP MS is not a viable option.

An alternative to this is the measurement of Sr stable isotopes using TIMS, whereby a solid sample is ionised by thermal heating. During thermal ionization, the light isotope is preferentially evaporated causing a within instrument mass fractionation, and this results in the fractionation of all isotope ratios during the course of the measurement. The extent and nature of this mass fractionation varies during the time of the analysis, as well as differing between filaments and methods of loading. This in turn makes any correction for instrumental mass bias based on comparisons with isotopic analyses of standards difficult to achieve, potentially unreliable, and inconsistent. If the element in interest has four or more isotopes, as is the case for Sr, then an alternate reliable technique, double spiking, can be used to correct for mass bias. Addition of a double spike in combination with TIMS enables measurement precisions of $\delta^{88}Sr$ to ±10ppm, a three-fold improvement over most published MC-ICP-MS data.

If an isotope ratio varies due a non-mass dependent process, then both a spiked and un-spiked measurement is required (e.g. Galer, 1998; Albarède and Beard, 2004). As the $^{87}Sr/^{86}Sr$ ratio can vary as a result of radiogenic in-growth, a separate spiked and un-spiked measurement is required for Sr analysis, in turn allowing an evaluation of coupled mass dependent variations in $^{84}Sr/^{86}Sr$ and $^{88}Sr/^{86}Sr$ ratios along with radiogenic $^{87}Sr/^{86}Sr$ ratios in terrestrial samples. Furthermore, this approach has the advantage of enabling the detection of any nucleosynthetic variations in $^{84}Sr/^{86}Sr$ ratios in extra-terrestrial samples. This double spike and TIMS techniques allows us to measure all three Sr isotope ratios to a high-precision in natural samples including measuring $^{87}Sr/^{86}Sr$ ratios to ~±7 ppm and $\delta^{88}Sr$ to ±10 ppm external precision, fulfilling all the pre-requisites of this study.

2.2. Analytical Method

2.2.1. Laboratory conditions and protocol

All chemistry was carried out under ultra clean laboratory conditions under laminar flow controlled fume hoods at the Department of Earth Science, Oxford. Two hoods were used, which were regularly cleaned and maintained. Special care was taken to separate the double-spike and non-spiked chemistry in order to avoid cross contamination. This is crucial for accurate stable Sr analyses as the Sr composition of the double spike contrasts greatly when compared with the natural range of ratios encountered in the environment. Thus, mixing of even a relatively minor amount of spike with a natural sample (and non-spiked sample run) has the potential to drastically alter its measured composition, and vice versa. Spiked and non-spiked beakers were cleaned separately and ascribed their own sets of cleaning acids and beakers, and where possible, separate hoods were used for column chemistry.

2.2.1.1. Preparation of reagents

All acids (HNO_3, HCl, HF,) used were prepared by in house sub-boiling distillation to at least Quartz-Distilled (QD) grade or Ultra-Purity acids (HCl and HNO_3) purchased from ROMIL were used. The acetic acid ($C_2H_4O_2$) used was distilled in-house to glacial grade (99%) and the sodium acetate of analytical grade (≥99.0 %), purchased from Fisher Scientific. Any acetone and ethanol used in cleaning were reagent grade purchased from Fisher Scientific. Water was deionised using a MilliQ-element water polisher to achieve high purity MQ water with a resistivity of 18.2 MΩ cm^{-1}. All acids and reagents were sealed with Parafilm® and stored in thrice cleaned PTFE or Teflon bottles and a clean ventilated cupboard when not being used in the fume hood.

2.2.1.2. Savillex Teflonware cleaning

All Savillex used was thoroughly cleaned before and after use to ensure minimal contamination. Savillex and bottles were cleaned following the procedure summarised as follows.

1. Rinsed first with ethanol and subsequently several times with MQ followed by bulk cleaning (in a single large beaker) on the hotplate for a week at 130°C in 35% reagent grade HNO_3.
2. Rinsed three times in MQ followed by individual cleaning on a hotplate for 5 days at 130°C in 20% QD HNO_3. Acid is discarded following this step.
3. Rinsed in MQ, and stored in fresh (previously unused) 20% HNO_3 at room temperature in a sealed plastic box.

2.2.2. Sample preparation

All samples were rock samples and provided in whole rock, crushate, or powdered form. The lunar samples were processed (crushed) in a dedicated preparatory lunar laboratory. Whole rock samples and crushates were converted to powdered form, to facilitate dissolution. Specific details on sample processing are provided in the relevant chapters, and general processing techniques are outlined below. All samples and standards were prepared and processed using identical techniques and reagents as outlined in this section, unless specifically stated.

2.2.2.1. Crushing

Whole rock samples, crushates and mineral separates were powdered in an alumina mortar and pestle. A specific mortar and pestle were used for the lunar samples to avoid cross contamination. Both mortar and pestle were cleaned with ethanol and Kim-wipes, ultrasonically cleaned in MQ several times, rinsed, and air-dried before and after use. Clingfilm was used to seal the mortar to avoid chips flying out during crushing and contamination.

2.2.2.2. Picking

Terrestrial oceanic basalts, provided in the form of chips, were crushed and picked using an optical microscope and weighing paper. Any chips or grains showing signs of weathering or alteration were removed. Minerals were separated under a binocular microscope to ensure optical purity of the minerals and any grains showing signs of weathering or containing visible inclusions were removed.

2.2.2.3. Cleaning and leaching

Rock chips were rinsed in MQ before and after crushing and picking. Oceanic basalt samples or mineral separates were also leached after crushing and picking in weak HCl (2M) for half an hour in a room temperature ultrasonic bath. This is to remove any possible contamination (for example, from Fe-Mn oxyhydroxides or seawater), which has the potential to affect isotope systems, particularly in ocean floor basalts or those subject to sub-aerial weathering. In most cases, the terrestrial oceanic basalts were fresh glasses and provided in finer grained crushate form.

2.2.2.4. Shale sample preparation

Carbonate fractions in shales were removed by leaching with 1M acetic acid buffered with 1M sodium acetate to pH 5 in clean 15 mL centrifuge tubes following the method detailed by Kryc et al. (2003). The solutions were left for 5-6 hours until CO_2 production ceased, left to settle, and the buffered solution pipetted out. Addition of MQ water and centrifuging was repeated several times to ensue near complete acid removal. The samples were transferred to Teflon beakers, dried out, and re-weighed to determine the fraction of carbonate removed by mass.

2.2.3. Sample dissolution

2.2.3.1. Basalts and silicate minerals

Silicates were digested by conventional methods comprising a 3:1 ratio of concentrated HF to concentrated HNO_3, scaling roughly1.3 mL for each 60 mg of sample according to sample size in order to ensure complete silicate dissolution. The volumes stated in the following protocol are for similar sample sizes and were scaled as necessary. After at least 48 hours of digestion at 130°C, the sample solution was evaporated to dryness and taken up in 0.5 mL concentrated HNO_3, left at 130°C overnight and evaporated. This stage was repeated as necessary until no insoluble fluorides remained. The remaining residue was fully dissolved in 2 mL 6M HCl and stored until aliquots were taken.

2.2.3.2. Bomb dissolution in an oven

Samples with high organic carbon contents, such as shales, required extensive oxidation for complete digestion. These samples were digested in pre-cleaned Teflon bomb vessels overnight at 150°C with caps on, in a 3:1:0.5 ratio of concentrated

HNO_3:HCl:HF totalling 2.7 mL for 30-50 mg sample mass. The caps were tightened before undergoing oven digestion at 120°C for 48 hours. Sample solutions were dried down, re-dissolved in 1 mL concentrated HNO_3, placed in an ultrasonic bath for 15 minutes and left on the hotplate at 140°C overnight. This re-dissolution step was repeated with 1 mL concentrated HCl, followed by 2 mL 6 M HCl, and agitated in the ultrasonic bath as necessary in between steps, until the solutions were clear and samples fully dissolved.

2.3. Double spike

2.3.1. Spike preparation

The concentrated spike solution was prepared at the Open University by Ian J Parkinson in 2007 and has been used by both the Oxford and OU groups to maintain consistency. Two enriched ^{84}Sr and ^{87}Sr carbonate single spikes were purchased from Oakridge National Laboratories, weighed and dissolved in concentrated HNO_3 and mixed in roughly a 1:1 ratio to produce an $^{84}Sr/^{87}Sr$ ratio of 0.912. The spike was calibrated by ICP-MS using a gravimetric NBS 987 solution and the Sr isotopic composition of the double spike determined as listed below:

$^{84}Sr/^{87}Sr = 0.912665$

$^{86}Sr/^{87}Sr = 0.0496697$

$^{88}Sr/^{87}Sr = 0.223677$

2.3.2. Aliquots and spike addition

Previous investigations in chemistry related to Sr resulted in the discovery that column induced fractionation can occur during Sr separation (Charlier et al., 2006). These variations were found to be significantly greater than the analytical reproducibility of the method. This requires sample spiking prior to chromatographic separation (Parkinson et al., 2007; Krabbenhöft et al., 2009). Optimal spiking is calculated based on the amount of Sr per sample and spiked accordingly. Two aliquots equivalent to 700-800ng of Sr were taken from each sample solution and to one of these a double spike was added and left to equilibrate at room temperature for 24 hours. These were later dried down, taken up in 0.5mL 2M HNO_3, and left on the hotplate to reflux for several hours prior to column chemistry to ensure total dissolution.

2.4. Chemical separation

2.4.1. Column fabrication and maintenance

Columns were hand made from shrink-wrap Teflon using metal column moulds and a heating-quenching technique. Stainless steel moulds with a reservoir equating to 2 mL were heated with lengths of Teflon tubing around them for 15 minutes in an oven, removed quickly and quenched with cold water and left to cool for several minutes. The columns were carefully removed, rinsed with MQ water and cleaned for several days in 20% HNO_3. Frits, punched out of polypropylene (30μm pore-size) material, were inserted into the columns and left to clean in 20% HNO_3 for several weeks. The columns were thoroughly rinsed in MQ several times before and after use and stored at room temperature in 2-5% HNO_3, replaced monthly.

2.4.2. Resin cleaning

The Sr spec resin (particle size 50-100um) was purchased from Eichrom Technologies Inc and cleaned and calibrated before use. Resin was cleaned in 3 mL batches by eluting the following set of QD acids and water through a large column three times; 200 mL 6 M HCl followed by 200 mL MQ water, and 200 mL 3 M HNO_3 followed by 200 mL MQ water. The clean resin was later stored in a weak HNO_3 slurry at room temperature in low-light conditions as light and heat have been known to affect Sr spec resin.

2.4.3. Column calibrations

Prior to starting chemistry on actual rock samples the clean Sr spec resin was calibrated. The terrestrial basalt (MD57 D10-1) was first used to calibrate the column both with 100uL and 150uL of pre-cleaned Sr spec resin. Continuous 100uL cuts of the column elute, following the procedure outlined in section 2.4.4 were collected and analysed by ICP-MS, firstly, to establish the separation of Sr from the two major contaminants, Ca and Rb, and secondly, to determine which column fraction contained Sr and lastly to determine if 150 or 100ul of resin is optimal for the chemical protocol. Results are shown in Figures 2.1 and 2.2 below, and the elute fractions showed a distinct separation of Sr from Ca and Rb for both volumes of resin. The calibration using 150uL of Sr resin (Figure 2.2) provides a better separation of Sr from the matrix and less tailing during Sr elution compared to the column with 100uL of resin (Figure 2.1), thus 150ul was used during chemistry for optimal separation. New batches of Sr spec resin were calibrated, as well as all batches of cleaned resin in order to routinely check separation and column yields with a stock solution of BHVO-2. Selected results of these calibrations are given in Appendix B.

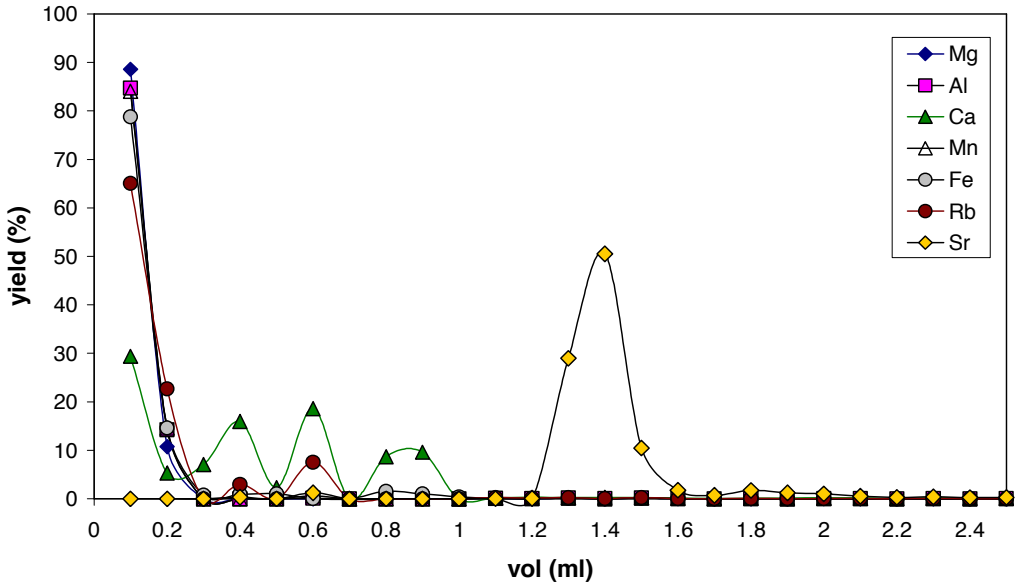

Figure 2.1: Sr calibration using 100µl resin

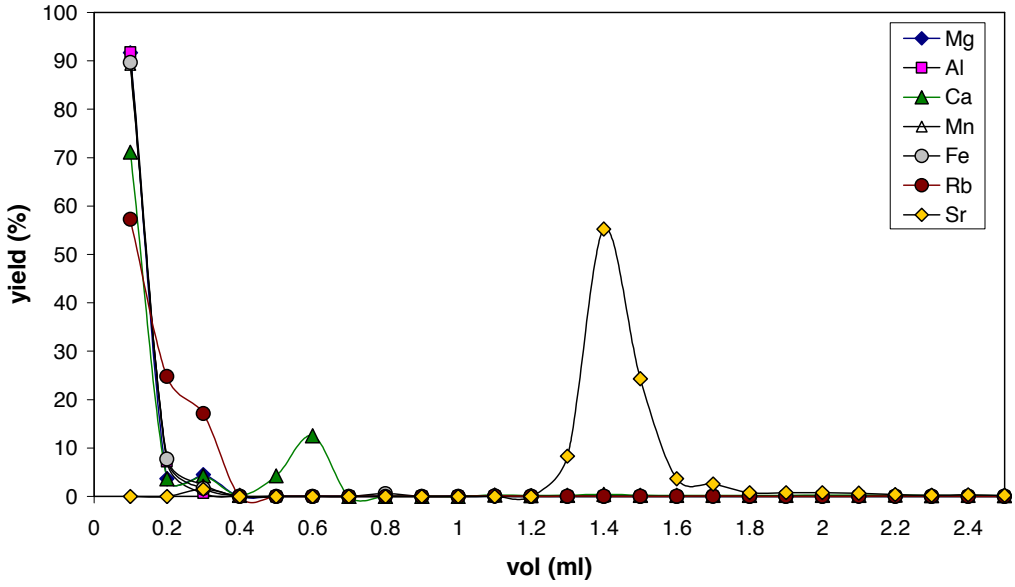

Figure 2.2: Sr calibration using 150µl resin

Column yields were routinely checked throughout for a total number of 10 times, and found to be consistently within the range 77-95%, giving an average yield of 87.5%. Column yields of 100% are not required as the samples are spiked before chemistry, and any fractionation that may occur during column chemistry is corrected for by the double-spike technique. Although this is true for most single elements and at relatively low concentrations, careful chemical separation of Sr from matrix elements is still required for high-precision isotopic ratio determinations.

2.4.4. Chemical separation procedure

The Sr is isolated from matrix elements by passing the sample solution through Sr spec extraction chromatographic resin in columns, and eluting matrix elements with several acids based upon the procedure outlined by Deniel and Pin (2001) with minor modifications, as outlined below.

1. Step 1: Addition of 150µl resin slurry, wash with 200µl MQ
2. Step 2: resin pre-clean with 2 mL 6 M HCl, followed by 2 sets of 2 mL MQ
3. Step 3: resin clean with 1 mL 7 M HNO_3
4. Step 4: Precondition: 1 mL 2 M HNO_3
5. Step 5: Sample load: in two sets of 250 µL 2 M HNO_3
6. Step 6: Wash sample out with 250 µL and 150 µL 2 M HNO_3
7. Step 7: Elute matrix with 1 mL 7 M HNO_3
8. Step 8: Collect Sr in 1.5 mL 0.05 M HNO_3

The eluted Sr fraction is dried down overnight at 90°C ready for TIMS analysis. Eichrom state the maximum capacity of the resin for Sr is approximately 21 mg per 2

mL according to Horwitz et al. (1992). For this reason a maximum a mass of 50mg of total sample was passed through a single column and sample solutions were split accordingly.

2.5. Mass spectrometry

2.5.1. Filament preparation

Strips of high purity (99.98-99.99%) rhenium ribbon were cut with ceramic scissors into lengths of roughly 2cm, attached at right angles to single-filament posts using a "dog", and fixed into place using a spot welder. These filaments were outgassed in a set of either 15 or 30 filaments, at 4 A for 60 minutes in a ThermoFisher Degassing Device, and left to stand for at least 4 hours prior to sample loading.

2.5.2. Filament cleaning

Following analysis, used Re ribbon was removed from the filament posts using tweezers, and stored for recycling. Abrasive cleaning using zinc oxide combined with drops of MQ on a cotton bud removed stains on used extraction plates. All filament posts, side plates, extraction plates and source slits (in the wheel of the TIMS) were then cleaned by boiling in 30% H_2O_2 for 30 minutes followed by 30 minutes boiling in MQ. All components were air dried at 130°C in an oven overnight and left to cool. When not in use, clean components were wrapped in cling film and stored in clean plastic boxes.

2.5.3. TaF_5 activator

Activators are commonly used in TIMS methodology to optimise the ionisation efficiency of the element in question and increase beam intensity during heating by increasing the work function of the filament surface and allowing ionisation at lower temperatures. For Sr, a Ta emitter is used as an activator. A high-purity, low-blank TaF_5 activator solution was prepared at the OU following the procedure detailed by Charlier et al. (2006). In summary, approximately 20g TaF_5 is produced from repeat HF dissolutions of 250mg Ta_2O_5 powder, and $Ta(OH)_5$ crystals precipitated by drop by drop addition of ammonia. High purity crystals were produced by repeated cycles of this, and dissolved in a combination of HF, concentrated H_3PO_4, 3M HNO_3 and MQ H_2O.

2.5.4. Filament and sample loading

Dried down samples of 700-800ng of Sr were loaded onto outgassed single filaments in a clean fume hood in the TIMS laboratory as nitrate salts. A volume of 1µL of concentrated HNO_3 was added to all samples, and left to dissolve. An outgassed filament was then attached to the heating apparatus, heated to ~0.9A, and a piece of Parafilm levelly and carefully melted in two strips at the centre of the filament to leave a 2mm gap. The amp was turned off and 0.8µl of TaF_5 activator and the sample carefully loaded into the 2mm gap using an Eppendorf 10µL pipette. The filament was slowly heated to ~0.7A and the solution left for 5 minutes to dry down. Once dry, the filament was slowly, incrementally, heated until the Parafilm started to smoke (roughly ~1.1A), at which point it was left to smoke out until being heated some more. This was repeated in increments until all the Parafilm had burned off and the filament glowed red, left for 1-2 seconds until it flashed white and quickly turned to 0A.

2.5.5. Wheel loading

Sample filaments were loaded into the detached magazine of the TIMS, twenty-one at a time, inside a laminar-flow cabinet. Side plates and blank plates, to secure the filament, were clipped on and the magazine transferred back into the turret of the TIMS. A clean extraction plate was exchanged for the used one after every magazine, particularly between spiked and non-spiked runs. The wheel was rotated using the software to check for snags and ensure full rotation, the door closed and sealed and the pumps switched on to create a vacuum in the ion source. After a reasonable pressure had been reached (HV=10^{-4} mbar and FV=10^{-1}mbar), the sample wheel was calibrated to ensure contact at all filament posts, and the machine left to pump down overnight to the optimal pressure values of; Fore Vacuum Press= $2x10^{-2}$ mbar, High Voltage Source Press= $2x10^{-7}$ mbar or lower and Ion Getter Press= $5x10^{-9}$ mbar or lower.

2.5.6. Sample runs

2.5.6.1. Method set-up

All measurements were made in positive ion mode. Although the exact positioning of cups used in the cup configuration differed between the two TIMS, the same masses and order of masses collected on cups remained the same. Six cups were used to collect ^{84}Sr, ^{85}Rb, ^{86}Sr, ^{87}Sr, ^{88}Sr and a dummy mass. This dummy mass, and the amplifiers routine rotation in one direction after each block (to the right) minimised any signal decay signature being passed on from ^{88}Sr, as it is the most abundant isotope. The interference of ^{87}Rb on ^{87}Sr is corrected for, either online or offline, by measuring ^{85}Rb and assuming a constant natural ratio of $^{87}Rb/^{85}Rb$ = 0.385041. Gain calibrations were performed daily, before measurements, to monitor the amplifiers in the long term and ensure no “sparks”, otherwise gains were re-run. A peak centre was run at the start of

every measurement, and a baseline run every block. All these parameters were consistent for both methods used at the OU and Durham. However, the methods set up for the actual measurement of Sr isotopes differed between the institutions, partly due to the preferences of the group responsible for maintaining the TIMS and partly due development of a more efficient method later during the data collection.

At the OU, longer measurement times of ~4 hours per single analysis were used for beams voltages of ~8V by measuring a total of 540 ratios in 54 blocks of 10 cycles per block. At Durham, an alternative method was devised of shorter measurement times with higher beam voltages in which a total of 200 ratios were measured in 10 blocks of 20 cycles per block. For both methods, an idle time of 3 seconds in between measurements was set, with an integration time of 16.777s and a baseline run every block. Both methods are equivalent in terms of counting statistics and internal precision on a single measurement. However, the higher beam voltages in the second method allowed for shorter measurement times and a faster rate of sample analysis in one session, translating to a higher number of samples.

2.5.6.2. Heating the filament

Filaments were heated by increasing the current through the filaments at a slow, steady rate over 45 minutes to an hour to ensure Rb burn-off, and optimise beam intensity and stability, following the procedure outlined below (whilst the analyser gate is shut):

1. Heat filament from 0-1500mA at 500mAmin^{-1}.
2. Heat filament from 1500-1800mA at 100Amin^{-1}.
3. Heat filament from 1800-2400mA at 50Amin^{-1}.

4. Open analyser gate, tune (A), heat filament from 2400-2500mA at 50Amin^{-1}.
5. Tune (B), heat filament 2500-2600mA at 50Amin^{-1}.
6. Samples were then heated up in 50-100mA increments at 50Amin^{-1} and tuned (B) in between until reaching either ~8V (OU) or ~18-20V (Durham).
7. Method set, analysis started.

Tune A: Extraction Left, Extraction Right, fine wheel tune, Z- focus, Extraction Left, Extraction Right, Condenser, X-Symmetry and Z-focus lenses.
Tune B: fine wheel tune, Z- focus, Extraction Left, Extraction Right, Condenser, X-Symmetry and Z-focus lenses.

In Durham, higher voltages were needed for measurement requiring that the filaments were heated to higher temperatures than at the OU (up to 2900mA compared to 2700-2800mA at the OU- never exceeding 1460°C, although Durham lacked a pyrometer).

2.5.6.3. Deconvolution calculations

Both a spiked and un-spiked sample is measured. The interference of ^{87}Rb on ^{87}Sr is corrected for offline, using a ratio of ^{87}Rb/^{85}Rb = 0.385041. As explained in section 2.1 the un-spiked measurement is used to monitor and correct for radiogenic in-growth in the double spike method. The two runs are deconvolved with any fractionation induced by the column added to the instrumental mass fractionation and the double-spike equations are solved in ^{87}Sr denominator space. Exponential mass fractionation deconvolution equations are used, outlined by Albarede and Beard (2004), which involve an iterative solution using a Newton-Raphson technique. This deconvolution yields the true isotope composition of the three Sr isotope ratios (^{84}Sr/^{86}Sr, ^{87}Sr/^{86}Sr and

$^{88}Sr/^{86}Sr$). Uncertainties on the three Sr isotope ratios are calculated by use of a Monte Carlo simulation that incorporates the uncertainties from both the un-spiked and spiked analyses.

2.6. Reproducibility

2.6.1. Manufactured Sr standard NBS 987

As two different TIMS machines were used, it was important to monitor any differences between the two by repeat measurements of an internationally accepted and used standard; NBS 987 (sometimes known as NIST 987 and SRM 987) as distributed by the National Bureau of Standards (currently the National Institute of Standards and Technology). To achieve this, NBS 987 was analysed several times during each measurement session by both instruments to give a long-term external precisions. All measurements of NBS-987 were of a single stock solution used at both universities to maintain consistency, and these were unprocessed through chemistry. The results are shown in Figure 2.3 and 2.4 for the Open University and Durham respectively, along with their long-term averages. Measurements were made at the OU from April 2010 to May 2012 over four analytical sessions, and at Durham from Jan 2012 to December 2013 over two sessions.

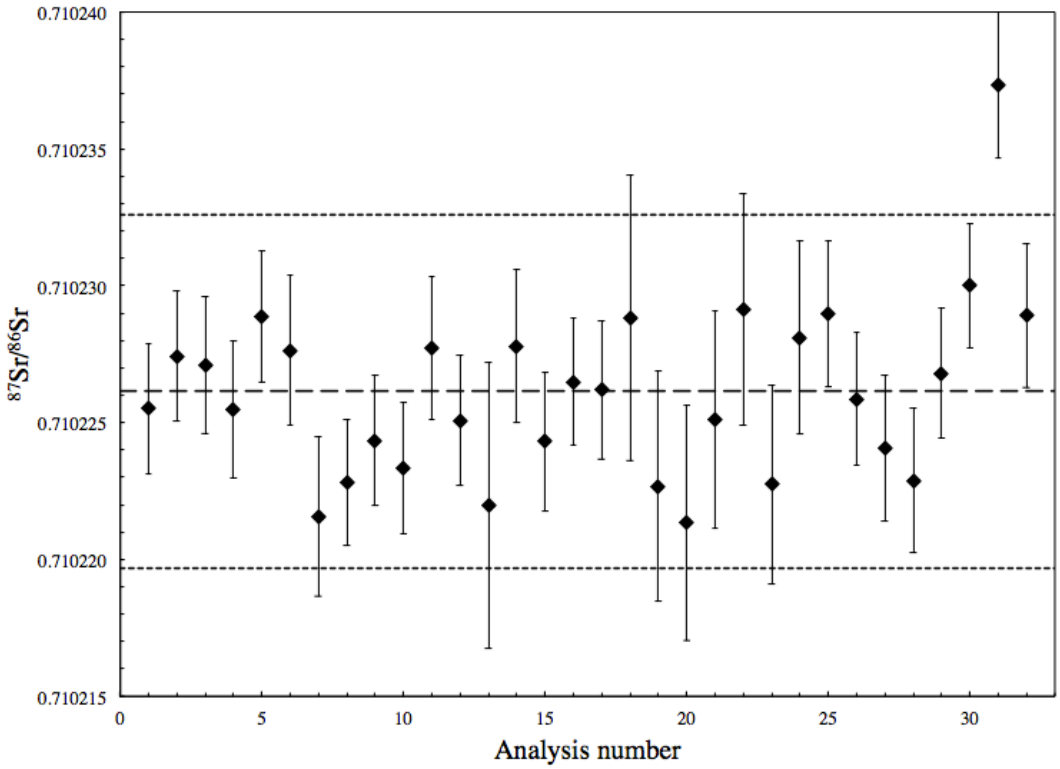

Figure 2.3: Plot of $^{87}Sr/^{86}Sr$ data for NBS-987 from The Open University (2011-2012). The dashed line represents the long-term average with 2 SD uncertainty, which equates to a reproducibility of ±9.1 ppm.

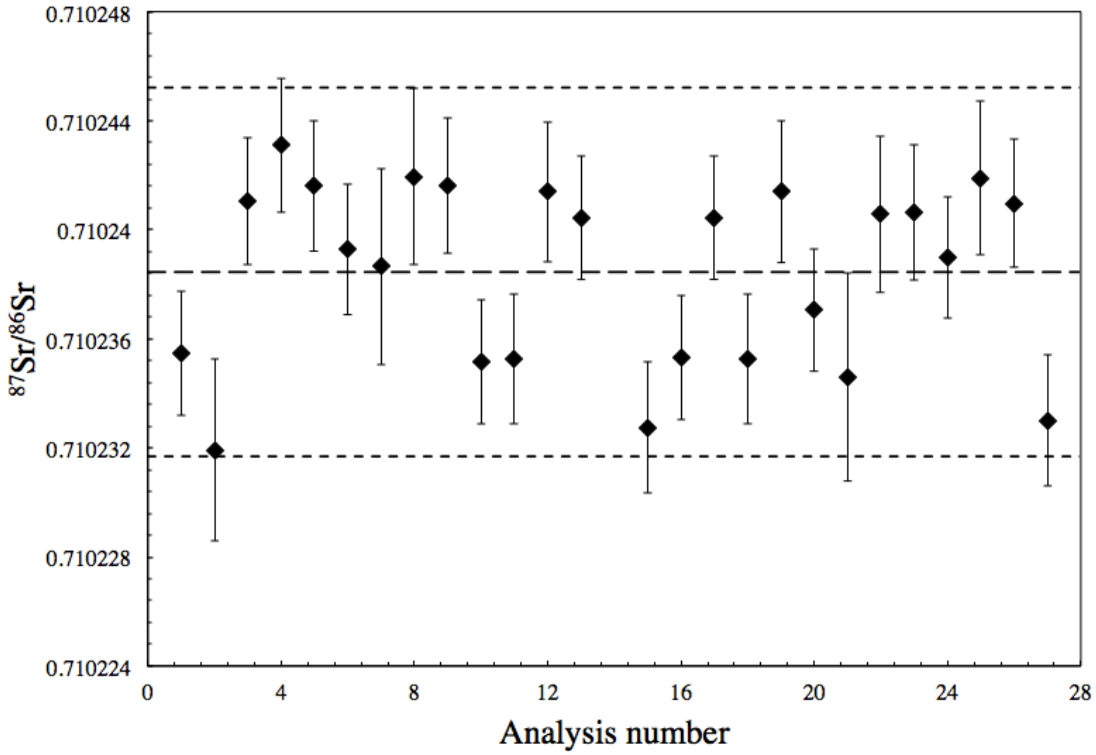

Figure 2.4: Plot of $^{87}Sr/^{86}Sr$ data for NBS-987 from Durham University (2012-2013). The dashed line represents the long-term average with 2 SD uncertainty, which equates to a reproducibility of ±9.5 ppm.

The internal precision on a single measurement of NBS 987 was usually less than ±4 ppm and always better than the external precision. The internal precision is that of a single measurement whilst the external is given by multiple analyses of NBS 987. The average value of NBS 987 measurements at the OU (Fig. 2.3) is $^{87}Sr/^{86}Sr$= 0.7102261 ± 0.0000065 (2SD; n=32) which equates to an external reproducibility of ±9.1 ppm for $^{87}Sr/^{86}Sr$. The long-term average at Durham (Fig. 2.4) is $^{87}Sr/^{86}Sr$= 0.7102385 ± 0.0000068 (2SD; n=26) which equates to an external reproducibility of ±9.5 ppm.

2.6.2. Rock standards

To further test the external reproducibility and ensure sure that no isotopic fractionation is created during the dissolution, independent dissolutions and measurements of BHVO-1 were duplicated on both TIMS instruments and are shown in Figure 2.5. These are indistinguishable within error and result in an average of $\delta^{88}Sr$ = 0.268 ± 0.009‰ (2 SD; n=4), which equates to an external precision of ±9.5 ppm.

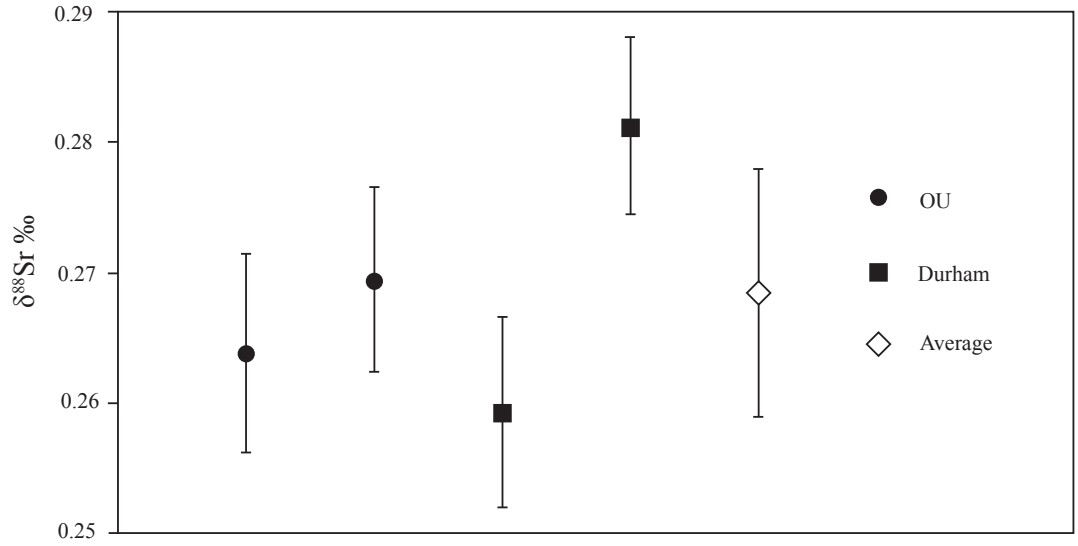

Figure 2.5: Duplicate measurements of BHVO-1 at the OU and Durham are replicated in $\delta^{88}Sr$ within error (after normalisation of OU data to Durham). The BHVO-1 average is also shown to 2 SD.

2.6.3. Internal normalisation

The long-term $^{87}Sr/^{86}Sr$ average of NBS 987 at Durham is near identical to the commonly accepted value of $^{87}Sr/^{86}Sr$= 0.71024, whereas that of the OU is less radiogenic. For this reason, all $^{87}Sr/^{86}Sr$ data (and thereby $\delta^{88}Sr$ data) were normalised to the accepted value of 0.71024. All NBS 987 measurements and both instrument averages lay within the commonly accepted NBS values today of 0.71024.

A comparison of $^{87}Sr/^{86}Sr$ data for repeated measurements of BHVO-1 and the average of these (to 2SD) is shown along with selected average values from literature (2SD) in Fig 2.6. The $^{87}Sr/^{86}Sr$ data for BHVO-1 compare well with selected values from literature.

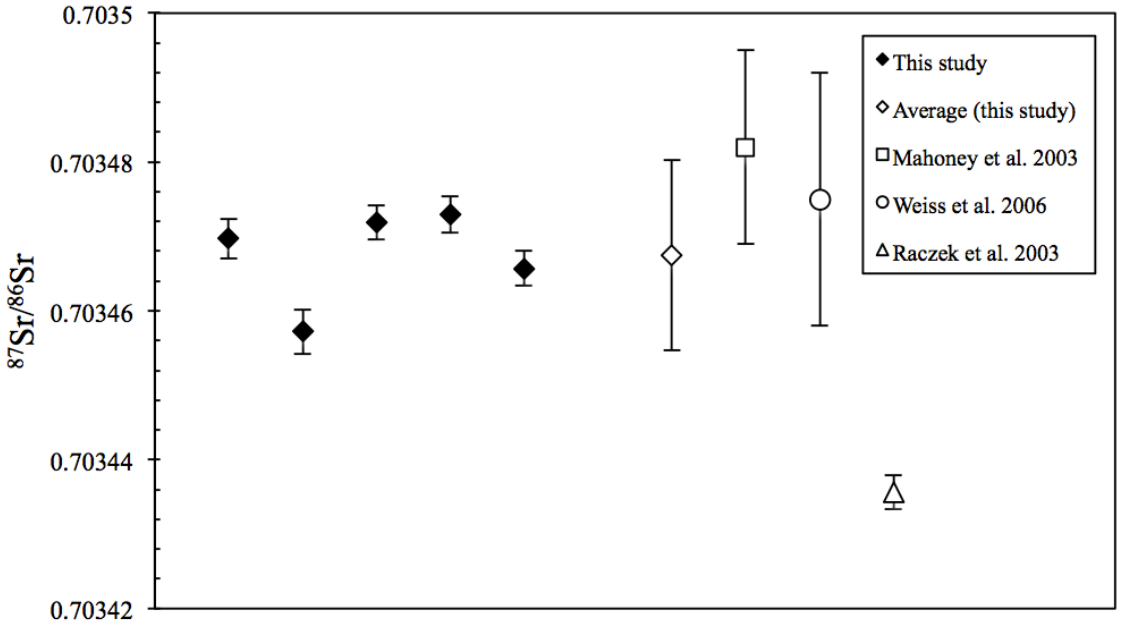

Figure 2.6: A comparison of $^{87}Sr/^{86}Sr$ data for BHVO-1 from this study with from selected representative average values from literature (Mahoney et al., 2003; Weiss et al., 2006; Raczek et al., 2003). Averages are given to 2SD.

2.7. Blanks

Total procedural blanks (TPBs) were routinely measured for every set of sample dissolutions through chemistry, and for each type of digestion procedure. These include the column blank and the loading blank. When varying volumes of aliquots were taken for column chemistry, the maximum volume was taken for the blank. Approximately 0.1g of a single spike highly enriched in ^{84}Sr (0.99%) was accurately weighed several times and added to the total procedural blank aliquot and left to equilibrate for 24 hours at room temperature. This was dried down and re-dissolved in 1 mL 2 M HNO_3, weighed accurately, and processed through Sr separation chemistry. Four TPBs (total procedural blanks) were analysed by the SEM by TIMS to include the loading blank, and were found to never be greater than 76pg. For a measurement load of 800ng this is equivalent to a maximum blank contribution of less than 0.0095% of the total measured Sr. Blanks for every other set of columns and dissolutions were measured by ICP-MS (Element, ThermoFisher) and were never detectable over the background limit (LOD, limit of detection), signifying they were less than 63.83pg minus the loading blank. Overall, total procedural blanks were routinely less than 76pg and considered negligible in comparison to the >700ng of Sr used for sample analysis.

CHAPTER THREE

Stable and radiogenic Sr isotope variations in oceanic basalts

Abstract

Radiogenic Sr ($^{87}Sr/^{86}Sr$) is a widely used tracer of mantle chemistry, which when paired with stable Sr ($^{88}Sr/^{86}Sr$) offers a unique opportunity to trace both melt sources and melting and differentiation processes. This study presents high precision DS-TIMS $^{87}Sr/^{86}Sr$ and $^{88}Sr/^{86}Sr$ data for a geographically widespread suite of young MORBs and OIBs, including MORBs from the FAMOUS ridge section of the Mid-Atlantic Ridge. Resolvable variations in $\delta^{88}Sr$ of ~0.14‰ are found for MORB, and within the FAMOUS segment. These range from $\delta^{88}Sr$ = +0.312 ± 0.007 to +0.176 ± 0.010‰. In contrast, OIB possess a relatively restricted range of compositions from $\delta^{88}Sr$ = +0.224 ± 0.008 to + 0.280 ± 0.008‰. Variations in $^{87}Sr/^{86}Sr$, as well as $\delta^{88}Sr$, are found for the FAMOUS MORB from 0.702868 (±3) to 0.703503 (±3), which are not correlated with indices of seawater contamination. Plagioclase mineral data for two FAMOUS samples are heavier in $\delta^{88}Sr$ than the complementary glasses, suggesting that plagioclase crystallisation can cause variations in $\delta^{88}Sr$ by the preferential incorporation of the heavier isotopes of Sr into this phase. The variations in $\delta^{88}Sr$ compositions of MORB are most likely due to a combination of plagioclase crystallisation and inherited source heterogeneity. The relatively restricted compositions of OIB, and preliminary analyses of marine sediment and continental basalts, suggest that subduction and recycling have little effect on the $\delta^{88}Sr$ value of mantle melts, or, that these processes reduce the magnitude of any variations that may be present in the recycled material.

3.1. Introduction

An essential step in the application of a new isotope system, stable or radiogenic, is to understand the fundamental processes that control its behaviour in the silicate Earth. One approach is to examine material from the principal silicate reservoirs on Earth - the mantle and the continental crust. Ultramafic peridotites exposed at Earth's surface or carried as xenoliths in volcanic rocks can be used to characterise the composition of the upper mantle. However, problems can arise as not all ultramafic rocks are considered representative of the mantle, since they may not represent equilibrium residues of melting. In addition, secondary processes such as metamorphism or metasomatism can affect such rocks during their passage to the surface. This is particularly important when investigating relatively small variations in the radiogenic and stable isotopes of an element as mobile as Sr. To circumvent such potential problems, mantle-derived magmas are also used, as, in principle, their composition should reflect that of their mantle source. In this way, the chemical variations preserved by volcanic rocks at mid-ocean ridges and ocean islands can provide insights into the compositional variations preserved in the upper mantle.

The radiogenic isotopes of Sr, Nd and Pb are arguably the most widely used tools to determine and define mantle heterogeneity and significant variations in both elemental and radiogenic isotope compositions in all major ocean basins indicate that the upper mantle has not been effectively mixed (Hofmann, 2003). Variations in the $^{87}Sr/^{86}Sr$, $^{143}Nd/^{144}Nd$ $^{206}Pb/^{204}Pb$, $^{207}Pb/^{204}Pb$, and $^{208}Pb/^{204}Pb$ compositions of oceanic basalts are attributed to the mixing of several mantle components which are also defined by these same parameters, illustrated in Figure 3.1 (Hofmann, 2003; White 1985). These end-members are defined are discussed in Chapter 1. Although there is some overlap, basalts

formed at spreading centres (MORB) due to relatively large degrees of melting (10-20%), and intra-plate basalts formed by lower degrees of melting (<10%) and found at oceanic islands (OIB), possess different isotopic compositions, and are thought to sample distinct reservoirs. The former are thought to sample the relatively trace element depleted mantle (DMM) in the spinel stability field (Turner et al., 2000), characterised by incompatible trace element depletion that resulted from the formation of the continental crust (Hofmann, 1988; Sun and McDonough, 1989). The OIB sample both this depleted reservoir and varying extents and combinations of the four enriched components, most likely in the garnet stability field possibly as the result of upwelling mantle plumes. Traditionally, OIBs are viewed as being sourced from primitive, less depleted, or enriched parts of the mantle than MORB sources (e.g. Wasserburg and DePaolo, 1979). As a consequence of a number of processes, OIBs show larger compositional variation both chemically and isotopically than MORBs (Hofmann, 2003). These processes include variable extents of mantle depletion by prior partial melting, mantle metasomatism through the infiltration of silicate melts or fluids, and recycling of lithospheric material into the mantle. For example, the upper mantle is thought to be depleted in incompatible elements relative to the lower mantle due to continuous melt extraction, as well as the entrainment of recycled material into the lower mantle. For this reason, MORB and OIB are often studied in parallel to reveal information on all mantle components, their mixing, and resulting mantle heterogeneity.

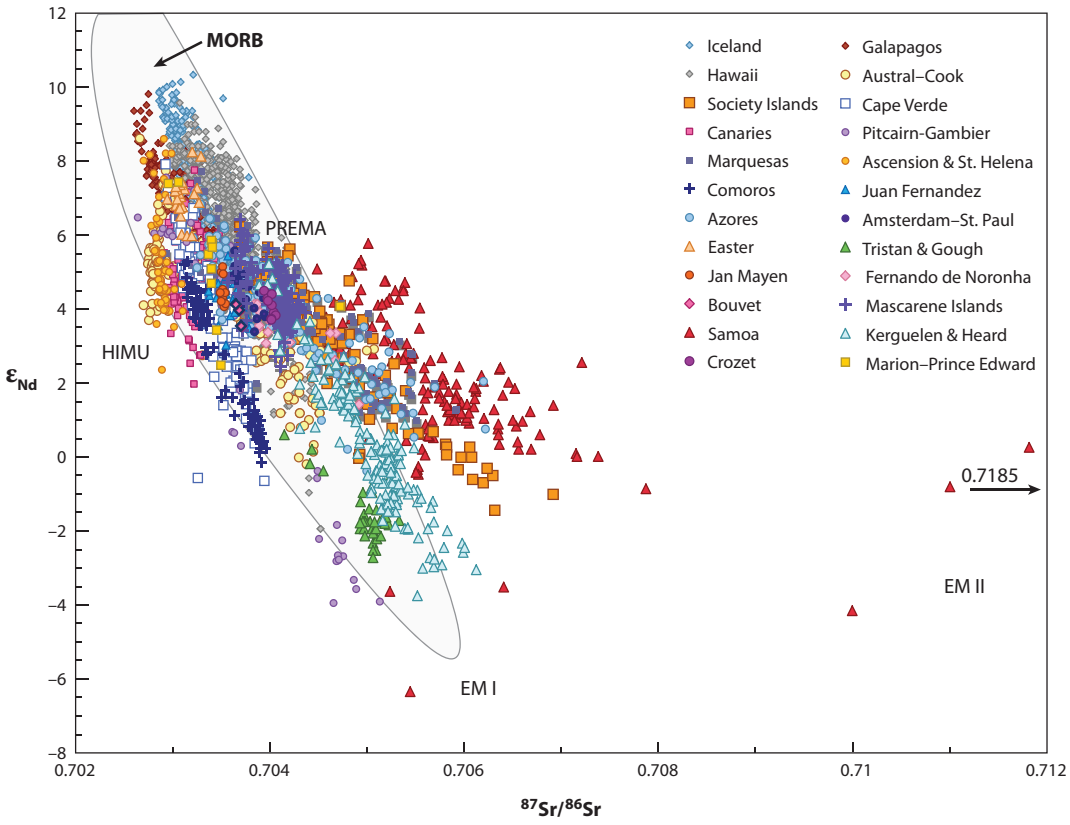

Figure 3.1: $^{87}Sr/^{86}Sr$ versus ε(Nd) for OIB and MORB from the GEOROC database, from White (2010).

Stable isotope variations in magmatic rocks can arise from mass dependent processes including partial melting, diffusional exchange or fractional crystallisation. For example, Teng et al. (2013) attribute differences in the stable Fe isotope composition of mantle rocks and OIB to fractionation during partial melting of the mantle. The stable isotopes of Si, Fe and Sr have all been shown to fractionate during magmatic differentiation (Savage et al., 2011; Schuessler et al., 2009; Charlier et al., 2012), and diffusion can cause stable isotope fractionation both in nature and experiments (Richter et al., 2009a,b; Huang et al., 2010; Lundstrom et al., 2005; Teng et al., 2006; Parkinson et al., 2007). However, to date there is little precise data for the stable $^{88}Sr/^{86}Sr$ composition of mantle melts. Aside from geostandards, only two MORB from the Indian ridge (MD57) and one from the Atlantic have been analysed for their $^{88}Sr/^{86}Sr$ compositions, and variations cannot be detected at the ~30ppm precision of this earlier

MC-ICP-MS study (Charlier et al., 2012). This work presents high precision DS-TIMS $^{88}Sr/^{86}Sr$ data for an extensive suite of whole rock MORBs and OIBs and several mineral separates to investigate the composition of the mantle, any heterogeneity that may exist, and processes such as fractional crystallisation, partial melting, and recycling. Trace element and $^{87}Sr/^{86}Sr$ data were obtained for the same basalts to complement this data and add further to understanding their petrogenesis. Radiogenic isotopes can reveal information regarding mantle sources and stable isotopes on mass dependent processes, so taken together, $^{88}Sr/^{86}Sr$ and $^{87}Sr/^{86}Sr$ data are used to unravel source variations from the effects of melting and magmatic processes. The effect of recycling material into the mantle is investigated by analyses of crustal material and marine sediment. Marine sediments play a pivotal role in crust-mantle recycling as they comprise a significant fraction of the material subducted, but whilst much of the crustal low temperature environment is well characterised for stable Sr isotopes (Fietzke and Eisenhauer, 2006; De Souza et al., 2007; Ohno and Hirata, 2007; Halicz et al., 2008; Ruggeberg et al., 2008; Krabbenhoft et al., 2010; Ohno et al., 2008; De Souza et al., 2010), there is a lack of stable Sr data reported for marine sediments such as shale. As such, $^{88}Sr/^{86}Sr$ data for shale and other crustal components can provide insights into the $^{88}Sr/^{86}Sr$ composition of inputs into the mantle and the effects of recycling this material.

This study aims to address key questions including: 1) whether variations in $^{88}Sr/^{86}Sr$ exist due to mass dependent processes and if they do, the potential processes responsible for their development, 2) if there are differences between OIB and MORB and for what reasons, 3) the extent to which coupled $^{87}Sr/^{86}Sr$ and $^{88}Sr/^{86}Sr$ data can be used to disentangle source heterogeneity from variations due to the effects of partial melting and magmatic processes, and 4) whether an estimate of the expected inputs of recycling into mantle match up with that of the BSE.

3.2. Geological background of samples

Oceanic basalts were selected from a geographically diverse range of sites, both spreading ridges and intra-plate settings, so as to sample a number of mantle components and thus mantle heterogeneities at a global scale. A detailed analysis of MORB from the FAMOUS section of the Mid-Atlantic Ridge, thought to retain the signatures of mantle heterogeneities and magmatic processes, allowed an investigation into these processes on a small scale. Sample localities are shown in Figure 3.2. All MORB analysed here are quenched aphyric submarine glasses. Most of the OIBs are subaerial though a few submarine glasses were also analysed. The MgO contents of the MORB glasses are lower than those in primary MORB (<9% versus 10-15%).

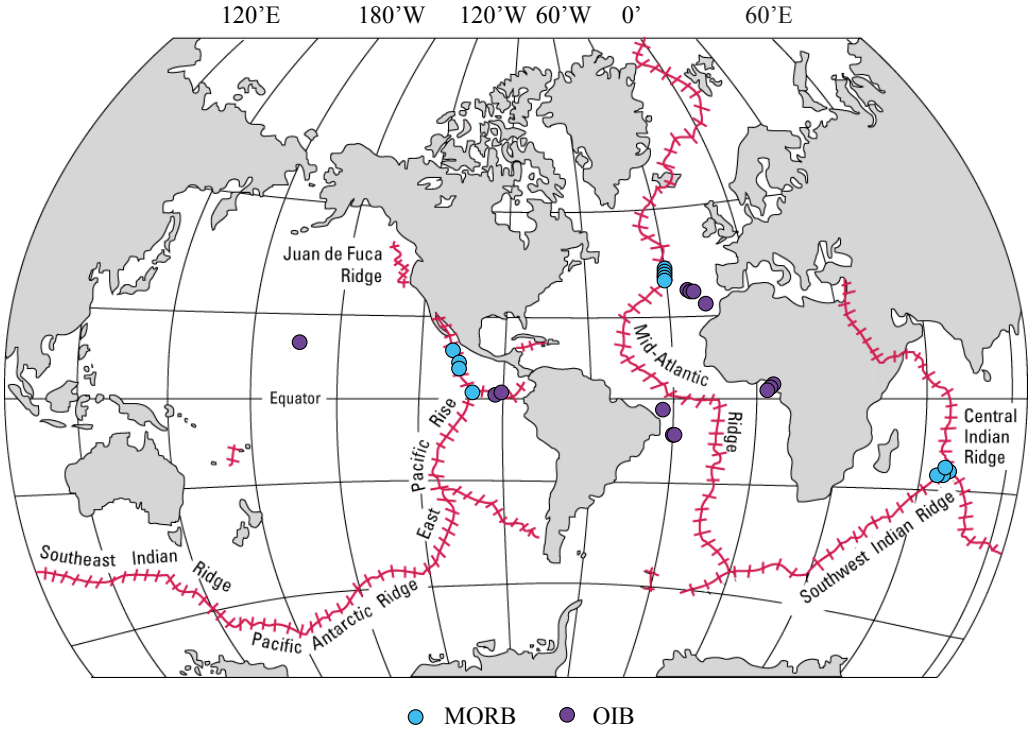

Figure 3.2: Map showing global localities of MORB and OIB samples. Map from USGS.

3.2.1. MORB

To assess the variability of stable Sr on a global scale, glasses from the ridges of several of the major oceans, the Indian Ocean, the Pacific Ocean, and Atlantic Ocean, were analysed. These basalts were dredged or collected by submersible in the axial rift valley, and as such are relatively young "zero age" and optically pure glasses. The three ridges span a range of spreading rates, to enable an investigation into any effect this may have on the stable Sr isotope composition. The FAMOUS segment has slow spreading rates of ~2cm/year, the Indian Ridge faster rates of 2-3 cm/year and the East Pacific Rise (EPR) the fastest rates of up to 13 cm/year. Basalts from these three ridges sample the depleted mantle, and are briefly described below.

3.2.1.1. Indian Ocean MORB and the DUPAL anomaly

The isotope compositions of mid-ocean-ridge basalts (MORB) from the Indian Ocean have led to the identification of a large-scale isotope anomaly relative to Pacific and Atlantic Ocean MORB (Dupré and Allègre, 1983), characterised by low $^{206}Pb/^{204}Pb$, $^{143}Nd/^{144}Nd$ and high $^{207}Pb/^{204}Pb$, $^{208}Pb/^{204}Pb$ and $^{87}Sr/^{86}Sr$ ratios. Such isotope signatures, termed DUPAL by Hart (1984), are thought to indicate the presence of a mantle source that has experienced a long-term evolution with high Th/U and Rb/Sr ratios and low U/Pb and Sm/Nd ratios relative to those of the Atlantic and Pacific mantle. The distinctive signature of the DUPAL anomaly has been attributed to the presence of recycled continental lithosphere, old subcontinental lithosphere, or sediments associated with oceanic crust (e.g. Hamelin and Allègre, 1985; Hamelin et al., 1985; Michard et al., 1986, Price et al., 1986; Dosso et al., 1988; Mahoney et al.,

1989; Mahoney et al., 1992; Rehkämper and Hofmann, 1997). To investigate any effect of this DUPAL signature on the stable Sr composition, four basalts from the region were analysed, all of which have been analysed previously for their Sr-Nd-Pb compositions, and two solely for their Re-Os and $\delta^{11}B$ compositions (Escrig et al., 2004; Schiano et al., 1997; Gannoun et al., 2007). Three of the glasses, denoted MD57, were collected on the Central Indian Ridge during the 1988 cruise MD57, and the remaining are from the Southwest Indian Ridge sampled on the MD 23 cruise (Schiano et al., 1997).

3.2.1.2. Pacific

Four basalts from the fast-spreading EPR were studied, two of which were previously analysed for their Sr-Nd-Pb, Re-Os, and $\delta^{11}B$ compositions, another for its Sr-Nd composition, and the last its Re-Os, and $\delta^{11}B$ composition (Gannoun et al., 2007). DR7-1 and Searise 2 DR07 were collected from the northern axis on the Clipperton cruise, 1981, and the 1980 Searise 2 cruise respectively, SO12 206-1 on the SO012 cruise, 1980, from the Hess Deep along the Cocos-Nazca triple junction, and lastly CY82 18-01 from the CYATHERM (1982) cruise along the axial graben.

3.2.1.3. Mid-Atlantic Ridge (FAMOUS segment)

In many cases mantle heterogeneity appears to occur on a small scale, and the petrogenesis of such magmas cannot be investigated using only regional scale sampling of just a few samples per ridge. For this reason, 10 basalts were selected from the

FAMOUS (French American Mid-Ocean Undersea Study) ridge segment to explore the magnitude of stable Sr isotope variation at a small spatial scale along a single segment (45 km long), and the extent to which mantle heterogeneity, partial melting, and crustal processes play a part in dictating these lava compositions. The FAMOUS ridge segment of the Mid-Atlantic Ridge, which lies south of the Azores platform at 36.5°N, provides an opportunity to study chemical variations of, and the processes affecting, oceanic ridge basalts at the segment scale.

Basalts from the FAMOUS region show a significant range in trace element concentrations (Langmuir et al., 1977), which correspond to a wide range of radiogenic isotope compositions (Laubier et al., 2012; Gale et al., 2013). On the basis of early isotope data, in particular the uniform radiogenic Sr isotope compositions (White and Schilling, 1978), it was presumed that these melts result from magma chamber processes or dynamic melting of a homogeneous mantle source and all trace element variations were produced by melting processes (e.g. Langmuir et al., 1977; White and Bryan, 1977). More recently, largely on the basis of high precision Sr-Nd-Pb data for a greater number of samples, it is apparent that these variations correspond to both variations in mantle composition and magmatic processes (Gale et al., 2013, Laubier et al., 2012). Although resolvable variations in $^{87}Sr/^{86}Sr$ are evident, these authors exclude the Sr data from the discussion and base their conclusions solely on Nd and Pb data. This was justified on the basis that Nd and Pb show a strong correlation, but little co-variation with Sr. The Re-Os and Cl data for the same samples have been taken to indicate contamination by seawater, and a comparison between these and high precision $^{87}Sr/^{86}Sr$ data may allow a definitive answer as to whether these samples have experienced seawater contamination.

Gale et al. (2013) consider the FAMOUS lavas to be isotopically intermediate between the depleted mantle and the signature of the Azores islands and based on a narrow Pb-Pb linear trend the samples form, the authors suggest the source of isotopic enrichment is related to the Azores plume, which has undergone extensive metasomatism. In contrast, recent high precision unpublished Pb data (Burton et al., in prep) suggest there is a minimal involvement, if any, of the Azores plume, at least for the samples analysed here. A comparison of new high precision Sr with Pb data, and correlations between the two, could be used to evaluate the involvement of the Azores plume, and the reasons for these variations in the mantle. Finally, Laubier et al., (2012) attribute positive elemental Sr anomalies found in mineral inclusions from FAMOUS MORB to the assimilation of plagioclase-rich cumulates (troctolite) in the crust, the presence of which would be confirmed by the existence of correlation between stable Sr and the Eu anomaly of the FAMOUS basalts.

3.2.2. OIB

As with the MORB, the OIB samples were chosen for their geographic diversity, in order to sample multiple mantle components and any effects of recycling. Most OIB and MORB data possess a limited range of compositions defined by the four end-members in $^{87}Sr/^{86}Sr$-$^{143}Nd/^{144}Nd$-$^{206}Pb/^{204}Pb$ space (Hart et al., 1992). Ocean island basalts that sample mantle domains with different geochemical and isotopic compositions dominate the magmatism of oceanic island groups. The radiogenic isotope compositions of these form linear arrays that have been interpreted as binary mixing between mantle reservoirs. In brief, basalts sampled in this study from the Galapagos, Iceland, and Hawaii are predominantly tholeiitic and sample the DMM (although

samples from the Galapagos are thought to be pre-dominantly FOZO; Harpp and White, 2001; Geist et al., 1988; White et al., 1993), whilst those of the Azores islands selected are thought to possess an EM1 composition, and those of the Cameroon Line and Madeira have HIMU signatures (Halliday et al., 1988; Halliday et al., 1990; Lee et al., 1994; Mata et al., 1998). Basalts from Trindade and Fernando de Noronha are also analysed, which have a combination of DMM and EM1 signatures (Marques et al., 1999; Siebel et al., 2000; Gerlach et al., 1987; Lopes, 1997). Most of these basalts are taken from oceanic islands in the Atlantic, as this is far removed from the DUPAL anomaly and any recent subduction zones that might affect their isotope composition, but some islands from the Pacific Ocean were also sampled. These basalts are fresh, relatively young (less than 3.5 Myr). Aside from those from Fernando de Noronha, Loihi, and Bioko (Cameroon), the Sr-Nd-Pb isotopic compositions of the basalts have been measured previously (Halliday et al., 1992; Halliday et al., 1990; Halliday et al., 1988; Harpp and White, 2001) and are illustrated in Figure 3.3 along with MORB compositions and representative mantle source end-members. The lithologies of these lavas are given in Table 3.1; most are alkali basalts with the exception of a tholeiite from Galapagos, two basanites from Madeira and Principe (Cameroon), and a nephelinite from Trindade.

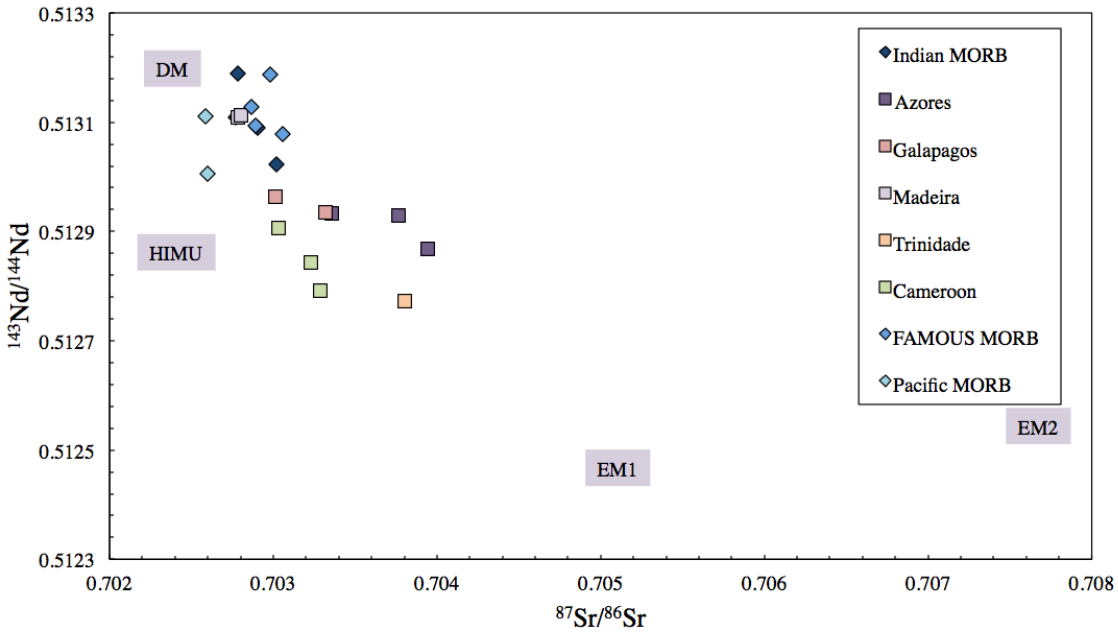

Figure 3.3: Previously published Sr-Nd data for the OIB and MORB in this study. Most of the FAMOUS basalts are missing, as are FDN25, D5-1, and SO12 206-1. Symbols are larger than error bars. Data from Escrig et al. (2004), Schiano et al. (1997), Dupre et al. (1981), Gale et al. (2013), White (1979), Yu and Schilling (1997), Gannoun et al. (2007), Prinzhofer et al. (1989), Halliday et al. (1992), Halliday et al. (1990), Halliday et al. (1988), and Harpp and White (2001).

3.2.3. Mineral separates

Plagioclase mineral separates from two FAMOUS MORB samples, 522-1-1 and ARP 74 11-18, were analysed to investigate the effects of plagioclase growth and fractional crystallisation on the $^{88}Sr/^{86}Sr$ composition of oceanic basalts. These sub-mm crystals were picked under an optical microscope for their purity, leached, and analysed by MC-ICP-MS in Durham University.

3.2.4. Shale and continental basalt samples

Two USGS shale standards and two continental basalts were analysed to investigate recycling. SGR-1b is a hydrocarbon and carbonate rich shale from the Eocene Green River Formation, Colorado and SCo-1 is an Upper Cretaceous silty marine shale from the Cody Shale, Wyoming. The location and lithology of each sample is given in Table 3.2. Carbonate fractions were removed from these, to eliminate any effect this may have on the composition of shale. The silty marine shale (SCo-1) was analysed both as a whole rock, as well as with carbonate removed. Both continental basalts are from the USA: a Pleistocene basalt from Kilbourne Hole, situated in the Potrillo Volcanic Field (PVF) on the axis of the Rio Grande Rift (Harvey et al., 2012), and the continental flood basalt USGS standard BCR-2 from Portland, Oregon.

3.3. Analytical technique

Each MORB glass sample was handpicked under a microscope to exclude any alteration products and cleaned ultrasonically by rinsing in ethanol and distilled water. Following handpicking and cleaning, all samples were powdered and digested following the methods outlined in Chapter 2. Also outlined in this chapter are further details regarding Sr chemistry and TIMS analysis. All TIMS analyses were performed at the University of Durham. Trace elements and REE concentrations of the OIB and MORB were measured by ICP-MS (Element 2, ThermoFisher Instruments) at the University of Oxford and are given in Appendix C. Rock standards BHVO-1, BHVO-2 and BCR-2 were run with every analysis along with in-house elemental standards, and the standard addition technique was used.

3.4. Results

The $\delta^{88}Sr$ and $^{87}Sr/^{86}Sr$ data for MORB and OIB are given in Tables 3.1 and 3.2, along with sample localities, co-ordinates, and spreading rates, MgO wt%, SiO_2 wt%, Eu/Eu*and Rb/Sr ratios. All major element data for the samples are from the references listed in Figure 3.3. Mineral data for the two MORB plagioclase separates are given in Table 3.1. The $\delta^{88}Sr$ and $^{87}Sr/^{86}Sr$ data for the shale and continental basalt samples are given in Table 3.3. Trace element and REE concentration data for the OIB and MORB are given in Appendix C.

Mid-Ocean Ridge Basalts

Sample name	**Location**	**Co-ordinates**	**Spreading rate**	**Eu/Eu*$_{PM}$**	**$^{87}Sr/^{86}Sr$ ± 2se**	**$\delta^{88}Sr$ ± 2se (‰)**
MD57 D9-1	Central Indian Ridge	8°01'S 68°07'E		1.17	0.702753 ± 0.000003	0.273 ± 0.008
MD57 D10-1	Central Indian Ridge	6°22'S 68°25'E	3.09	0.92	0.703105 ± 0.000003	0.252 ± 0.008
MD57 D13-7	Central Indian Ridge	1°48'S 67°65'E	2.69	0.89	0.702937 ± 0.000003	0.277 ± 0.007
MD23 Site 4	SW Indian Ridge	25°864'S 70°323'E	4.40	1.06	0.702814 ± 0.000003	0.290 ± 0.007
					Indian Average	0.273 ± 0.016
SO12 206-1	East Pacific Rise	2°182'N 100°672'W	12.87	0.95	0.702468 ± 0.000002	0.298 ± 0.007
Searise 2 DR07	East Pacific Rise	20°1153'N 113°7118'W	6.60	0.88	0.702533 ± 0.000002	0.312 ± 0.007
CY82 18-01	N East Pacific Rise	12°858'N 103°963'W	6.15	0.94	0.702624 ± 0.000002	0.242 ± 0.007
DR7-1 EPR	N East Pacific Rise	11°43'N 103°783'W	-	1.01	0.702789 ± 0.000003	0.261 ± 0.007
					Pacific Average	0.278 ± 0.032
ARP 74 11-18	FAMOUS Mid-Atlantic Ridge	36°85'N 33°25'W	2.04	0.96	0.702869 ± 0.000003	0.255 ± 0.007
ARP 74 12-19	FAMOUS Mid-Atlantic Ridge	36°858'N 33.258'W	2.04	0.92	0.703055 ± 0.000003	0.267 ± 0.007
ALV 518 3-1	FAMOUS Mid-Atlantic Ridge	36°818'N 33°255'W	2.04	0.96	0.702875 ± 0.000002	0.258 ± 0.009
ALV 518 3-2	FAMOUS Mid-Atlantic Ridge	36° 82'N 33° 26'W	2.04	0.97	0.702875 ± 0.000003	0.297 ± 0.007
ALV 523-1	FAMOUS Mid-Atlantic Ridge	36°827'N 33°252'W	2.04	0.90	0.702906± 0.000002	0.262 ± 0.007
ALV 519-2-1	FAMOUS Mid-Atlantic Ridge	36°818'N 33°262'W	2.04	1.07	0.702894 ± 0.000002	0.191 ± 0.009

]522-2-2	FAMOUS Mid-Atlantic Ridge	36°812'N 33°265'W	2.04	0.98	0.702910 ± 0.000003	0.209 ± 0.007
522-1-1	FAMOUS Mid-Atlantic Ridge	36°812'N 33°265'W	2.04	0.98	0.702896 ± 0.000002	0.106± 0.011
525-5-1	FAMOUS Mid-Atlantic Ridge	36° 812'N 33°273'W	2.04	1.00	0.702982 ± 0.000004	0.299 ± 0.008
525-5-2	FAMOUS Mid-Atlantic Ridge	36°812'N 33°273'W	2.04	1.00	0.702926 ± 0.000003	0.254 ± 0.006
525-5-3	FAMOUS Mid-Atlantic Ridge	36°812'N 33°273'W	2.04	0.96	0.702924 ± 0.000003	0.176 ± 0.009
					Atlantic Average	0.247 ± 0.026
					MORB group average	**0.260 ± 0.017**
Plagioclase separates						
522-1-1	FAMOUS Mid-Atlantic Ridge		2.04	0.98	0.702946 ± 0.000013	0.31 ± 0.03
ARP 74 11-18	FAMOUS Mid-Atlantic Ridge		2.04	0.96	0.702939± 0.000016	0.34 ± 0.03

Table 3.1: Eu/Eu^*_{PM} normalised to Primitive Mantle values given by McDonough and Sun (1995). Group average error given as 2 s e =2*SD√n. All $^{87}Sr/^{86}Sr$ data normalised to an NBS 987 value of $^{87}Sr/^{86}Sr = 0.71024$.

Table 3.2 (next page): Eu/Eu^*_{PM} normalised to Primitive Mantle values given by McDonough and Sun (1995). Group average error given as 2 s e =2*SD√n. All $^{87}Sr/^{86}Sr$ data normalised to an NBS 987 value of $^{87}Sr/^{86}Sr = 0.71024$. BHVO-1 value given as an average of all four measurements.

Ocean Island Basalts

Sample	Location	Lithology	Type	SiO_2 wt %	MgO wt %	Eu/Eu^*_{PM}	$^{87}Sr/^{86}Sr \pm 2se$	$\delta^{88}Sr \pm 2se$ (‰)
AZF2	Azores Flores	Alkali basalt	Subaerial	47.47	6.12	1.05	0.703334 ± 0.000003	0.240 ± 0.008
AZP8	Azores Pico	Alkali basalt	Subaerial	47.46	13.21	1.00	0.703914 ± 0.000003	0.268 ± 0.006
AZFY2	Azores Fayal	Alkali basalt	Subaerial	46.35	10.18	1.04	0.703798 ± 0.000003	0.280 ± 0.008
MD40	Madeira	Alkali basalt	Subaerial	45.18	10.69	1.04	0.702779 ± 0.000003	0.224 ± 0.008
MD64	Madeira	Basanite	Subaerial	44.74	8.14	1.01	0.702785 ± 0.000003	0.230 ± 0.008
PL02 30-1	Galapagos Seamount	Tholeiitic basalt	Submarine	48.67	8.32	1.04	0.703046 ± 0.000003	0.259 ± 0.007
PL02 25-1	Galapagos seamount	Alkali basalt	Submarine	46.71	5.15	1.01	0.703330 ± 0.000003	0.264 ± 0.008
TD4	Trindade	Nephelinite	Subaerial	37.02	5.61	0.96	0.703788 ± 0.000002	0.230 ± 0.006
FDN25	Fernando de Noronha		Subaerial	44.06	10.71	1.00	0.704708 ± 0.000003	0.245 ± 0.008
D5-1	Loihi, Hawaii	Alkali basalt	Submarine	47.60	5.20	0.99	0.703574 ± 0.000002	0.269 ± 0.006
C195	Mt Cameroon, Cameroon	Alkali basalt	Subaerial	-	6.20	-	0.703280 ± 0.000002	0.250 ± 0.007
FP23	Bioko, Cameroon	Alkali basalt	Subaerial	45.34	9.44	0.98	0.703191 ± 0.000003	0.233 ± 0.007
P19	Principe, Cameroon	Basanite	Subaerial	41.88	8.94	-	0.702976 ± 0.000002	0.238 ± 0.007
BHVO-1 (*av*)	Kilauea, Hawaii	Tholeiitic basalt	Subaerial	49.94	7.23	1.05	0.703457 ± 0.000003	0.249 ± 0.006
BHVO-2	Kilauea, Hawaii	Tholeiitic basalt	Subaerial	49.90	7.23	1.04	0.703470 ± 0.000002	0.268 ± 0.009
							OIB group average	**0.248 ± 0.009**

Sample name	Location	Lithology	Sr ppm	$^{87}Sr/^{86}Sr$ (2 se)	$\delta^{88}Sr$ ‰ (2 se)
Shale					
SCo-1	Wyoming, USA	Silty marine shale	170 ± 15	0.725789 ± (3)	0.106 ± 0.006
SCo-1[C]				0.718339 ± (8)	0.116 ± 0.012
SGR-1b	Green River Formation, USA	Petroleum and carbonate-rich shale	420 ± 30	0.713087 ± (3)	0.302 ± 0.007
				Shale average	0.204 ± 0.200
Continental basalt					
BCR-2	Columbia River, Oregon, USA	Continental flood basalt	358 ± 5	0.705000 ± (3)	0.241 ± 0.007
KH03-10	Kilbourne Hole, USA	Basalt	655 ±20	0.703974 ± (3)	0.181 ± 0.014
				Continental basalt average	0.211 ± 0.060
				Total average	0.203 ± 0.088

Table 3.3: Sr isotope data for USGS shale standards analysed. Carbonate fractions were removed, apart from "SCo-1 with carbonate". Errors for $\delta^{88}Sr$ and $^{87}Sr/^{86}Sr$ are given in ppm as 2 s e from the mean. Group average discounting SCo-1 with carbonate, and error given as 2 s e where 1se=SD√n. Elemental data for standards from USGS and for KH03-10 from Harvey et al., (2012). All $^{87}Sr/^{86}Sr$ data normalised to an NBS 987 value of $^{87}Sr/^{86}Sr = 0.71024$. [C] = whole rock sample with carbonate fraction.

3.4.1. Major, trace, and REE data for oceanic basalts.

All MORB have MgO contents between 5-10%, and all OIB between 5-11% (Figure 3.4) indicative of relatively primitive, unfractionated compositions. Aside from three basanites and a nephelinite, the majority are alkaline or tholeiitic basalts. Figures 3.5 and 3.6 below illustrate the REE patterns for MORB and OIB respectively and highlight the enrichment of these basalts relative to the primitive mantle (values taken from McDonough and Sun, 1995). The [La/Sm] ratio (normalised to the PM) is often used as an index of enrichment and also in the classification of basalts. Following the classification scheme used by Niu et al. (2012), the intra-plate OIBs are enriched in incompatible elements with [La/Sm] >>1. Following the classification scheme whereby depleted MORB (D-MORB) have [La/Sm] values of less than 1, enriched MORB (E-MORB) posses [La/Sm] ratios of more than 1.5,

and transitional MORB (T-MORB) have [La/Sm] ratios in between, all MORB analysed are depleted relative to the primitive mantle (D-MORB) as illustrated in Figure 3.7.

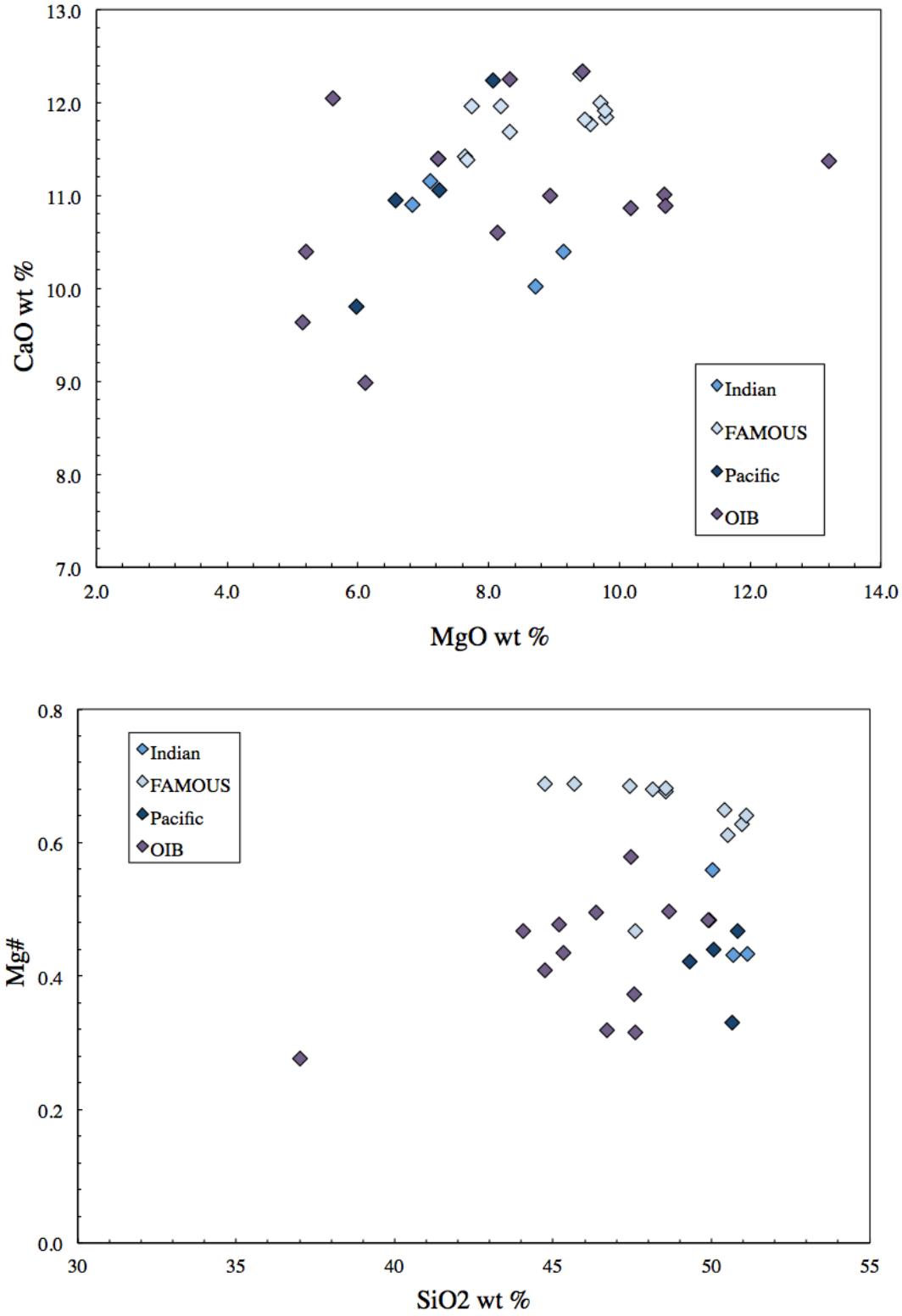

Figure 3.4: Major element data, SiO_2 and MgO (wt %), of the OIB and MORB samples.

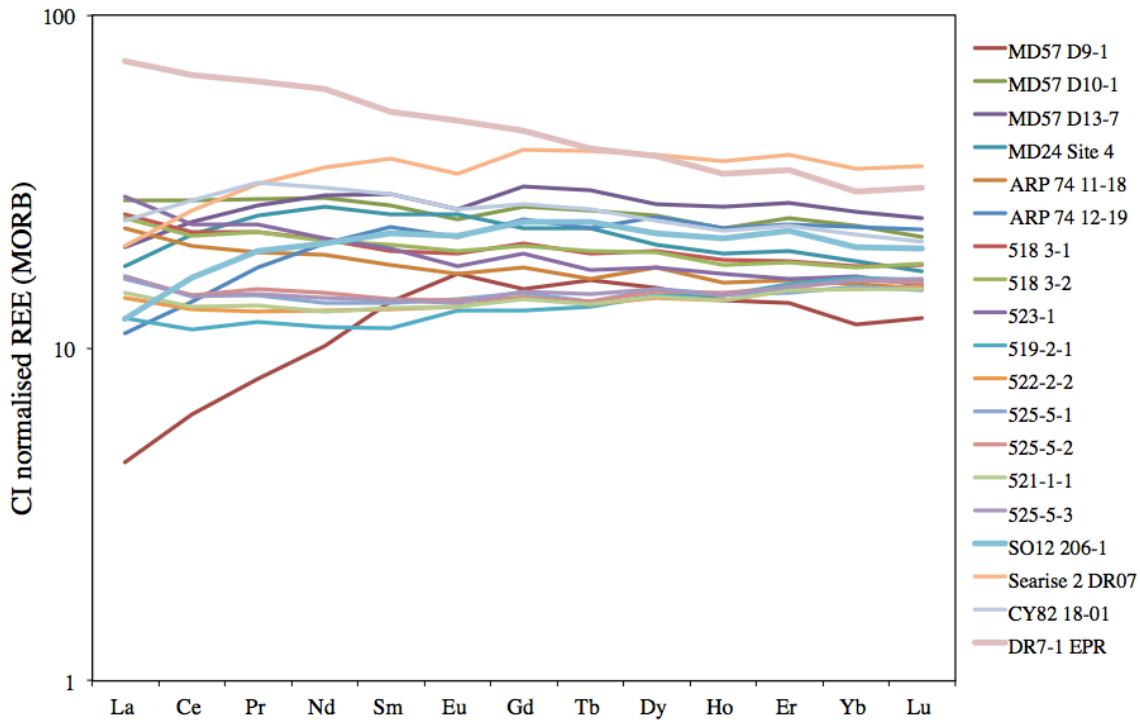

Figure 3.5: Spidergram of MORB REEs normalised to CI values (Anders and Grevesse, 1989).

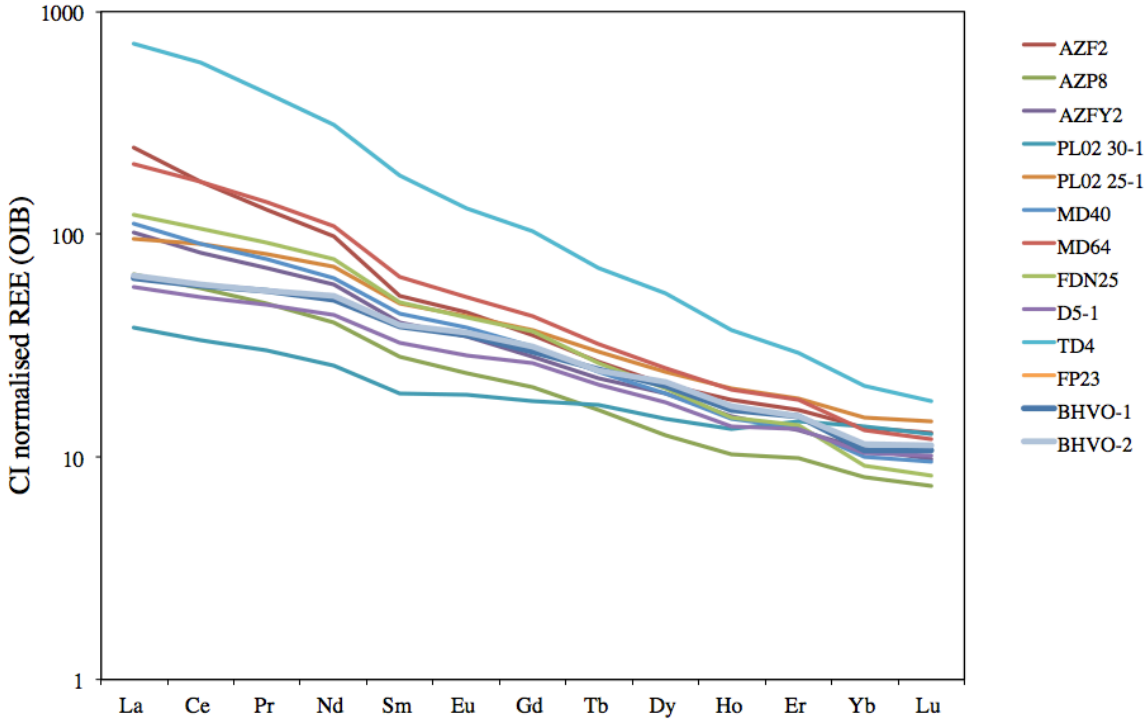

Figure 3.6: Spidergram of OIB REEs normalised to CI values (Anders and Grevesse, 1989).

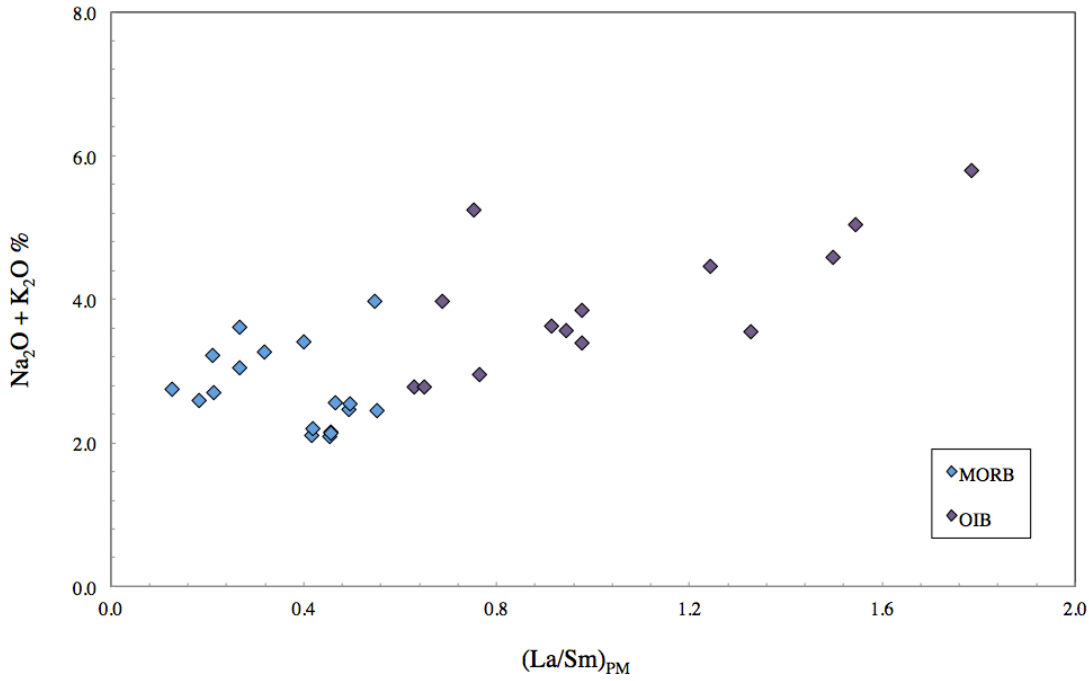

Figure 3.7: (La/Sm), normalised to PM, versus alkali content for the MORB and OIB samples.

3.4.2. Radiogenic $^{87}Sr/^{86}Sr$ data for oceanic basalts

The $^{87}Sr/^{86}Sr$ values of MORB fall within a restricted range from $^{87}Sr/^{86}Sr$ = 0.702468 (±3) to 0.703105 (±2) (Fig 3.8). The MORBs from both the Indian and Pacific Ocean Ridges have $^{87}Sr/^{86}Sr$ compositions that overlap. Those from FAMOUS are grouped closer together, aside from one slightly more radiogenic sample, ARP 74 12-19, but also display variations that are resolvable outside the analytical precision.

Basalts from oceanic islands possess a wider range of $^{87}Sr/^{86}Sr$ values, from 0.702779 (±3) to 0.704708 (±3), than those from spreading ridges (Fig 3.9). Multiple samples from Madeira and Kīlauea possess near identical $^{87}Sr/^{86}Sr$ compositions, whereas those from the Galapagos Islands, Azores and the Cameroon Line vary outside of analytical uncertainty. The sample from Flores Island in the Azores has a less radiogenic $^{87}Sr/^{86}Sr$ composition

than those from Pico and Faial. Samples FDN25 and D5-1 have extremely radiogenic compositions ($^{87}Sr/^{86}Sr$ = 0.704706 ±3 and 0.703573 ±2 respectively), and FDN25 the most radiogenic composition of all (marked with a dashed line), which extends towards the HIMU/ EM1/EM2 end-members.

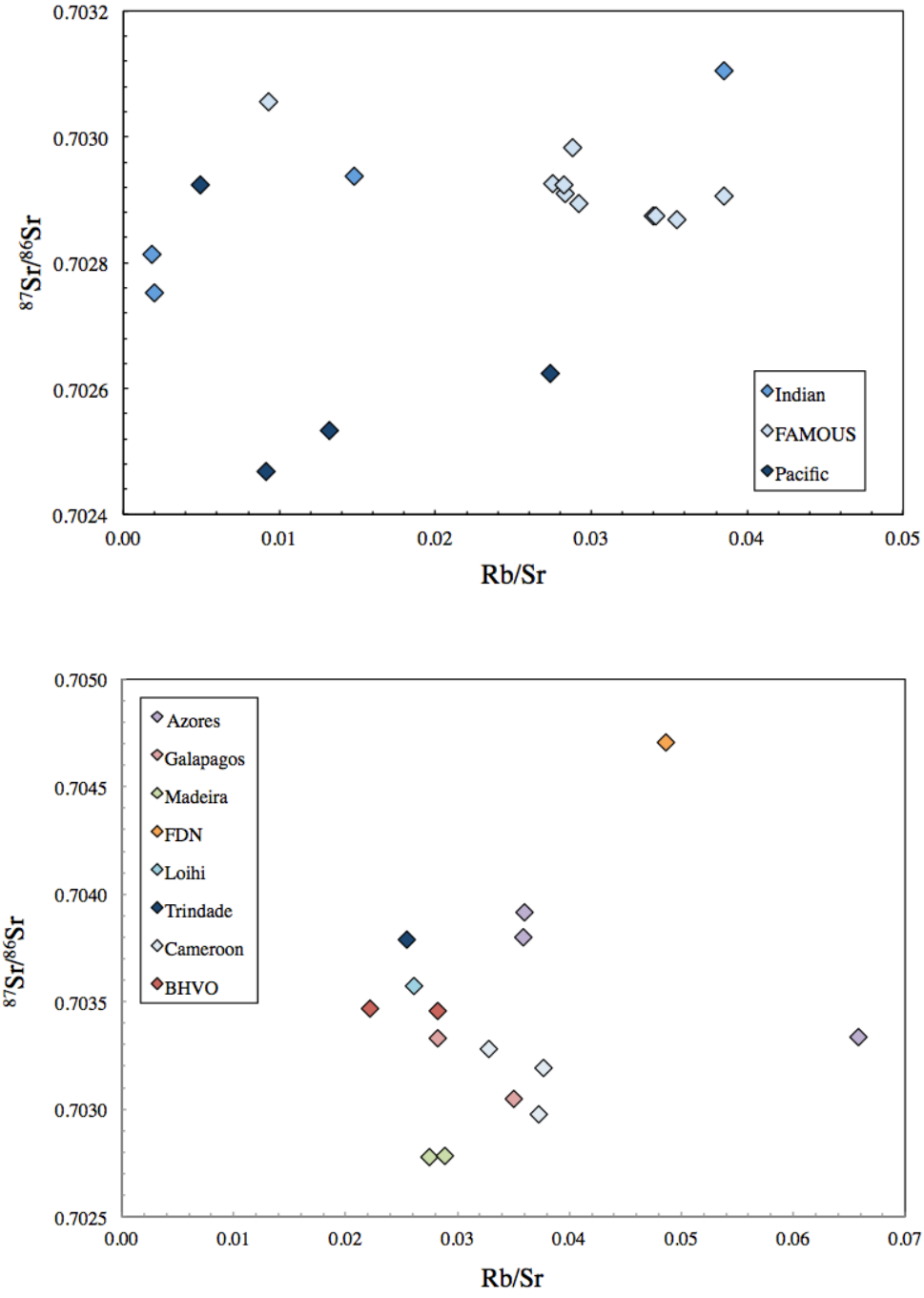

Figure 3.8 and 3.9: The $^{87}Sr/^{86}Sr$ ratios of MORB and OIB shown with Rb/Sr. The analytical precision is smaller than the symbols.

The $^{87}Sr/^{86}Sr$ ratios of 23 of the 31 basalts analysed in this study have been determined previously (Escrig et al., 2004; Schiano et al., 1997; Gale et al., 2013; Dupré et al., 1981; Yu et al., 1997; Prinzhofer et al., 1989; White, 1979; Halliday et al., 1988; Halliday et al., 1990; Halliday et al., 1992; Harpp and White, 2001), and are shown in Figure 3.3. Overall, the $^{87}Sr/^{86}Sr$ isotope compositions determined in this study compare well with existing data, with a maximum difference of 20 ppm between the MORB sample ALV525-5-3 and its $^{87}Sr/^{86}Sr$ composition determined by Yu et al. (1997). There is no existing $^{87}Sr/^{86}Sr$ data for five basalts from the Atlantic, one from the Pacific, and the OIBs FDN25 and D5-1. Combined, the MORB and OIB cover a restricted area of the total global spread in radiogenic isotopes. Aside from FDN25 and D5-1, all samples have $^{87}Sr/^{86}Sr$ compositions within the range of the remaining samples in Figure 3.3. The MORB samples possess more restricted $^{87}Sr/^{86}Sr$ compositions, resulting in a tighter grouping, typical of MORB with a depleted mantle source, whilst OIB extend to far more radiogenic values, as high as that typically seen for the enriched EM signature.

3.4.3. Stable $\delta^{88}Sr$

The $\delta^{88}Sr$ compositions of MORB samples ranges from $\delta^{88}Sr = +0.312 \pm 0.007$ to $+0.176 \pm 0.010$‰. The data show clearly resolvable variations of ~0.14‰ in $\delta^{88}Sr$, far greater than the analytical precision. The majority of this variation is seen within a single sample area; the FAMOUS segment, although this may be a sample bias given the greater number of samples analysed for Atlantic MORB relative to those from the Pacific and Indian ridges. The MORB samples possess an average a $\delta^{88}Sr$ value of 0.260 ± 0.009‰ (2 se; n= 18) with a variance of $0.0013‰^2$.The $\delta^{88}Sr$ composition of OIB samples range from $\delta^{88}Sr$

= +0.280 ± 0.008 to +0.224 ± 0.018‰. The δ^{88}Sr values for the OIB cannot be resolved from one another and are homogenous with a low variance of 0.0003‰^{2} and an average value of δ^{88}Sr =0.248 ± 0.004‰ (2 se; n= 15). The MORB data show a variation four times larger than that of OIB, and are clearly resolved from one another. The average values for MORB and OIB are indistinguishable from one another within 2 se of the mean (Figure 3.10).

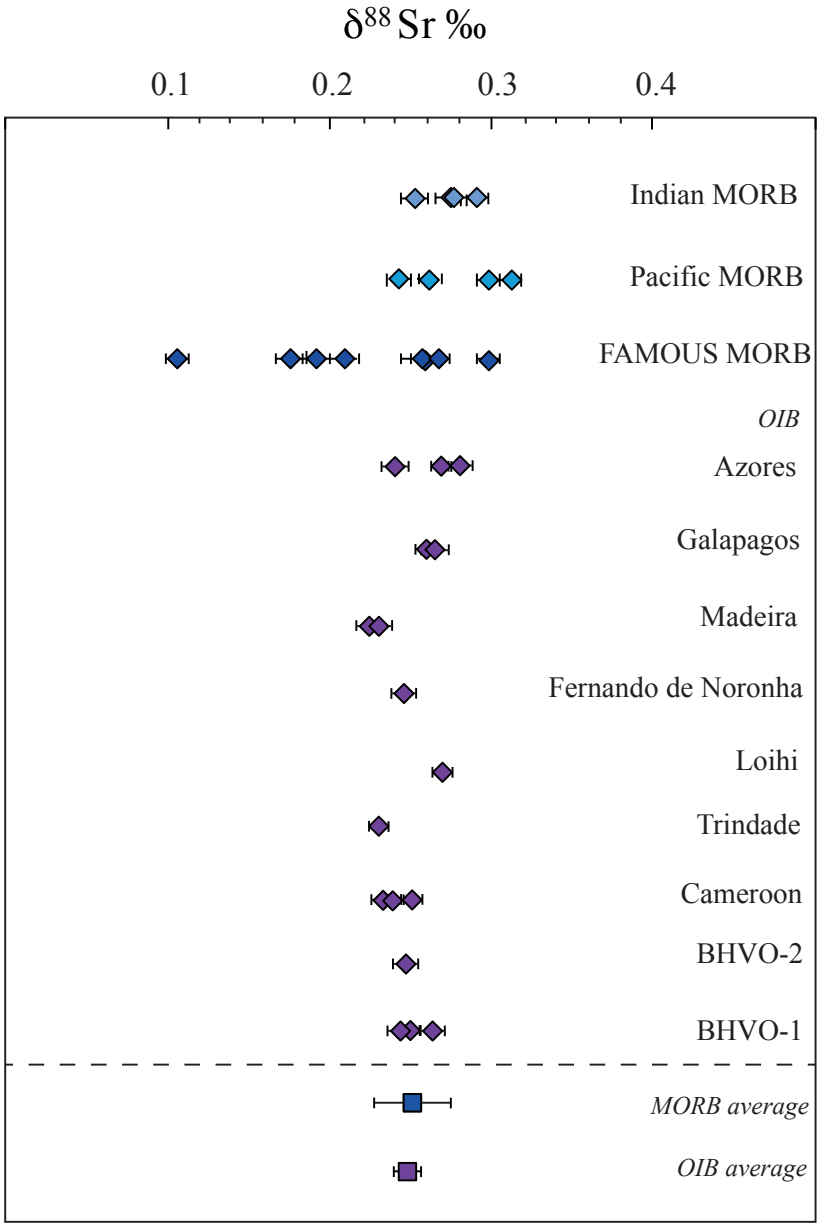

Figure 3.10: A comparison of MORB and OIB δ^{88}Sr compositions, shown with their respective averages to 2se of the mean.

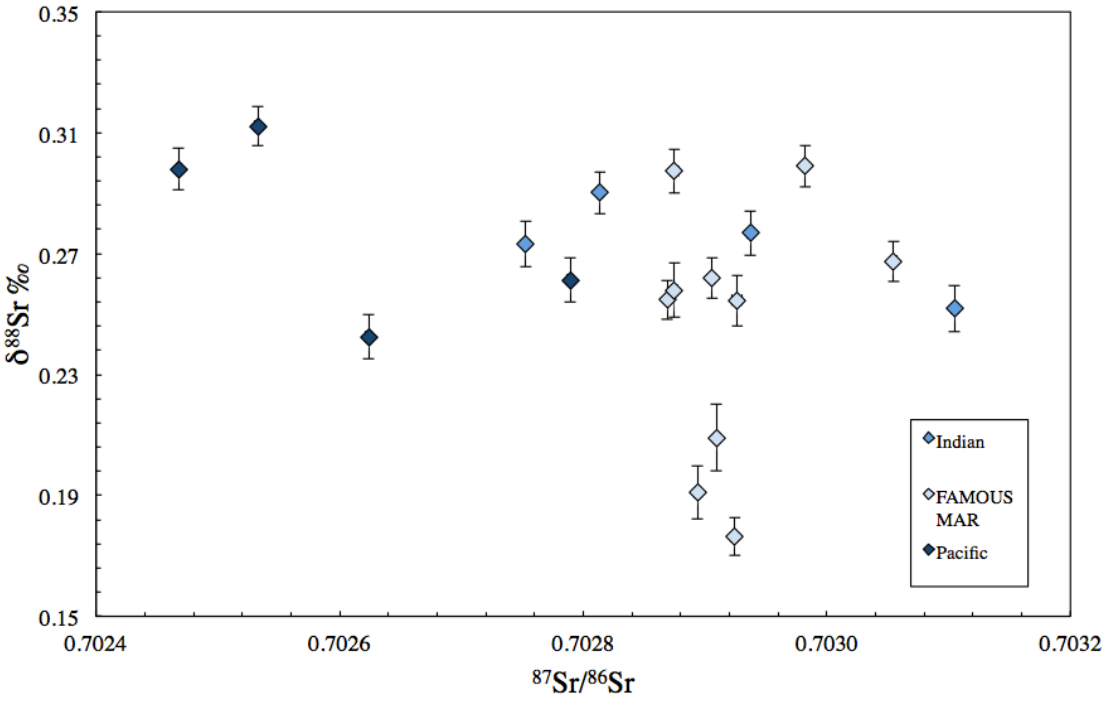

Figures 3.11: Plot of $\delta^{88}Sr$ versus $^{87}Sr/^{86}Sr$ for MORB.

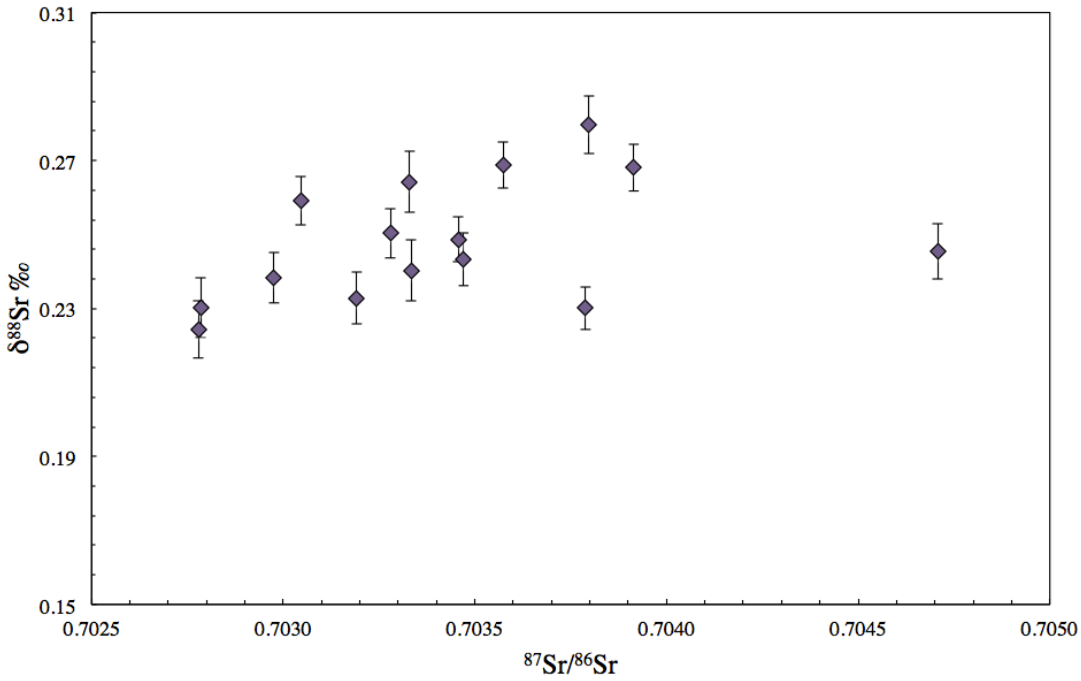

Figures 3.12: Plot of $\delta^{88}Sr$ versus $^{87}Sr/^{86}Sr$ for OIB.

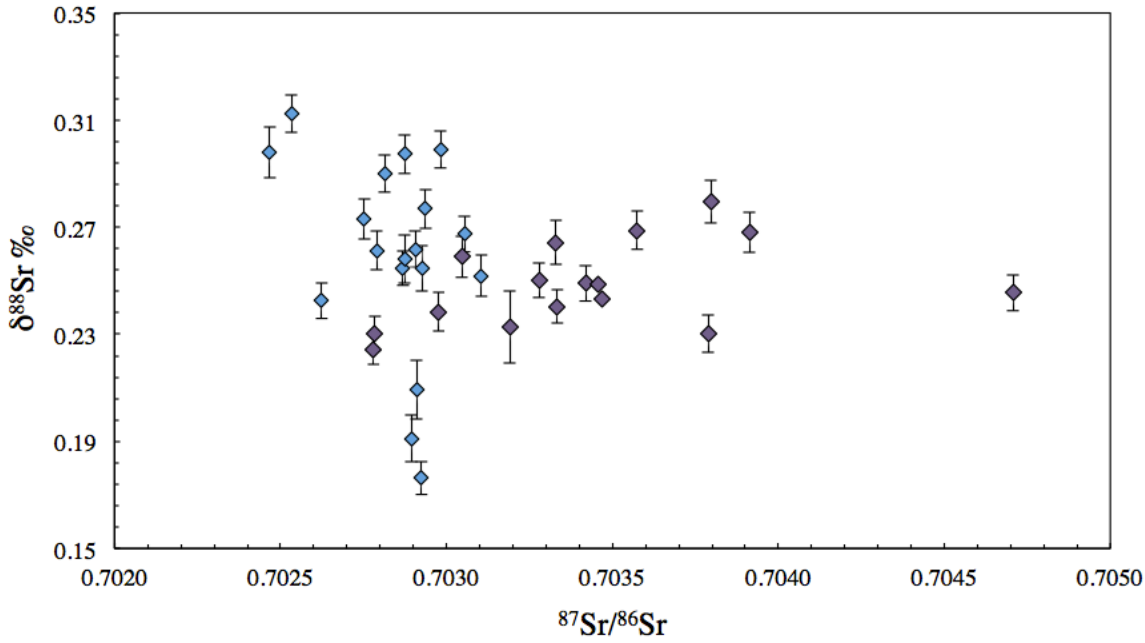

Figures 3.13: A comparison of $\delta^{88}Sr$ versus $^{87}Sr/^{86}Sr$ for OIB and MORB.

The average stable $\delta^{88}Sr$ compositions of MORB analysed here are comparable to those determined in previous studies of $\delta^{88}Sr$ = 0.27‰ ±0.05 (2 se; n=8), 0.29‰, and 0.26‰ ±0.01 (Moynier et al., 2010; Charlier et al., 2012; Ohno and Hirata, 2007) but range to much lighter compositions and show larger variations, only resolvable with the precision of DS-TIMS measurements (Figure 3.14). Nevertheless, these are restricted in composition when compared to variations in $\delta^{88}Sr$ reported for evolved crustal material which extend to much lighter values of $\delta^{88}Sr$ = -0.19‰ for a rhyolite glass (Charlier et al., 2012). However, based on the homogenous $\delta^{88}Sr$ composition of oceanic basalts, Charlier et al., (2012) concluded that mantle-melting delivers homogenous melts to the surface whereas this study clearly shows resolvable variations to lighter values than those previously observed. There is a lack of existing OIB data, aside from rock reference standards, with which to compare the OIB data of this study with. As with MORB, however, these data span a comparatively small range of $\delta^{88}Sr$ values in the wider context of the range of $\delta^{88}Sr$ fractionation in terrestrial materials.

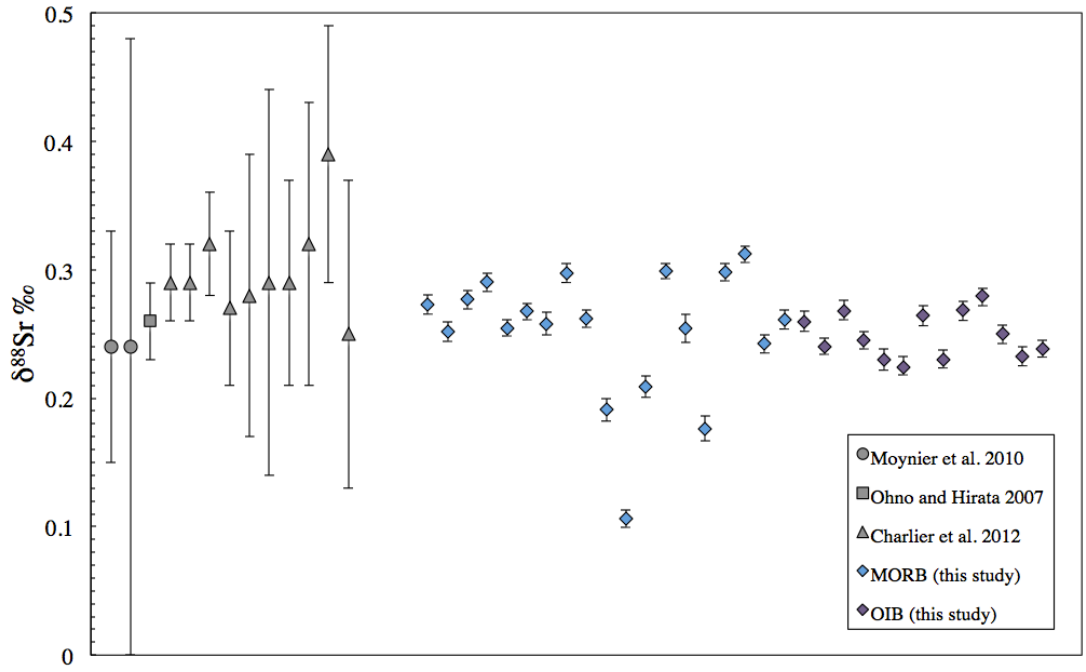

Figure 3.14: A comparison of DS-TIMS MORB and OIB data (this study) with previous basalt MC-ICP-MS data (Moynier et al., 2010; Ohno and Hirata, 2007; Charlier et al., 2012).

3.4.4. Scales of variations in the $^{87}Sr/^{86}Sr$ and $\delta^{88}Sr$ ratios of oceanic basalts

For OIB, resolvable variations in $^{87}Sr/^{86}Sr$ are found on a global scale as well as on a local scale for multiple samples from all islands excluding Madeira, which are identical within error. Resolvable variations in $^{87}Sr/^{86}Sr$ are found for MORB on several scales, globally, regionally (DUPAL anomaly) and locally (FAMOUS segment). On a larger global scale, the MORB analysed here are characterised by more restricted $^{87}Sr/^{86}Sr$ compositions, when compared to basalts from continental regions or oceanic islands. On a regional scale, variations in $^{87}Sr/^{86}Sr$ from 0.702753 (±3) to 0.703103 (±3) are found for the Indian Ridge samples, with a maximum $^{87}Sr/^{86}Sr$ value of ~0.703. Hart (1988) used an $^{87}Sr/^{86}Sr$ value of >0.705 to define the DUPAL anomaly. By this reasoning, the Indian MORB analysed in this study do not show the typical characteristics of a DUPAL signature for Sr. On a smaller local scale, resolvable variations in $^{87}Sr/^{86}Sr$ are found for

MORB from the FAMOUS ridge segment, only 45km long, from 0.702868 (±3) to 0.703503 (±3). Variations in radiogenic isotopes, including Sr, have been reported for several other sections along the MAR, AMAR and Narrowgate (le Reox et al., 1996; le Reox et al., 1981), as well as for FAMOUS basalts previously (Gale et al., 2013), where $^{87}Sr/^{86}Sr$ was found to vary outside analytical error. However, as no correlations between $^{87}Sr/^{86}Sr$ and other isotope systems, particularly Pb, were found for MORB from the FAMOUS region, these authors speculated that the variations might be caused by seawater alteration. Figure 3.15 shows clearly resolvable variations in the $^{87}Sr/^{86}Sr$ ratios of FAMOUS samples relative to previous data.

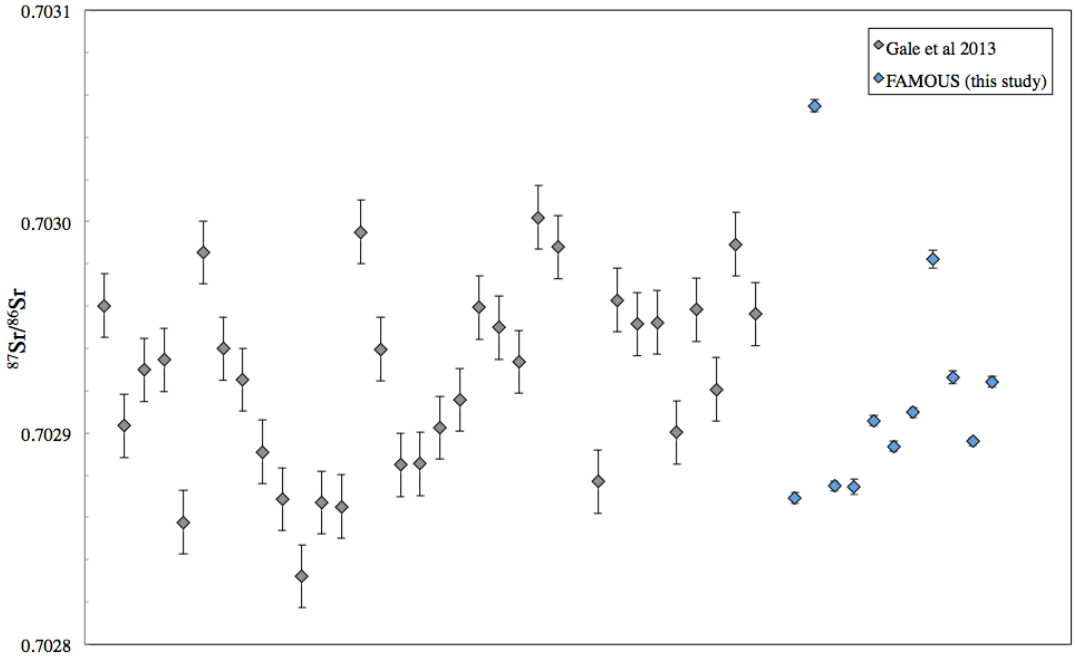

Figure 3.15: A comparison of $^{87}Sr/^{86}Sr$ from this study with that of Gale et al. (2013) for FAMOUS MORB.

Similarly, resolvable differences in the $\delta^{88}Sr$ compositions of MORB are found on all three scales. The most surprising of these is the large extent of variation seen in samples from a single ridge segment 45km long (FAMOUS). The $\delta^{88}Sr$ compositions of OIB are overall relatively homogenous, but on a global scale resolvable variations do exist the

lightest sample, MD40, is resolvable from the heaviest, AZFY2 ($\delta^{88}Sr$ = 0.224 ± 0.008‰ and $\delta^{88}Sr$ = 0.280 ± 0.008‰ respectively). On a smaller local scale, samples from the Cameroon Line, Galapagos, Madeira and Hawaii are not resolvable from one another and variations are not evident. Only one sample from Flores Island in the Azores lies outside of analytical error from the others.

3.4.5. FAMOUS mineral separates

The $\delta^{88}Sr$ compositions of two plagioclase separates from the FAMOUS suite are consistently heavier than their complementary glasses (Figure 3.16). Mineral-melt fractionation factors are derived from Equation 3.1 and the $\delta^{88}Sr$ composition of the glasses, and are $\Delta_{522plag\text{-}melt}$ = 0.21‰ and $\Delta_{ARPplag\text{-}melt}$ = 0.08‰.

$$\Delta_{A\text{-}B} = \delta_A - \delta_B \qquad \textit{Equation 3.1}$$

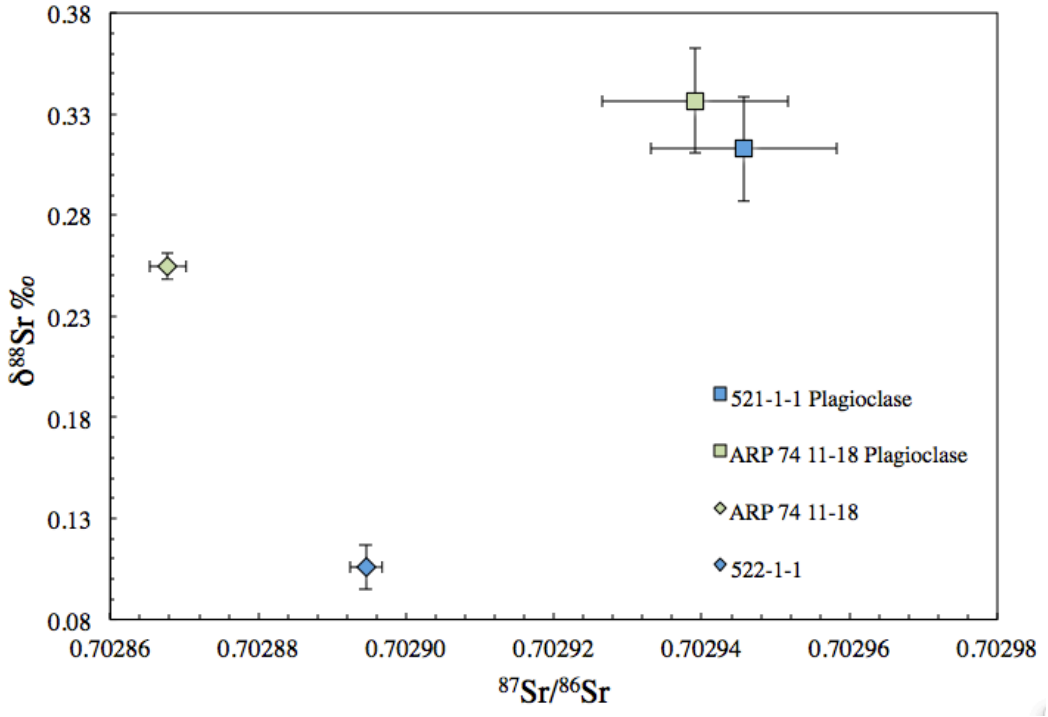

Figure 3.16: $^{87}Sr/^{86}Sr$ and $\delta^{88}Sr$ data for the FAMOUS MORB plagioclase minerals and glasses.

3.4.6. Shale and continental basalt samples

The three shale samples span a wide range of $\delta^{88}Sr$ compositions from $\delta^{88}Sr$=0.106 ± 0.006‰ to 0.302 ± 0.006‰. There is no measureable difference between the $\delta^{88}Sr$ value of the whole-rock SCo-1 sample and that with the carbonate fraction removed. The two continental basalts possess lighter $\delta^{88}Sr$ values than the oceanic basalts, from $\delta^{88}Sr$ =0.241 ± 0.007 to 0.181 ± 0.014‰, with an average $\delta^{88}Sr$ value of 0.211 ± 0.060. The $^{87}Sr/^{86}Sr$ value obtained for sample KH03-10, 0.703974 ± (3), compares well with that measured by Harvey et al. (2012) of 0.70395 (±1).

3.5. Discussion

The elemental and isotope compositions of magmas that form at mid-ocean ridges and oceanic islands are controlled by their mantle source composition, partial melting, and magma mixing, and prior to eruption on the ocean floor, fractional crystallisation and secondary alteration. In the following discussion, the mechanisms by which each process can generate the variations observed in $\delta^{88}Sr$ in MORB and OIB are presented and evaluated. Where appropriate, the origins of variations in stable Sr are discussed along with complementary radiogenic Sr data, as when considered together this potentially offers greater insights into the processes controlling radiogenic and stable isotope fractionation.

3.5.1. Origin of variations in $^{87}Sr/^{86}Sr$ and $\delta^{88}Sr$

3.5.1.1. Seawater contamination or assimilation of altered oceanic crust

Seawater can alter the composition of oceanic basalts either prior to their eruption by direct interaction with magma or by the assimilation of altered oceanic crust (e.g., Michael and Schilling, 1989; Schiffman et al., 2010), or post eruption by surface alteration of erupted lavas. This is particularly pertinent when considering Sr isotope data, as seawater has both high concentrations of Sr (90 μmol kg^{-1}) and isotopically contrasting signatures ($^{87}Sr/^{86}Sr$ = 0.70917, $\delta^{88}Sr$ = 0.387‰; e.g. Hodell et al., 1990; Krabbenhoft et al., 2010) from those of typical mantle melts. Consequently, even a relatively small extent of seawater interaction with fresh basalt has the potential to alter its composition significantly. Samples were specifically chosen for their optical purity, handpicked, and leached prior to dissolution. Therefore, it is unlikely that their isotope compositions are compromised by surface alteration, which leaves the possibility of assimilation of altered material in the source. Chlorine is enriched in seawater and can be used as a sensitive indicator of seawater contamination. The absence of correlations between Cl and $^{87}Sr/^{86}Sr$ and $\delta^{88}Sr$ (Fig. 3.17) implies that seawater has had no measurable effect on the Sr composition of MORB.

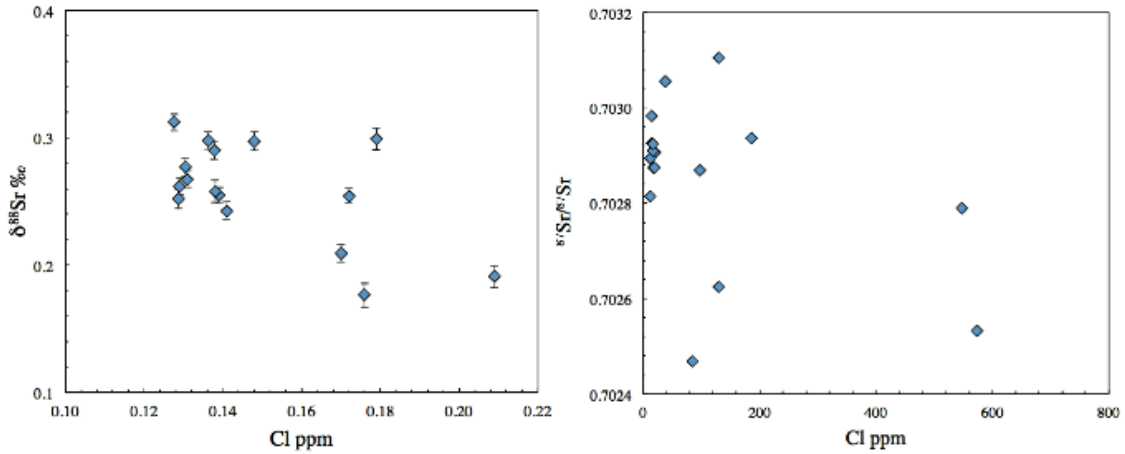

Figure 3.17: Plots of Cl versus $^{87}Sr/^{86}Sr$ and $\delta^{88}Sr$ in MORB.

However, as Cl is incompatible and is susceptible to change during fractional crystallisation and partial melting, a more robust tracer of seawater is ideally required. Seawater possesses $^{11}B/^{10}B$ isotope composition far removed from mantle values, making it an ideal tracer for detecting the presence of seawater in mantle-derived basalts. Additionally, for the same MORB samples analysed in this study, $^{187}Os/^{188}Os$ variations were found to co-vary with $^{11}B/^{10}B$ consistent with the assimilation of roughly 5 to 10% of older oceanic crust altered by seawater (Gannoun et al., 2007). Despite the detection of an altered oceanic crust signature, correlations between $^{187}Os/^{188}Os$ and $\delta^{11}B$ with both $^{87}Sr/^{86}Sr$ and $\delta^{88}Sr$ are absent (Figure 3.18), suggesting that the cause of the variations in $^{187}Os/^{188}Os$ and $\delta^{11}B$ is not linked to Sr isotopes. Thus, the possibility of seawater interaction as a potential cause for significant variations in $^{87}Sr/^{86}Sr$ and $\delta^{88}Sr$ in MORB can be ruled out, leaving primary mantle melting (including mantle heterogeneity) or magmatic processes as the potential causes of the Sr isotope variations.

Unfortunately, Cl concentration and Os isotopic data are lacking for the OIB samples, making it difficult to definitively assess the extent of seawater alteration. However, all

OIBs were selected for their optical purity and based on this observation alone seawater interaction is unlikely. Additionally, any influence of seawater would shift the $\delta^{88}Sr$ composition to heavier values, rather than the slightly lighter values of OIB observed relative to MORB.

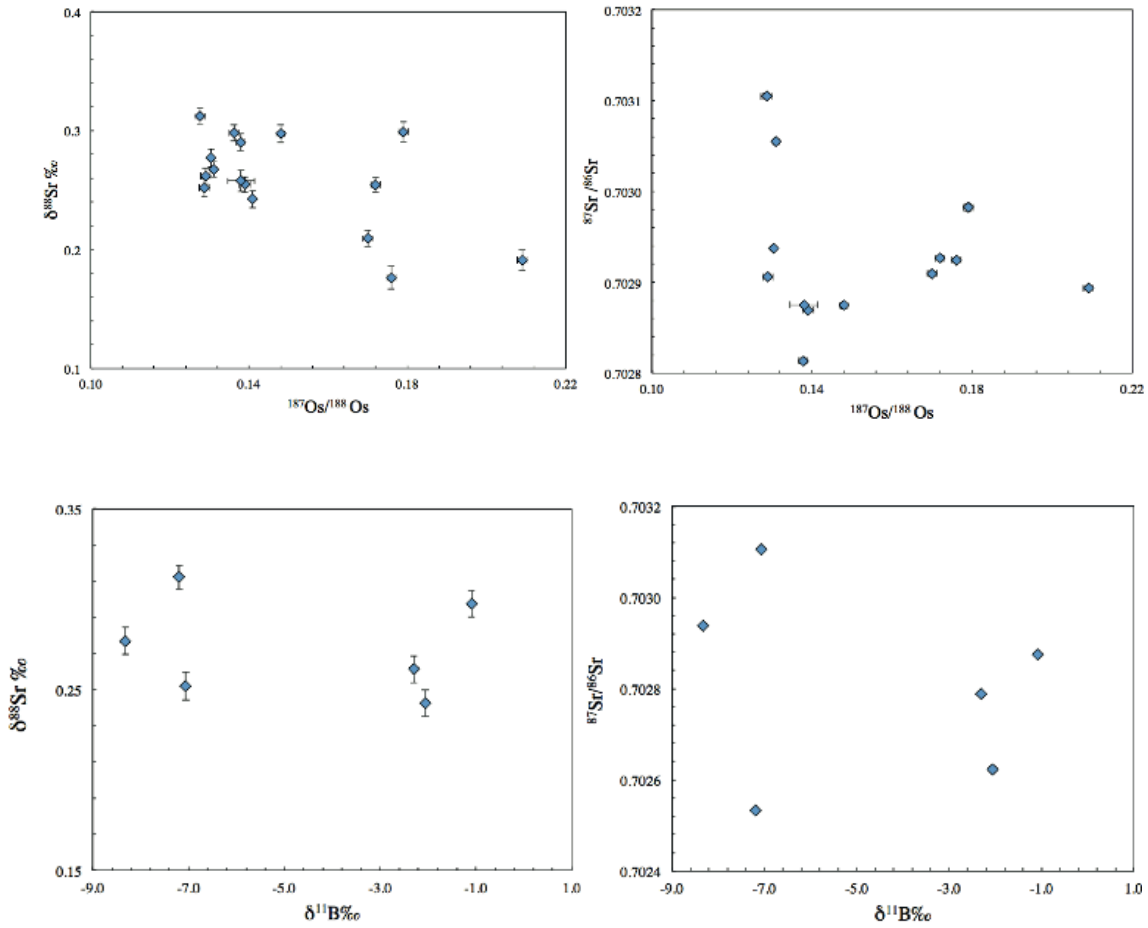

Figures 3.18: MORB $\delta^{88}Sr$ and $^{87}Sr/^{86}Sr$ compositions with indices for seawater, $^{187}Os/^{188}Os$ and $\delta^{11}B$.

3.5.1.2. Mantle processes

3.5.1.2.1. Partial melting (fractionation during melting)

A fundamental assumption in the application of radiogenic isotopes to mantle-derived basalts is that they are in equilibrium with their mantle source (e.g Hofmann and Hart, 1978; Zindler and Hart, 1986). Over the meter scale of melting, at the temperatures and pressures typical of the mantle, diffusion is considered to result in elemental and isotope equilibrium. Following this rationale, radiogenic isotopes cannot fractionate during melting of a single source, and any fractionation cause would be corrected for during internal normalisation to a fixed $^{88}Sr/^{86}Sr$ ratio. Thus, the variations in $^{87}Sr/^{86}Sr$ are not caused by partial melting and cannot be used as indicator of this for $^{88}Sr/^{86}Sr$.

Stable isotope fractionation during partial melting can potentially arise by the release of one isotope preferentially to another. This is thought to occur for Fe isotopes, based on differences between the average Fe compositions of mantle melts and mantle rocks (Teng et al., 2013). In particular, MORBs and OIBs were found to have heavier $\delta^{56}Fe$ compositions than mantle peridotites, inferred to reflect Fe isotope fractionation during partial melting, possibly moderated by redox conditions. Small differences between mantle peridotites and oceanic basalts were similarly observed for $\delta^{51}V$, however, it was concluded that they are unlikely to have resulted from partial melting (Prytulak et al., 2013). Fractionation of stable Sr isotopes during partial melting can potentially be identified using indices of the degree of melting, such as Mg#, La/Yb, Zr/Y and Rb/Sr. Ratios of incompatible elements to compatible elements are particularly robust indicators, as incompatible elements, by definition, preferentially partition into melt. Figures 3.19 and 3.20 show $\delta^{88}Sr$ compositions of MORB and OIB against some typical indices of partial melting.

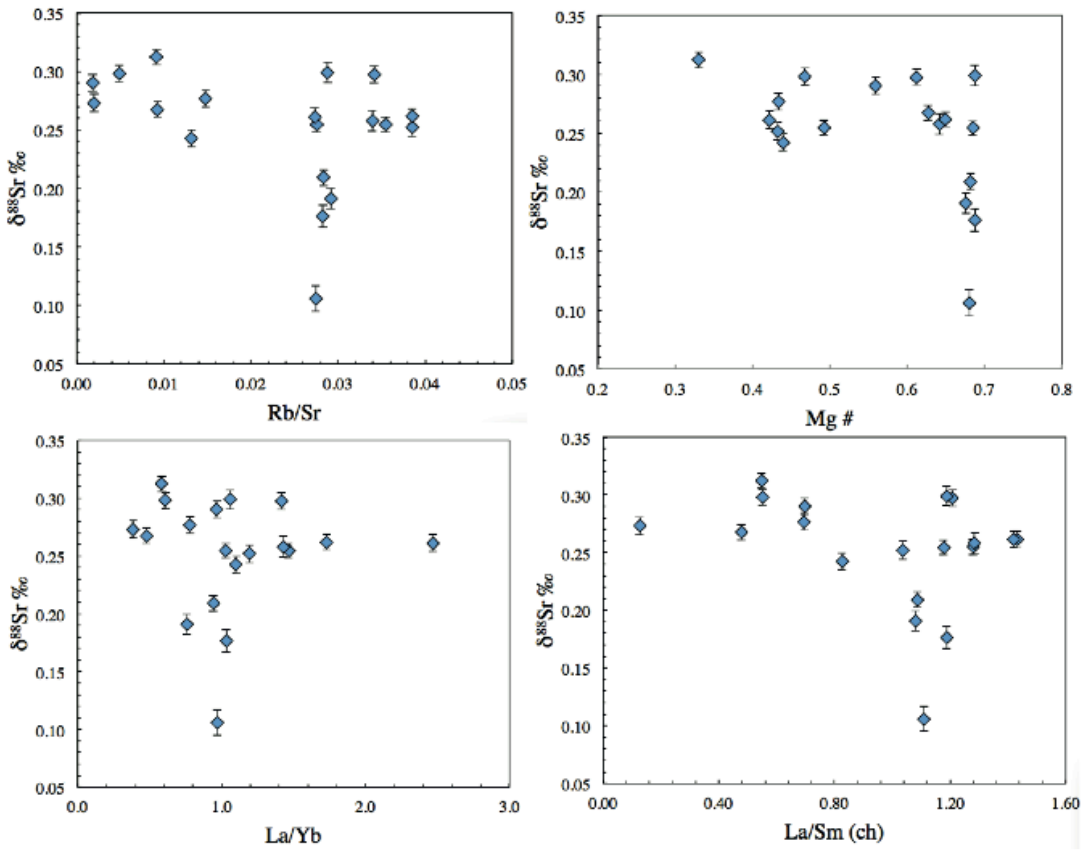

Figure 3.19: δ^{88}Sr compositions of MORB with indices of partial melting.

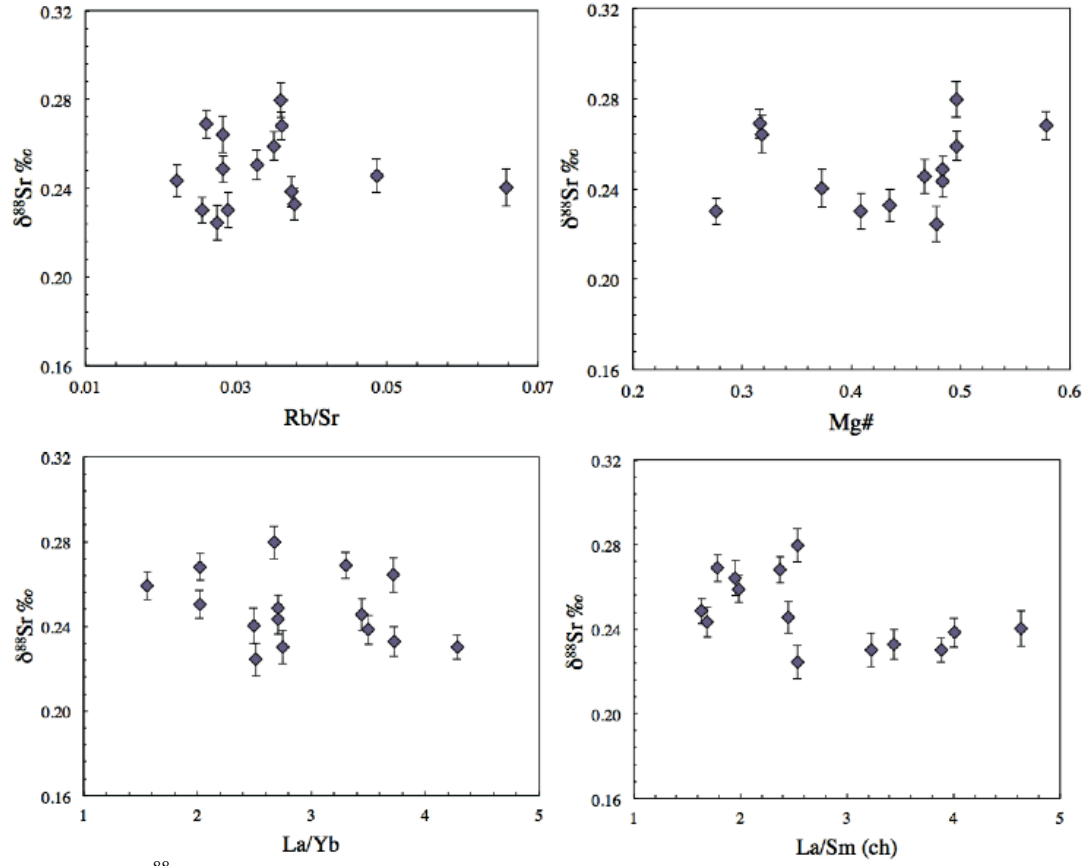

Figure 3.20: δ^{88}Sr compositions of OIB with indices of partial melting.

Overall, the MORB analysed do not show a significant range in the degree of partial melting, which is rather a feature more usually observed for OIBs that are considered to reflect smaller and variable degrees of partial melting (Figure 3.7). Globally, correlations for MORB with $\delta^{88}Sr$ and indices of partial melting are absent, which is also true at the smaller local scale of the FAMOUS samples. For OIB there is a tentative negative correlation between $\delta^{88}Sr$ and La/Yb with samples that might be attributed to smaller degree partial melts, such as TD4, extending to lighter values. However, many of these indices can also be affected by mantle heterogeneity and differentiation, which may obscure any trend caused by partial melting. However, the absence of any correlation with other indices such as Mg#, La/Sm and Rb/Sr suggests that the degree of partial melting has little or no effect of the $\delta^{88}Sr$ composition of mantle melts. Overall, there is little evidence to suggest fractionation of $\delta^{88}Sr$ during partial melting of either MORB or OIB, though further analyses of OIB that possess the chemical characteristics of smaller degree melts may confirm the potential co-variation with La/Yb.

3.5.1.2.2. Heterogeneity in the mantle source

The large variations in the $^{87}Sr/^{86}Sr$ compositions of OIBs observed in this study, that extend to very radiogenic values of ~0.7037, are thought to be the signatures of mantle heterogeneity resulting from incomplete mixing of various enriched and depleted components. These source components could be from a depleted mantle, enriched mantle resulting from recycled crustal material, and metasomatised material (e.g. see reviews by Niu et al., 2012; White, 2010), as discussed in Chapter 1. Variations in the radiogenic isotopes of MORB are similarly thought to result from recycling, metasomatism, or

differences in lithologies (for example pyroxenite compared to peridotite). Global variations are considered to be due to an inherited heterogeneity in the mantle source as a result of incomplete mixing of various source components, from depleted mantle (DMM) to enriched or metasomatised components, and this is the cause of global scale resolvable variations in $^{87}Sr/^{86}Sr$ ratios of MORB and OIB analysed. On smaller length scales, for basalts from the FAMOUS segment, previous studies have dismissed variations in $^{87}Sr/^{86}Sr$ as being due to seawater contamination, and attributed the variations in other radiogenic isotopes due to mixing between a DMM source and a metasomatised Azores plume member (Gale et al., 2013). Considering seawater is unlikely to be the cause of the $^{87}Sr/^{86}Sr$ variations of FAMOUS basalts in this study, they are, in this case, most likely due to inherited source heterogeneity. This view is supported by arguments based on evidence that suggest that mantle heterogeneity in both MORB and OIB sources exists on a much smaller scale than previously thought (e.g. Sobolev et al., 2000; White, 2010). The exact cause of variability in $^{87}Sr/^{86}Sr$ is difficult to determine based on Sr isotopes alone, however, new Pb data for the FAMOUS samples analysed in this study preclude the involvement of the Azores plume, as has been previously suggested by Gale et al. (2013), at least for the samples studied here (Burton et al., in prep). There is also the potential for certain mantle minerals, such as phlogopite (commonly linked to metasomatism in ultramafic rocks), to have more radiogenic $^{87}Sr/^{86}Sr$ ratios relative to other silicates, and varying amounts of these minerals in the source could result in differences in the $^{87}Sr/^{86}Sr$ composition of its melts (e.g. O'Nions and Pankhurst, 1974). Despite this, in all likelihood the variations in $^{87}Sr/^{86}Sr$ of MORB and OIB basalts on global, regional and local scales are due to mantle heterogeneity in the sources of these melts.

It is less clear whether the variations in $\delta^{88}Sr$ compositions of OIB and MORB can also be attributed to mantle heterogeneity. Using the $^{87}Sr/^{86}Sr$ composition of oceanic basalts as

a proxy for mantle heterogeneity, it is possible to compare these with the $\delta^{88}Sr$ composition of mantle source components, assuming there is no extensive fractionation during melting or homogenisation of isotopic signature. Clear correlations between the radiogenic and stable Sr isotopes of oceanic basalts are absent (Figs. 3.11 and 3.12), which suggests either that the stable and radiogenic Sr are not controlled by the same processes, or that stable isotopes are controlled by additional factors that obscure any trend. There is also no clear correlation between $\delta^{88}Sr$ and K_2O/TiO_2 (Figure 3.21), an indicator of incompatible element enrichment of the source (e.g. Schilling et al., 1983). Combined, the OIBs analysed sample a number of source components including EM1 and HIMU signatures. Despite this, the limited degree of stable isotope variation, and the absence of any clear trends with either location or mantle source type, suggests that the established mantle source components do not exert a major control on the stable isotope composition of mantle melts for OIB, or else that any variations or obscured by melting and magmatic differentiation.

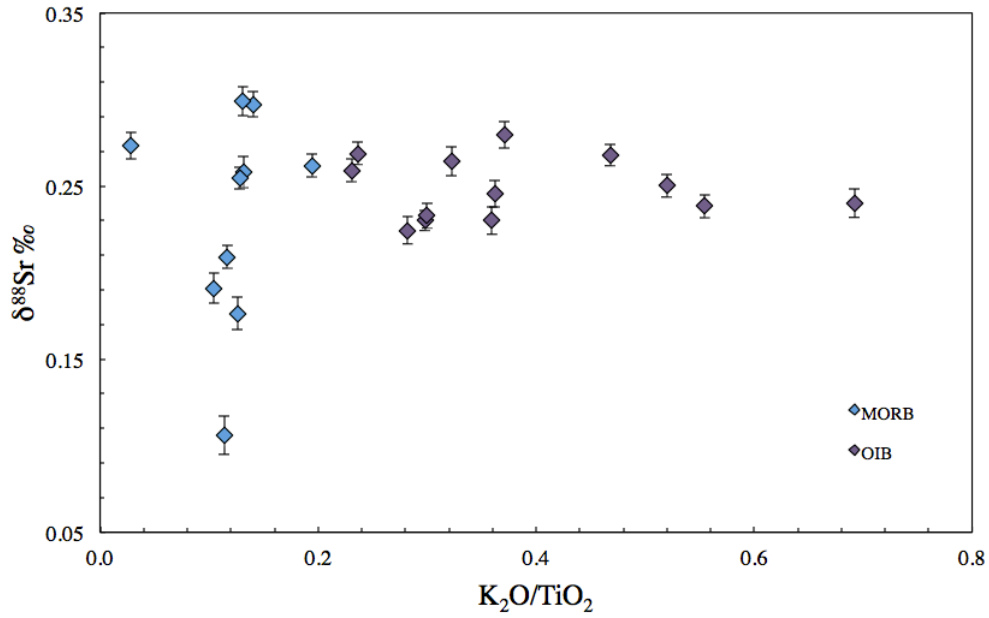

Figure 3.21: $\delta^{88}Sr$ data for OIB and MORB, shown with their K_2O/TiO_2 ratios.

There is also the potential for certain mantle minerals to possess distinct $^{88}Sr/^{86}Sr$ ratios relative to other silicates, and varying proportions of these minerals in the source could result in differences in the $^{88}Sr/^{86}Sr$ composition of melts. At present it is difficult to determine any such effects because of the absence of $\delta^{88}Sr$ data for minerals and ultramafic mantle rocks, limiting speculation on the stable isotope compositions of pyroxenite and peridotite, and whether differences between these lithologies could result in inherited signatures in the products of mantle melting. Chemically, these vary in composition; pyroxenite is predominantly composed of pyroxene, whereas peridotite comprises both olivine and pyroxene. Should these minerals have contrasting $\delta^{88}Sr$ compositions, melting of these variable sources could result in variations in basalts. However, pyroxene, olivine and refractory minerals such as spinel, typically have low partition coefficients for Sr and as such will exert a minimal influence on the isotope composition of the melt, unless they possess extreme $\delta^{88}Sr$ compositions. Unfortunately without ultramafic whole rock and mineral data little more can be stated with any degree of certainty.

3.5.1.3. Magmatic processes

Fractional crystallisation

Fractional crystallisation and AFC (assimilation with fractional crystallisation) processes have long been suggested as a means of generating the variable degree of elemental enrichment and chemical variations of oceanic basalts (e.g. O'Hara, 1977; O'Hara and Matthews, 1981). Processes such as fractional crystallisation are unlikely to be responsible for the variations in $^{87}Sr/^{86}Sr$ seen in both MORB and OIB as they cannot fractionate

radiogenic isotopes if the basalts are in isotopic equilibrium with their mantle source. This is reflected by the absence of any correlation between $^{87}Sr/^{86}Sr$ of MORB and OIB samples with indices of fractional crystallisation such as SiO_2, Ba, and Eu/Eu* for plagioclase crystallisation, and thus $^{87}Sr/^{86}Sr$ is not useful as a tracer of this process for $^{88}Sr/^{86}Sr$.

Stable isotope fractionation, however, can occur during igneous differentiation as a result of the preferential partitioning of isotopes into particular minerals during fractional crystallisation (e.g. Schuessler et al., 2009; Teng et al., 2008; Weyer and Seitz, 2012; Telus et al., 2012; Savage et al., 2011). This has been proposed to occur for Sr, based on lighter $\delta^{88}Sr$ (up to~-0.20‰) values of evolved rocks such as rhyolites as a result of plagioclase crystallisation, into which Sr is preferentially partitioned (Charlier et al., 2012). A co-variation between $\delta^{88}Sr$ and Eu/Eu*, often used as an index of plagioclase crystallisation, can be modelled by ^{88}Sr being preferentially partitioned into plagioclase, where the melt composition is driven to lighter $\delta^{88}Sr$ values during fractional crystallisation. As fractional crystallisation commonly occurs in magma chambers within which MORB melts, and Sr largely partitions into plagioclase, this process may be responsible for the varied $\delta^{88}Sr$ compositions. Figure 3.22 illustrates Eu/Eu* with $\delta^{88}Sr$ compositions for MORB. This could be interpreted as two negative trends with considerable scatter for both, but overall a general negative trend is seen with no clear correlation between Eu/Eu* and $\delta^{88}Sr$. This is not unexpected, as a clear correlation would only be expected for melts fractionating with the same initial composition.

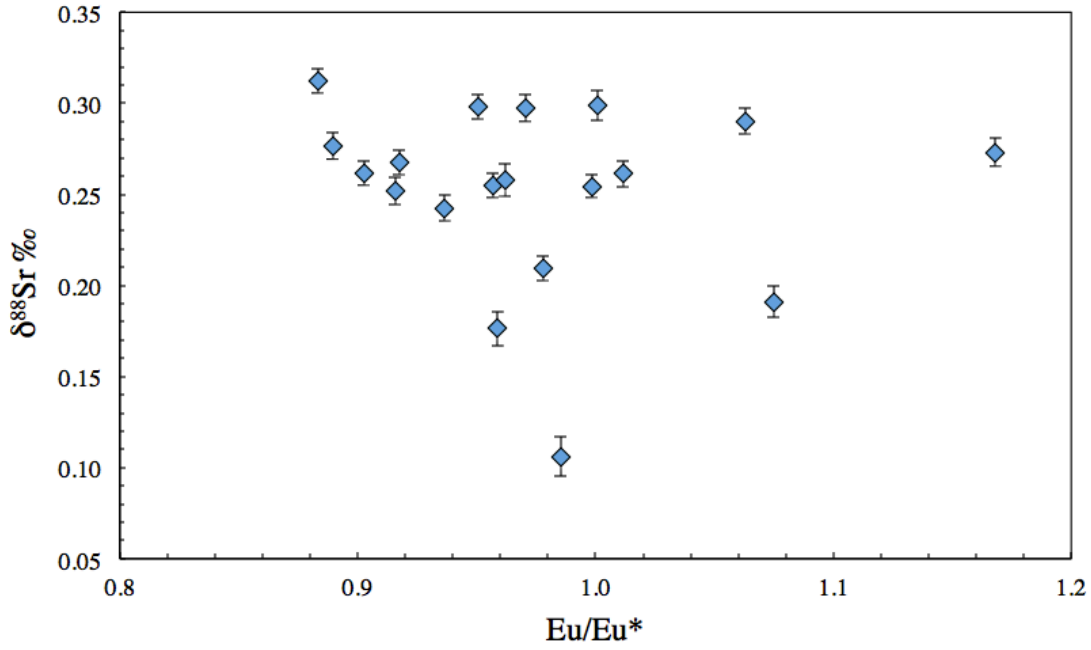

Figures 3.22: δ^{88}Sr versus Eu/Eu* for all MORB.

Although the FAMOUS segment is thought have undergone melt replenishment as well as fractional crystallisation, it may give a better indication of the relationship with fractional crystallisation than the global MORB trends. A correlation between Eu/Eu* and Sr concentration demonstrates that plagioclase fractionation is clearly occurring within the FAMOUS MORB suite, albeit to a minor extent as the lowest Eu anomaly value is Eu/Eu*= 0.87. There is also a suggestion of a negative trend between Eu/Eu* and δ^{88}Sr (Figure 3.23), however, the absence of a clear correlation indicates that plagioclase crystallisation is not the only process responsible for the variations observed.

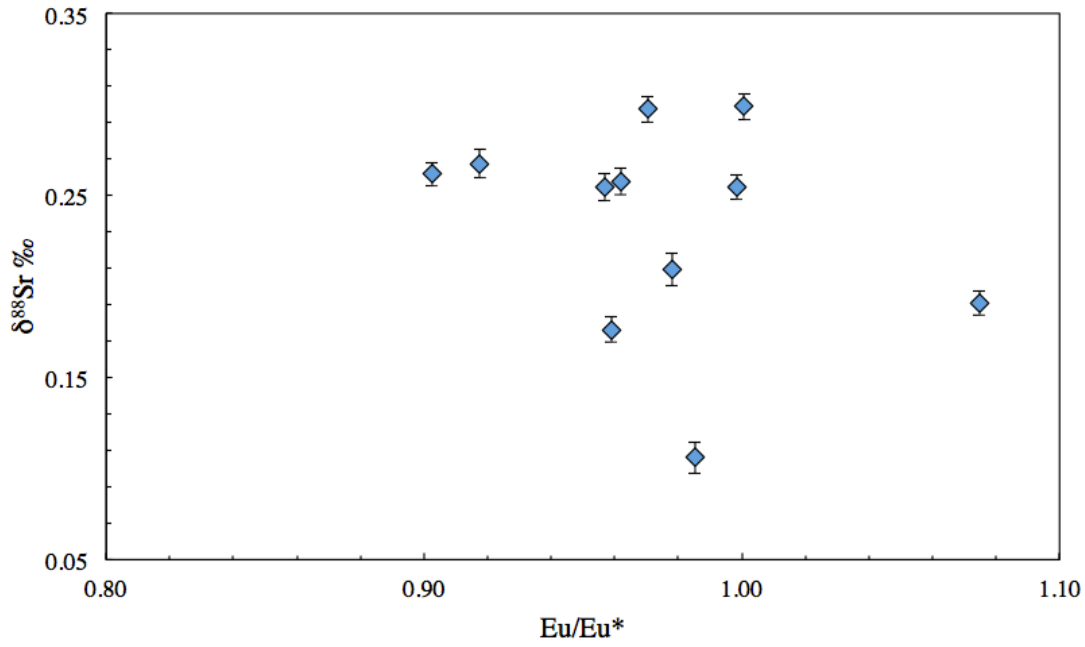

Figure 3.23: The δ^{88}Sr compositions of FAMOUS MORB shown with their Eu anomalies.

One reason for this may be that there is an additional mineral phase responsible for δ^{88}Sr fractionation. As Sr can also partition into clinopyroxene, this has the potential to fractionate the stable isotopes of Sr. However, a correlation between δ^{88}Sr and Sc (often taken as an indicator of pyroxene crystallisation) is absent (Figure 3.24), which implies that this phase plays only a minor role. Alternatively, it may be that another factor, such as mantle source heterogeneity, also exerts some control on the δ^{88}Sr composition of melts.

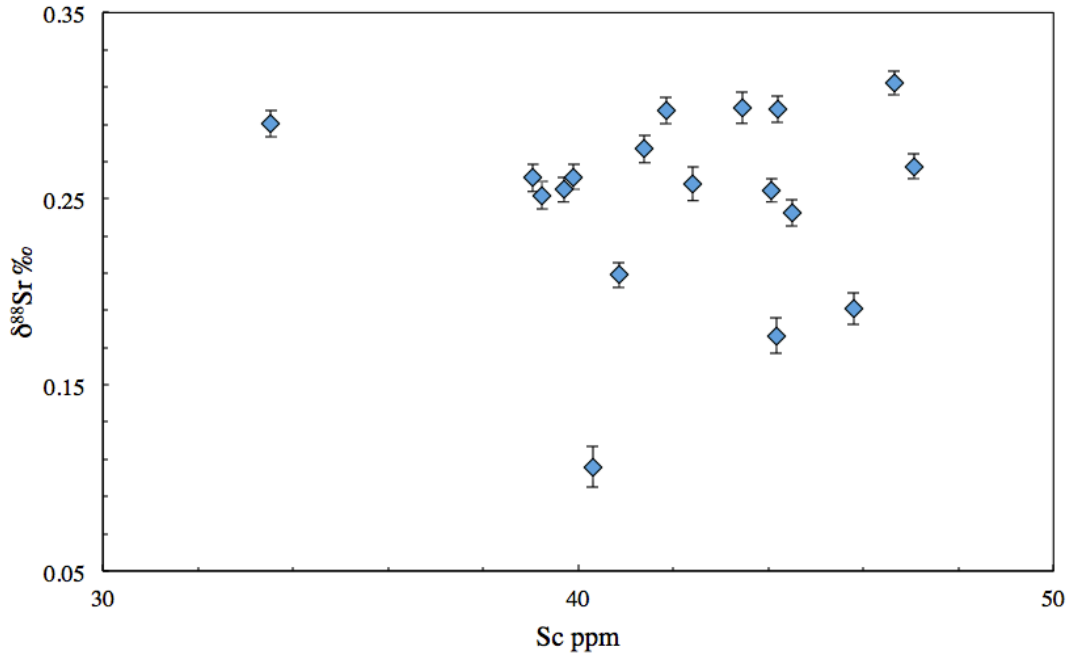

Figure 3.24: δ^{88}Sr compositions with Sc content for the MORB analysed in this study.

Analyses of plagioclase separates from two FAMOUS basalts appear to confirm that fractional crystallisation of plagioclase can cause variations in the δ^{88}Sr compositions of MORB by the preferential partitioning of the heavier isotopes of Sr into the mineral to leave a lighter residual melt (Figure 3.16). Using plagioclase-melt fractionation factors calculated for these minerals, the fractionation of δ^{88}Sr for the FAMOUS MORB suite can be modelled as a function of crystallisation using the Eu/Eu* ratios of the samples as a proxy for the melt fraction remaining. Mineral-melt fractionation factors for both clinopyroxene and plagioclase were used to model the effect of crystal fractionation on the δ^{88}Sr of the remaining melt using clinopyroxene data ($\Delta_{Silv\text{-}cpx\text{-}melt}$ = .0.23‰) discussed elsewhere (Chapter 4). Concentrations of trace elements in the melt, C_L, are calculated using the fractional crystallisation equation (3.2):

$$C_L = C_0 F^{(D-1)} \qquad \textit{Equation 3.2}$$

where C_0 is the initial melt composition, F is the melt fraction remaining and D is the partition coefficient. For plagioclase, C_0 is estimated to be ~80ppm based on the Sr concentration of sample 525-5-1, and D taken to be ~3.5. The δ^{88}Sr composition of the melt, $\delta^{88}Sr_L$, is then calculated using Equation 3.3:

$$\delta^{88}Sr_L = [\delta^{88}Sr_0 + 1000]F_L^{f-1} - 1000 \qquad \textit{Equation 3.3}$$

where $\delta^{88}Sr_0$, is the initial stable Sr isotope composition and F_L is the fraction of Sr remaining in the melt. The results are shown in Figure 3.25 for two sets of models using different starting compositions. The model used by Charlier et al. (2012) is shown for comparison. The first set of models uses sample 525-5-1 as the initial unfractionated starting composition, as it has a Eu/Eu* value of 1.00 and the heaviest δ^{88}Sr composition of +0.299 ± 0.008‰, and is represented by long dashed lines. The second set of models uses the lightest sample, 522-1-1, as the starting composition (δ^{88}Sr= +0.106 ± 0.011‰, Eu/Eu* = 0.99), for comparison and is illustrated with short dashed lines.

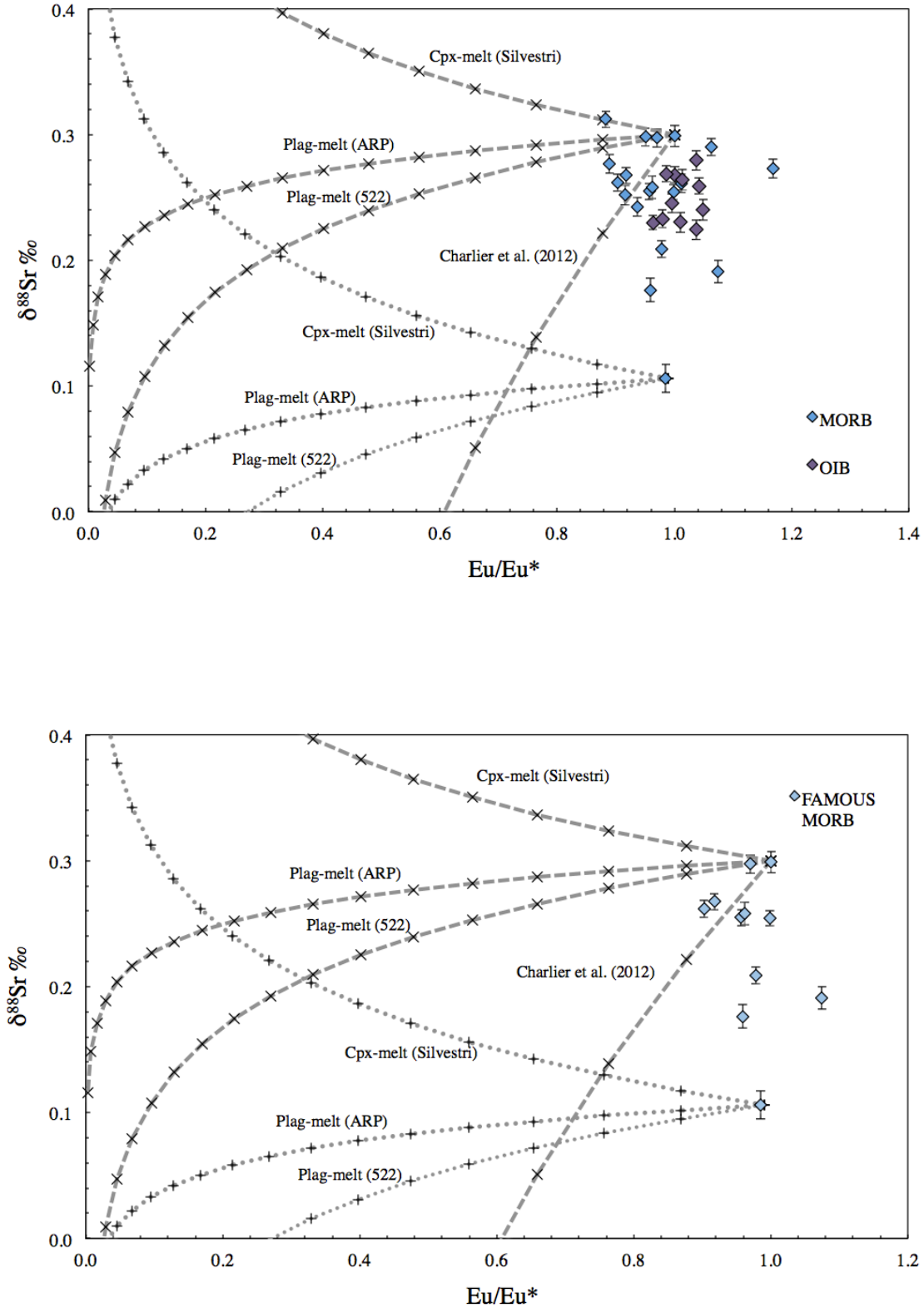

Figure 3.25: Upper graph shows the results of modelling with MORB and OIB analysed in this study, and the lower with solely FAMOUS MORB. Long dashed curves represent models with a starting composition based on sample 525-5-1, whilst the short dashed curves use a composition based on sample 522-1-1. The curves are annotated with the mineral data that were used in the calculations.

The modelling indicates that the calculated effects of removal of plagioclase or clinopyroxene on $\delta^{88}Sr$ are inconsistent with the OIB and MORB $\delta^{88}Sr$ data of this study. A possible cause for the inconsistency between the models and the data is the difficulty in modelling Eu/Eu* data in an open system: the FAMOUS basalts exhibit a substantial range in incompatible element fractionation, larger than can be explained by a single fractionation crystallisation event, requiring multiple supplies of magma along the segment (Langmuir et al., 1977; Laubier et al., 2012; Gale et al., 2013). Alternatively, as the plagioclase mineral data confirm that plagioclase fractionation can drive the melt composition to lighter $\delta^{88}Sr$ values, the models may illustrate the involvement of an additional factor or process, such as assimilation or mantle heterogeneity.

Further support for the involvement of another process or source control is the observation that OIBs exhibit a similar range of plagioclase crystallisation as MORB, with Eu anomalies extending to values of 0.96, yet lack the extreme $\delta^{88}Sr$ compositions of MORB. Whilst the two OIB samples that show the largest extent of plagioclase crystallisation, TD4 and FP23 (Eu/Eu*= 0.96 and 0.98 respectively), also possess the lightest $\delta^{88}Sr$ values ($\delta^{88}Sr$= 0.230 and 0.233‰ respectively), there is no clear correlation between $\delta^{88}Sr$ and plagioclase (Figure 3.26) or clinopyroxene crystallisation with Sc (Figure 3.27). The apparent absence of a relationship between fractional crystallisation and the $\delta^{88}Sr$ composition of OIBs suggests that assimilation or mantle heterogeneity also play a part, although at this stage partial melting cannot be ruled out as an additional process and more analyses are required.

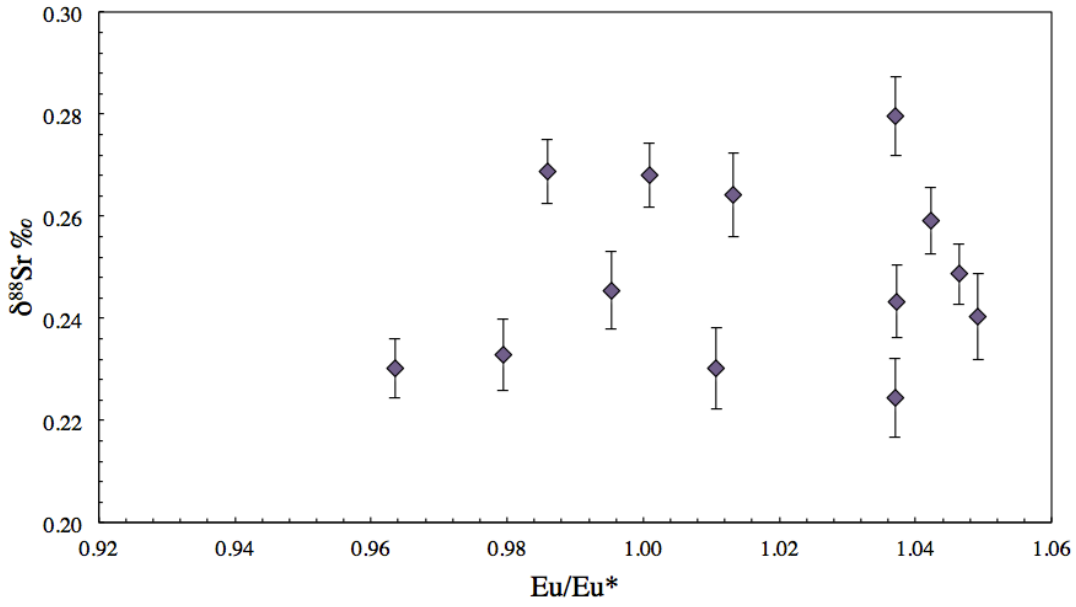

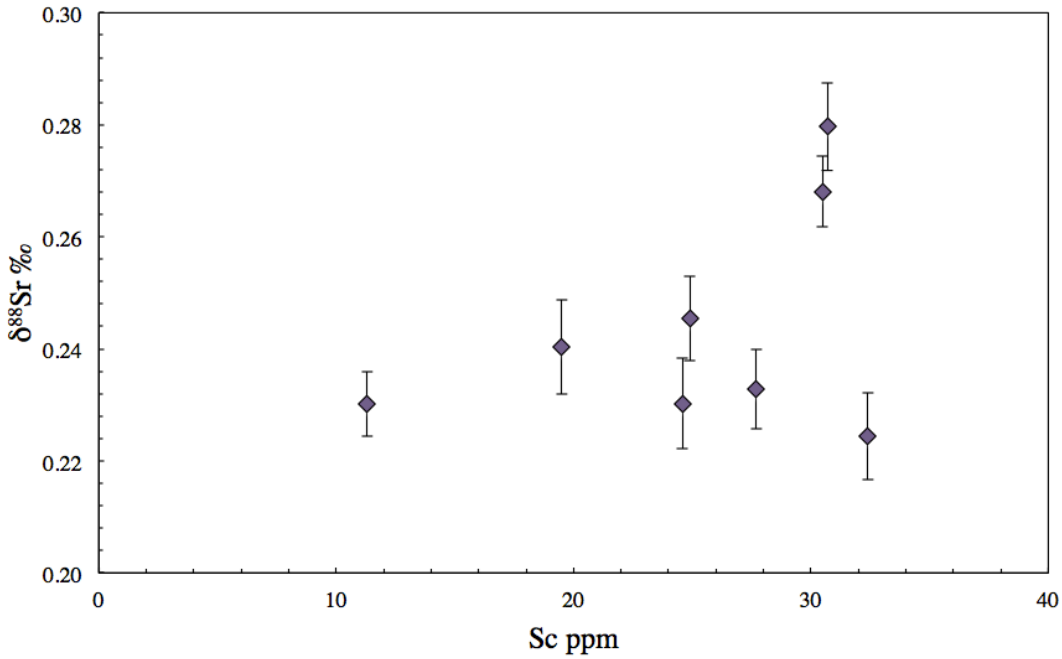

Figures 3.26 and 3.27: No relationship exists between stable $\delta^{88}Sr$ and Sc, or Eu/Eu* for OIB samples analysed in this study.

Assimilation

Isotopic variations in both $^{87}Sr/^{86}Sr$ and $\delta^{88}Sr$ may arise through assimilation of oceanic crust through which ocean basalts are typically erupted. Gabbro typically surrounds

magma chambers in which MORB form, but the absence of any δ^{88}Sr data for this lithology makes it difficult to comment on its possible assimilation. However, considering that gabbro is compositionally similar to basalt, and that both are comprised of similar minerals (pyroxene, plagioclase, amphibole and olivine) in comparable proportions, there is theoretically little reason to suggest they would possess distinct δ^{88}Sr compositions. For both OIB and MORB, the assimilation of altered oceanic crust can potentially cause the variations seen should the δ^{88}Sr composition of the assimilant be distinct. Although the δ^{88}Sr composition of altered oceanic crust is unknown, the expected effect of the incorporation of various proportions of an assimilant can be modelled by choosing end-members with hypothetical $^{87}Sr/^{86}Sr$ and δ^{88}Sr compositions. This is achieved using mass-balance calculations, based on Equation 3.4 below:

$$R_M^X = \frac{R_A^X X_A f + R_B^X X_B (1-f)}{X_A f + X_B (1-f)} \qquad \textit{Equation 3.4}$$

where R_M^X is an isotope ratio of X in a mixture of components A and B, X_A and X_B are concentrations of X in A and B, and f is the weight fraction of A.

Three hypothetical end-members were chosen to calculate the mixing lines and effects of varying degrees of assimilation. The average δ^{88}Sr value for oceanic basalts (δ^{88}Sr = 0.25) is chosen as the basalt end-member composition and the $^{87}Sr/^{86}Sr$ composition assumed to be that of MORB (~0.7029). A value of $^{87}Sr/^{86}Sr$ = 0.7069 is taken as the altered basalt end-member (Spooner et al., 1977), and end members with the following isotopic compositions were chosen: A1 δ^{88}Sr= 0.35‰ and $^{87}Sr/^{86}Sr$= 0.7069, A2 δ^{88}Sr= 0.15‰ and

$^{87}Sr/^{86}Sr$= 0.7069, and A3 $\delta^{88}Sr$= 0.35‰ and $^{87}Sr/^{86}Sr$= 0.703. The results are shown in Figure 3.28 below, where the dashed lines represent mixing lines and the symbols indicate 1, 10, 20, 30, 40% etc. additions of hypothetical assimilated material to the basalts.

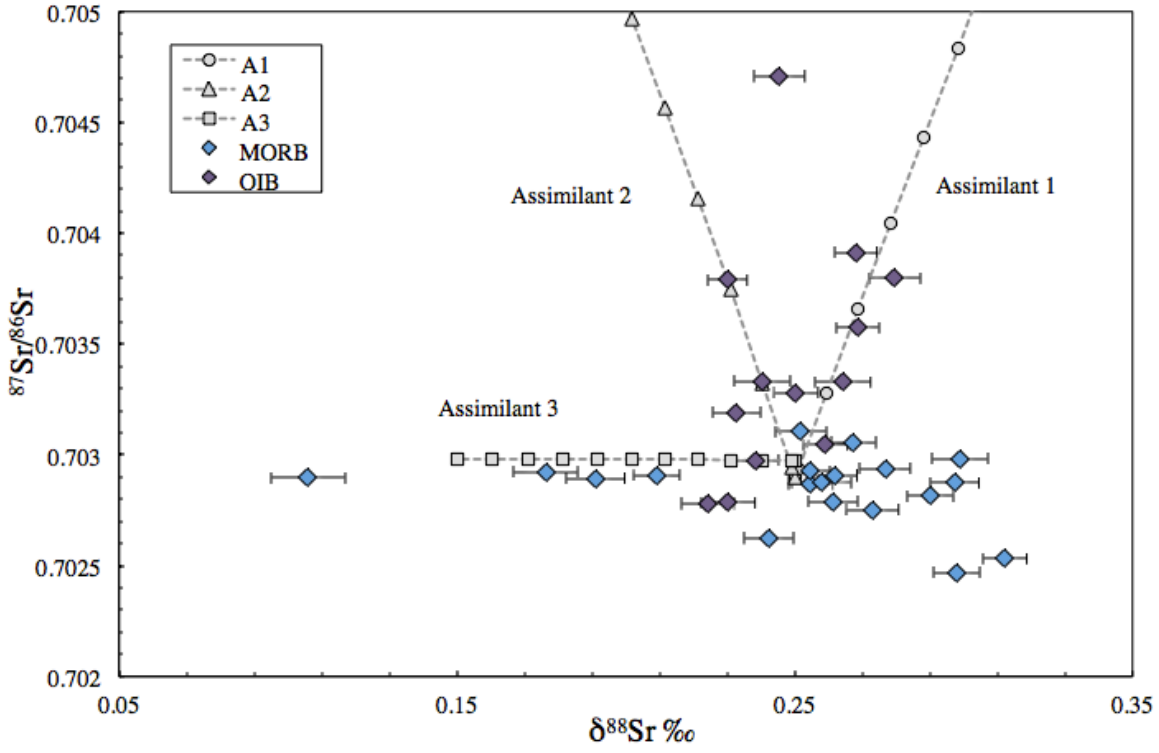

Figure 3.28: Models of the effects assimilation on the $\delta^{88}Sr$ compositions of MORB. The effects of the addition of three hypothetical end-members to the isotopic composition of basalt are shown with OIB and MORB data measured for comparison. The symbols represent additions of the assimilant in 10% increments.

Despite a substantial degree of scatter in the OIB and MORB $\delta^{88}Sr$ data, the mixing lines in Figure 3.28 indicate that a combination of several end-members can potentially cause the variations in $^{87}Sr/^{86}Sr$ and $\delta^{88}Sr$ of the OIB samples, specifically end-members A1 and A2. The composition of the first assimilant (A1) is based on an estimate of seawater-altered oceanic crust with a heavy $\delta^{88}Sr$ composition, intermediate between seawater and basalt. This model fits a number of the OIB data and suggests that assimilation of such altered crust may be responsible for the variations in $^{87}Sr/^{86}Sr$ and $\delta^{88}Sr$ observed.

However, the absence of correlations between $\delta^{88}Sr$ and indices of seawater precludes the involvement of this as a cause for $\delta^{88}Sr$ fractionation. Assimilant A2 is also based on a hypothetical value for altered oceanic crust with a light $\delta^{88}Sr$ composition closer to that of carbonates. This model also fits a number of OIB data, however, the likelihood of such an assimilant is uncertain, as the existence of an end-member with such isotopic compositions is unknown. Assimilant A3 fits the MORB data well, but has an $^{87}Sr/^{86}Sr$ composition identical to those of MORB and thus is difficult to assign to a realistic end-member component. It most closely represents the expected effects of fractional crystallisation due to the invariable $^{87}Sr/^{86}Sr$ trajectory. As such, fractional crystallisation best suites the trend in MORB samples.

3.5.2. Implications for recycling

Considering that significant heterogeneities in the source of OIBs are evident from variations in $^{87}Sr/^{86}Sr$ ratios, the relatively limited range of $\delta^{88}Sr$ compositions is surprising and contrary to expectation. A number of the sources of the OIB basalts in this study have been linked to the recycling of continental crust. Limited $\delta^{88}Sr$ data is available for much of the terrestrial environment, but that which exists suggests that rhyolites are far lighter than mantle rocks, and granites often extend to lighter compositions but are, on average, at mantle values (Charlier et al., 2012; Ohno et al., 2008; JinLong et al., 2012; Ohno and Hirata, 2007). Sediments and carbonates also possess $\delta^{88}Sr$ compositions that extend to lighter values (Ohno and Hirata, 2007; Krabbenhoft et al., 2010; Halicz et al., 2008). Given that overall it is reasonable to assume that much of the subducted material has lighter $\delta^{88}Sr$ values than oceanic basalts, it is remarkable that OIB do not differ from

MORB, nor exhibit any significant variations. One reason for this could simply be that on average, subducted material has an average $\delta^{88}Sr$ composition that is indistinguishable from the mantle, and from consideration of mass balance, evolved crustal material with light values plays a minor role and is present in small quantities.

Results from the preliminary analyses of crustal material and marine sediment suggest that generally material with a varied $\delta^{88}Sr$ composition is subducted into the mantle. The average composition of shale is $\delta^{88}Sr = \sim 0.20 \pm 0.2‰$ whilst the average of all 4 shale and basalt samples is $\delta^{88}Sr = 0.21 \pm 0.08‰$. As these do not differ drastically from one another, a simplified mass balance calculation can be made using the latter value as a representative $\delta^{88}Sr$ composition for subducted material into the mantle. Plank and Langmuir (1998) estimate subducted sediment into the mantle to have a Sr concentration of 327ppm and calculate that over 1.6 Ga, subduction of 1 km^3 of sediment per year would contribute ~0.1% by mass to the entire mantle. Assuming the mantle to have a Sr concentration of 14ppm (Condie, 1997) and a $\delta^{88}Sr$ composition of +0.25‰, taken from the average of the oceanic basalts, the expected composition of the mantle can be calculated by substituting these values into Equation 3.4. This yields a $\delta^{88}Sr$ value for the mixture of +0.248‰, which is marginally lighter than the average value of the oceanic basalts. Increasing the input of subducted material into the mantle to 4% only shifts the $\delta^{88}Sr$ value to +0.214‰. The latter value is resolvably lighter than the current estimate of the mantle based on averages of the oceanic basalts, but it is uncertain whether this amount of sediment is realistic given that an independent appraisal of subducted material has also been placed in the same region as the former calculation of 0.1% (1.65km^3 per year; Clift et al., 2009).

The expected isotopic shifts in $\delta^{88}Sr$ and $^{87}Sr/^{86}Sr$ can be modelled using mass-balance calculations to predict mixing lines between a basalt end-member and the addition of increasing fractions of subducted material. The estimate of the average $^{87}Sr/^{86}Sr$ composition of subducted material from Plank and Langmuir (1998) is used, $^{87}Sr/^{86}Sr$ = 0.71730. The results of these calculations are shown in Figure 3.29 for two end-members of material inputs. The first mixing model (Subduction 1) uses the average composition used in calculations above, and the second uses a lighter value of $\delta^{88}Sr$ = 0.15‰ (Subduction 2).

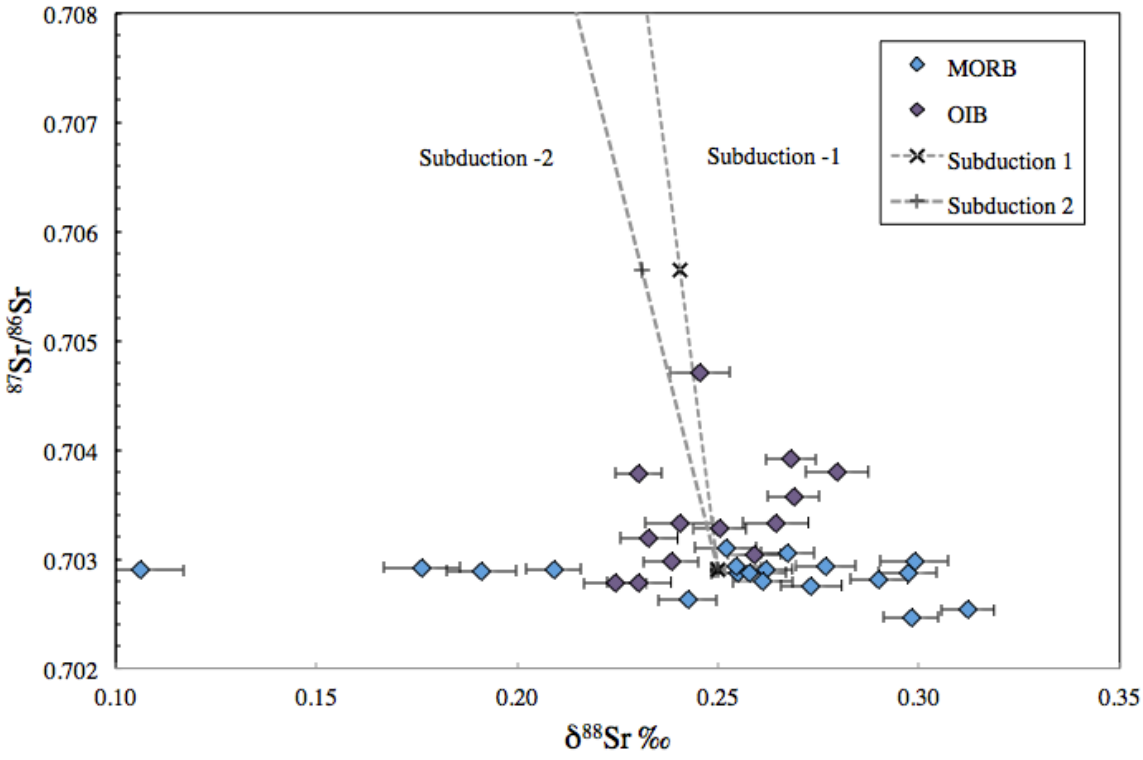

Figure 3.29: Model of the effects of subduction on the Sr isotopic composition of the mantle. The symbols represent additions of subducted material in increments of 10%.

Overall, the MORB and OIB data do not lie on these mixing lines. However, sample FDN25 is consistent with the first model and implies a contribution of roughly ~0.5% subducted sediment into the mantle source. The Sr and Nd isotopic compositions of the volcanics from Fernando de Noronha are thought to exhibit a combination of DMM and

EM1 signatures (Gerlach et al., 1987; Lopes, 1997), which is consistent with sediment in the mantle source. However, more detailed analyses are required to accurately constrain the range and $\delta^{88}Sr$ composition of subducted material before such conclusions can be made. On the whole, these simple mass-balance calculations suggest that the $\delta^{88}Sr$ composition of the mantle is not considerably transformed by inputs into the mantle from subduction and recycling despite the lighter compositions of the inputs relative to the mantle melts. To a small degree, however, they can account for the $^{87}Sr/^{86}Sr$ and $\delta^{88}Sr$ data of the OIB samples analysed here.

3.6. Conclusions

This work has shown that high precision DS-TIMS analyses are required to reveal the variations in the $\delta^{88}Sr$ composition that exist for oceanic basalts, previously considered to possess a relatively uniform composition. Mid-ocean ridge basalts show large resolvable variations in $\delta^{88}Sr$ of ~0.14‰, from $\delta^{88}Sr = +0.312 \pm 0.007$ to $+0.176 \pm 0.010$‰. Much of this variation is seen within a single sample area; the FAMOUS segment. The average composition of basalts from the Atlantic, Indian and Pacific Ridges are indistinguishable. These MORB possess an average $\delta^{88}Sr$ value of 0.260 ± 0.009‰ (2 se; n= 18) with a variance of 0.0013; four times greater that seen in OIBs. Negative covariations between $\delta^{88}Sr$ and Eu/Eu*, and heavy $\delta^{88}Sr$ values of plagioclase separates, are consistent with fractionation due to fractional crystallisation through the preferential partitioning of the heavy isotopes of Sr into plagioclase. However, the tenuous $\delta^{88}Sr$ - Eu/Eu* trend suggests an additional factor affects the $\delta^{88}Sr$ compositions of basalts, most likely mantle source heterogeneity on small scales. Models of the expected shifts in the $^{87}Sr/^{86}Sr$ and $\delta^{88}Sr$

composition of two-component mixing between basaltic melts and hypothetical end-members indicate that the assimilation of altered oceanic crust can, to some degree, account for the Sr isotope variations observed MORB. However, the $\delta^{88}Sr$ composition of such an assimilant are undetermined, and thus the probability of such a process accounting for the variations in $\delta^{88}Sr$ compositions is uncertain. The absence of correlations between Sr isotopes and indices of seawater suggests that the assimilation of seawater, and altered oceanic crust, has not demonstrably affected Sr isotopes.

Some of the first data for OIBs indicate that they exhibit relatively limited variations in $\delta^{88}Sr$, ranging from $\delta^{88}Sr$ = +0.280 ± 0.008 to +0.224 ± 0.018‰. The average compositions of MORB and OIB are indistinguishable from each other. Overall, OIBs are homogenous in $\delta^{88}Sr$ with a low variance of 0.0003 and an average value of $\delta^{88}Sr$ =0.248 ± 0.004‰ (2 se; n= 15). These restricted compositions reflect a moderately small degree of fractional crystallisation and an apparent uniform $\delta^{88}Sr$ composition of the mantle sources. This implies that various mantle source end-members have similar $\delta^{88}Sr$ compositions, or else they release melts of a similar composition. Correlations between the $\delta^{88}Sr$ values of OIB and indicators of plagioclase and clinopyroxene fractionation are absent; implicative that neither has a dominant role in causing the variations observed, though more analyses are required. In spite of overwhelming evidence for large scale heterogeneities in the mantle source based on $^{87}Sr/^{86}Sr$ data, the relatively uniform $\delta^{88}Sr$ composition of OIBs globally suggests that the average composition of subducted material is indistinguishable from that of the mantle, regardless of the input of evolved continental crust which often possesses lighter values (Charlier et al., 2012). Mass-balance calculations using preliminary shale analyses support this view, and provide little evidence for an adjustment of the average mantle $\delta^{88}Sr$ composition with realistic amounts of subducted material.

CHAPTER FOUR

The stable Sr isotope composition of magmatic minerals

Abstract

Co-existing mineral pairs from three igneous systems have been analysed for their $\delta^{88}Sr$ and $^{87}Sr/^{86}Sr$ compositions to probe the causes of $\delta^{88}Sr$ fractionation on a mineral scale. Plagioclase, clinopyroxene and their complementary melt fraction were investigated from a MORB basalt from the Mid-Atlantic and a basalt from Mt. Silvestri in Italy. An additional plagioclase-clinopyroxene pair and anorthositic plagioclase cumulate were analysed from the layered Skaergaard intrusion in East Greenland. The $\delta^{88}Sr$ compositions of plagioclase vary from $\delta^{88}Sr = 0.004 \pm 0.007$ to 0.348 ± 0.008‰ and those of clinopyroxene range from $\delta^{88}Sr = 0.241 \pm 0.006$ to 0.324 ± 0.008‰. Fractionation of these minerals, relative to the melt, varies from -0.26 to 0.21‰ and 0.06 to -0.02‰, respectively. Overall, there are considerable differences in the behaviour of $\delta^{88}Sr$ in the minerals of these three systems. However, resolvable variations in the $^{87}Sr/^{86}Sr$ ratios of the minerals and melts indicate they may have undergone contamination, or are not in equilibrium.

4.1. Introduction

Measurements of the isotopic composition of magmatic minerals provide evidence of the fractionation effects caused by mineral – melt separation, which allow a more accurate insight into the control that phases have on the whole rock composition. These allow a better determination of what phases certain isotopes of an element partition into, and thus what processes are responsible for isotope fractionation and how this occurs. Mineral phases in a given rock may not always be in equilibrium with one another or with the melt from which they crystallise. In this regard, for sufficiently young rocks, measurement of the radiogenic isotopes may offer an indication as to whether phases are in equilibrium with one another, as they are not fractionated by mass dependent processes and thus if in equilibrium should be identical for all the phases present.

The data presented in chapter 3 outlines evidence of fractionation of $\delta^{88}Sr$ in whole rock MORB samples. Analyses of two plagioclase feldspar separates and the corresponding glasses from which they crystallised provides clear evidence that $\delta^{88}Sr$ fractionation accompanies plagioclase crystallisation, with the heavier isotopes of Sr partitioning into the mineral phase, which is in agreement with previous studies (Charlier et al., 2012). Aside from these and a K-feldspar geostandard SRM607, found to be isotopically light ($\delta^{88}Sr = -0.07 \pm 0.06$ ‰), there is a lack of $\delta^{88}Sr$ data for minerals, particularly other than feldspar. This study aims to determine the $\delta^{88}Sr$ composition of magmatic minerals that commonly constitute igneous rocks that have the potential to influence the Sr isotope composition. Common major rock forming silicate minerals likely to affect the isotopes of Sr (i.e. partition coefficients of >1) were analysed: plagioclase and clinopyroxene, whereas minerals present in minor quantities, such as apatite, were not analysed due to their low Sr concentrations.

4.2. Geological background of samples

4.2.1. Skaergaard mineral separates

The layered Skaergaard intrusion in East Greenland is a classic example of in-situ differentiation of basic magma (e.g. McBirney, 1975). The intrusion is thought to have formed from a single pulse of tholeiitic magma during the opening of the North Atlantic 55 Ma years ago (Schwarz et al., 1979; Hirschmann et al., 1997; McBirney, 1996) and differentiated by fractional crystallisation upon cooling after its emplacement forming a layered sequence of cumulate differentiates in a closed system (Wager and Deer, 1939; Wager and Brown, 1968;). As such, it offers a unique opportunity to investigate the effect that crystal formation during magmatic differentiation might have on stable Sr isotopes, and clinopyroxene and plagioclase separates from whole rock samples from two sections in the layered sequence were separated and analysed. Sample 5321 is located from the Upper Zone (UZa) and is described by Wager (1960) as a plagioclase-magnetite cumulate or anorthositic ferrodiorite, and sample 5112 is from the Lower Zone (LZb) and described as an olivine gabbro (average rock). Sample 5321 is thought to have formed after 97.7% of magma had solidified, and sample 5112 after 86.6% solidification (Dissanayake, 1976). Strontium and Nd isotope studies suggest minimal (<4%) contamination of the magma by crustal sources (Stewart and DePaolo, 1990; McBirney and Creaser, 2003), but the variable $\delta^{18}O/^{16}O$ compositions of several samples suggest alteration throughout the intrusion by meteoric waters (Taylor and Forester, 1979). Sample 5112 has a whole-rock $\delta^{18}O/^{16}O$ value of +5.9‰ (Taylor and Epstein, 1962), which is close to primary mantle values. There is no $\delta^{18}O$ data for sample 5321, but it is geographically located very close to 5181, which has a $\delta^{18}O_{\text{plagioclase}}$ value of +6.4‰, identical to that of sample 5112 (Taylor and Forester, 1979). The primary $\delta^{18}O$

signatures of both samples indicate that they are unlikely to have been affected by hydrous contamination. The minerals had been separated previously to 99% purity (Dissanayake and Vincent, 1972), and were further handpicked using an optical microscope.

4.2.2. Mt. Silvestri mineral separates

The Skaergaard intrusion is comprised entirely of cumulates and thus lacking a glass (melt) component. As such, only inter-mineral fractionation factors can be obtained unless the starting melt composition is known or can be reasonably estimated. As the stable Sr isotope composition of primary mafic melts has already been shown to vary (in Chapter 3), a mineral-melt system has also been analysed to allow the direct determination of mineral-melt fractionation factors. Mt. Silvestri is located on Mt. Etna, Italy, and historic lavas at Mt. Silvestri form part of a trachy-basaltic suite, considered to result partly from low-pressure crystal fractionation and partly as a consequence of mixing of distinct mantle sources (e.g. Clocchiatti and Metrich, 1984; Schiano et al., 2001). The lavas are hypocrystalline in texture, containing porphyritic minerals set in a groundmass of finer grained material or glass, which allows both the minerals and glass to be analysed. A plagioclase separate, clinopyroxene separate, and glass from a basalt (MgO = 5.73%) of the 1892 eruption have been analysed (Clocchiatti and Metrich, 1984). In addition to the minerals studied, the lavas contain phenocrysts of olivine, magnetite, spinel and Fe-Ti oxides in a fine-grained groundmass.

4.3. Results

The $\delta^{88}Sr$ and $^{87}Sr/^{86}Sr$ data of the minerals are given in Table 4.1. Calculated fractionation amounts for mineral-mineral pairs and mineral-melt pairs are given in Table 4.2, using Equation 4.1. For the Skaergaard samples, mineral-melt fractionation amounts are calculated assuming that they crystallised from a mafic melt with a composition of $\delta^{88}Sr$= 0.26‰, taken from the average of MORB analysed in Chapter 3.

$$\Delta_{A\text{-}B} = \delta_A - \delta_B \qquad \textit{Equation 4.1}$$

Sample	Mineral	Location	$^{87}Sr/^{86}Sr$	± 2 se	$\delta^{88}Sr$ ‰	± 2 se
5112 plag	Plagioclase	Skaergaard	0.704284	0.000002	0.248	0.006
5112 cpx	Clinopyroxene	Skaergaard	0.704593	0.000002	0.324	0.008
5321 plag	Plagioclase	Skaergaard	0.704375	0.000002	0.348	0.008
Silvestri plag	Plagioclase	Mt Silvestri	0.703482	0.000002	0.004	0.007
Silvestri cpx	Clinopyroxene	Mt Silvestri	0.703514	0.000002	0.241	0.006
Silvestri glass	Glass	Mt Silvestri	0.703560	0.000003	0.466	0.007
Other samples						
522-1-1 plag	Plagioclase	FAMOUS	0.702946	0.000013	0.31	0.03
522-1-1 glass	Glass	FAMOUS	0.702896	0.000002	0.106	0.011
ARP 74 11-18 plag	Plagioclase	FAMOUS	0.702939	0.000016	0.34	0.03
ARP 74 11-18 glass	Glass	FAMOUS	0.702869	0.000003	0.255	0.006

Table 4.1: $\delta^{88}Sr$ and $^{87}Sr/^{86}Sr$ mineral data for the Skaergaard, Silvestri and MORB samples.

Mineral-melt	Mineral $\delta^{88}Sr$ ‰	Melt $\delta^{88}Sr$ ‰	Fractionation, Δ ‰
$\Delta_{5112plag\text{-}melt}$	0.25	0.26	-0.01
$\Delta_{5112cpx\text{-}melt}$	0.32	0.26	0.06
$\Delta_{5321plag\text{-}melt}$	0.35	0.26	0.09
$\Delta_{Silvplag\text{-}melt}$	0.00	0.47	-0.26 ± 0.01
$\Delta_{Silvcpx\text{-}melt}$	0.24	0.47	-0.02 ± 0.08
$\Delta_{522plag\text{-}melt}$	0.31	0.11	0.21 ± 0.03
$\Delta_{ARPplag\text{-}melt}$	0.34	0.26	0.08 ± 0.03

Mineral-mineral	**Mineral δ^{88}Sr ‰**	**Mineral δ^{88}Sr ‰**	**Fractionation, Δ ‰**
$\Delta_{5112plag-cpx}$	0.25	0.32	-0.08 ± 0.01
$\Delta_{Silvplag-cpx}$	0.00	0.24	-0.24 ± 0.01

Table 4.2: Fractionation factors of both mineral-mineral and mineral-melt pairs. Uncertainties for 5112 and 5321 cannot be calculated, as the melt value is an assumption.

Figure 4.1 illustrates the $^{87}Sr/^{86}Sr$ composition of the Skaergaard samples with their $\delta^{88}Sr$ values. Figure 4.2 illustrates the same for the Mt. Silvestri system, and Figure 4.3 the MORB samples.

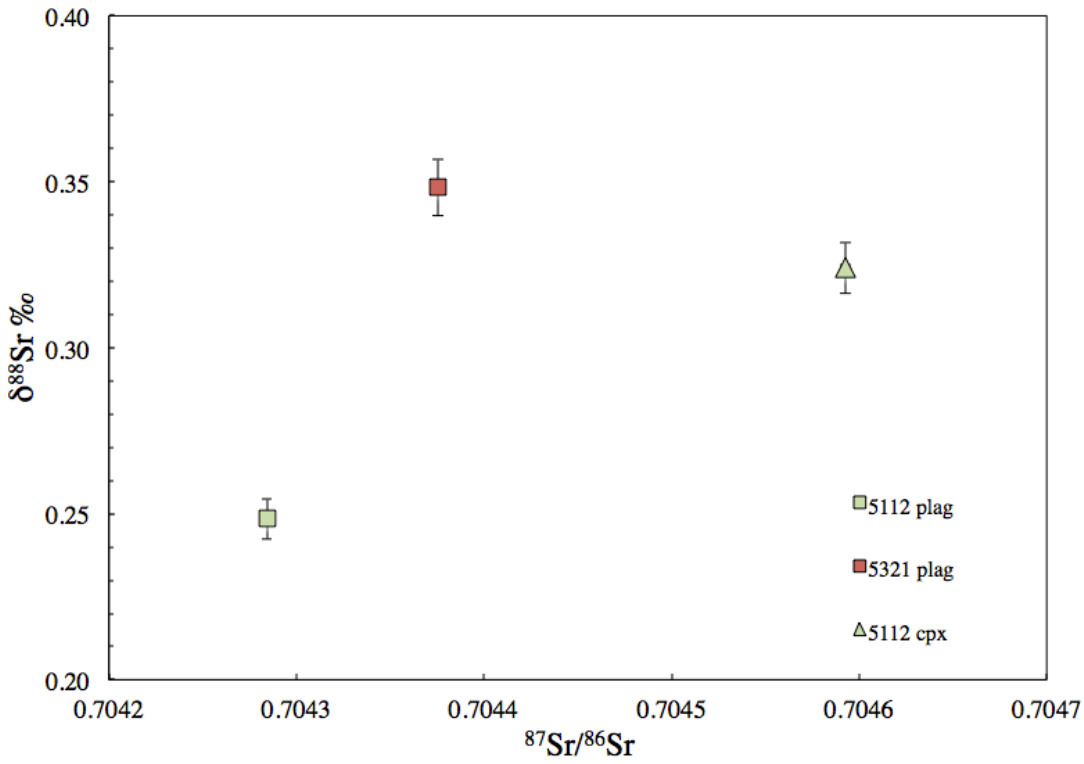

Figure 4.1: $^{87}Sr/^{86}Sr$ and $\delta^{88}Sr$ data for the Skaergaard minerals.

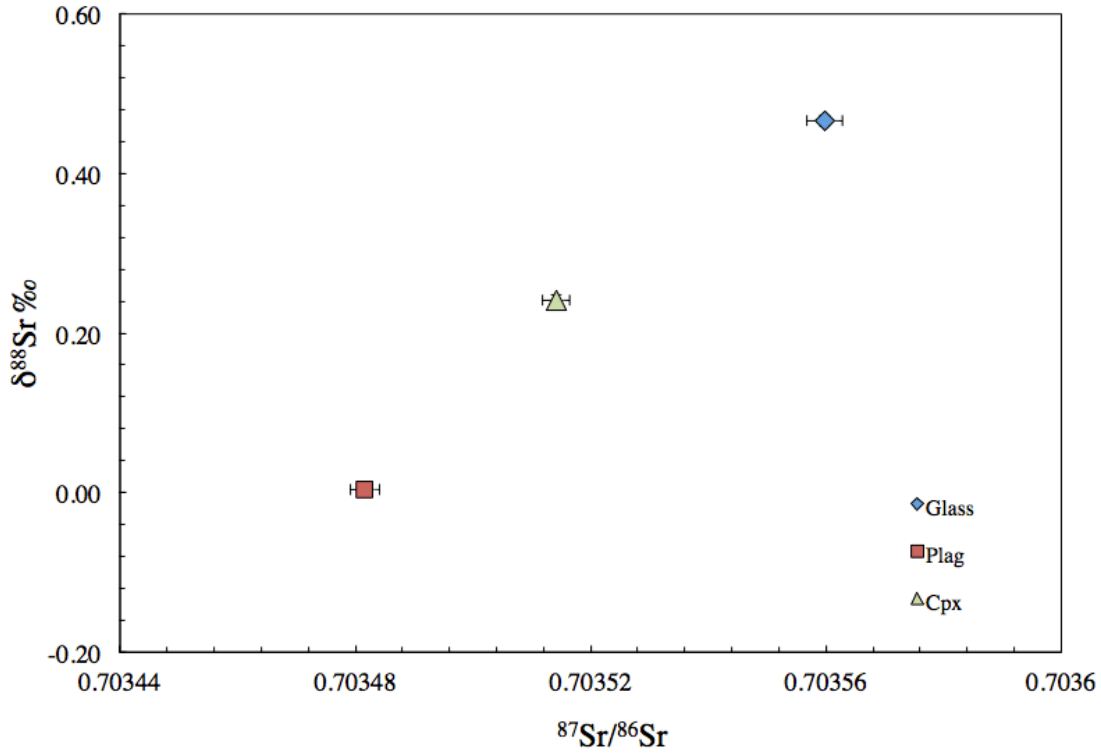

Figure 4.2: $^{87}Sr/^{86}Sr$ and $\delta^{88}Sr$ data for the Mt. Silvestri minerals and glass.

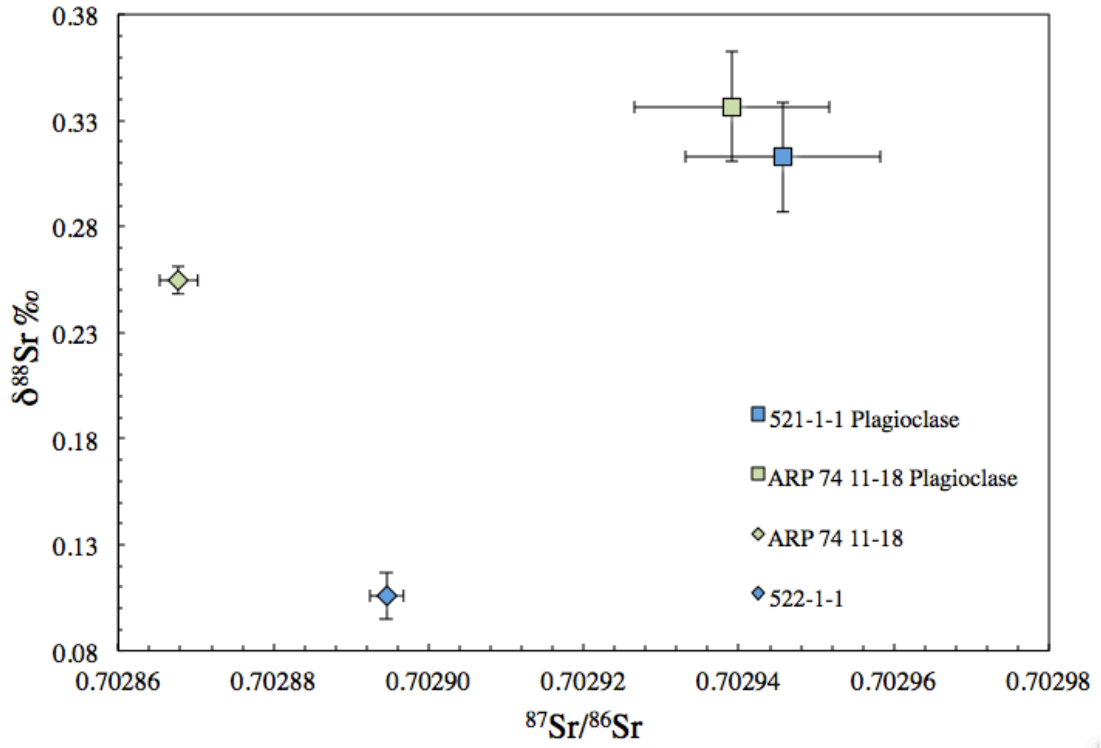

Figure 4.3: $^{87}Sr/^{86}Sr$ and $\delta^{88}Sr$ data for the FAMOUS MORB minerals and glasses.

4.4. Discussion

4.4.1. Mineral data

The minerals analysed span a wide range of $\delta^{88}Sr$ values from +0.004 ± 0.007‰ for the Silvestri plagioclase to +0.348 ± 0.008‰ for the Skaergaard 5321 plagioclase. In a single magmatic system, Silvestri, a variation in $\delta^{88}Sr$ of ~0.46‰ exists between the minerals and the glass, which is significant at high temperature.

4.4.2. Skaergaard

The plagioclase-clinopyroxene pair for sample 5112 shows resolvable offsets in both stable and radiogenic Sr isotope compositions. Clinopyroxene has a heavier $\delta^{88}Sr$ composition than the plagioclase, and a more radiogenic $^{87}Sr/^{86}Sr$ composition. The resolvable difference in $^{87}Sr/^{86}Sr$ may suggest that contamination has occurred during crystallisation, or that one of these phases has grown in an earlier melt with a different composition. Studies of the $\delta O^{18}/O^{16}$ composition of minerals from sample 5112 indicate a value of +6.8 ±0.2‰ for plagioclase and +5.6 ±0.1‰ for clinopyroxene, which suggests that these two phases are not in isotopic equilibrium, however, this is a common feature for many igneous rocks and not necessarily due to secondary processes (Taylor and Epstein, 1962). Given the antiquity of Skaergaard formation, the minerals may have been in equilibrium during fractionation but subsequently evolved contrasting radiogenic values due to different abundances of Sr and Rb. This is the most plausible explanation given that contamination due to hydrothermal or meteoric water is considered improbable in the Lower Zone section (McBirney and Creaser, 2003), as alteration by late stage liquids is thought to have permeated the upper levels of the intrusion, and contamination of the magma by surrounding host rock is considered minimal (2-4%; Stewart and DePaolo, 1990).

4.4.3. Mt. Silvestri

Both plagioclase and clinopyroxene of the Mt. Silvestri magmatic system are lighter in $\delta^{88}Sr$ than the melt, and the plagioclase is lighter than clinopyroxene. This suggests that the lighter isotopes of Sr partition into the minerals, and the lighter isotopes primarily into plagioclase, contrary to what is believed to occur from $\delta^{88}Sr$ studies of whole rock data and mineral data (Chapter 3). The very light composition of plagioclase feldspar is, however, similar to the value obtained for the alkali-feldspar standard SRM607 by Charlier et al. (2012), $\delta^{88}Sr$ = -0.07 ±0.06. However, the $^{87}Sr/^{86}Sr$ compositions of the minerals are resolvably different from one another as well as from their glass counterpart, which is again suggestive of contamination or isotopic disequilibrium between the minerals. As the lavas are historic, there is insufficient time for radiogenic in-growth of $^{87}Sr/^{86}Sr$ to account for the changes observed. There is a strong positive correlation between $^{87}Sr/^{86}Sr$ and $\delta^{88}Sr$- this could be indicative of a crystallisation sequence throughout the system, or pervasive contamination with material with an isotopically distinct $\delta^{88}Sr$ and $^{87}Sr/^{86}Sr$ composition. For the former, plagioclase may have crystallised first, from a melt with a less radiogenic $^{87}Sr/^{86}Sr$ and lighter $\delta^{88}Sr$ composition, and clinopyroxene later from a melt with an increasingly more radiogenic $^{87}Sr/^{86}Sr$ and heavier $\delta^{88}Sr$ composition to leave the melt with the most radiogenic $^{87}Sr/^{86}Sr$ and heaviest $\delta^{88}Sr$ values. The latter is also plausible given that contamination with a sedimentary component of the host rock through which it is erupted is thought to occur throughout the Mt. Silvestri lavas and minerals (Clocchiatti and Metrich, 1984). This sedimentary contaminant may be sandstone, carbonate, clay, or some combination of all three. Contamination by carbonate with a light $\delta^{88}Sr$ composition and low $^{87}Sr/^{86}Sr$ ratio can be responsible for the differences in both in the minerals of the system, and lead to unrepresentative

mineral fractionation factors. However, carbonates tend to possess a more radiogenic $^{87}Sr/^{86}Sr$ signature than mantle-derived melt (Ohno and Hirata, 2007; Krabbenhoft et al., 2010; Halicz et al., 2008), which would lead to increasingly more radiogenic values in contaminated minerals.

Based on variations in B, Sr, Nd isotope ratios in whole rock and mineral samples, Tonarini et al. (2001) proposed mixing between neighbouring Mt. Etna magmas and a subduction-like fluid phase with an $^{87}Sr/^{86}Sr$ composition of ~0.708. This would be applicable to the related Silvestri system, whose lavas have $^{87}Sr/^{86}Sr$ values in a similar range (0.7034). However, again, the contamination appears to be the reverse to that expected from the order of crystallisation unless both phases crystallised prior to extensive contamination with such fluids. Under these circumstances, it is highly likely that the minerals and glass show contamination with a sedimentary component typical of Silvestri lavas, or simply a crystallisation sequence reflecting a melt of variable $^{87}Sr/^{86}Sr$ and $\delta^{88}Sr$ composition. In either case, it is unclear to what extent the $\delta^{88}Sr$ value of the minerals relative to the melt is representative of the true $\delta^{88}Sr$ fractionation factor.

4.4.4. Fractionation factors

The $\delta^{88}Sr$ fractionation factors for both inter-mineral and mineral-melt pairs based on the mineral data are variable, ranging from -0.24 ± 0.01 to -0.08 ± 0.01 for $\Delta_{plagioclase\text{-}clinopyroxene}$, -0.26 ± 0.01 to +0.21 ± 0.03 for $\Delta_{plagioclase\text{-}melt}$, and -0.02 ± 0.08 to 0.06 for $\Delta_{clinopyroxene\text{-}melt}$. For Skaergaard, the only reliable fractionation factors calculated from the mineral data are for the inter-mineral pair for sample 5112, as the mineral-melt fractionation factors are calculated assuming a melt $\delta^{88}Sr$ composition, whilst $\delta^{88}Sr$ values of primary basaltic melts are know to vary (Chapter 3). It is

interesting to note that for both 5112 and Silvestri plagioclase is consistently lighter in $\delta^{88}Sr$ than clinopyroxene, resulting in negative $\Delta_{plagioclase\text{-}clinopyroxene}$ values, whereas it has been commonly considered (Chapter 3; Charlier et al., 2012) that plagioclase play a dominant role in causing $\delta^{88}Sr$ fractionation of melts to light values. It is unknown if, and to what extent, either of these systems are contaminated, however, which places a significant uncertainty on the validity of the mineral data and derived $\delta^{88}Sr$ fractionation factors. The same applies to the MORB mineral data, as the $^{87}Sr/^{86}Sr$ values of the minerals differ from those of the glass, suggestive of disequilibrium between the mineral-melt pairs (Figure 4.3). Nevertheless, the fractionation factors determined for the MORB plagioclase-melt pairs, (0.08 ± 0.03 and 0.21 ± 0.03) are positive, suggesting that plagioclase crystallisation causes $\delta^{88}Sr$ fractionation by the heavier isotopes of Sr preferably partitioning into plagioclase to leave the residual melt isotopically light. This is what is expected from whole rock MORB data (Chapter 3), and also consistent with previous modelling by Charlier et al. (2012).

4.5. Conclusions

The $\delta^{88}Sr$ compositions of plagioclase were found to vary from $\delta^{88}Sr$ = 0.004 ± 0.007 to 0.348 ± 0.008‰ and those of clinopyroxene from $\delta^{88}Sr$ = 0.241 ± 0.006 to 0.324 ± 0.008‰. Fractionation factors for these minerals, relative to the melt, vary from -0.26 ± 0.01 to 0.21 ± 0.03, and 0.06 to -0.02 ± 0.08, respectively. Plagioclase is always light in $\delta^{88}Sr$ relative to clinopyroxene in both Skaergaard and Mt. Silvestri, and both clinopyroxene and plagioclase are found to be isotopically light relative to the melt in Mt. Silvestri lavas. However, variations in radiogenic $^{87}Sr/^{86}Sr$ in addition to evidence for contamination of the Silvestri lavas, combined with the absence of melt data for Skaergaard, question the validity of the fractionation factors calculated

for $\delta^{88}Sr$ for these systems. Fractionation factors for the MORB plagioclase-glass pairs, of $\Delta_{plagioclase\text{-}melt}$ = +0.08 to +0.21 are obtained. However, resolvable variations in $^{87}Sr/^{86}Sr$ between plagioclase and the melt imply that the mineral-melt pairs may not be in equilibrium.

CHAPTER FIVE

Well-resolved stable and radiogenic Sr isotope variations associated with magmatic differentiation at Hekla

Abstract

A suite of co-genetic rocks ranging from basaltic to rhyolitic in composition from Hekla, Iceland, have been analysed for their $^{87}Sr/^{86}Sr$ and $\delta^{88}Sr$ isotope compositions by DS-TIMS. Variations in $^{87}Sr/^{86}Sr$ from 0.703166 ± 0.000002 for a basalt to $^{87}Sr/^{86}Sr$ = 0.703220 ± 0.000005 for a rhyolite are reported, which are correlated with SiO_2 content. These variations in $^{87}Sr/^{86}Sr$ are the first reported for Hekla as such small variations can only be detected by the high precision of the TIMS measurements of this study. Resolvable variations in $\delta^{88}Sr$ are also observed, ranging from +0.29 ± 0.01‰ for basalt to +0.15 ± 0.01‰ for rhyolite. Shifts to more radiogenic $^{87}Sr/^{86}Sr$ values and lighter $\delta^{88}Sr$ compositions may either be coupled and due to assimilation of an altered basalt with secondary carbonate present, or de-coupled and a result of two super-imposed processes; assimilation of unaltered basalt and magmatic differentiation. For the latter, fractional crystallisation and removal of plagioclase and/or clinopyroxene during magmatic differentiation could be responsible for driving the melt composition to isotopically light $\delta^{88}Sr$ values.

5.1 Introduction

Chapter 3 investigates the range of stable Sr fractionation in mafic products of mantle melts. This largely concerns the processes involved in mantle melting and the resulting basaltic oceanic curst. The continental crust constitutes a minor percentage of the bulk silicate earth (0.6%), but comprises ~70% of the total volume of the crust and exhibits a far wider range of compositions than the oceanic crust. The processes involved in generating these extreme compositions have the potential to fractionate the stable isotopes of Sr, like many other heavy stable isotopes (e.g. Fe, V, Si). Another motivation for studying evolved crustal material is the impact of weathering and surface run-off from such material on low temperature environments such as rivers and the marine realm. The considerable interest in the low temperature environment regarding stable Sr merits investigation and quantification of the extent of stable Sr fractionation in evolved continental crust, as weathering of such crust may play an important role in the global weathering cycle of Sr.

The stable Sr isotope composition of evolved crustal igneous rocks has been investigated previously. Andesitic geostandards have previously shown no fractionation in $\delta^{88}Sr$ relative to basalts: JA-2 has a $\delta^{88}Sr$ value of 0.25‰± 0.01‰ (Ohno and Hirata, 2007) and AVG-2 a composition of $\delta^{88}Sr$ = 0.27‰± 0.09‰ (Moynier et al., 2010). Charlier et al. (2012) analysed a more comprehensive range of terrestrial igneous samples including 5 basalts, an andesite, a granodiorite, granite, quartz latite and 5 rhyolites. The quartz latite and rhyolites possess distinctly lighter $\delta^{88}Sr$ values, ranging from $\delta^{88}Sr$ = + 0.20 ± 0.06 to - 0.19 ± 0.13‰, than the remaining samples which possess a restricted range of $\delta^{88}Sr$ = + 0.30 ± 0.07‰ (2 s.d.). These data suggest that the more evolved igneous rocks, such as rhyolites, may possess lighter Sr stable isotope

compositions, which in turn indicates that these isotopes are fractionated by magmatic processes (Chapter 1; Figure 1.2). However, as these authors used MC-ICP-MS in combination with sample standard bracketing, the variations found in stable Sr isotope compositions are relatively small compared to the ~±60 ppm precision and cannot be resolved from one another. Moreover, the evolved rocks studied came from a variety of localities rather than from a single suite of co-magmatic rocks. This is potentially problematic, as each of the melts may possess varying initial Sr and Rb contents and fractionation between samples is then difficult to relate to one other should their initial δ^{88}Sr composition vary. Nevertheless, these authors found a co-variation between europium anomalies and the stable Sr isotope compositions, and on this basis hypothesised that isotope fractionation was caused by the preferential incorporation of the heavy isotopes of Sr into plagioclase with a fractionation factor of ~1.0007 for ^{88}Sr/^{86}Sr. The possibility that the stable isotopes of Sr fractionate during magmatic evolution invites further investigation. In order to better understand the processes that control the isotope variations the suite of rocks should ideally be from a single source, and measured to a higher precision.

The volcano of Hekla and its eruptive products provide the ideal opportunity to investigate the effects of fractional crystallization and other magmatic processes on the stable isotopes of Sr from a single suite of primitive to evolved igneous rocks, considered relatively unaffected by crustal and secondary processes. Hekla has been widely studied for a number of reasons, which work to the advantage of the study undertaken here. Firstly, Hekla is situated in SW Iceland which itself lies along the oceanic Mid-Atlantic Ridge spreading centre. At oceanic spreading centres mafic magmas are primarily erupted, which comprise the majority of rocks in Iceland thereby avoiding the potential contamination of material erupting through older more evolved

continental crust. Secondly, Hekla is unusual as it one of few volcanoes that produce a range of rock types, from basalt to rhyolite, from a single co-genetic source. This eruption of both mafic and felsic material, with little or none of intermediate composition, from a single volcanic centre is known as bi-modal volcanism. The lavas at Hekla have been the subject of a number of studies of other stable isotope systems including O, Fe, Li, Si, and V (Sigmarsson et al., 1992b; Schuessler et al., 2009; Savage et al., 2011; Prytulak et al., 2012). The results of these studies have been taken to rule out sedimentary, meta-sedimentary or hydrothermal processes, which may also affect stable isotopes (e.g Schuessler et al., 2009; Sigmarsson et al., 1992b; Thirlwall, 2006). Lastly, Hekla is a currently active volcano and has erupted the entire range of materials in recent, historic, times, negating any radiogenic in-growth effects on the $^{87}Sr/^{86}Sr$ ratio.

An additional point of interest when investigating the Sr isotopic composition of Hekla and its magmatic products is the much-disputed radiogenic Sr composition of the volcano and Iceland in general. Many studies have been undertaken in this regard, both for Hekla and Iceland (e.g. Hemond et al., 1988; Condomines et al., 1983; Hart et al., 1973; Sigmarsson et al., 1992a; Sigmarsson et al., 1992b; Chekol et al., 2011; O'Nions and Grönvold, 1973; O'Nions and Pankhurst, 1973). Most of these analyses were carried out several decades ago by methods delivering data of a much lower precision than that achievable at the present day. More recent analyses such as that undertaken by Sigmarsson et al. (1992b) report no measurable variation in $^{87}Sr/^{86}Sr$ for the wide compositional range of Hekla lavas, while an ID-TIMS study find varying $^{87}Sr/^{86}Sr$ compositions in the very recent dacites from the 2000 eruption at Hekla, but infer these to be the products of crustal melting and therefore have a different source to the less evolved lavas (Chekol et al., 2011). Thus far, it has been assumed that a range of

primitive to evolved material from Hekla possess indistinguishable $^{87}Sr/^{86}Sr$ compositions. The external precision of the former study is not specified, but the average internal precision (~±30 ppm) is a factor of 10 larger than the current analytical precision of DS-TIMS techniques, while the latter study only investigated material of basaltic to basaltic andesite compositions. Variations may, however, exist below the detection limit of such studies. If present, variations in the $^{87}Sr/^{86}Sr$ ratio have the potential to reveal information regarding processes such as contamination, assimilation or mixing with a magmatic or non-magmatic contaminant. On the other hand, a homogenous $^{87}Sr/^{86}Sr$ composition limits the absence of such processes. The DS-TIMS technique can act as a more sensitive measure to further constrain whether variations do exist in the $^{87}Sr/^{86}Sr$ ratio in the Heklas lavas.

In this chapter, $\delta^{88}Sr$ and $^{87}Sr/^{86}Sr$ data are presented for a suite of co-genetic extrusive rocks collected from Hekla, spanning the extent of the silica range. This work investigates the products of crustal differentiation ranging in composition from basaltic to rhyolitic, and as such, the effects of fractional crystallisation and crustal evolution on stable Sr isotopes. This study contributes to our understanding of the processes that occur during igneous differentiation, the causes of Sr isotopic variation (both stable and radiogenic) and the consequences for the weathering of such rocks and the global Sr cycle in general.

5.4 Geological background

The volcano of Hekla lies in the South Iceland Volcanic Zone in the south-western part of the island, which itself is situated along the Mid-Atlantic Ridge in the Atlantic Ocean (Fig. 5.1). Hekla is an active fissure volcano and, as one of the most active volcanoes in Iceland, has erupted 18 times since 1104 A.D., most recently in 2000. Hekla itself is estimated to be less than 7000 years old, with the oldest documented eruption dating back to ~1000 BC (Sigmarsson et al., 1992b). The samples analysed were collected from flows dating back to an oldest age of 4000 years (Savage et al., 2011) and a youngest age of 23 years. Eruptions on Hekla typically begin with an explosive Plinian or sub-Plinian phase followed by quieter effusive activity and lava outpouring, during which most of the extrusive material is ejected. During these eruptions the composition of the eruptive products changes from more differentiated and evolved acidic SiO_2-rich andesite, dacite or rhyolite initially, to more primitive and less evolved SiO_2-poor basaltic andesite. The initial SiO_2 content of the primary Plinian stage products correlates with the repose time between eruptions, where longer inactive periods produce the most SiO_2-rich tephras (Thorarinsson and Sigvaldason, 1972). Basalt is erupted from fissure vents on the flanks of Hekla, mainly to the North of Hekla at the present time (Jakobsson, 1979), never from the central vent, completing the range of lavas from basalt to rhyolite (46-72% SiO_2).

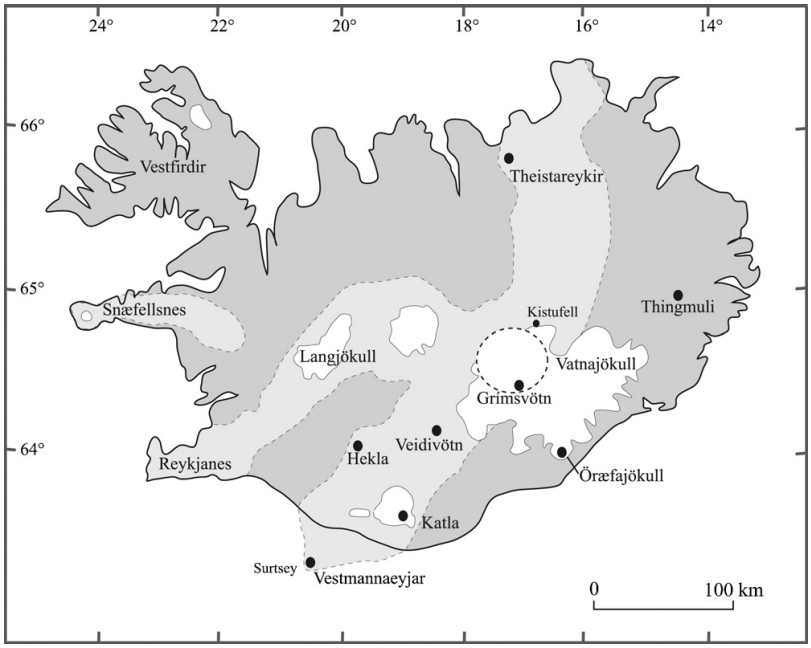

Figure 5.1: Map of Iceland showing the location of Hekla. From Sigmarsson and Steinthorsson (2007).

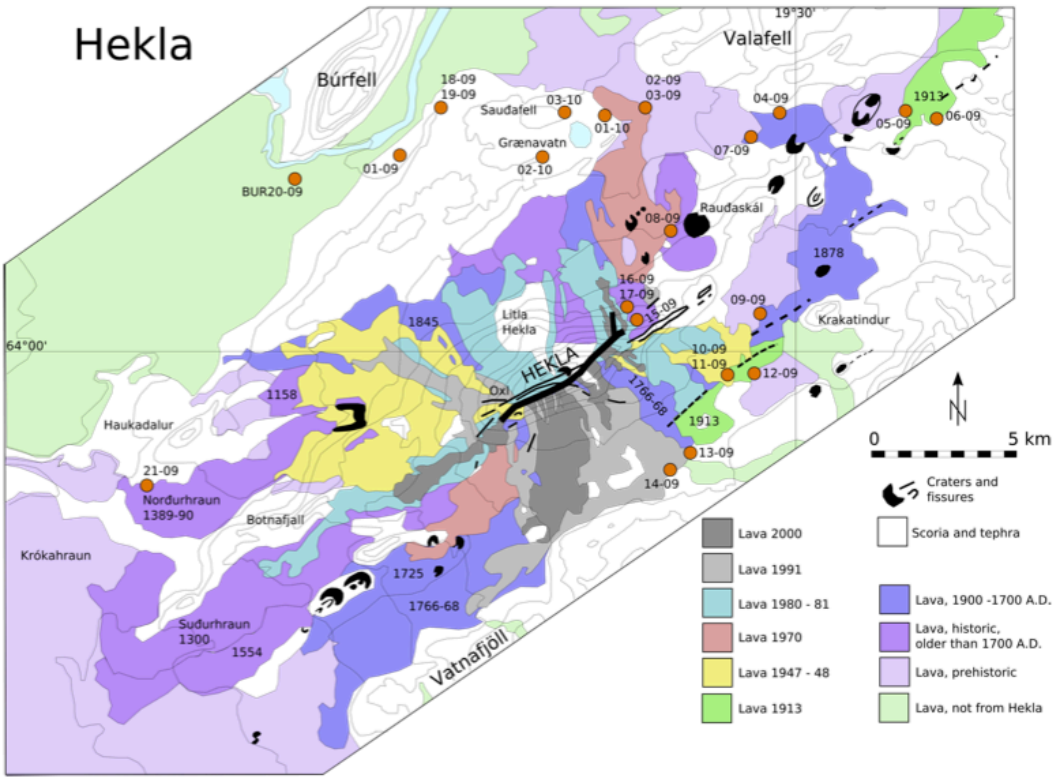

Figure 5.2: Geographical location of Hekla and samples (Savage et al., 2011). Samples analysed in this study: (HEK) 06-09, 12-09, 14-09, 16-09, 10-09, 15-09, 18-09, 19-09, 03-10 and BUR 20-09.

The evolution of Hekla has been disputed in recent decades. The major and trace element composition of Hekla volcanics point to the simple magmatic evolution of a transitional alkaline series, with enrichment of incompatible elements in the melt during differentiation along the liquid line of descent (Schuessler et al., 2009; Sigmarsson et al., 1992b). This increase in incompatibles with magma evolution is most likely a result of fractional crystallisation within the magma chamber. Sigmarsson et al. (1992b) propose a three-stage model, based on Th, Sr and O isotope data, to generate the wide range of silica contents. Firstly, basaltic magma rises and pools at the base of a shallow (8–15 km depth) magma chamber, at which point it undergoes fractional crystallisation to form basaltic andesite. This hot basaltic magma causes partial melting of crustal meta-basalt and meta-gabbro to form dacitic magma, which in turn mixes with basaltic andesite to form andesite. Lastly, rhyolite forms following fractional crystallisation of the dacitic melt. This model has been contested on the basis of more recent ^{238}U–^{230}Th–^{226}Ra disequilibria and Sr–Nd–Pb–Hf isotope data which instead point to a two-stage evolution via assimilation and fractional crystallisation (Chekol et al., 2011). In this case, the trace element and isotopic data of Hekla are attributed to a series of small lenses of magma that are intruded into the shallow crust and evolve via a combination of fractional crystallisation and assimilation of a dacitic crust to andesitic compositions. Additionally, seismological evidence (Soosalu and Einarsson, 2004) points to the absence of a single shallow magma chamber as suggested by Sigmarsson et al. (1992b). Regardless of whether the volcanism on Hekla results from a simple fractional crystallisation suite following a single liquid line of descent, or a combination of AFC processes, such systems in nature rarely behave in a straightforward manner, but nevertheless this offers a near ideal system for documenting the effects of magmatic differentiation.

5.3 Sample description

The samples were collected and prepared (washed, crushed and powdered) between September 2009 and July 2012 by Savage et al. (2011) and provided in powdered form for this study. Where possible, the youngest and freshest material possible was collected from flow cores. Tephra from prehistoric eruptions dating back to up to 4000 years before present was also collected (ages are given in Table 5.1 and sample sites are shown in Figure 5.2). Major and trace element abundances were measured by XRF at the Open University (Savage et al., 2011). The samples lie on a transitional alkali series along a liquid line of descent (Savage et al., 2011). The rocks are aphyric, with phenocryst contents normally below 5%. Thin sections show that the major crystallising phases present are olivine, clinopyroxene and plagioclase feldspar, along with accessory apatite, magnetite and minor zircon (Savage et al., 2011). A basalt, BUR-20-09, genetically unrelated to Hekla but collected within its vicinity, was also analysed.

5.4 Analytical technique

Sample quantities ranging from 10-40 mg of the homogenised sample powder were dissolved and spiked, and the Sr separated from the solutions and analysed by TIMS at the Open University and Durham University as detailed in Chapter 2. The REE concentrations were measured by ICP-MS (Element 2, ThermoFisher Instruments) at the University of Oxford and are given in Appendix D.

5.5 Results

The $\delta^{88}Sr$ and $^{87}Sr/^{86}Sr$ data of the samples are given in Table 5.1, along with their ages, rock type, SiO_2 wt %, Sr contents and Eu anomalies. The equivalent $\delta^{18}O$ data of corresponding lava flows (Sigmarsson et al., 1992b), as well as $\delta^{30}Si$ data (Savage et al., 2011) of the same samples, are also shown.

Sample name	**Eruption date**	**Rock Type**	**Silica wt %**	**Sr ppm**	**Eu/Eu***	**δ^{30}Si ‰ (2 sd)**	**δ^{18}O ‰ (SMOW)**	**$^{87}Sr/^{86}Sr$ (2 se)**	**δ^{88}Sr ‰ (2 se)**
Hekla lavas									
HEK 06-09	1913 A.D.	Basalt	46.20	366	1.02	-0.31 ± 0.09	4.73 ± 0.04	0.703161 ± 0.000002	0.251 ± 0.007
HEK 12-09	1913 A.D.	Basalt	46.42	371	1.02	-0.29 ± 0.10	4.73 ± 0.04	0.703166 ± 0.000002	0.278 ± 0.010
								Basalt average	0.265 ± 0.027
HEK 14-09	1991 A.D.	Basaltic andesite	53.71	392	0.95	-0.26 ± 0.06		0.703176 ± 0.000003	0.253 ± 0.006
HEK 16-09	1980 A.D.	Basaltic andesite	54.81	381	0.95	-0.27 ± 0.07	4.90 ± 0.07	0.703171 ± 0.000003	0.262 ± 0.008
								Basaltic andesite average	0.244 ± 0.035
HEK 10-09	1947 A.D	Andesite	57.67	362	0.97	-0.25 ± 0.03	4.80 ± 0.10	0.703186 ± 0.000002	0.232 ± 0.007
HEK 15-09	1980 A.D.	Andesite	59.64	361	0.97	-0.22 ± 0.01	4.90 ± 0.07	0.703171 ± 0.000003	0.229 ± 0.008
								Andesite average	0.217 ± 0.023
HEK 18-09	2800 B.P.	Dacite	68.41	211	0.74	-0.17 ± 0.04	4.90 ± 0.03	0.703208 ± 0.000003	0.228 ± 0.010
HEK 19-09	2800 B.P.	Dacite	68.88	203	0.70	-0.21 ± 0.01	4.90 ± 0.03	0.703191 ± 0.000003	0.197 ± 0.011
								Dacite average	0.200 ± 0.005
HEK 03-10	4000 B.P.	Rhyolite	72.07	122	0.55	-0.17 ± 0.04	4.86 ± 0.001	0.703220 ± 0.000005	0.146 ± 0.012
Other Icelandic samples									
BUR 20-09	~1700 A.D.	Basalt	49.05	162	1.03	-0.31 ± 0.04	4.70 ± 0.10	0.703117 ± 0.000003	0.287 ± 0.007

Table 5.1: δ^{18}O values taken from Sigmarsson et al. (1992a) and reported relative to SMOW (standard mean ocean water) and NBS-28 = 9.45‰, for which errors are the maximum deviation observed for duplicate runs. REE's normalized relative to PM values as given by Anders and Grevesse (1989). Eu/Eu* calculated as [Eu]/√ ([Sm]*[Gd]). δ^{30}Si, major and trace element data taken from Savage et al. (2011), reported in relative to NBS-28 and given to 2 sd uncertainty. Group average errors are given as as 2 s e from the mean.

5.5.1. Stable $\delta^{88}Sr$

The $\delta^{88}Sr$ values for the Hekla samples range from $\delta^{88}Sr = +0.278 \pm 0.010$ to $+0.146 \pm 0.012‰$. This variation in $\delta^{88}Sr$ of ~0.13‰ is significant, yet smaller than that reported by Charlier et al. (2012) for rocks of equivalent compositions. There is a clear, positive, linear relationship between stable Sr isotopic values and SiO_2 and Ba content (Figs. 5.3 and 5.4), and a robust negative correlation with $\delta^{30}Si$ (Fig. 5.5). The $\delta^{88}Sr$ values of the samples shift to lighter values with increasing silica contents and magmatic differentiation. Although though there is some degree of overlap between adjacent rock types on individual samples measurements, the average $\delta^{88}Sr$ value for each becomes heavier with silica content: $\delta^{88}Sr_{basalt} = 0.265 \pm 0.027$ ‰ (2 se; n=2); $\delta^{88}Sr_{basaltic\ andesite} = 0.244 \pm 0.035$ ‰ (2 se; n=2); $\delta^{88}Sr_{Andesite} = 0.217 \pm 0.023$ ‰ (2se; n=2); $\delta^{88}Sr_{Dacite} = 0.200 \pm 0.005$ ‰ (2 se; n=2) and $\delta^{88}Sr_{Rhyolite} = 0.15 \pm 0.01‰$ (2 se; n=1).

The $\delta^{88}Sr$ composition of the basalts reported in this study compare well with an average of all basalts measured to date: 0.29‰ ± 0.02‰, (2 se; n=13) (Charlier et al., 2012; Moynier et al., 2010; Ohno and Hirata, 2007). However, all three studies report minimal variation in $\delta^{88}Sr$ to lighter values with magmatic evolution up to andesitic compositions, of $\delta^{88}Sr = 0.25‰$ (Moynier et al., 2010) $\delta^{88}Sr = 0.32‰$ (Charlier et al., 2012), and $\delta^{88}Sr = 0.25 \pm 0.01‰$ (Ohno and Hirata, 2007). In contrast, we observe a clear fractionation in $^{88}Sr/^{86}Sr$ to compositions as light as $\delta^{88}Sr = 0.200 \pm 0.005‰$ for andesites, and even lighter values for rhyolites. We report an overall variation in $\delta^{88}Sr$ of 0.15‰, considerably smaller than the ~0.5‰ variations observed by Charlier et al. (2012). The rhyolitic glass analysed by Charlier et al. (2012) extend to values as light as $\delta^{88}Sr = -0.19‰ \pm 0.13$ (2 se) whereas those of this study posses compositions of $\delta^{88}Sr = 0.146‰ \pm 0.012$ (2 se). However, the variation seen by Charlier et al. (2012) is difficult

to resolve to the analytical precision of the technique (~±50 ppm) whereas the variation observed in this study is clearly resolvable with the improved current analytical precision.

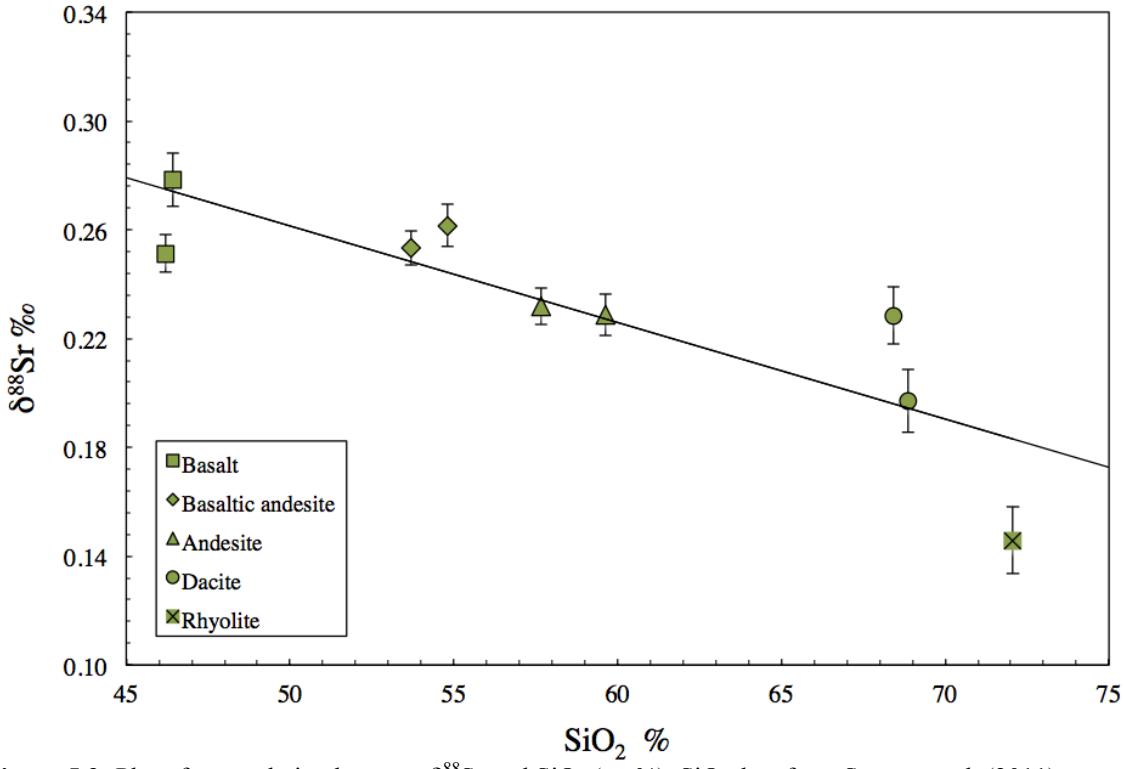

Figure 5.3: Plot of a correlation between $\delta^{88}Sr$ and SiO_2 (wt %). SiO_2 data from Savage et al. (2011).

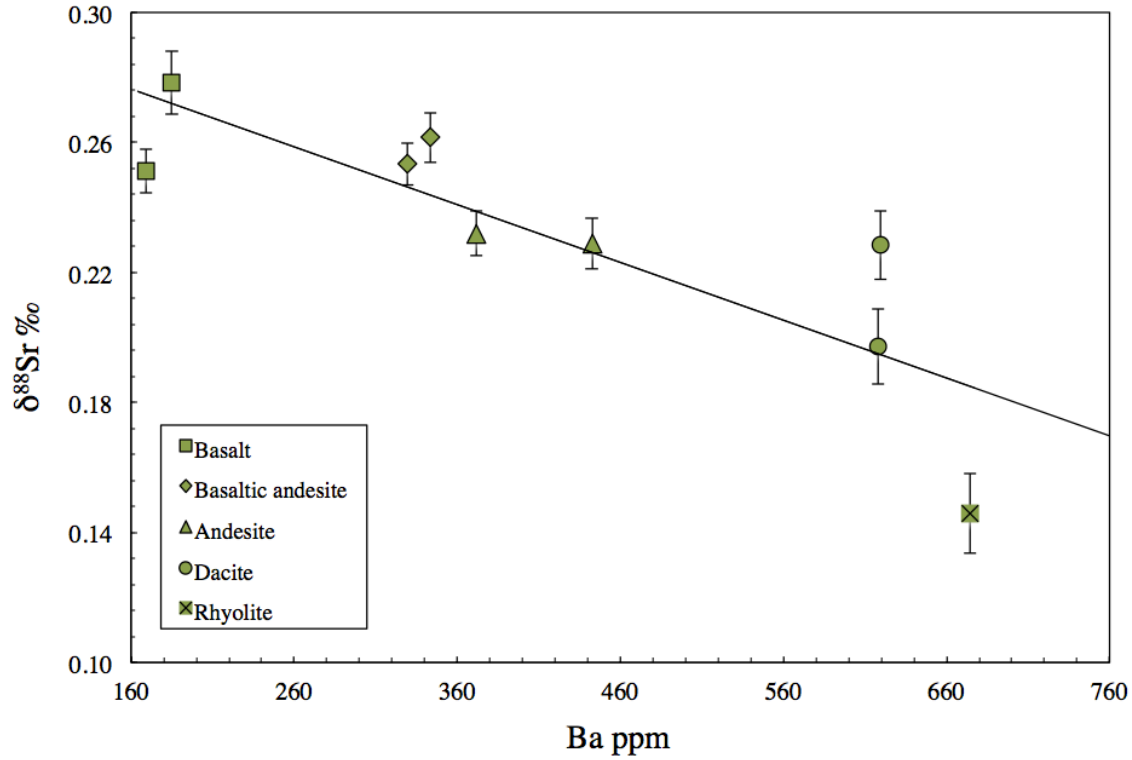

Figure 5.4: Plot of a correlation between $\delta^{88}Sr$ and Ba (ppm). Ba data from Savage et al. (2011).

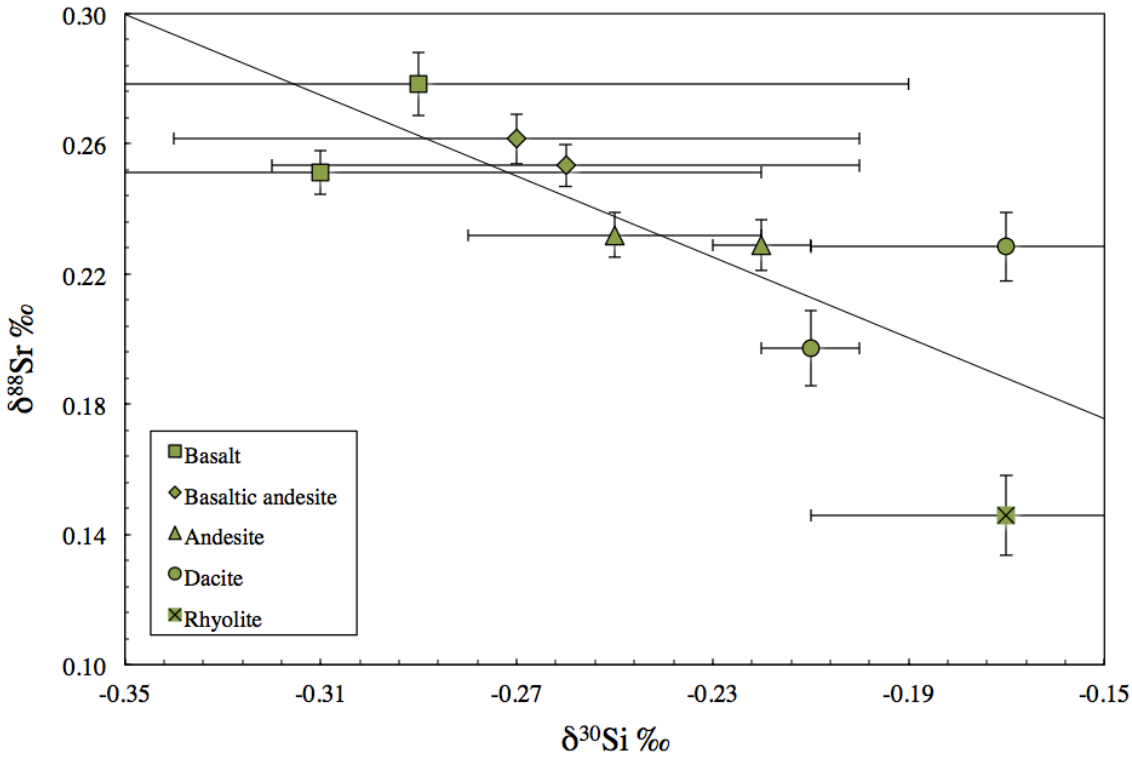

Figure 5.5: Plot of a linear correlation between $\delta^{88}Sr$ and $\delta^{30}Si$. $\delta^{30}Si$ data from Savage et al. (2011).

5.5.2. Radiogenic $^{87}Sr/^{86}Sr$

Variations in $^{87}Sr/^{86}Sr$ are detected in the Hekla samples, ranging from $^{87}Sr/^{86}Sr$ = 0.703161 (±2) for a basalt to $^{87}Sr/^{86}Sr$ = 0.703220 (±5) for a rhyolite. With the exception of the genetically unrelated BUR 20-09, there is a linear correlation of the $^{87}Sr/^{86}Sr$ ratio with silicic content, increasing from (Fig. 5.6), as well as with other indicators of magmatic differentiation such as Ba. Figure 5.7 shows a positive correlation between $^{87}Sr/^{86}Sr$ and $\delta^{88}Sr$. On a plot of $^{87}Sr/^{86}Sr$ against Sr concentration, Fig. 5.8, the samples plot along a hyperbolic mixing curve and Fig. 5.9 shows the inverse of this ($1/Sr \approx 1/^{86}Sr$) gives a linear array.

Sigmarsson et al. (1992b) report an average $^{87}Sr/^{86}Sr$ isotope composition for basalts to rhyolites on Hekla of 0.70316 (±3) with no measurable variation for a wide range of rock compositions. Chekol et al. (2011) report a limited range in the $^{87}Sr/^{86}Sr$ ratio of basalts of 0.70319–0.70322. These results are in good agreement with the average $^{87}Sr/^{86}Sr$ in rocks analysed in this study of 0.703176 with a range of 0.703161 - 0.703220. The variation in $^{87}Sr/^{86}Sr$ was not observed in the analyses of Sigmarsson et al. (1992b), as the precision of the measurements was too low. Variations were observed by Chekol et al. (2011), however the contrasting $^{87}Sr/^{86}Sr$ ratios of the basalts and dacites were attributed to different origins.

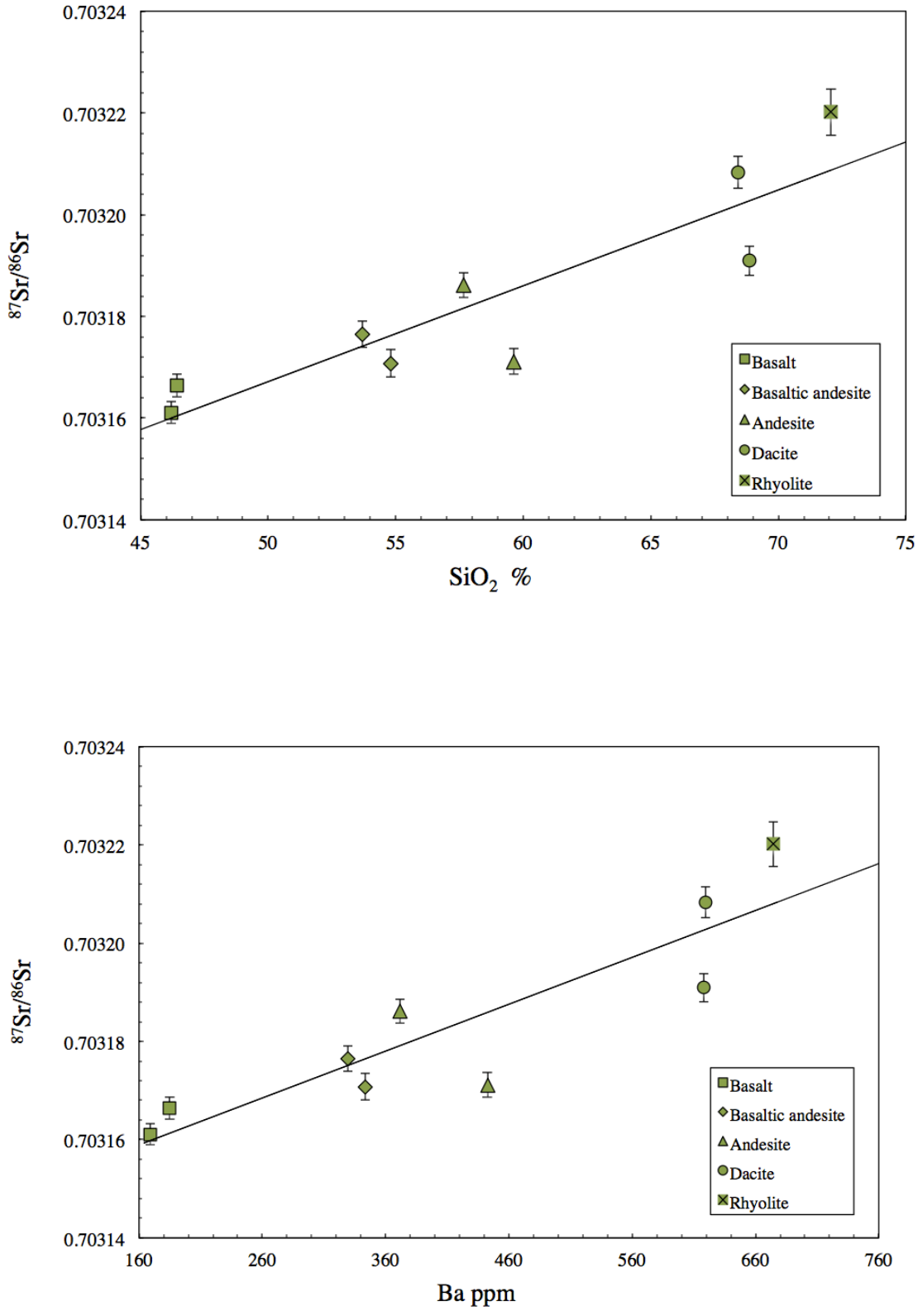

Figure 5.6: Correlations between $^{87}Sr/^{86}Sr$ and indicators of magmatic differentiation SiO_2 (wt%) and Ba (ppm). Ba and SiO_2 data from Savage et al. (2011).

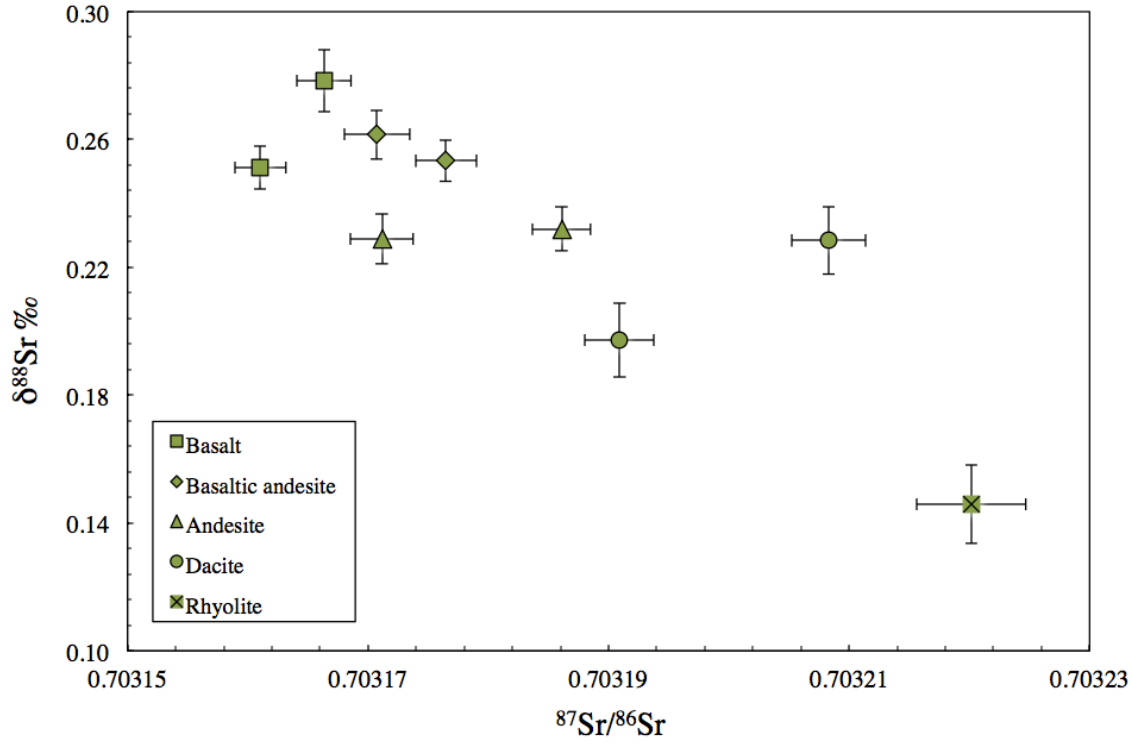

Figure 5.7: Radiogenic variations in $^{87}Sr/^{86}Sr$ correlated with variations in stable $\delta^{88}Sr$.

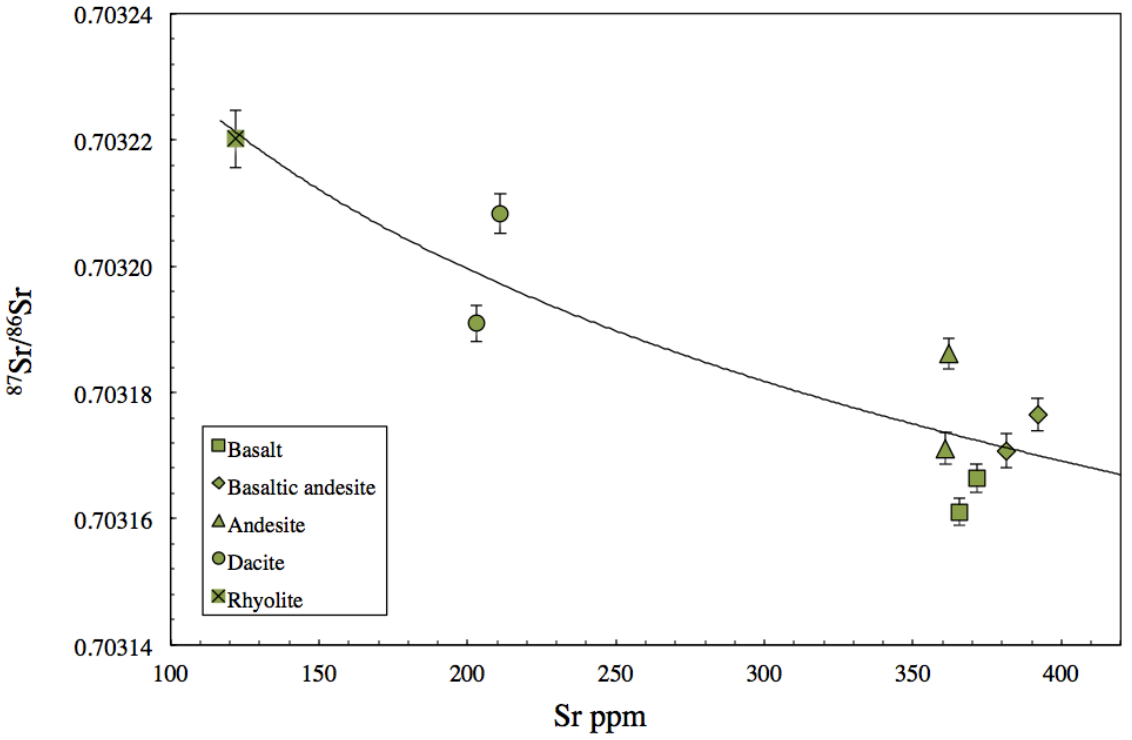

Figure 5.8: Plot of hyperbolic mixing between Sr and $^{87}Sr/^{86}Sr$.

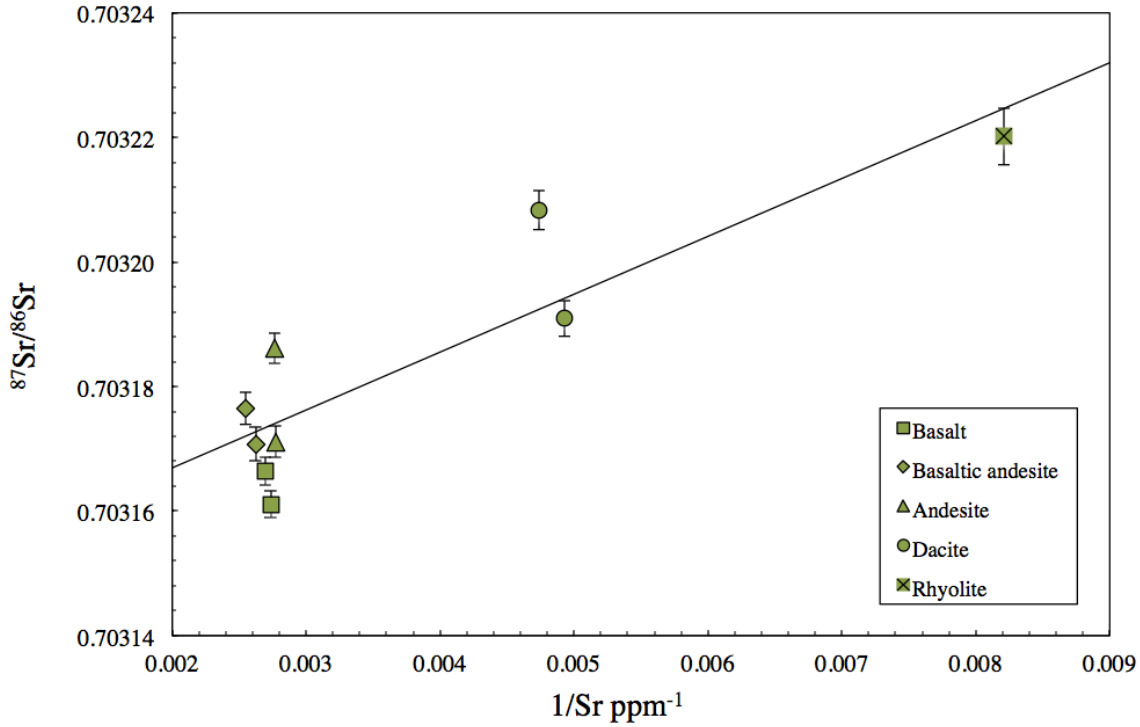

Figure 5.9: Plot of a mixing line between $^{87}Sr/^{86}Sr$ and $1/^{86}Sr$.

5.5.3. Sample BUR 20-09

Sample BUR 20-09 has an $^{87}Sr/^{86}Sr$ isotope composition isotopically unlike the rest of the Hekla suite. The $\delta^{88}Sr$ composition is resolvably heavier than the equivalent Hekla basaltic rocks. Additionally, it has different major and trace element concentrations, consistent with the sample being genetically unrelated to the Hekla suite (Savage et al., 2011). For this reason, it is excluded from any discussion comparing the $\delta^{88}Sr$ and $^{87}Sr/^{86}Sr$ data as it has a source isotopically distinct from those of the co-genetic Hekla suite and is incomparable when interpreting a single magmatic system.

5.6. Discussion

5.6. Origins of variations

The systematic shift to lighter $\delta^{88}Sr$ values with increasing silica content to evolved compositions demonstrates that there is a process, or several processes, fractionating the stable isotopes of Sr during magmatic evolution. The additional correlation of the radiogenic isotopes of Sr with silica content suggests that both radiogenic and stable isotopes are responding to the same process. There are several secondary near surface processes such as interaction with hydrothermal or geothermal fluids that could affect the radiogenic isotopes of Sr as well as a number of potential fractionation mechanisms in high temperature magmatic systems that can occur either during the evolution and emplacement of the magma. As low temperature processes can potentially fractionate radiogenic and stable isotopes of Sr to a greater extent than high temperature process, these need to be considered and assessed for their contribution to the observed stable isotope fractionation. In the following, the possible causes of this systematic progression of radiogenic isotopes with magma evolution are considered, as is the likelihood of their affecting the stable Sr composition.

5.6.1. Analytical error in DS calculations

The correlation between $^{87}Sr/^{86}Sr$ and $\delta^{88}Sr$ coupled with the unusual shift to lighter stable isotope compositions with magmatic evolution (in contrast to other isotopic systems such as Si; Savage et al., 2011), raises a concern that this may be a false trend resulting from systematic error propagated through calculations of the stable isotopic composition from the deconvolution of the double spike data. The radiogenic $^{87}Sr/^{86}Sr$

data is used to calculate the $^{88}Sr/^{86}Sr$ ratio by deconvolution of a spiked and un-spiked run, in this particular case there is a shift to increasing radiogenic $^{87}Sr/^{86}Sr$ values with magmatic differentiation. In order to address this, the $^{87}Sr/^{86}Sr$ ratio determined through double spike deconvolution calculations (sometimes termed $^{87}Sr/^{86}Sr_{norm}$) can be normalized to the "true" $^{88}Sr/^{86}Sr$ ratio of the sample, rather than a fixed ratio of $^{88}Sr/^{86}Sr = 0.1194$, and compared to the natural $^{87}Sr/^{86}Sr$ ratio attained through the un-spiked run (e.g. Krabbenhoft et al., 2010). The relationship between the traditional radiogenic $^{87}Sr/^{86}Sr$ ratio the $^{87}Sr/^{86}Sr_{norm}$ ratio and the deconvolved $^{87}Sr/^{86}Sr$ ratio is defined by Equation 5.1:

$$\frac{\left(\frac{^{87}Sr}{^{86}Sr}\right)_{Norm}}{\left(\frac{^{87}Sr}{^{86}Sr}\right)} = \left[\frac{\left(\frac{^{88}Sr}{^{86}Sr}\right)_{Nier}}{\left(\frac{^{88}Sr}{^{86}Sr}\right)}\right]^{\frac{ln(m_{87}/m_{86})}{ln(m_{88}/m_{86})}} \qquad \textit{Equation 5.1}$$

When calculated for the Hekla samples, the re-normalised $^{87}Sr/^{86}Sr$ ($^{87}Sr/^{86}Sr_{norm}$, following the notation in Krabbenhoft et al., 2010) are near identical to the un-spiked $^{87}Sr/^{86}Sr$ data, Table 5.2, and Figure 5.10 shows a positive correlation between the two, with minor deviation from the line of best fit. This good agreement clearly demonstrates the robustness and accuracy of the double spike technique as well as ensuring that no false trends result from the double spike deconvolution.

Sample name	$^{87}Sr/^{86}Sr$	2 s e	$^{87}Sr/^{86}Sr$ deconvolved	$^{86}Sr/^{88}Sr$	f	$^{87}Sr/^{86}Sr_{nom}$
HEK 06-09	0.703160	0.000002	0.703249	0.119370	-0.010936	0.703160
HEK 12-09	0.703152	0.000002	0.703244	0.119369	-0.011252	0.703152
HEK 20-09	0.703115	0.000003	0.703217	0.119366	-0.012491	0.703116
HEK 14-09	0.703163	0.000003	0.703243	0.119373	-0.009847	0.703163
HEK 16-09	0.703169	0.000003	0.703262	0.119369	-0.011384	0.703169
HEK 10-09	0.703172	0.000002	0.703245	0.119375	-0.008956	0.703172
HEK 15-09	0.703170	0.000003	0.703251	0.119373	-0.009960	0.703170
HEK 19-09	0.703189	0.000003	0.703259	0.119376	-0.008582	0.703189
HEK 03-10	0.703219	0.000005	0.703270	0.119383	-0.006348	0.703219

Table 5.2: The $^{87}Sr/^{86}Sr_{norm}$ value is determined from the $\delta^{88}Sr$ and the $^{87}Sr/^{86}Sr$ deconvolved value renormalized to $\delta^{88}Sr = 0$. $^{87}Sr/^{86}Sr_{nom}$ refers to the deconvolved $^{87}Sr/^{86}Sr$ ratio renormalized to a $^{88}Sr/^{86}Sr$ ratio of 8.375209. f= $\ln(^{88}Sr/^{86}Sr_{NBS}/^{88}St/^{86}Sr_{sample})/\ln(m_{86}/m_{88})$.

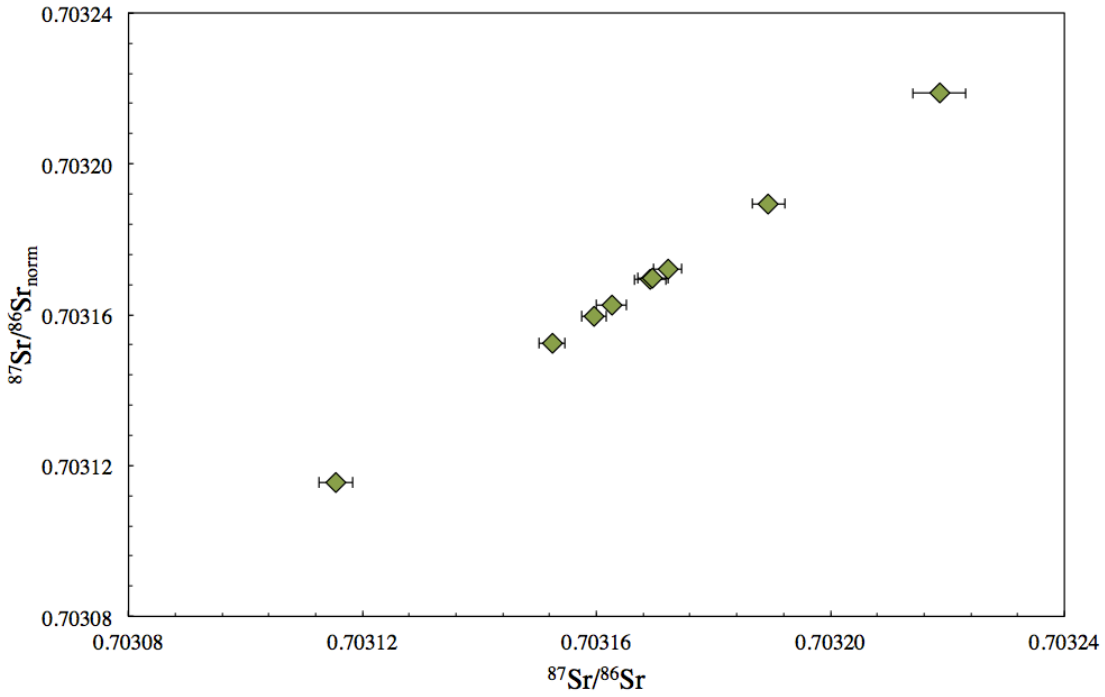

Figure 5.10: Plot of $^{87}Sr/^{86}Sr_{norm}$ with (unspiked) $^{87}Sr/^{86}Sr$.

5.6.2. Non-magmatic causes of stable isotopic variation

5.6.2.1. Non-equilibrium (kinetic) isotopic fractionation

As previously explained in Chapter 1, isotopic fractionation can result from non-equilibrium (kinetic) processes. At the formation temperatures of molten basalt to rhyolite, it has been experimentally shown that the isotopes of major magmatic components can fractionate due to non-equilibrium (diffusional) processes such as chemical diffusion (Richter et al., 1999; Richter et al., 2003**;** Richter et al., 2008; Richter et al., 2009b) and thermal (Soret) diffusion (Kyser et al., 1998; Richter et al., 2003; Richter et al., 2009b; Huang et al., 2010). Although these experimental models do not take into account other high temperature processes that occur with a natural igneous body such as partial melting, assimilation and fractional crystallisation, and assume a constant (unrealistically unperturbed) thermal gradient, these isotopic variations can be significant- for example as up to 8‰ for Mg (Richter et al., 2008) and have been predicted to occur in magma chamber processes under certain conditions (Lundstrom, 2009). However, as Sr has a higher atomic mass and smaller relative mass difference between isotopes, it would be expected that Sr fractionation due to non-equilibrium processes would be significantly smaller than that observed for the lighter major element components that constitute silicates. Very little diffusion data exists for Sr, and in addition the mass dependent slopes for kinetic and equilibrium Sr isotope fractionation are so similar at low fractionation degree, it is difficult to distinguish between the two fractionation types (Figure 1.1; Chapter 1). As there is restricted experimental and natural evidence to either prove or disprove the affect of such processes on Sr, we will discuss arguments for and against these mechanisms being responsible for the variations in Sr stable isotopes seen here.

Thermal (Soret) diffusion arises from the internal redistribution of species within a substance in response to an imposed temperature gradient and has the potential to fractionate stable isotopes such as Li and Mg (Richter et al. 2009a,b; Lundstrom et al., 2005). There is experimentally based evidence to suggest isotopic fractionation of Sr by thermal diffusion at temperatures and pressures of 1200°C and 0.5 GPa within a basaltic melt (Lacks et al., 2012). However, there are a number of reasons why thermal diffusion can be discounted as contributing to the stable isotope fractionation seen for Sr. The first and most obvious of these is that the observed stable isotope fractionation is in the opposing direction to that expected from thermal diffusion. Diffusive species move up or down a thermal gradient so as to equalize the internal energy distribution, which results in the light species being accumulated at the hot end and the heavier species at the cold end, and this has been consistently demonstrated from experimental work (e.g. Huang et al., 2010; Richter et al., 2009b). However, the cold end of the Hekla magmatic system, i.e. the rhyolites, possess lighter stable isotope compositions contrary to the predicted effects of thermal diffusion. Such experiments were based on temperature gradients of roughly 100°C, which are probably not attained, should the alternative magma chamber model for Hekla by Chekol et al. (2011) be correct. Additionally, the time scales required to generate thermal diffusion isotopic fractionation in a large magma chamber are most likely to be on the scale of millions of years (Lundstrom, 2009) rather than thousands of years as appears to be the case for magma chamber longevity for Hekla. Lastly, linear correlations between isotope systems affected by thermal diffusion were observed for all experiments and as no such relationships exist between these isotope systems and Sr, and no effects that could be attributed to thermal diffusion have been observed for other stable isotope systems such as Fe, Si and O. To

this end, it is reasonable to assume that thermal diffusion does not play a major role in producing the stable isotopic fractionation of Sr.

Another non-equilibrium process that can cause stable isotopic fractionation is chemical diffusion, which arises from the redistribution of species as a result of a chemical gradient and mainly favours the lighter isotopes of an element as these diffuse faster relative to the heavier species. This results in the lighter isotopes of an element diffusing towards areas of lower elemental concentration, and this has been experimentally shown to occur in all stable isotope systems studied thus far (e.g. Richter et al., 2009b). However, to date there is an absence of experimental or field based data regarding Sr stable isotope fractionation due to chemical diffusion. For Hekla, the basalts possess higher concentrations of Sr and the rhyolites lower concentrations, thus the observed stable isotope shift is in line with the expected stable isotope fractionation via chemical diffusion. However, several lines of evidence suggest that this is not a contributing factor for stable isotope fractionation at Hekla.

The first is that a single zoned magma chamber is required to produce such an effect in a closed system, and although this has been suggested by Schuessler et al. (2009), others have argued against this based on the absence of seismological data for a large shallow magma chamber and suggest several smaller lenses of intruded magma (Chekol et al., 2011). Moreover, it has long been observed that basalt does not erupt from the central vent of Hekla, but on the flanks, which strengthens the argument that the basalt source may well be physically detached from the evolving fractionating differentiates, in which case chemical diffusion is not likely to occur because of physical restrictions, i.e. they are not connected.

Secondly, Li stable isotopes are far more susceptible to isotopic fractionation by chemical diffusion, than heavier elements such as Sr, and as no shifts in the stable Li isotopic composition are observed for Hekla (Schuessler et al., 2009) it is highly unlikely that they exist for Sr. It might be argued that as an element as light as Li diffuses over such short time scales, the system has time to re-equilibrate and homogenize the isotopic effects resulting from diffusion, whereas a heavier isotope system such as Sr would take longer to diffuse, and may well have "frozen' in the isotopic signature resulting from chemical diffusion at the time of eruption. However, no stable isotopic fractionation could be attributed to chemical diffusion for either Si or Fe (Savage et al., 2011; Schuessler et al., 2009), the atomic masses of which are more comparable to Sr, suggesting that chemical diffusion has not affected either light and heavy isotope systems.

A third line of argument is that it has been found that thermal diffusion always results in the heavy isotopes being enriched at the cold end of the gradient regardless of whether the concentration of the parent element increases or decreases, as well as causing larger isotope fractionation than that observed for chemical diffusion (Richter et al., 2009b; Huang et al., 2010). Thus, it is possible to rule out Sr stable isotope fractionation as a result of thermal diffusion, likewise it is unlikely to account for the variations observed in other isotope systems.

5.6.2.2. Radiogenic in-growth

The decay of ^{87}Rb to ^{87}Sr may well account for the increases in ^{87}Sr compared to stable ^{86}Sr ratio of a rock and its minerals over enough time. The $^{87}Rb/^{86}Sr$ ratio of the

samples can be calculated from their Rb and Sr concentrations using Equation 5.2, and these correlate with the $^{87}Sr/^{86}Sr$ composition through which an isochron can be plotted (Figure 5.11). Assuming a closed system and using sample HEK 12-09 as the initial parental magma yields a minimum time period of 2.3 ± 0.9 Myr to evolve to an $^{87}Sr/^{86}Sr$ ratio of the most radiogenic sample (HEK 03-10) via radiogenic in-growth. HEK 03-10 was collected from a lava flow dating back to as recently as 4000 years ago, and Hekla itself is thought to be 6000-7000 years old, thus assuming a closed system, radiogenic in-growth alone cannot have caused the differences seen in $^{87}Sr/^{86}Sr$.

$$^{87}Rb/^{86}Sr = (Rb/Sr).\left(\frac{Ab^{87}Rb.WSr}{Ab^{86}Sr.WRb}\right) \qquad \textit{Equation 5.2}$$

where *Ab* is the isotopic abundance and *W* is the atomic weight. The atomic weight of Rb, *WRb*, is 85.46776 and the isotope abundance of ^{87}Rb, $Ab^{87}Rb$, is 85.46776. The abundance of ^{86}Sr ($Ab^{86}Sr$) and the atomic weight of Sr (*WSr*) is calculated for each sample.

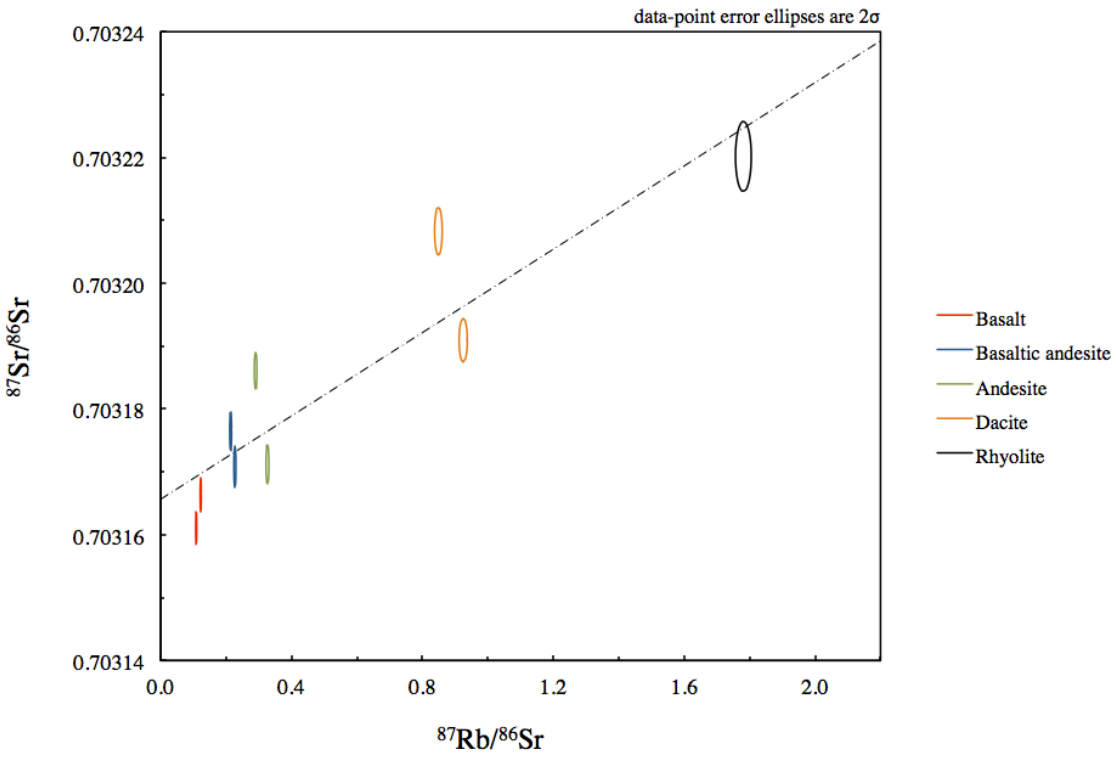

Figure 5.11: Isochron plot of the Heka samples, using Isoplot, gives an age of 2.3 ± 0.9 Ma with an MSWD of 39.

Although radiogenic in-growth cannot wholly account for the shifts in $^{87}Sr/^{86}Sr$, re-melting or assimilation of older basaltic crust with a more radiogenic $^{87}Sr/^{86}Sr$ value could cause the variations. Re-melting and assimilation of older basaltic crust has been proposed to have occurred for Hekla before (Sigmarsson et al., 1992b), and is discussed further in Section 6.2.2.5.

5.6.2.3. Low-temperature secondary fluid/alteration process

Hydrothermal and geothermal fluids have the potential to alter magmatic rocks and overprint their original igneous isotope source signature. The stable isotopes of lighter elements (e.g H, O, Cl) can be used to fingerprint processes such as hydrothermal and geothermal interaction, as they extremely sensitive due to the large relative mass

difference between isotopes. Hydrogen and oxygen are the major components of alteration fluids and their stable isotopes retain this secondary isotopic signature, which can be detected upon analysis. In addition, the compositions of surface reservoirs, such as seawater, are often isotopically distinct from the relatively restricted range of pristine compositions in the mantle. Sigmarsson et al. (1992b) reported oxygen isotope data from Hekla with a restricted range of $\delta^{18}O$ values, between +4.5 and +5.3‰. Although these values are slightly lower than average mantle values ($\delta^{18}O = +5.5 \pm 0.7$‰; Mattey et al., 1994), which may be indicative of contamination by hydrothermal alteration (Hemond et al., 1993), they are a common feature on Iceland and thought to be a characteristic feature of the Icelandic plume (Thirlwall et al., 2006). Additionally, the enrichment of the heavier isotopes of oxygen with magmatic evolution is more likely to be a result of equilibrium fractionation through fractional crystallization than a low temperature-kinetic process.

Estimates of the Sr isotope compositions of a hydrothermal end-member were made by Krabbenhoft et al. (2010) to be $^{87}Sr/^{86}Sr = 0.7045 \pm 0.0005$ and $\delta^{88}Sr = 0.27 \pm 0.03$‰. This $^{87}Sr/^{86}Sr$ value is far more radiogenic than the pristine mantle and could hypothetically have shifted the radiogenic Sr isotope composition of the Hekla rocks, resulting in a more radiogenic signature with continued mixing during magmatic evolution. However, Krabbenhoft et al. (2010) documented a range in the $\delta^{88}Sr$ values of hydrothermal fluids sourced from the mid-Atlantic Ridge (4°48'S) extending from +0.25‰ to values as heavy as +0.36‰. In general, the hydrothermal fluids with the heaviest $\delta^{88}Sr$ values also possessed the most radiogenic $^{87}Sr/^{86}Sr$ values, consistent with these waters containing a greater proportion of seawater. For Hekla, if hydrothermal fluids are responsible for the radiogenic values seen with differentiation, it then follows that the more evolved rocks should also possess heavy stable Sr

compositions. However, the opposite trend is actually observed for Hekla, and in this case hydrothermal fluids are unlikely to be responsible for the shifts observed. Importantly, and particularly pertaining to the following discussion of causes of stable isotope fractionation, even if hydrothermal fluids affected Hekla magmas they cannot account for the light stable isotope compositions of the more evolved magmas as they only fall within the heavier range of ocean basalts and do not extend to the lighter values observed in more evolved rocks.

Lithium is a mobile trace element, and its elemental concentrations and isotope compositions can be used to trace magma-fluid interaction, for example the exsolution of late stage aqueous magmatic fluids. If Li behaved as a mobile element during fluid exsolution one would expect its concentrations to decrease during differentiation. In contrast, Schuessler et al. (2009) found that Hekla volcanics exhibit increasing Li concentrations with magma evolution, consistent with incompatible elemental behaviour during fractional crystallization in the absence of extensive fluid exsolution. The authors also report stable δ^7Li values typical for the upper mantle, rather than variations towards fluid δ^7Li compositions, suggesting that there has been no fluid alteration (via degassing or metasomatism) in the magmatic system. For an element system as mobile as Li, the uniformity of the stable isotopes and concentrations suggest that the various processes that could potentially perturb this element, such as diffusion, fluid loss from or addition to the magma, or assimilation of fluid altered country rock have not occurred, or at the very least, not to an extent that can be detected within the precision of this work.

5.6.2.4. Seawater

Modern day seawater has a well-constrained Sr composition of $^{87}Sr/^{86}Sr = 0.709312 \pm 0.000009$ and $\delta^{88}Sr = 0.386 \pm 0.007‰$ (e.g. Hodell et al., 1990; Vance et al., 2009; Allègre et al., 2010 Krabbenhoft et al., 2010) both of which are very different from the closest Hekla values of $^{87}Sr/^{86}Sr = 0.703220$ and $\delta^{88}Sr = \sim0.278‰$ respectively. Although seawater can theoretically account for the increasingly radiogenic composition with magmatic evolution by mixing in the magma chamber, the corresponding stable isotopic shift to heavier values expected is not observed. The $\delta^{88}Sr$ composition of more evolved rocks at Hekla are in fact lighter. Consequently the involvement of seawater, and its involvement in generating the light stable compositions, is unlikely.

5.6.2.5. Crustal contamination; AFC

Mixing of a crustal component with a magma system during its evolution commonly occurs and is a highly likely cause of contamination for the case of Hekla. Mixing can occur either in the source region of the melts (the mantle) between the magma and subducted sediment or crust, within the magma chamber involving assimilation of the surrounding country rock, or during magma emplacement due to interaction with the wall rock into which magma is intruded. Trends in radiogenic isotopes will then fall on mixing lines. Langmuir et al. (1978) used a general mixing equation that can be applied to radiogenic isotope ratios, in which contaminated samples lie on a hyperbolic curve, or on a straight line with a common denominator. For the radiogenic Sr isotope system, the initial $^{87}Sr/^{86}Sr$ can be plotted against the Sr concentrations and the stable isotope ^{86}Sr not affected by in-growth is usually used for concentration. Mantle derived magmas that assimilate or are contaminated by older crustal, would acquire more radiogenic

$^{87}Sr/^{86}Sr$ compositions than those found in the mantle and extend to values of the contaminant. In Fig. 5.8 the Hekla suite does indeed show some suggestion of hyperbolic mixing curve indicating that these rocks may have been affected by contamination or assimilation by older crustal rocks. This mixing is also evident from the straight-line trend in Fig. 5.9 between $^{87}Sr/^{86}Sr$ plotted against $1/^{86}Sr$. These trends although faint are nevertheless distinct, and are consistent with some degree of contamination.

Using combined stable and radiogenic isotope plots, it is possible to differentiate between contamination in the magma source and crustal (assimilation) contamination. Oxygen isotopes are effective in distinguishing rocks formed in equilibrium with the mantle from those formed from the continental crust, as the latter is enriched in ^{18}O relative to the mantle following extensive reaction with the hydrosphere. Any correlation between the stable isotopes of O and the radiogenic Sr isotopes would provide compelling evidence for contamination in the mantle source region (James, 1981). This is clearly not the case for Hekla, based upon the correlation of the O data from Sigmarsson et al. (1992b) matched to the $^{87}Sr/^{86}Sr$ data in this study by lava flows shown in Figure 5.12. No correlation is seen between the two for the Hekla suite, ruling out contamination in the source, and leaving contamination by assimilation as the only possibility.

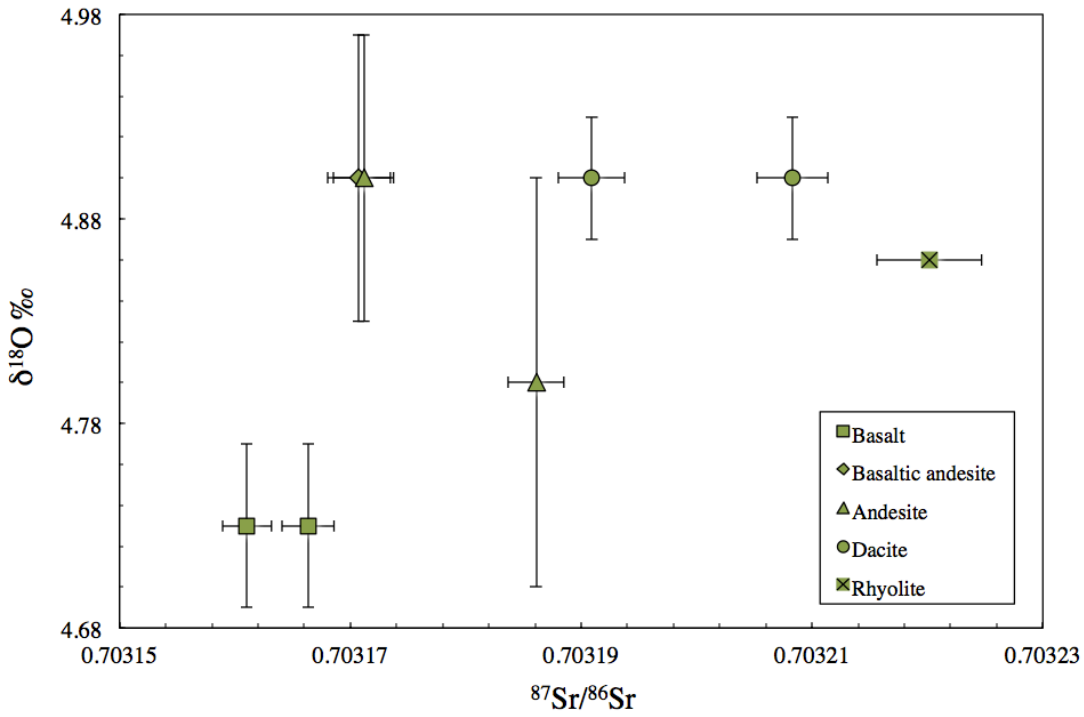

Figure 5.12: Plot of $\delta^{18}O$ data from Sigmarsson et al. (1992b) with the $^{87}Sr/^{86}Sr$ composition of the lavas.

Assimilation of country rock either within the magma chamber or during transport of magma occurs commonly through partial melting of the wall rock at high magmatic temperatures (ca.1300°C). Crystal fractionation has been shown to occur at Hekla as evidenced by both stable isotope and elemental analysis. The frequency of the coupling between crystal fractionation and assimilation is largely due to the latent heat released during crystallisation of differentiating magmas melting the surrounding wall rock of the magma chamber. This Assimilation Crystal Fractionation (AFC) can occur over a wide range of temperatures, and has been modelled (DePaolo, 1981) and documented extensively in nature. Sigmarsson et al. (1992b) suggest that AFC processes are responsible for the magmatic differentiation of the dacites seen at Hekla. These AFC processes have also been suggested to account for two types of basalts in the SIVZ (Sigmarsson et al., 1992a) in which primary alkali basalt and olivine tholeiite melts 'erode' and assimilate the base of the crust.

Based on the constancy of the Hekla $\delta^{18}O$ over time, Thirlwall et al. (2006) concluded that lavas from Hekla are unlikely to have been generated by contamination from the lower crust, although this was not definitive. These near constant values and the absence of any correlation between $\delta^{18}O$ and either the radiogenic or stable values of Sr in combination with the similarity of all these values with surrounding rocks indicate that the contamination appears to be relatively minor. Given the relatively young mafic rocks in the vicinity of Hekla, the most likely contaminant is pre-existing basaltic crust, with only marginally more radiogenic Sr. A basalt from the vicinity of Hekla may have more radiogenic composition than Hekla due to a number of reasons. The first is radiogenic ingrowth, although as previously argued, this is unlikely given the relatively young age of Iceland basalts. An alternative is through source heterogeneity in the mantle, which we know from Chapter 2 can occur as various basalts sourced globally have differing $^{87}Sr/^{86}Sr$ compositions. Although the basalts from Chapter 2 overall have heavy $\delta^{88}Sr$ compositions, samples from a single ridge have been shown to range to light values. The possibility of this occurring at Hekla is tenuous, but overall unlikely, as the correlation between $\delta^{88}Sr$ and silica content is undeniably systematic and not random. Furthermore, although technically MORBs, Icelandic basalts are considered to be closer to OIBs in terms of chemistry, and thus most likely possess a more restricted $\delta^{88}Sr$ composition as observed in Chapter 2.

An alternate contaminant however, is basalt that has undergone chemical weathering and contains an altered secondary component. In Icelandic basalts, calcium carbonate is a common secondary weathering mineral, and is stable at the high pH (>9.5) typically found in Icelandic groundwaters. Carbonates possess radiogenic $^{87}Sr/^{86}Sr$ ratios close to 0.708 (Allègre et al., 2010) and a range of $\delta^{88}Sr$ compositions from heavy to as light as ~ -0.4‰ (Fietzke and Eisenhauer, 2006; Ruggeberg et al., 2008; Halicz et al., 2008;

Krabbenhoft et al., 2010). The lighter $\delta^{88}Sr$ carbonate compositions far exceed those of the Hekla lavas, and as such could be responsible for the signature seen at Hekla. However, the decrease in stable Sr to lighter values is near constant throughout sequence including over the likely "mixing" regime that has been identified using Fe stable isotopes (Schuessler et al., 2009), at which point assimilation of altered country rock would most likely occur due to AFC. This suggests that either secondary mineral formation has not affected stable Sr isotopes, or that assimilation has not occurred.

In summary, AFC is most likely responsible for the increasingly radiogenic Sr isotope signature of more evolved rocks. If the assimilant is altered basalt containing secondary carbonate phases, this can result in fractionation to lighter stable isotopic compositions. Given the systematic fractionation over the mixing regime, there is also the possibility that the assimilant is unaltered basalt, which would be unlikely to affect the stable Sr signature. This would imply that the correlations between $^{87}Sr/^{86}Sr$ and $\delta^{88}Sr$ are the result of two superimposed processes.

5.6.3. Stable isotope fractionation with magmatic differentiation

Magmatic differentiation clearly occurs at Hekla, and is considered to be the process responsible for the fractionation of other stable isotopes, including O, Si and Fe (Sigmarsson et al., 1992b; Savage et al., 2011; Schuessler et al., 2009). The strong correlations observed between $\delta^{88}Sr$ and indices of fractional crystallisation such as SiO_2 and Ba content (Fig. 5.2 and 5.3) indicate that fractionation of stable Sr could also have occurred during magmatic differentiation. An obvious mechanism to modify the Sr isotope composition of a melt is by the removal of isotopically lighter or heavier strontium through crystallisation of minerals. For Hekla, as $\delta^{88}Sr$ evolves to lighter compositions with increasing silica content this would require the removal of

isotopically heavy minerals from the melt to result in isotopically lighter residual lavas. Unfortunately, aside from those analysed in this thesis and a K-feldspar standard analysed by Charlier et al. (2012), isotopic mineral data for stable Sr and isotope fractionation factors between silicate minerals and melts are lacking, making it difficult to definitively assign the cause of isotopic fractionation to single or combined mineral phases. To circumvent this need, trace elements can be used as indicators for particular minerals and correlated with stable Sr compositions.

5.6.3.1. Trace element data

An obvious start to determining the cause of isotopic fractionation is firstly determining the mineral phases into which Sr partitions. Given the relatively well constrained bulk partition coefficients for Sr, D_{Sr}, (GERM; EarthRef) and the known crystallising phases at Hekla (olivine, plagioclase, clinopyroxene, magnetite, apatite and zircon), the phases Sr is most likely to partition into and thus fractionate isotopically as a consequence of this are plagioclase and clinopyroxene, as well the minor phase apatite. Of these, plagioclase has the highest D_{Sr} and is most likely to cause isotopic fractionation. Using the Eu anomaly as a proxy for plagioclase fractionation, the strong correlation between Eu/Eu* and $\delta^{88}Sr$ (Fig 5.13) suggests that the lighter isotopes of Sr are preferentially incorporated into plagioclase, and removal of this mineral from the melt during fractional crystallisation may be responsible for generating the lighter isotopic compositions of more evolved components. This is in good agreement with the conclusions of Charlier et al. (2012) for stable Sr fractionation by crystallisation and removal of isotopically heavy plagioclase.

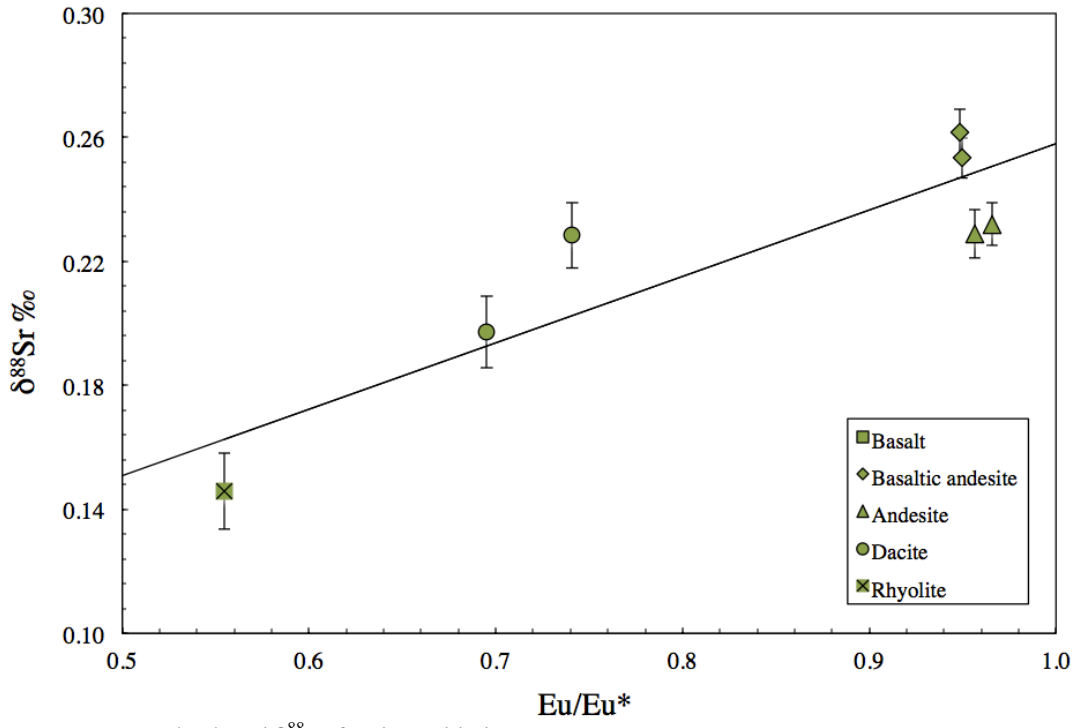

Figure 5.13: Eu/Eu* and δ^{88}Sr for the Hekla lavas.

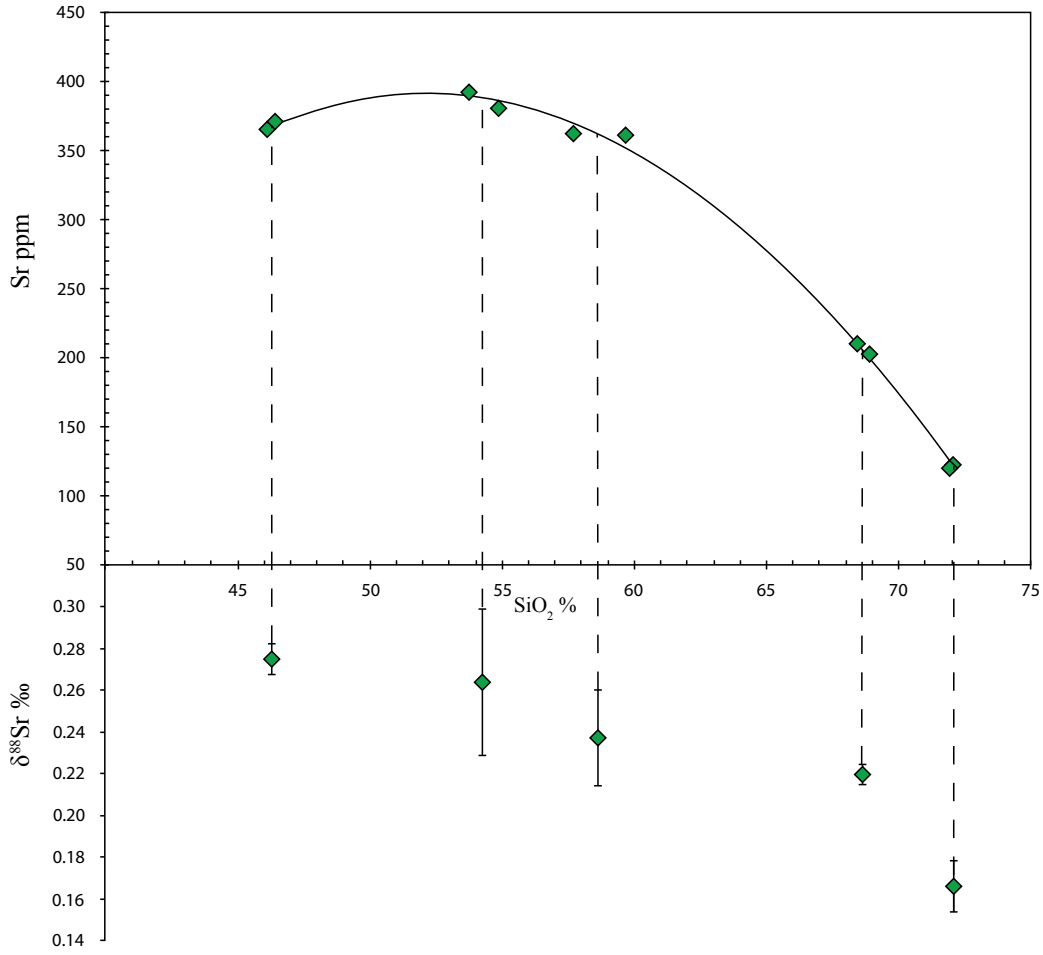

Figure 5.14: The Sr contents of the lavas are shown with corresponding group average δ^{88}Sr values for the lithologies, both with increasing SiO_2 during differentiation. SiO_2 data from Savage et al. (2011).

The onset of plagioclase crystallisation and removal can be identified on Fig. 5.14 by the peak of Sr abundance, at SiO_2 ~52%, after which the Sr content declines as a result of compatible behaviour. Although difficult to define with certainty, there is a suggestion that the Sr stable composition may decrease from 0.265‰ to 0.244‰ before the removal of plagioclase, which implies that another mineral phase aside from plagioclase may be responsible for fractionating the stable isotopes of Sr. Additionally, the strong correlation between $\delta^{30}Si$ and $\delta^{88}Sr$ (Figure 5.4) suggests that as Si isotopes are fractionated by mineral phases in addition to plagioclase at Hekla (Savage et al., 2011), this is also the case for stable Sr. Figure 5.15 shows constant clinopyroxene crystallisation throughout the entire differentiation sequence, as demonstrated by the decrease in CaO/Al_2O_3 ratio with decreasing MgO content. An equally robust correlation exists between $\delta^{88}Sr$ and CaO/Al_2O_3 as well as with Sc, known to exclusively substitute into pyroxene and not plagioclase (Fig. 5.16). Taken together, the implication is that clinopyroxene may also drive the $\delta^{88}Sr$ of the melt to lighter values by preferential partitioning of the heavier isotopes into the mineral. It is noted that such a process would require a significant fractionation factor, as Sr concentrations are typically low in clinopyroxene.

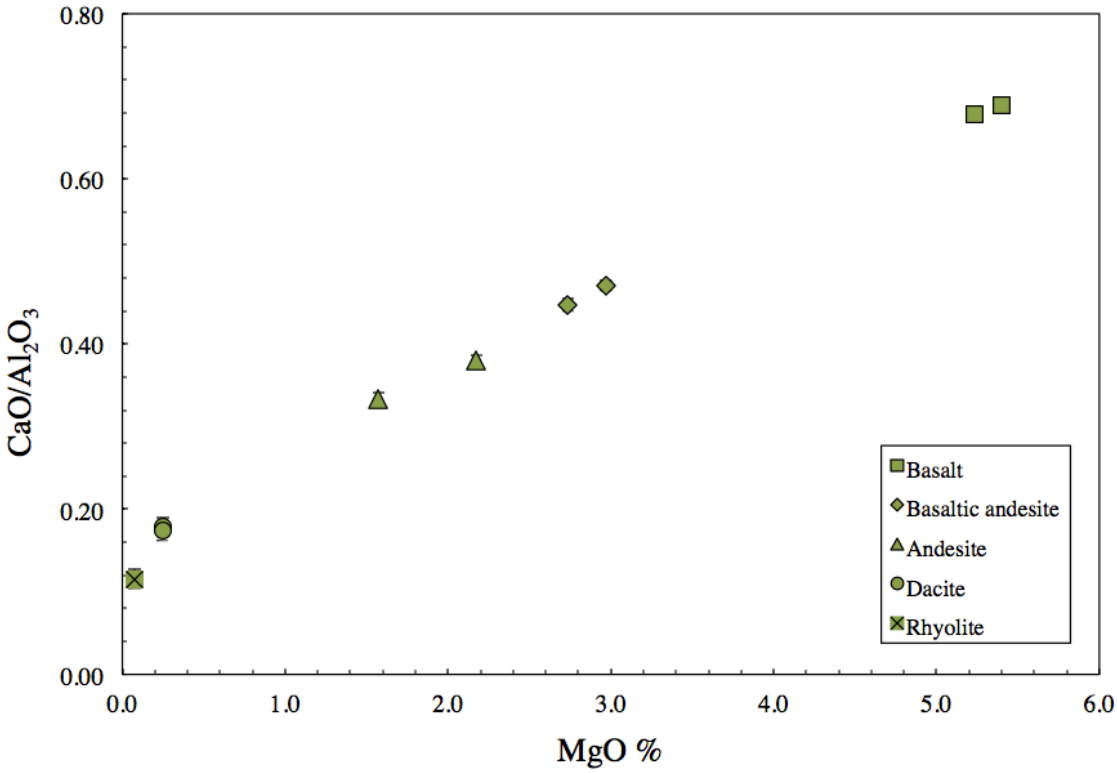

Figure 5.15: Evidence for clinopyroxene fractionation during magmatic evolution- with MgO (wt %). MgO data from Savage et al. (2011).

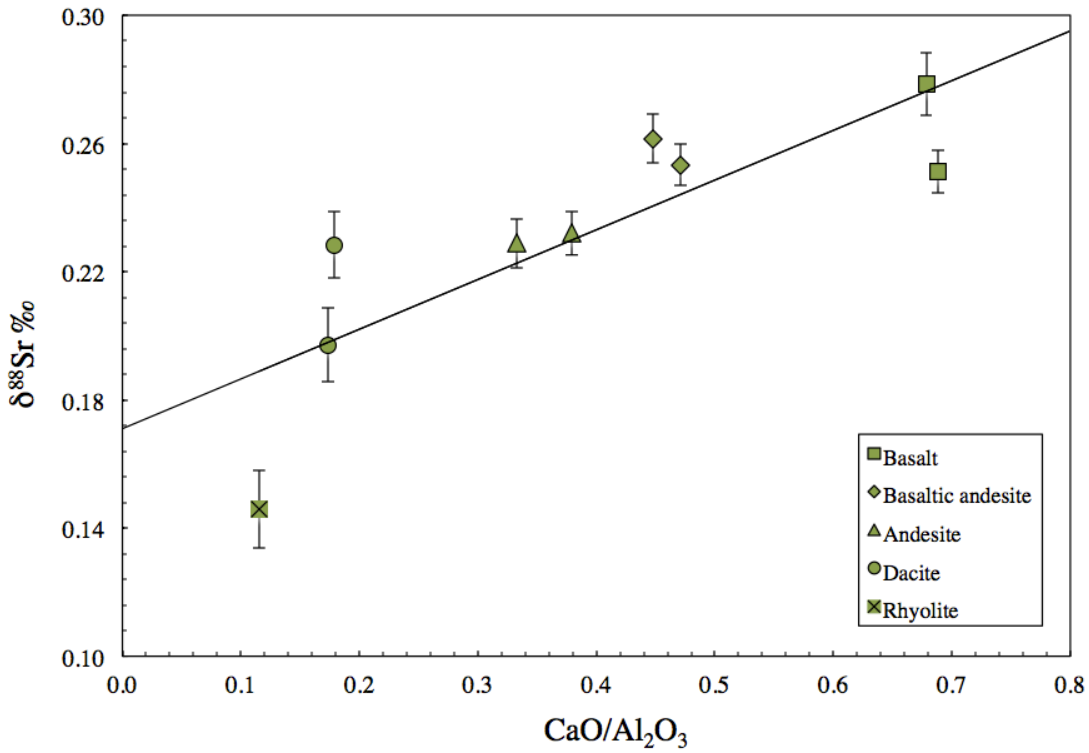

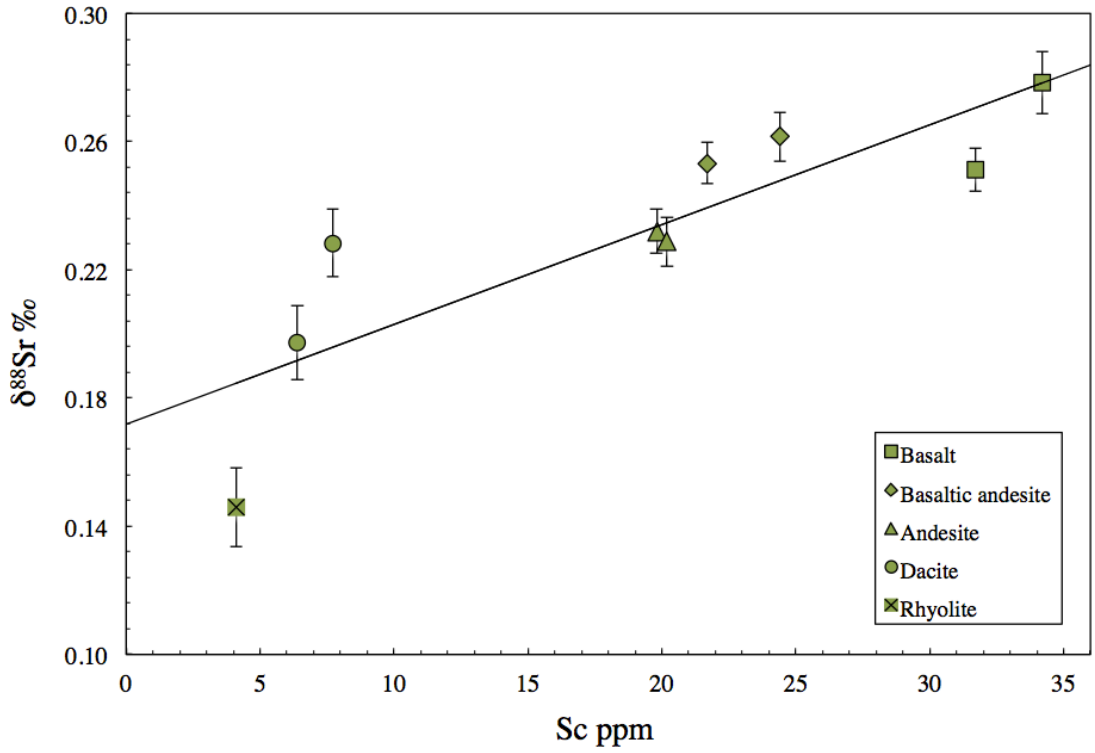

Figure 5.16: Correlation between $\delta^{88}Sr$ and indices of clinopyroxene fractionation, CaO/Al_2O_3 and Sc. Elemental data from Savage et al. (2011).

Theoretically, apatite would be the least likely phase of the three to fractionate stable Sr to such a large degree due to its occurrence as an accessory mineral and its relatively low Sr concentrations. However, as Sr is known to partition into apatite (D_{Sr} ~1-4; GERM; EarthRef; Prowatke and Klemme, 2006) this possibility must also be considered. Apatite is an early crystallising and long-lasting phase that reaches saturation during the evolution of a range of silicate melts (Hoskin et al., 2000). Prowatke and Klemme (2006) show that during experimental apatite/melt trace element partitioning in a silicate melt, REE elements behave compatibly with apatite, whereas LILE are strongly incompatible. The concentrations of Lu and Ba both increase during magmatic differentiation at Hekla, however the Lu/Ba ratio decreases indicating apatite fractionation. Using this as a proxy when compared with $\delta^{88}Sr$, apatite removal cannot account for the evolution to lighter isotopic values (Fig. 5.17). In fact, prior to

plagioclase removal, apatite crystallisation appears to drive the lava composition to heavier values. Using P_2O_5 as an indicator of apatite crystallisation, apatite only commences to fractionate when the sequence produces basaltic-andesite compositions, which is in agreement with the observations of Chekol et al. (2011). The lack of correlation with stable $\delta^{88}Sr$ suggests that apatite plays a minimal role in fractionating the stable isotopes of Sr. Although apatite crystallisation may account for some of the Sr isotopic fractionation seen at Hekla, it is unlikely to be the major phase responsible for driving the rocks to the light isotopic compositions seen. However, it may account for some isotope fractionation prior to plagioclase removal. Nevertheless, there is a limit to how far isotope fractionation can be assigned to particular phases using trace elements alone as mineral proxies.

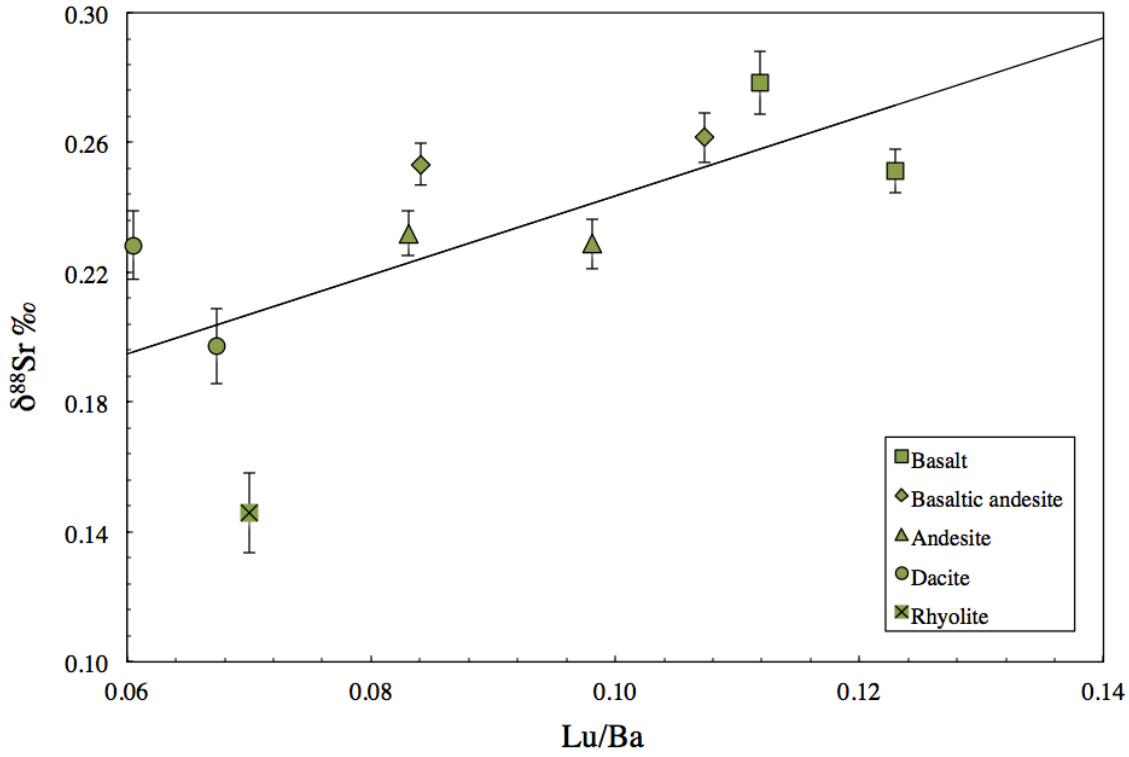

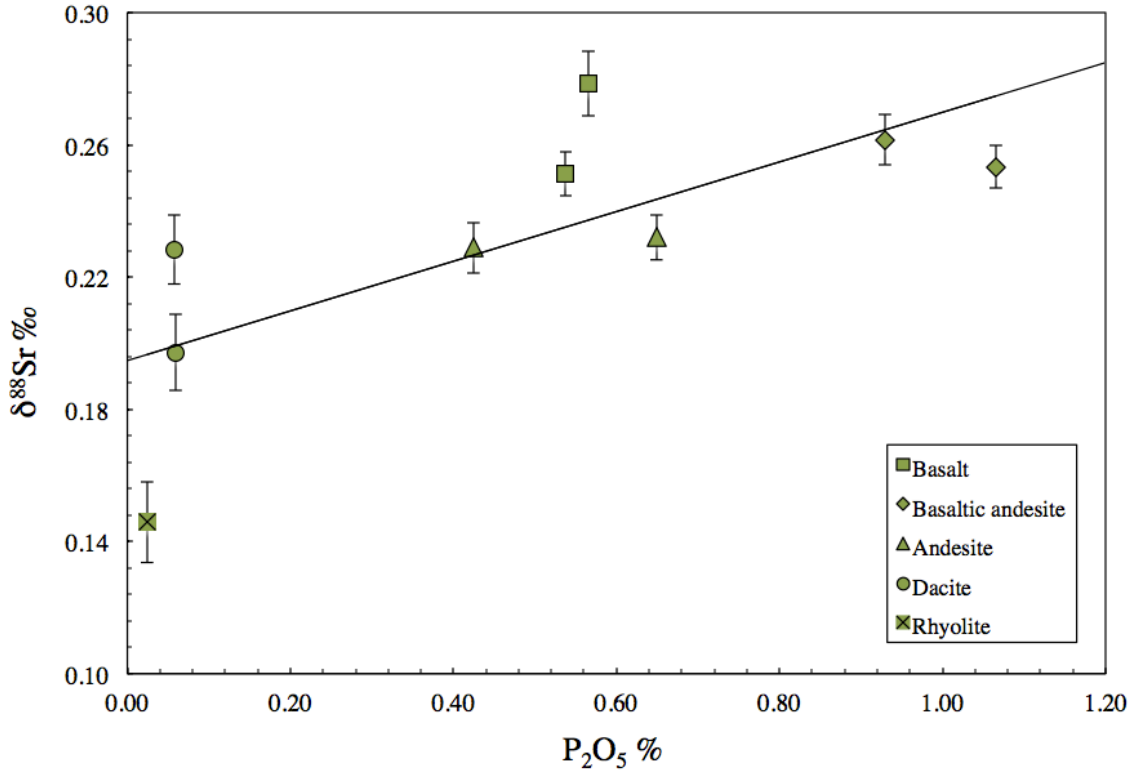

Figure 5.17: $\delta^{88}Sr$ with indices of apatite crystallisation; Lu/Ba ratio and P_2O_5 (%). Elemental data from Savage et al. (2011).

5.6.3.2. Mineral data

The evolution of strontium isotopes are modelled according to Rayleigh fractional crystallisation (Equation 5.3), and used to estimate the overall Sr isotope fractionation factor between the silicate melt and all mineral phases. For this, various values for the bulk mineral-melt isotopic fractionation factor, $\Delta Sr_{solid\text{-}melt}$ (where $1000 \cdot \ln\alpha^{88/86}Sr_{mineral/melt} \approx \Delta^{88}Sr_{mineral\text{-}melt} = \delta^{88}Sr_{mineral} - \delta^{88}Sr_{melt}$), were used and assumed to remain constant and there is no re-equilibration of solids with the liquid.

$$\delta^{88}Sr_{melt} = (\delta^{88}Sr_{source} + 1000)f^{(\alpha-1)} \qquad \textit{Equation 5.3}$$

As a simple linear correlation between $\delta^{88}Sr$ and SiO_2 is observed, HEK 06-09 is taken as the initial composition as it has the lowest SiO_2 and Ba content (169ppm) and

heaviest $\delta^{88}Sr$ composition, (+0.251‰). Ba behaves incompatibly and can be used as a proxy for the fraction of melt remaining, *F*, as described in the following equation:

$$F = \left(\frac{Ba_{initial}}{Ba_{melt}}\right) \qquad \textit{Equation 5.4}$$

Using Ba proves to be a robust method for calculating F, as it suggests that basaltic andesite forms after ~48% crystallisation, and rhyolite after ~75% consistent with similar estimates made by Chekol et al. (2010) and Savage et al. (2011). The results of this modelling are the plotted along with the Hekla in Figure 5.18. From this, a bulk fractionation factor between all minerals and melts of $\Delta^{88}Sr_{solid\text{-}melt}$~ 0.07‰ best describes the Hekla suite, starting from a basaltic composition. Also shown in Figure 5.19, are results of the same modelling, but using a starting composition of +0.278‰, closer to the composition of HEK 12-09.

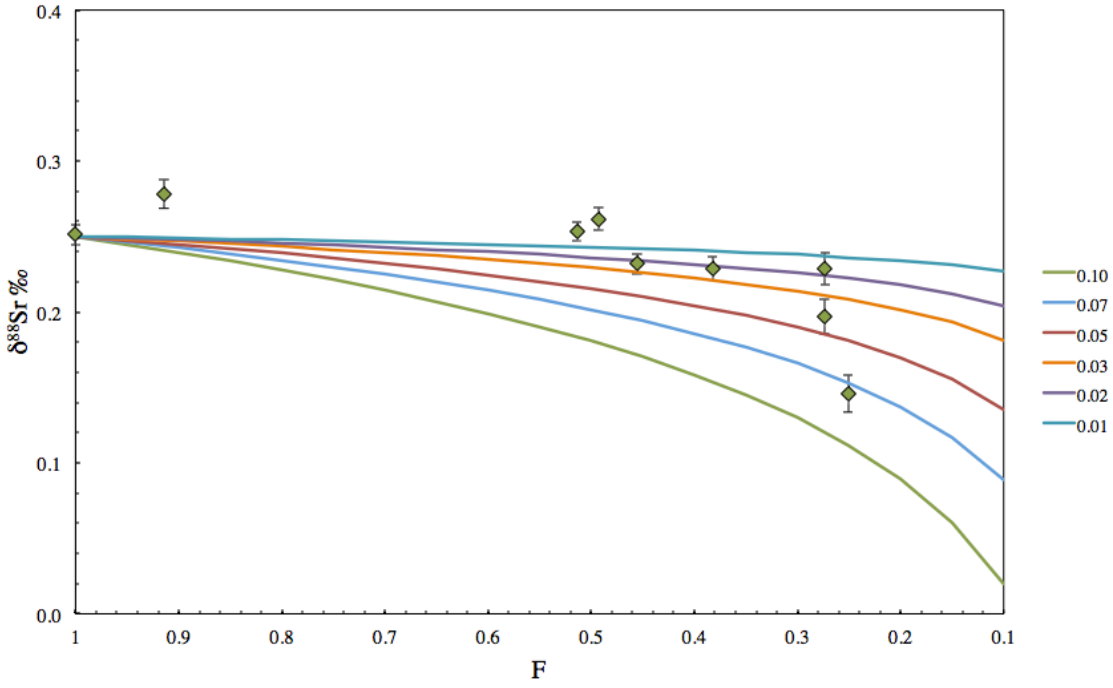

Figure 5.18: Results of modelling Rayleigh fractionation in a magma chamber with varying values of the bulk fractionation factor, Δ. Hekla data shown for comparison. A bulk fractionation factor of 0.07 best fits the Hekla data.

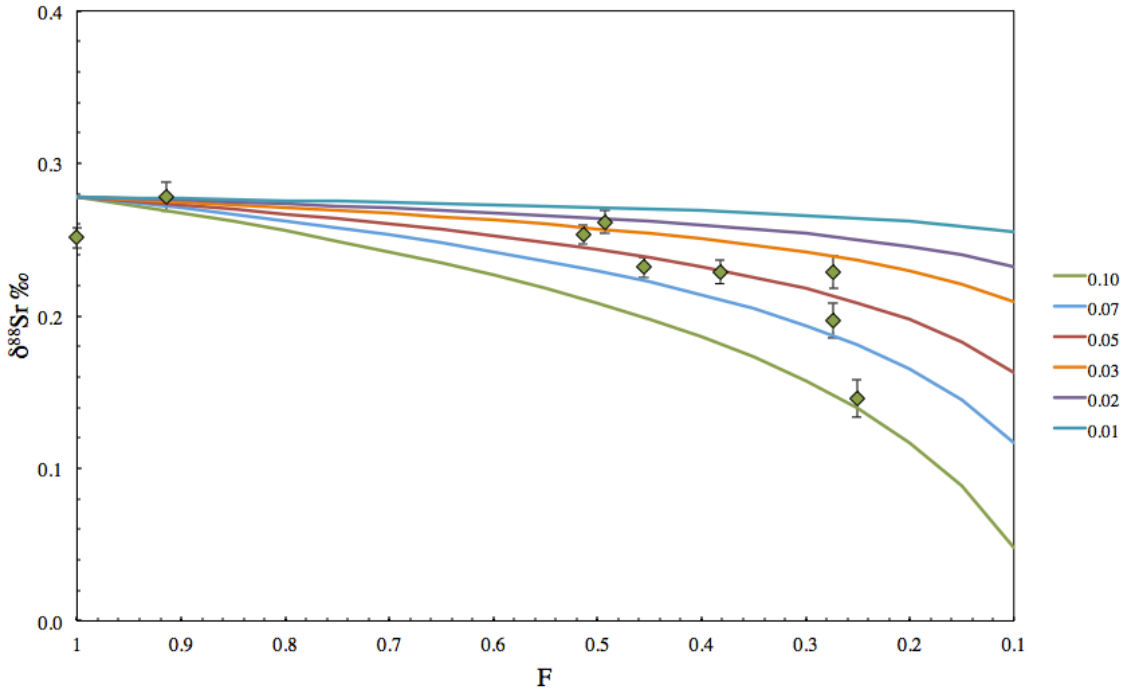

Figure 5.19: Results of modelling Rayleigh fractionation in a magma chamber with varying values of the bulk fractionation factor, Δ. Hekla data shown for comparison. A bulk fractionation factor of 0.06 best fits the Hekla data when a heavier starting composition of $\delta^{88}Sr$= 0.278‰ based on HEK 12-09 is used.

From the mineral analyses of Skaergaard, Mt. Etna and MORB (Chapter 1), individual mineral fractionation factors for minerals crystallising at Hekla can be calculated. An important assumption made in calculating the fractionation factors for the Skaergaard minerals is that they form from a liquid with an initial composition of ~0.26‰. This value was taken from the average of MORB data, and assumes no variation between samples. It should be noted that this assumption is tenuous, considering that variations are observed for MORB in Chapter 3 and thus the chosen initial melt composition is unlikely to be representative. This renders the Skaergaard mineral data non-ideal. For Mt. Etna and MORB, the fractionation factors are calculated using the composition of the glass melt as the starting composition, which again is a less-than-perfect assumption as it is more than likely that the composition of the glass will have changed with crystallisation of the phases of interest. Additionally, there is considerable doubt

surrounding the validity of using this data for purely magmatic purposes as several minerals and whole rock samples from the area (Silvestri) were found to have a sedimentary component in their genesis (sandstones, carbonates and clay-discussed in Chapter 4). With this in mind, and for the purpose of discussion all minerals from both systems are applied to the system at Hekla. Fractionation factors for both systems are given in Table 4.2 in Chapter 4. Using these, the effect of a single mineral crystallising from a melt on the stable Sr composition is modelled for a magma system. This, again, assumes that they behave according to Rayleigh fractionation and isotope fractionation factors remain constant between minerals and melt. Figure 5.20 shows the results of this modelling using a starting composition of HEK 06-09 (δ^{88}Sr =0.251‰) along with the actual data for Hekla. Figure 5.21 shows the results of the same modelling using a starting composition of HEK 12-09 (δ^{88}Sr =0.278‰).

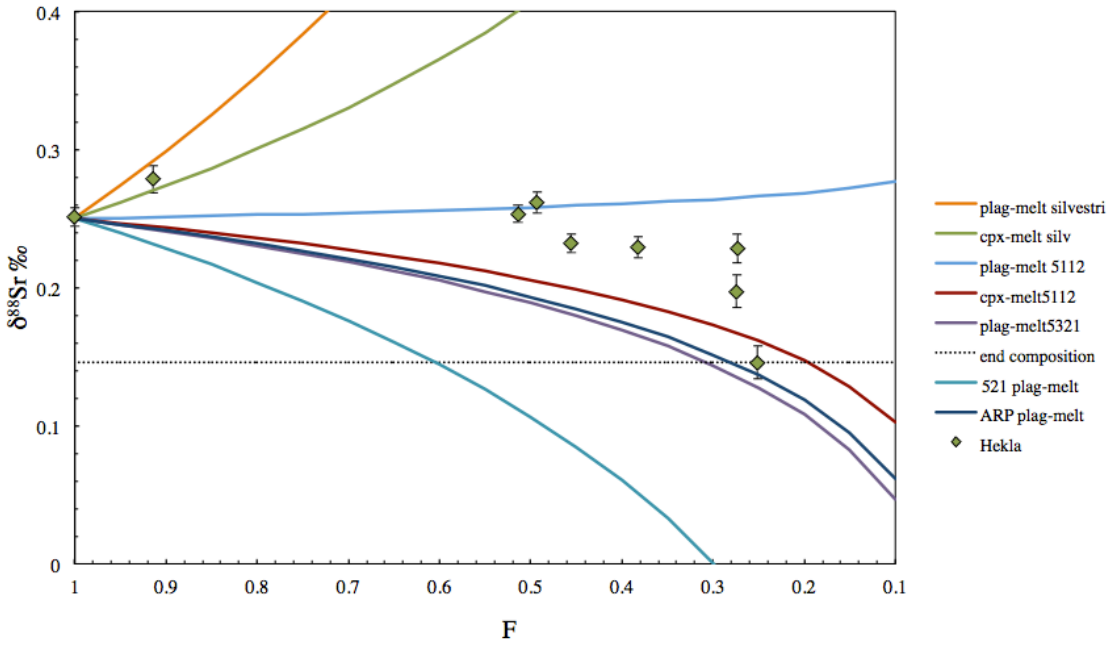

Fig 5.20: Rayleigh modelling of δ^{88}Sr evolution of a magma showing the effects of fractionating plagioclase and clinopyroxene, using a starting composition of HEK 06-09.

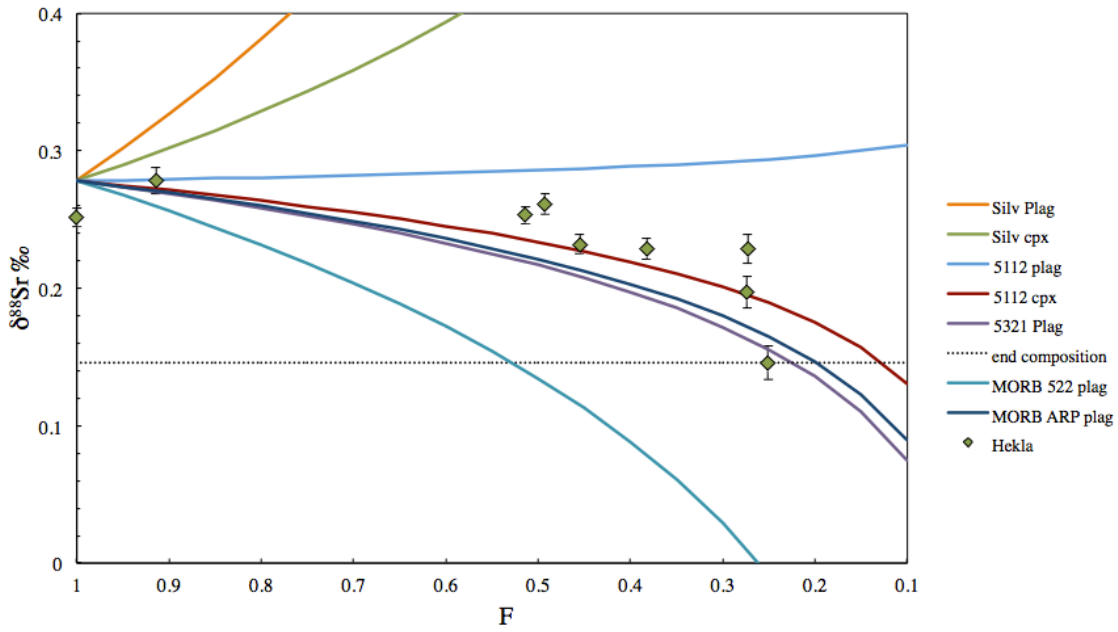

Fig 5.21: Rayleigh modelling of $\delta^{88}Sr$ evolution of a magma showing the effects of fractionating plagioclase and clinopyroxene, using a heavier starting composition of HEK 12-09.

Only two types of mineral (plagioclase and clinopyroxene) were measured and thus the effects of any other minerals cannot be examined in this way. However, it is clear from such modelling that all minerals vary significantly in terms of their Sr isotope composition. Both plagioclase and clinopyroxene can be either light or heavy relative to the melt from which they crystallise, assuming the melt compositions used for these are correct. Plagioclase and clinopyroxene are light relative to the melt for the Silvestri data, and the opposite is true for the Skaergaard system, assuming these crystallised from a melt with an average MORB composition. Figures 5.20 and 5.21 illustrate models calculated by assuming only the mineral in question affects the Sr composition of the melt which is highly unlikely as plagioclase, clinopyroxene and apatite are known to be present in thin section, which can affect Sr. As such, alternative trends can be calculated for the combined effect of the fractionation factors for various combined mineral assemblages. This can be achieved by substituting the known bulk mineral

fractionation factor (Δ_{bulk} = 0.07‰) and individual mineral fractionation factors into the following equation, (assuming a 1:1 ratio of minerals present):

$$\Delta_{bulk} = 0.5\Delta_{plagioclase} + 0.5\Delta_{clinopyroxene} \qquad \textit{Equation 5.5}$$

This equation disregards the role of apatite in contributing to the bulk fractionation factor solely as there is no mineral data for it yet. Combinations of the Skaergaard 5112 clinopyroxene and the Skaergaard 5321 plagioclase, and the Silvestri clinopyroxene with the 521-1-1 plagioclase can generate an isotopically light melt and thus the isotopic trend observed at Hekla (although chosen from different samples). To generate a bulk fractionation factor of 0.07‰ require ratios of plagioclase to clinopyroxene ratios of 1:3 and 2:3 for the mineral combinations respectively.

With the limited mineral data and fractionation factors calculated based on broad assumptions, it is difficult to model the exact isotope evolution at Hekla. This is due to a number of reasons. The first is that the δ^{88}Sr compositions (and thus fractionation factors) of only two minerals present at Hekla are known. For example, the composition of apatite and thus its range of possible fractionation factors, are unknown. The second is that the exact initial melt composition is difficult to either determine or assume, and this may lead to large differences in the calculated fractionation factors. The third is that there is a clear range in the measured stable Sr compositions of plagioclase and clinopyroxene from three systems (Skaergaard, Mt. Etna and MORB). By inference, it is quite possible that the fractionation factors between these minerals and coexisting melt are variable, dependent upon mineral and/or melt composition. Therefore, it is difficult to apply the fractionation factors derived from minerals from Silvestri and Skaergaard to the magmatic system at Hekla. A surprising observation is that at both Skaergaard and Silvestri, the plagioclase is consistently lighter relative to

clinopyroxene, contrary to the MORB plagioclase minerals and the predictions made by correlations drawn between Eu/Eu* and $\delta^{88}Sr$ at Hekla and other systems (Charlier et al., 2012), which assume the removal of isotopically heavy plagioclase as the main driving force to light compositions in the melt. The role of clinopyroxene in this has not been discussed and is assumed to play a minor part. It is also surprising that although the fractionation factors largely depends on the initial composition assumed for the melt, plagioclase and clinopyroxene could be both isotopically heavy and light relative to this. From this, we can conclude from trace element and isotope data that plagioclase is the main mineral controlling stable Sr isotope fractionation in the differentiation sequence at Hekla, with a minor role of clinopyroxene and/or apatite. Mineral data from the two Skaergaard and Etna systems are, in general, unsuitable when applied to Hekla as it is found that there are dramatic differences in the behaviour of minerals in different systems.

5.7. Conclusions

The volcanic suite at Hekla suite show resolvable variations in the $^{87}Sr/^{86}Sr$ ratio of 0.703161 (±2) to 0.703220 (±5), as well as in the $\delta^{88}Sr$ ratio of +0.278 ± 0.010 to +0.146 ± 0.012‰. These igneous rocks shows a linear increase in the radiogenic ratio and in the stable $\delta^{88}Sr$ with increasing silica content and other indices of magmatic differentiation. Variations in $^{87}Sr/^{86}Sr$ have not been reported before for Hekla, either because the precision was not sufficient to detect such small variations (Sigmarsson et al., 1992b) or because a limited range of rock types were analysed (Chekol et al., 2011). When the observed trend in $^{87}Sr/^{86}Sr$ is combined with stable Sr, contaminants with heavy $\delta^{88}Sr$ compositions such as seawater can be ruled out. Hydrothermal fluids have been dismissed by previous studies (Schuessler et al., 2009), but even if present, are

unlikely to drive the stable Sr composition to such light values. Having ruled out alternatives such as diffusion, radiogenic in-growth, and secondary overprinting, the most likely contaminant is a crustal component, assimilated during on-going fractional crystallisation. Given the young age of Iceland and its overall mafic composition, this is likely to be pre-existing basaltic crust with a more radiogenic signature. However, if the assimilant is weathered basalt containing calcium carbonate as a secondary weathering mineral with light Sr compositions, it could be responsible for the shifts to lighter stable isotopic compositions and increasingly radiogenic values. Given the linearity of the trends before and during the inferred mixing regime where AFC is likely to occur, this may not necessarily be the case. Strong, linear correlations between δ^{88}Sr and indices of magmatic differentiation imply that magmatic evolution is capable of fractionating stable Sr to light isotopic values, which can be explained by the removal of lighter isotopes by crystal settling. Correlations with the Eu anomaly of the rocks implies that plagioclase fractionation is responsible for driving the isotopic composition of the melt to such light values, through the preferential partitioning of the heavy isotopes of Sr into plagioclase, in good agreement with previous work (Charlier et al., 2012). The possibility of stable isotope fractionation prior to plagioclase removal combined with correlations between the former and indices for clinopyroxene fractionation suggest other minerals, such as clinopyroxene, in addition to plagioclase have the potential to fractionate Sr stable isotopes (e.g. apatite). This is further supported by mineral analyses of MORB, Skaergaard and Mt Etna samples, which show that in all cases both clinopyroxene and plagioclase have a composition isotopically distinct from that of the melt. Overall, the data for Skaergaard and Silvestri minerals are not fully consistent with whole-rock Hekla data as both plagioclase and clinopyroxene can be isotopically lighter (as well as heavier) than the melt, and in both cases, plagioclase is consistently

determined to be isotopically lighter than clinopyroxene. The fractionation of $\delta^{88}Sr$ to lighter values in the melt during differentiation of Hekla is consistent with the heavier compositions of MORB plagioclase separates relative to glass (Chapter 3). A bulk fractionation factor between all minerals and the melt is calculated from Rayleigh fractional crystallisation to be $\Delta^{88}Sr_{mineral\text{-}melt}$=0.07‰. Rayleigh modelling using two mineral combinations (5112 cpx and 5321 plagioclase in a 3:1 ratio and Silvestri clinopyroxene with 521-1-1 plagioclase in a 2:3 ratio) of a melt with a starting composition of Hekla 06-09 ($\delta^{88}Sr$ =0.26‰) is consistent with the Hekla sequence. It is difficult to comment on the role of apatite, into which Sr can partition, due to a lack of mineral data. Further work would involve the measurement of minerals crystallising throughout the differentiation sequence as well as that of the glass melt, which is unfortunately difficult for Hekla given the aphyric texture of the samples. This would constrain the effect that each mineral has on the isotopic composition of the melt during different stages during the evolution of the magma as well as giving exact fractionation factors for the minerals relevant to that precise magmatic system. As the mineral data vary to such an extent, it would be interesting to constrain the effects of changing magma composition, tectonic setting, and other such factors on the fractionation factors for various minerals, and hence their effect on the isotopic composition of the melt.

CHAPTER SIX

Stable Sr isotope constraints on the formation and evolution of the Moon

Abstract

Using double-spiking TIMS techniques significant variations in the $^{88}Sr/^{86}Sr$ of lunar rocks of ~0.3‰ are determined that cannot be resolved from one another at the level of precision typically achieved by MC-ICP-MS. Variations in the $\delta^{88}Sr$ composition of high-Ti mare basalts likely reflect melting of residual cumulates variably depleted in plagioclase, and fractionated in $\delta^{88}Sr$, formed after extensive plagioclase crystallisation during magma ocean differentiation. The $^{84}Sr/^{86}Sr$ ratios of terrestrial and lunar rocks are identical within the uncertainty of this study, and lie on a single mass-dependent fractionation line with $^{88}Sr/^{86}Sr$, ruling out any excesses or deficiencies in ^{84}Sr that might reflect remnant nucleosynthetic effects. High-precision $^{87}Sr/^{86}Sr$ data are used in combination with ID Rb-Sr data to place precise constraints on Rb-Sr model ages for the Moon. Based on the ferroan anorthosite (FAN) 60015, an age of 4.523 ± 0.019 Ga (equivalent to 44 ± 13 Ma after the start of the solar system) is determined, and used to constrain a youngest possible age of ~31 million years after the start of the solar system.

6.1. Introduction

The most prevalent theory for the formation of the Moon is the condensation and coalescence of silicate-rich vapour and debris from a Giant Impact between a Proto Earth and a Mars-sized body named Theia, anywhere between 30-200 Myr after the formation of the Solar System (e.g. Hartmann and Davis, 1975; Cameron and Benz, 1991; Cameron, 1986; Canup and Asphaug, 2001; Touboul et al., 2007; Pahlevan and Stevenson, 2007; Halliday, 2008; Borg et al., 2011). The accretion of hot material is thought to have led to the formation of a lunar magma ocean (LMO). For the last decade, smooth particle hydrodynamics (s.p.h.) models of the Giant Impact have been most consistent with the Moon being mainly derived from Theia (Cameron, 2000; Canup and Asphaug, 2001), which is in contrast to the expectation from isotope data, given the isotopically identical compositions of the Moon and Earth. This is particularly relevant for oxygen, the isotope composition of which is extremely variable in the Solar System, yet isotopically identical in the Earth and Moon to within ±5ppm (Wiechert et al., 2001; Spicuzza et al., 2007), but also holds for the stable isotopes of refractory heavier elements including Si, Cr, Ti and W (Armytage et al., 2012; Touboul et al., 2007; Zhang et al., 2012; Lugmair and Shukulyokov, 1998).

The Moon is enriched in refractory lithophile elements such as Sr, but strongly depleted in moderately volatile lithophile elements such as Rb (Taylor, 1980; Wanke, 1981). It has been conjectured that this volatile element depletion was caused by the Moon–forming Giant Impact. Radiogenic Sr isotopes provide evidence of significant loss of moderately volatile elements during the late (>10 Myr) accretion history of the material that formed the Moon (Halliday and Porcelli, 2001). Recently, Zn stable isotope data for lunar rocks (Paniello et al., 2012) has been taken as the first evidence

for isotope fractionation of moderately volatile elements, previously unresolved using K (Humayun and Clayton, 1995), providing further evidence for the Giant Impact theory through fractionation during evaporation, and consistent with the observation that the Moon is depleted in volatile elements relative to Earth.

Although a difference is unlikely given the refractory nature of Sr, there remains a question as to whether the average Sr stable isotope composition of the Earth and Moon are the same. There is a suggestion that lunar rocks may be isotopically lighter in $\delta^{88}Sr$ (+0.16 ± 0.07‰) than terrestrial mantle-derived basalts ($\delta^{88}Sr$ = +0.30 ± 0.07‰) but this cannot be resolved at the current analytical precision of MC-ICP-MS, illustrated in Figure 1.2 in Chapter 1 (Moynier et al., 2011; Charlier et al., 2012). Constraining the bulk lunar Sr isotopic composition could provide information on the Giant Impact, the impactor Theia, and the extent to which Sr is homogenous across inner solar system bodies. Variations in $\delta^{88}Sr$ in lunar basalts have also been shown to be linked with the europium anomaly (Eu/Eu*), usually taken as an index of plagioclase crystallisation, and can be successfully modelled through the heavy isotopes of Sr being preferentially partitioned into plagioclase (Charlier et al., 2012). Aside from this study, only a single lunar meteorite has been analysed for its stable Sr composition (Moynier et al., 2011). However, taken together, these observations are based on a limited sample selection most of which are soils or meteorites, and these may not be representative of the mantle sources. Furthermore, each of these studies measured $\delta^{88}Sr$ by MC-ICP-MS, and any variations that do exist cannot be resolved at the ±50ppm precision reported. This study presents high-precision DS-TIMS data for an extensive suite of lunar highland rocks and mare basalts aimed at resolving these variations and understanding the causes of $\delta^{88}Sr$ fractionation.

Three lines of information can be acquired simultaneously using the DS-TIMS technique; stable $^{88}Sr/^{86}Sr$, nucleosynthetic $^{84}Sr/^{86}Sr$, and radiogenic $^{87}Sr/^{86}Sr$ (Chapters 1 and 2). As such, measurements of the Sr isotope composition of lunar rocks by this method can also address other key questions. One of these is that ^{84}Sr may serve as a potentially useful tracer of nucleosynthetic contributions (Chapter 1), as differences in nucleosynthetic anomalies between the Earth and the Moon could potentially be used to identify a primary isotopic signature retained by the impactor as they reflect the stellar sources from which planetary bodies accreted. However, only two lunar samples have been analysed and these lack complimentary $\delta^{88}Sr$ data, which is required to distinguish between ^{84}Sr and ^{86}Sr as the cause of isotope variation in a three-isotope plot (Moynier et al., 2012). A unique benefit of DS-TIMS relative to MC-ICP-MS is that it allows a precise comparison between $^{84}Sr/^{86}Sr$ and $^{88}Sr/^{86}Sr$ for lunar and terrestrial material for the first time in three-isotope space. Measurements of the radiogenic $^{87}Sr/^{86}Sr$ composition can be used to investigate another pertinent question: the age of the Moon, which itself may provide both evidence on the nature of the Giant Impact as well as key constraints on its timing. Precise measurements of the radiogenic $^{87}Sr/^{86}Sr$ composition of lunar samples can be used to calculate a model age for the Moon, made feasible by the low Rb/Sr ratio of the volatile-depleted Moon. Based on a compilation of data, a previous estimate of 90 ± 20 Myr after the start of the Solar System has been obtained (Halliday, 2008). However, the lunar $^{87}Sr/^{86}Sr$ data used to estimate a Rb-Sr age of the Moon have significantly lower precision than those that can currently be achieved using TIMS techniques. High precision $^{87}Rb/^{87}Sr$ and $^{87}Sr/^{86}Sr$ measurements of a range of lunar material, including the anorthosites 60015 and 60025, may better constrain the Rb-Sr model age of the Moon and could provide new insights into the timescales of its formation.

This study presents high-precision DS-TIMS $^{88}Sr/^{86}Sr$, $^{84}Sr/^{86}Sr$, and $^{87}Sr/^{86}Sr$ data for an extensive suite of lunar highland rocks and mare basalts, in order to:

1) Detect and determine the causes of resolvable variations in $^{88}Sr/^{86}Sr$ in contrasting lunar lithologies, which may yield information regarding their processes of formation;

2) Compare the $^{84}Sr/^{86}Sr$ composition of the Moon with that of the Earth, and other planetary bodies, to detect any resolvable differences due to nucleosynthetic anomalies, only achievable by pairing with precise $\delta^{88}Sr$ data;

3) Obtain very high precision $^{87}Sr/^{86}Sr$ data, in order to derive a precise Rb-Sr model age of the Moon, in combination with complementary $^{87}Rb/^{87}Sr$ data.

6.2. Sample description

Samples were selected from Apollo missions 11, 14, 15, 16 and 17 to reflect a range of compositions from anorthosites and other highland rocks, to high- and low-Ti mare basalts and picritic glasses. Two of the whole rock samples (67955 and 15555) have been previously analysed by Charlier et al. (2012) for $\delta^{88}Sr$. The lunar highland samples comprise two ferroan anorthosites, a noritic anorthosite, two norites and a troctolite. The lunar basalts include three low-Ti mare basalts; the aluminous basalt 14053 and two olivine normative basalts (15555 and 15016), eight high-Ti mare basalts and two picritic glasses; one green glass (74220) and an orange glass (15425).

6.3. Analytical technique

The lunar samples were provided in powdered form by NASA and underwent no further treatment prior to dissolution. Sample quantities ranging from 20-90 mg of the homogenised material were dissolved, spiked and Sr separated from the solutions and analysed by TIMS at the Open University (as detailed in Chapter 2). Aliquots from the same sample solutions were analysed for their trace and Rare Earth element concentrations (Appendix E) using quadrupole inductively coupled plasma mass spectrometry (ICP-MS) (Agilent) at the Open University, Milton Keynes. Rock standards, including BHVO-1, JB-2, BIR-1, BCR-2, JG-2, SDC- 1 and AGV-1, were analysed as an assessment of accuracy. The standard BHVO-1 was measured repeatedly during each sample run to correct for machine drift. The external reproducibility was determined by routinely analysing reference materials (BIR-1 and JB-2) and found to be better than ± 2% (2σ).

6.4. Results

The Sr isotope data for the lunar samples is given in Table 6.1. Separate $^{87}Rb/^{86}Sr$ data and Rb-Sr model ages are given in Table 6.2.

6.4.1. Trace elements

The samples exhibit the classic REE patterns of Eu enrichment and depletion in feldspathic rocks and basalts respectively, revealed by positive and negative Eu anomalies, and these are illustrated in Figures 6.1 and 6.2. This is thought to reflect the reduced nature of the Moon and the resulting substitution of Eu^{2+} for Ca^{2+} in plagioclase, leading to an enrichment in Eu relative to other 3+ oxidation state REEs in plagioclase rich anorthosite and troctolite, and a corresponding depletion in basalts that are later formed from the same source.

Sample name	Lithology	Eu/Eu*	ε^{84}Sr (2 se)	δ^{84}Sr (‰; 2 se)	^{87}Sr/^{86}Sr (2 se)	δ^{88}Sr (‰; 2 se)
Highland suite						
60015	Ferroan anorthosite	58.37	-0.46 ± 0.17	-0.33 ± 0.02	0.699170 ± 0.000002	0.285 ± 0.006
60025	Ferroan anorthosite	34.24	-0.64 ± 0.15	-0.55 ± 0.02	0.699078 ± 0.000002	0.448 ± 0.007
67955	Noritic anorthosite	1.19	-0.65 ± 0.17	-0.33 ± 0.02	0.700580 ± 0.000002	0.268 ± 0.006
77215	Norite	0.82	-0.64 ± 0.18	-0.35 ± 0.02	0.703319 ± 0.000002	0.288 ± 0.008
78235	Norite	1.30	+0.08 ± 0.20	-0.26 ± 0.03	0.700325 ± 0.000003	0.269 ± 0.007
76535	Troctolite	3.90	-0.17 ± 0.19	-0.29 ± 0.02	0.699660 ± 0.000003	0.271 ± 0.007
					Highland average	0.31 ± 0.06
Glasses						
74220	Orange glass	0.74	-0.42 ± 0.18	-0.33 ± 0.02	0.700145 ± 0.000003	0.289 ± 0.009
15425	Green glass	0.54	-0.74 ± 0.18	-0.38 ± 0.02	0.703015 ± 0.000002	0.310 ± 0.009
					Glass average	0.30 ± 0.02
Low-Ti basalts						
15016	Olivine normative basalt	0.63	-0.61 ± 0.18	-0.34 ± 0.02	0.700572 ± 0.000002	0.288 ± 0.007
14053	Aluminous basalt	0.52	+0.08 ± 0.26	-0.28 ± 0.03	0.703439 ± 0.000004	0.291 ± 0.011
15555	Olivine normative basalt	0.73	-0.43 ± 0.17	-0.25 ± 0.02	0.700271 ± 0.000002	0.212 ± 0.008
					Low-Ti basalt average	0.26 ± 0.05
High Ti-basalts						
75075	High-Ti basalt	0.36	-0.24 ± 0.18	-0.29 ± 0.02	0.699981 ± 0.000002	0.275 ± 0.010
71566	High-Ti basalt	0.53	-0.85 ± 0.19	-0.34 ± 0.02	0.699706 ± 0.000002	0.262 ± 0.007
77516	High-Ti basalt	0.48	-0.64 ± 0.16	-0.29 ± 0.02	0.699754 ± 0.000002	0.231 ± 0.009
10049	High-Ti basalt	0.28	-0.51 ± 0.18	-0.24 ± 0.02	0.704817 ± 0.000002	0.193 ± 0.009
74255	High-Ti basalt	0.30	-0.71 ± 0.17	-0.26 ± 0.02	0.702077 ± 0.000002	0.197 ± 0.012

70035	High-Ti basalt	0.40	-0.11 ± 0.21	-0.19 ± 0.02	0.699871 ± 0.000003	0.202 ± 0.006
71596	High-Ti basalt	0.52	-0.56 ± 0.19	-0.18 ± 0.03	0.699637 ± 0.000003	0.129 ± 0.011
70135	High-Ti basalt	0.35	-0.68 ± 0.19	-0.30 ± 0.02	0.700034 ± 0.000003	0.235 ± 0.006
					High-Ti basalt average	0.22 ± 0.03
					Lunar average	**0.26 ± 0.03**

Table 6.1: REE's normalized relative to CI values as given by Anders & Grevesse (1989). Eu/Eu* calculated as [Eu]/√ ([Sm]*[Gd]). $^{87}Sr/^{86}Sr$ data normalised to an NBS value of 0.71024. Errors in $\delta^{84}Sr$, $^{87}Sr/^{86}Sr$ and $\delta^{88}Sr$ are given as 2 s e from the mean, and errors in group averages given as 2 s e, calculated as 2(s.d.√n).

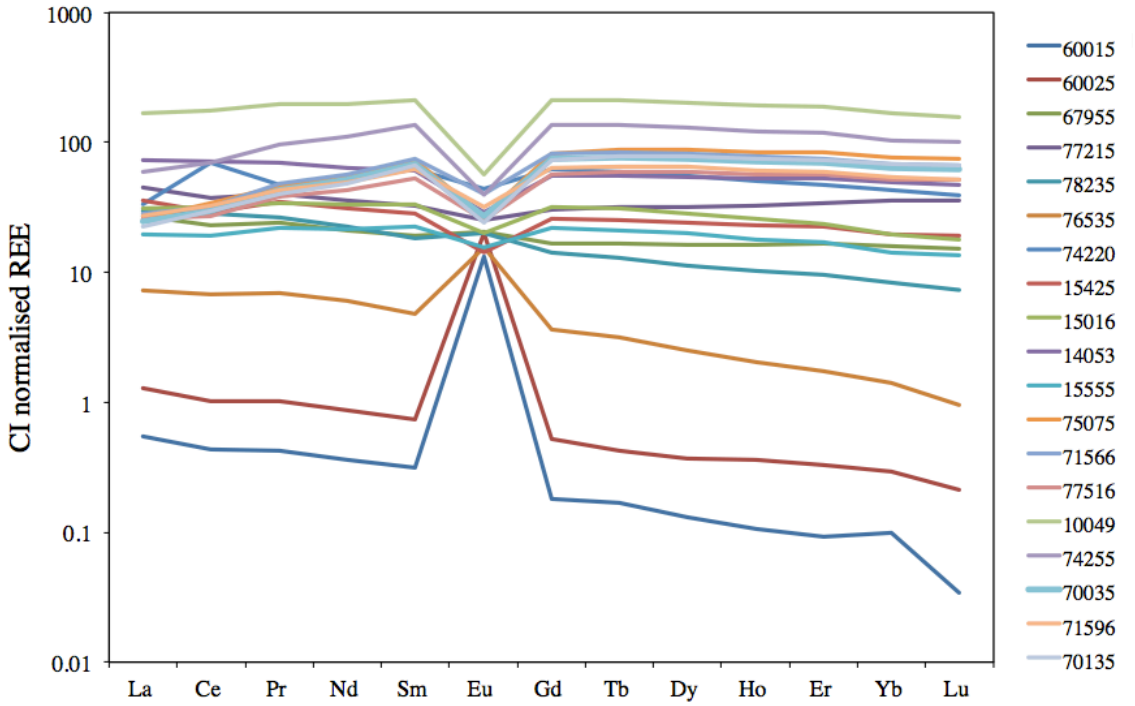

Figure 6.1: CI normalised REEs for individual samples. Chondrite values taken from Anders and Grevesse (1989).

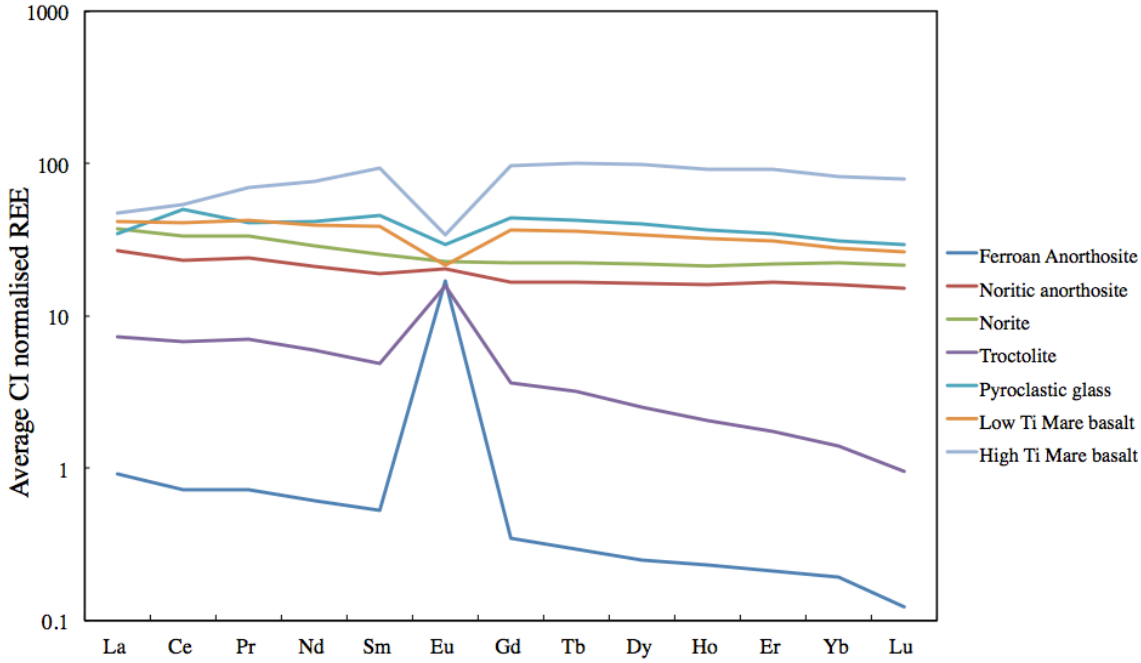

Figure 6.2: Average CI normalised REEs for lithological groups. The high-Ti mare basalt samples are the most depleted relative to plagioclase, as demonstrated by the most negative average Eu anomaly.

6.5.3. Nucleosynthetic variations in $^{84}Sr/^{86}Sr$

Variations in $^{84}Sr/^{86}Sr$ are reported in ε-units ($\varepsilon^{84}Sr$) for non-spiked internally corrected Sr measurements, and in δ-units for mass dependent stable Sr isotope variations ($\delta^{84/86}Sr$) determined from the double spike method. These represent 10^{-4} and 10^{-3} relative deviations from the average of NBS 987 respectively, after correction of mass fractionation using the $^{88}Sr/^{86}Sr$ ratio (assumed and true, respectively), and are normalised to the average $^{84}Sr/^{86}Sr$ value obtained from repeated measurement of NBS 987 of 0.0564893. By definition $\varepsilon^{84}Sr_{NBS\text{-}987} = 0$. The long-term external precision, obtained by numerous analyses of NBS 987, for $^{84}Sr/^{86}Sr$ is ±20 ppm (2SD).

The lunar samples possess $\varepsilon^{84}Sr$ values ranging from $\varepsilon^{84}Sr = -0.85\pm 0.19‰$ for the high-Ti mare basalt 71566 to $\varepsilon^{84}Sr = +0.11 \pm 0.21‰$ for the high-Ti mare basalt 70035, relative to terrestrial NBS-987. This results in a small, but resolvable, variation in $\varepsilon^{84}Sr$ of 1.04‰. Figure 6.3 shows the $\varepsilon^{84}Sr$ composition of the lunar samples compared with terrestrial OIB and MORB samples analysed in Chapter 3. On average, the lunar samples possess a slightly higher $\varepsilon^{84}Sr$ value of -0.46 ± 0.13‰ than the average of terrestrial samples ($\varepsilon^{84}Sr = -0.48 \pm 0.09‰$; n=34), but both overlap and are statistically indistinguishable within the error of this study. Recently published lunar $^{84}Sr/^{86}Sr$ data from Moynier et al. (2012) have been normalized to an undisclosed NBS 987 $^{84}Sr/^{86}Sr$ ratio other than the one used in this study. When normalized to the same NBS value, both lunar samples analysed by Moynier et al. (2012) fall within the range of the values obtained in this study, but the sample in common, 15555, is more positive by ~-0.6‰.

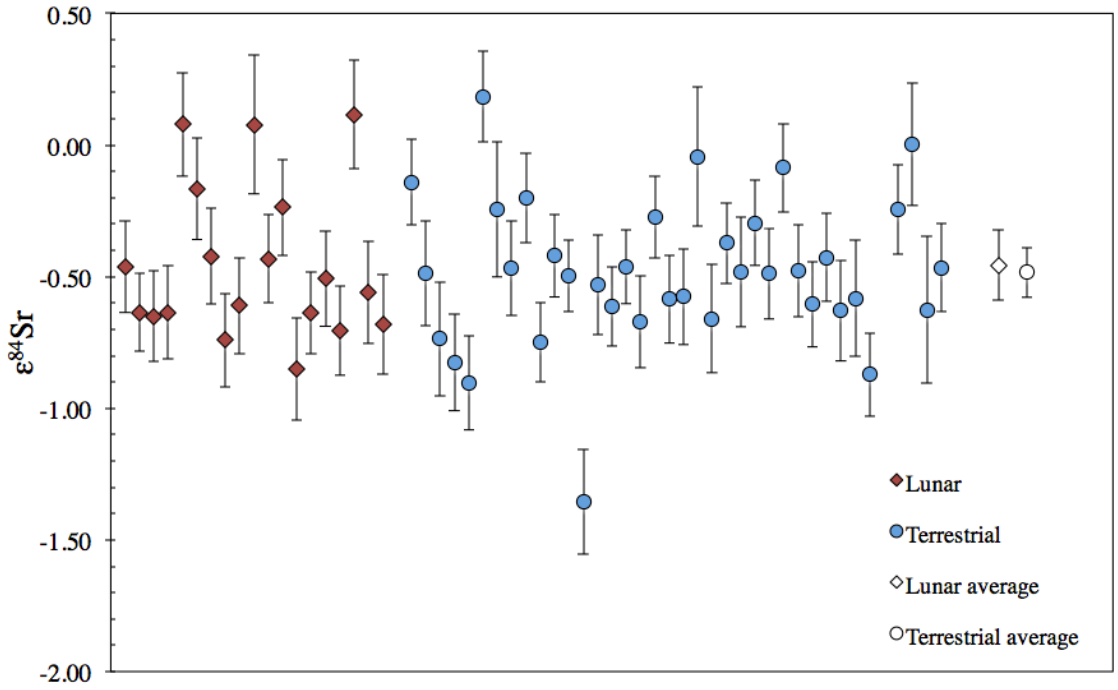

Figure 6.3: $\varepsilon^{84}Sr$ compositions of measured lunar and terrestrial rocks, shown with averages.

Although the average $\varepsilon^{84}Sr$ values of the two bodies are slightly offset from one another, due to the internal normalization to a fixed value of $^{88}Sr/^{86}Sr$, an apparent positive $^{84}Sr/^{86}Sr$ anomaly could either be attributed to a *p*-process excess on ^{84}Sr or to an *r*-process excess on ^{88}Sr, but without complimentary $\delta^{88}Sr$ data variations in $^{84}Sr/^{86}Sr$ cannot be unquestionably assigned to these excesses or deficiencies in ^{84}Sr or ^{86}Sr. This is the case for all existing $^{84}Sr/^{86}Sr$ data obtained in earlier studies. Both mass dependent processes and nucleosynthetic differences can cause variations in the $^{84}Sr/^{86}Sr$ ratio. For this reason, in order to investigate any nucleosynthetic effect on ^{84}Sr it is necessary to eliminate the effects of mass dependent fractionation by plotting the "true" $\delta^{84}Sr$ against $\delta^{88}Sr$. High precision $\delta^{84}Sr$ data can only determine any excesses or deficiencies in nucleosynthetic ^{84}Sr when paired with $\delta^{88}Sr$ data. Figure 6.4 illustrates a three-isotope Sr plot for all lunar samples, shown with terrestrial MORB and OIB. The lunar and

terrestrial samples show co-variations between $\delta^{84}Sr$ and $\delta^{88}Sr$ that fall on mass-dependent fractionation lines (Figure 6.4) that cannot be resolved from one another within the error of this study. The lunar data fall on a mass-dependent fractionation line with an equation of y = -1.00 (±0.01)x - 0.005 (±0.003) and the terrestrial with an equation y = -1.00 (±0.04)x - 0.008 ± 0.010.

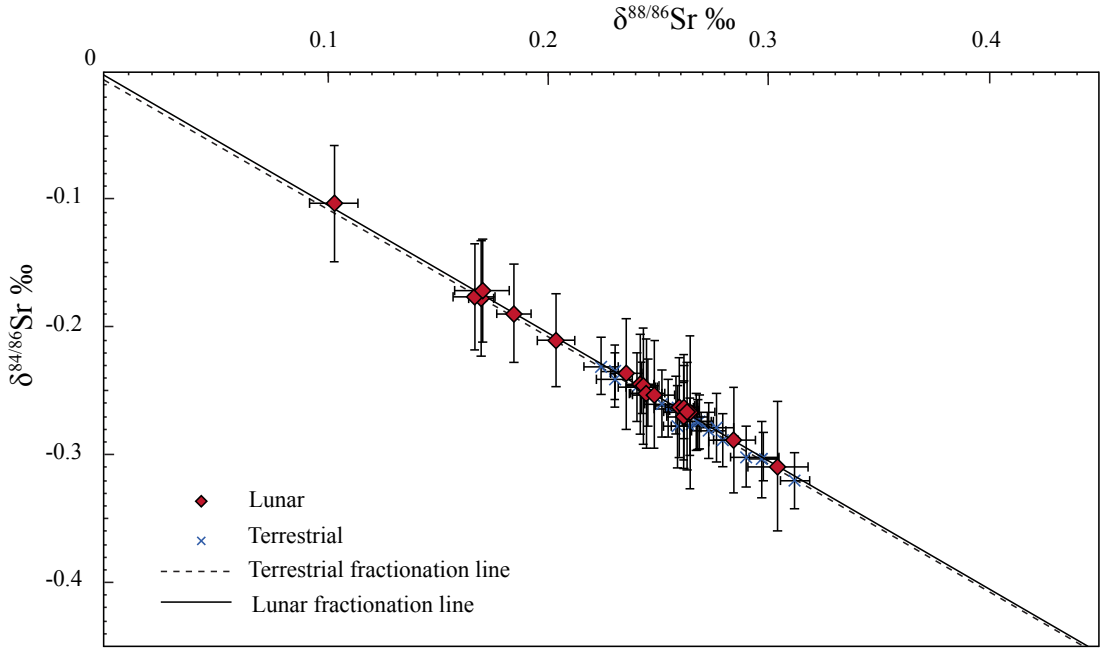

Figure 6.4: Three-isotope plot of $\delta^{84}Sr$ against $\delta^{88}Sr$ for lunar and terrestrial samples, which fall on a single mass fractionation line. Lunar samples are depicted in red and a solid mass fractionation line, whilst terrestrial samples are in blue with a dashed mass fractionation line.

6.5.3. Stable $^{88}Sr/^{86}Sr$

The $\delta^{88}Sr$ values for the samples are given in Table 6.1 along with their lithological rock type averages, and shown in Figure 6.5. The total range of $\delta^{88}Sr$ compositions of the lunar samples varies from $\delta^{88}Sr$ = 0.129 ± 0.011‰ to 0.448 ± 0.007‰. This is a relatively large spread (~0.32‰) in $\delta^{88}Sr$ compositions for high-temperature systems,

and comparable to the magnitude of $\delta^{88}Sr$ fractionation reported by Charlier et al. (2012), albeit with a shift to heavier $\delta^{88}Sr$ values ($\delta^{88}Sr$ = 0.00 ± 0.07‰ to 0.27 ± 0.13‰). The highland suite (including anorthosite, troctolite and norite) and picritic glasses possess a relatively restricted range of $\delta^{88}Sr$ values from +0.310 ± 0.009 to +0.268 ± 0.006 (a 0.04‰ variation), with the exception of the FAN sample 60025 that extends to the heaviest value of $\delta^{88}Sr$= 0.448 ± 0.007‰, giving a total variation of ~0.18‰. The averages of the highland rocks and lunar glasses are identical within error (2se): $\delta^{88}Sr_{Highland\ rocks\ av}$ = + 0.305 ± 0.058‰ (n=6); $\delta^{88}Sr_{\ Glasses\ av}$ = + 0.300 ± 0.021‰ (n=2). Mare basalts are distinctly lighter and range from $\delta^{88}Sr$ = +0.291 ± 0.011 to +0.129 ± 0.011 (0.16‰ variation). High-Ti basalts show a variation of 0.15‰ in $\delta^{88}Sr$ and possess the lightest group average ($\delta^{88}Sr_{High\text{-}Ti}$ = +0.216 ± 0.033). Fewer low-Ti basalt samples were analysed than high-Ti basalt samples (three as opposed to eight), but these also extend to lighter $\delta^{88}Sr$ compositions, and both rock types possess averages that are indistinguishable from one another and are fractionated, albeit to a lesser degree in low-Ti basalts. The isotope variations seen in the high-Ti basalts are taken to be representative of the lithology in general, as the lighter isotope compositions are seen in samples from both the Apollo 17 and Apollo 15 missions, and not restricted geographically.

Charlier et al. (2012) also found that highland rocks possess restricted isotope compositions ($\delta^{88}Sr$ = + 0.15 ± 0.05‰ to + 0.21 ± 0.10‰) and basalts exhibit variable and lighter $\delta^{88}Sr$ values ($\delta^{88}Sr$ = + 0.27 ± 0.13‰ to 0.00 ± 0.17‰), whilst the anorthositic breccia analysed by Moynier et al. (2010) falls within the heavier range of values determined for highland rocks in this study ($\delta^{88}Sr$ = + 0.33 ± 0.09‰). Of the two samples analysed in this study and by Charlier et al. (2012), one is found to be lighter

(15555) and the other heavier (67955), but both agree within the uncertainties of the MC-ICP-MS measurements.

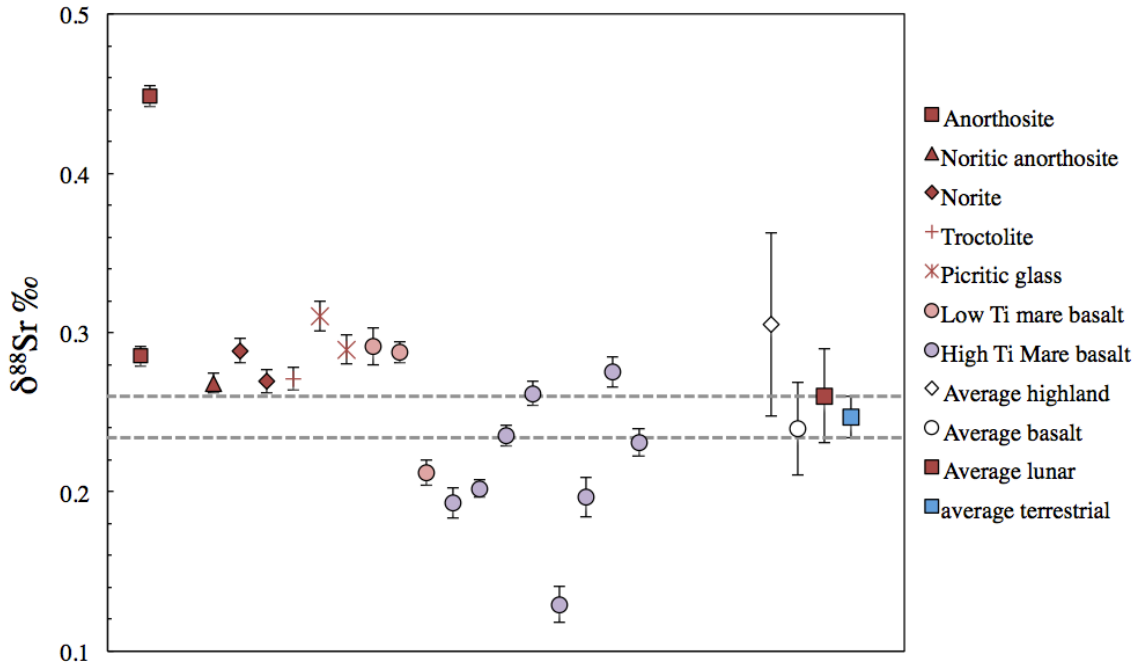

Figure 6.5: $\delta^{88}Sr$ isotope compositions of bulk lunar samples. Group averages are given for highland and basalt samples. The terrestrial average of OIB and MORB is also shown for comparison with dashed lines representing ± 2 se, within range of the lunar average, also shown.

6.5.3. Radiogenic $^{87}Sr/^{86}Sr$

The lunar rocks span a range of radiogenic compositions from $^{87}Sr/^{86}Sr$ = 0.699091 (±2) for the FAN 60025 to $^{87}Sr/^{86}Sr$ = 0.704817 (±2) for the low-Ti basalt 14053. The highland suite, especially the FANS 60015 and 60025, have the most unradiogenic compositions, whilst the basalts and glasses span a wide range of compositions extending to more radiogenic values. This study provides new $^{87}Sr/^{86}Sr$ data for samples 67955, 10049, 74420 and 15425, whilst those for which $^{87}Sr/^{86}Sr$ data already exist

yield comparable mean values to these existing data (Carlson and Lugmair, 1988; Evensen et al., 1973; Edmunson et al., 2009; Nyquist et al., 1974; Nyquist el al., 1975; Nyquist el al., 1976; Nakamura et al., 1976; Paces et al., 1991; Papanastassiou and Wasserburg, 1973; Papanastassiou and Wasserburg, 1976)

6.5.3. $^{87}Rb/^{86}Sr$ data and Rb-Sr model ages

The $^{87}Rb/^{86}Sr$ compositions of eight of the samples were determined to a high precision using isotope dilution and analysis on a Thermo Fisher Neptune at the Open University. For this, the $^{87}Rb/^{86}Sr$ ratio is calculated by the ratio of the ^{87}Rb (mol/g) to ^{86}Sr (mol/g), which are determined by the addition of a Rb-Sr spike and isotope dilution. Two splits of the anorthosite 60025 sample solution were analysed and yielded identical results. From the precise $^{87}Rb/^{86}Sr$ and $^{87}Sr/^{86}Sr$ ratios, the initial $(^{87}Sr/^{86}Sr)_I$ compositions for each sample is calculated by an age correction using crystallisation ages previously determined and listed in Table 6.2, and a decay constant of 1.40×10^{-11} (Equation 6.1) The total uncertainty on the initial $^{87}Sr/^{86}Sr_I$ ratio is calculated by the sum of the individual uncertainties for each component in Equation 6.1 (given in Table 6.2), aside from the decay constant uncertainty.

$$\left(^{87}Sr/^{86}Sr\right)_I = \left(^{87}Sr/^{86}Sr\right)_M - \left(^{87}Rb/^{86}Sr\right)_M \left(e^{\lambda_{87} t} - 1\right) \qquad \textit{Equation 6.1}$$

Where *I* is the sample initial, *M* is the measured sample, *t* is the crystallisation age of the sample and λ_{87} is the decay constant of ^{87}Rb. The initial $(^{87}Sr/^{86}Sr)_I$ compositions of the samples can then be used to determine the age of the Moon in two ways:

6.5.2.3. The isochron method of dating

From Equation 6.1, two simultaneous equations can be established in terms of the Earth's present day Sr isotopic composition. For the first, the present day value evolves from a Bulk Solar System Initial (BSSI) at the start of the Solar System at 4.567 Ga (T_{SS}). For the second, the present day value evolves from an initial $^{87}Sr/^{86}Sr$ of the Moon, $^{87}Sr/^{86}Sr_{LUNI}$, at the time of its formation (T_M). The $^{87}Sr/^{86}Sr$ evolution trajectories of both are shown with time in Figure 6.6.

$$\left(^{87}Sr/^{86}Sr\right)_P = \left(^{87}Sr/^{86}Sr\right)_{BSSI} - \left(^{87}Rb/^{86}Sr\right)_E\left(e^{\lambda_{87}T_{ss}} - 1\right) \qquad \textit{Equation 6.2}$$

$$\left(^{87}Sr/^{86}Sr\right)_P = \left(^{87}Sr/^{86}Sr\right)_{LUNI} - \left(^{87}Rb/^{86}Sr\right)_E\left(e^{\lambda_{87}T_M} - 1\right) \qquad \textit{Equation 6.3}$$

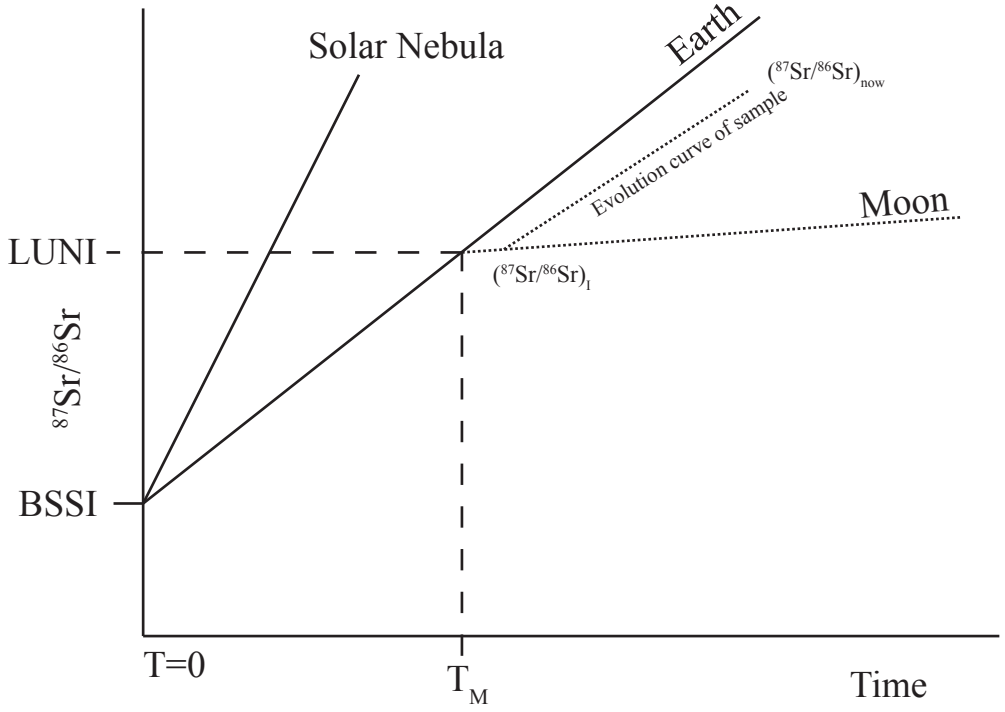

Figure 6.6: Schematic of the $^{87}Sr/^{86}Sr$ evolution curves of the Earth and the Moon with time. The model age of the Moon, T_M, is the time at which the Moon and Earth curves intersect. Also shown is the evolution curve (from $^{87}Sr/^{86}Sr_{now}$ to $^{87}Sr/^{86}Sr_I$) of a lunar sample relative to that of the bulk Moon.

A model age for the Moon, T_M, can be determined by calculating when the lunar Sr isotope composition was equal to the initial $^{87}Sr/^{86}Sr$ of the Moon, $^{87}Sr/^{86}Sr_{LUNI}$ (Figure 6.6), by combining and rearranging Equations 6.2 and 6.3 for T_M (Equation 6.4):

$$T_M = \left(\frac{1}{\lambda}\right) ln \left[e^{\lambda_{87} T_{ss}} - \frac{\left(^{87}Sr/^{86}Sr\right)_{LUNI} - \left(^{87}Sr/^{86}Sr\right)_{BSSI}}{\left(^{87}Rb/^{86}Sr_{E}\right)} \right] \qquad \textit{Equation 6.4}$$

A value for $^{87}Sr/^{86}Sr_{LUNI}$ can be calculated from the intercept of an isochron defined by the initial Sr compositions, $(^{87}Sr/^{86}Sr)_I$, and the $^{87}Rb/^{86}Sr$ ratios of lunar samples of different ages. This yields an initial of $^{87}Sr/^{86}Sr_{LUNI}$ =0.699059 ± 0.000081 based on the 8 samples analysed in this study (Figure 6.7). Using this as the initial lunar $^{87}Sr/^{86}Sr_{LUNI}$ value gives an age of T_M= 97 ± 74 Ma after the start of the solar system. For this, the decay constant of ^{87}Rb is taken to be 1.40 x 10^{-11} (Rotenberg et al., 2012), the age of the solar system, T_{ss}, to be 4567.1 ± 0.16 Ma (Amelin et al., 2006), the $^{87}Rb/^{87}Sr$ ratio of the Earth to be 0.0867 (Halliday, 2008) and the solar system Sr initial, $^{87}Sr/^{86}Sr_{BSSI}$, to be 0.698975 ± 0.000008 based on the group initial $^{87}Sr/^{86}Sr$ for CAI, which is identical to that found for eucrites and angrites (Hans et al., 2013).

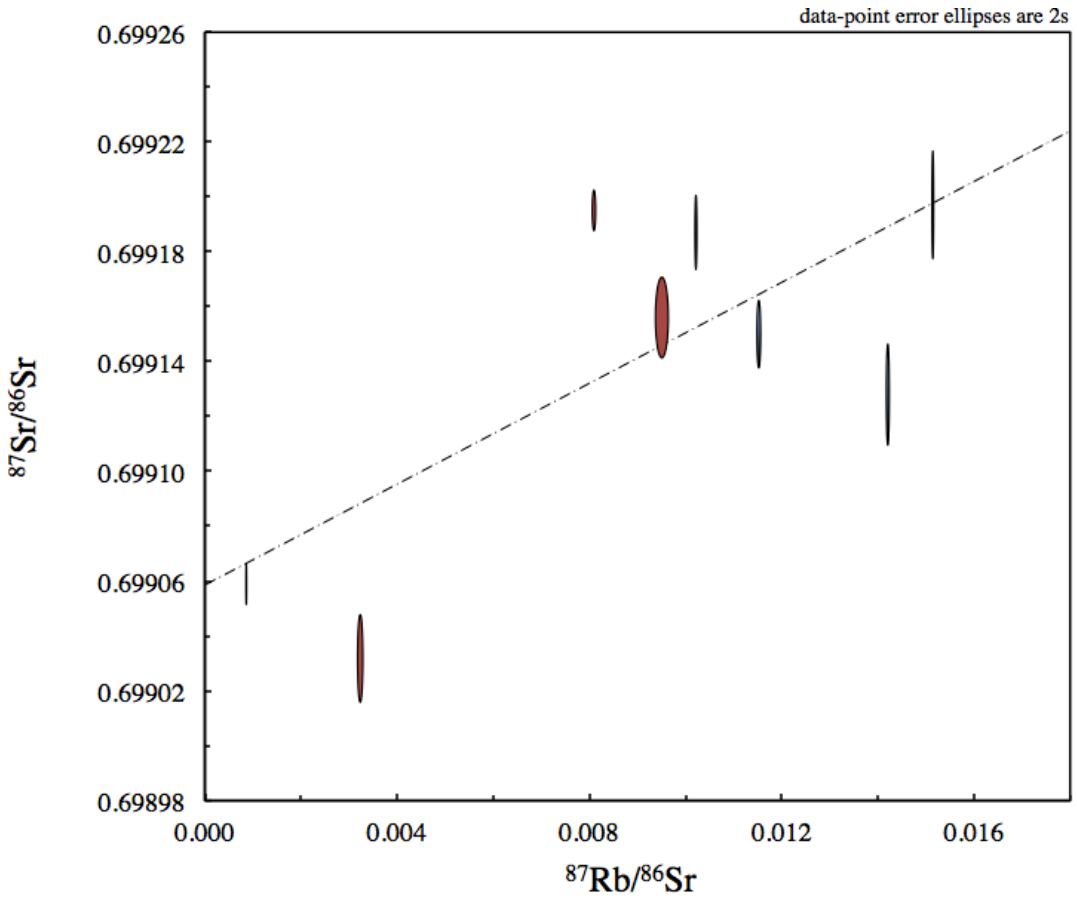

Figure 6.7: Errorchron plot of the $(^{87}Sr/^{86}Sr)_I$ and $^{87}Rb/^{86}Sr$ ratios of the lunar samples using Isoplot.

However, the eight samples analysed for their $^{87}Rb/^{86}Sr$ ratios are not co-linear, and instead lie on an errorchron (an isochron with a MSWD greater than 1) with a high MSWD of 92. Thus, they cannot reliably define a value for $^{87}Sr/^{86}Sr_{LUNI}$ with any degree of confidence.

6.5.2.3. Using the $(^{87}Sr/^{86}Sr)_I$ of individual samples as $(^{87}Sr/^{86}Sr)_{LUNI}$

An alternative to the isochron method is to assume there is little Sr evolution prior to crystallisation of the oldest lunar rock, such that LUNI is within error of the $(^{87}Sr/^{86}Sr)_I$ of the rock, and assume that the initial Sr of the rock is the same as the initial Sr of the Moon (i.e. the sample evolution curve in Figure 6.6 is close to the intersection of the Earth and Moon curves). A model age of the Moon is calculated for each individual

sample using its Sr initial as a substitute for the value for $^{87}Sr/^{86}Sr_{LUNI}$, and the sample that yields the oldest age is taken to best represent the initial isotope composition of the Moon. This can provide an upper limit of the age of the Moon, as any differences in model ages between individual lunar rocks must be due to processes that make the model ages younger, such as late crystallisation or re-melting upon impacts. In this way, model ages of the Moon were determined for each of the eight samples using the same parameters as above. The uncertainties for the model ages are determined by calculating the maximum and minimum possible model ages. All values and their uncertainties are given in Table 6.2. The model ages range from 44 ± 13 Myr for the oldest sample, the FAN 60015, to 172 ± 18 Myr for the high-Ti basalt 75075. Thus, the youngest model age of the Moon given by precise Rb-Sr dating is T= 44 ± 13 Myr after the solar system, and the new data constrains a youngest possible age of the Moon to ~31 years after the start of the solar system. The ages of the highland anorthosites are much younger (less than 100Myr) than those of the basalts, consistent with theories of their formation.

Sample name	Lithology	$^{87}Sr/^{86}Sr$ (2 se)	$^{87}Rb/^{86}Sr$ (2σ)	Age (Ga)$_a$	$^{87}Sr/^{86}Sr_I$ (2 se)	T_M (Ga)	T_M ss$_b$
60015	FAN	0.699170 ±(2)	0.00271 ±(5)	3.55 ± 0.05	0.69903 ±(1)	4.523 ± 0.013	44 ± 13
60025	FAN	0.699078 ±(2)	0.000312 ±(5)	4.360 ± 0.003	0.699059 ±(6)	4.502 ± 0.011	65 ± 11
60025 (duplicate)			0.000286 ±(6)				
71596	H-TiB	0.699637 ±(3)	0.0091 ±(1)	3.70 ± 0.07	0.69916 ±(1)	4.427 ± 0.015	140 ± 15
76535	Tr	0.699660 ±(3)	0.00764 ±(3)	4.236 ± 0.015	0.699195 ±(6)	4.397 ± 0.010	171 ± 10
71566	H-TiB	0.699706 ±(2)	0.00979 ±(2)	3.70 ± 0.07	0.69919 ±(1)	4.402 ± 0.014	165 ± 14
77516	H-TiB	0.699754 ±(2)	0.01111 ±(3)	3.79 ± 0.05	0.69915 ±(1)	4.431 ± 0.013	136 ± 13
70035	H-TiB	0.699871 ±(3)	0.01383 ±(2)	3.75 ± 0.07	0.69913 ±(2)	4.449 ± 0.017	118 ± 17
75075	H-TiB	0.699981 ±(2)	0.01478 ±(1)	3.70 ± 0.07	0.69920 ±(2)	4.395 ± 0.018	172 ± 18

Table 6.2: FAN= Ferroan anorthosite, H-TiB= high-Ti basalt and Tr= troctolite. a= values used for age correction taken from Schaeffer and Husain (1974), Borg et al. (2011), Nyquist and Shih (1992), Premo and Tatsumoto (1992), Paces et al. (1991), Stettler et al. (1973), and Lugmair et al. (1975). b: age after the start of solar system, taken as 4.567 Ga from Amelin et al. (2006), in Myr.

6.6. Discussion

6.5.3. $^{84}Sr/^{86}Sr$

The $\varepsilon^{84}Sr$ values of lunar and terrestrial samples analysed in this study are negative relative to the NBS 987 terrestrial reference standard, in agreement with previously published data (Moynier et al., 2012; Paton et al., 2013), suggesting that the standard NBS 987 is slightly fractionated relative to the Bulk Earth. The identical mass fractionation line between the Earth and the Moon implies that they possess an indistinguishable $^{84}Sr/^{86}Sr$ isotope composition, and that there are no distinct nucleosynthetic signatures in ^{84}Sr retained from different inputs of material to form the Moon. This suggests an origin for the Moon from a common, well-mixed Sr reservoir, consistent with the apparent isotope homogeneity seen for other elements, including O, Cr, Ti, and Mo (Clayton et al., 1984; Dauphas et al., 2002; Trinquier et al., 2007, 2009). This is also in accord with recent views on the formation of the Moon suggesting that it may comprise primarily of proto-Earth material rather than the impactor Theia (e.g. Reufer et al., 2012).

6.5.3. Variations in stable $^{88}Sr/^{86}Sr$

6.5.2.3. Highland suite

The generally accepted theory regarding the evolution of the lunar mantle involves cooling of the global lunar magma ocean and differentiation into cumulates comprising variable proportions of olivine and orthopyroxene with minor clinopyroxene, after significant (~75%) crystallisation the formation of a plagioclase-rich anorthosite crust (Snyder et al., 1992). The older highland suite comprises predominantly plagioclase-

rich anorthosite, the magnesian suite (including troctolite), and the alkali suite (including norite), whereas the younger mare basalts are thought to be the products of decompression melting after large impacts, of the earlier-segregated upper-mantle mafic cumulates which are depleted in plagioclase (e.g. Snyder et al., 1992; Shearer et al., 2006; Grove and Krawczynski, 2009). The crystallisation of plagioclase is reflected in complementary REE patterns seen in the highland rocks and mare basalts (Figure 6.1 and 6.2). In particular, the distinctive negative Eu anomalies (Eu/Eu*) of the mare basalts reflect the depletion of plagioclase relative to the anorthosites during this early differentiation event, which can be used as a proxy for the extent of plagioclase crystallisation. Strontium partitions strongly into plagioclase, in addition, the heavy isotope of Sr appears to be preferentially incorporated into this phase, thereby accounting for the variations in δ^{88}Sr observed in terrestrial samples (Chapters 3 and 4; Charlier et al., 2012). In this case, differentiation of the lunar mantle, involving plagioclase, is most likely to be responsible for the variations in lunar rocks. The positive correlation between Eu/Eu* and δ^{88}Sr, illustrated in Figures 6.8 and 6.9, is consistent with the interpretation of the Hekla differentiation sequence (Chapter 5) and plagioclase mineral data (Chapter 3), that crystallisation of plagioclase results in significantly lighter isotopic compositions in the evolving melt. This accounts for both the heavy δ^{88}Sr compositions of the highland suite, which are exceptionally rich in plagioclase, and the light δ^{88}Sr values of the plagioclase-depleted basalts. The ferroan anorthosites, 60015 and 60025 comprise more than 90% anorthositic plagioclase (Eu/Eu*= 28-44), and possess the heaviest δ^{88}Sr compositions as a result. Sample 60025 possesses the most extreme δ^{88}Sr composition, which is entirely plausible as although a bulk rock sample, it is essentially a plagioclase mineral separate and is considered to be one of the most pristine FANs returned to date. The variability in these highland rocks

is most likely due to variable extents of partitioning of Sr into plagioclase, and variable degrees of δ^{88}Sr fractionation.

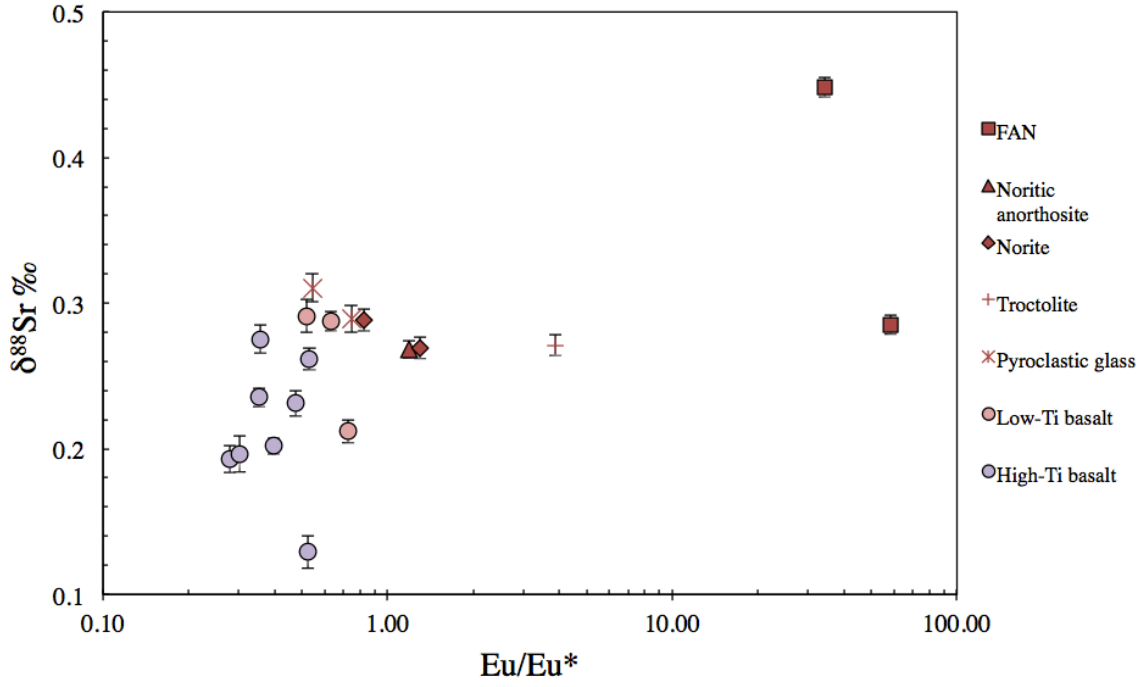

Figure 6.8: δ^{88}Sr versus Eu/Eu* for all lunar samples analysed.

6.5.2.3. Mare basalts

Charlier et al. (2012) attributed the δ^{88}Sr compositions of lunar basalts to the heavy isotopes of Sr being preferentially partitioned into plagioclase with a fractionation factor of $\alpha = 1.00016$. The basalts in this study can be modelled using a fractionation factor of modelled using an α value of 1.006 and a starting composition of 400ppm Sr with an isotopic value of δ^{88}Sr= 0.3‰ (Figure 6.10). Figure 6.9 highlights that whilst mare basalts with lower Eu anomalies tend to possess lighter δ^{88}Sr compositions, a clear co-variation between the two is absent and the low-Ti mare basalt 15555 and high-Ti mare basalt 71596 in particular do not fall along the same trend line as the majority of the

mare basalts (highlighted in Fig. 6.9). However, there is considerable scatter, particularly in the aforementioned basalts. Based on the δ^7Li composition of the olivine basalt 15555, it has been suggested that the sample equilibrated with a more evolved lunar magma ocean (Magna et al., 2006), which would also explain its anomalously light δ^{88}Sr composition in relation to the other Ti-basalts. Despite this, the trend shows considerable scatter and cannot be explained by derivation from a source with a singular composition. However, mare basalts are considered to represent partial melts of late-stage cumulates, with variable mantle source compositions, reflected in the high and low Ti basalts. There are also a number of additional processes capable of causing δ^{88}Sr fractionation in these basalts, such as partial melting and source heterogeneity in the cumulates, in addition to the primary plagioclase crystallisation during LMO differentiation.

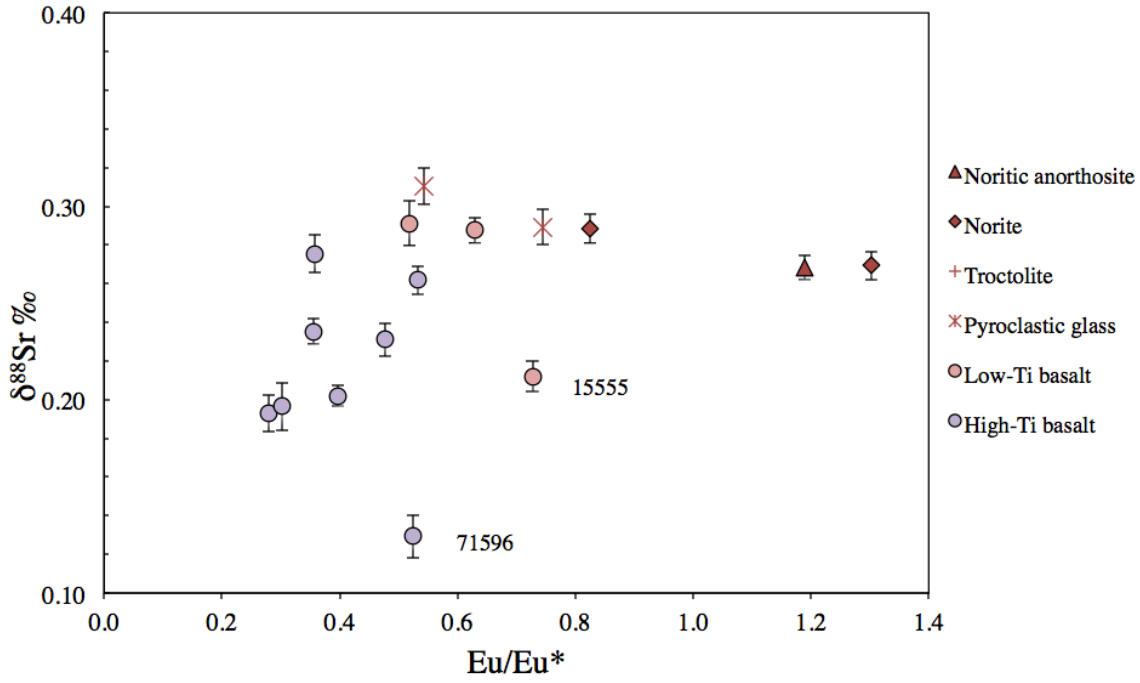

Figure 6.9: δ^{88}Sr of the basalts and glasses with their Eu/Eu*, for samples with an Eu/Eu*<1.4. Although there is a general positive trend, there is a lack of clear correlation.

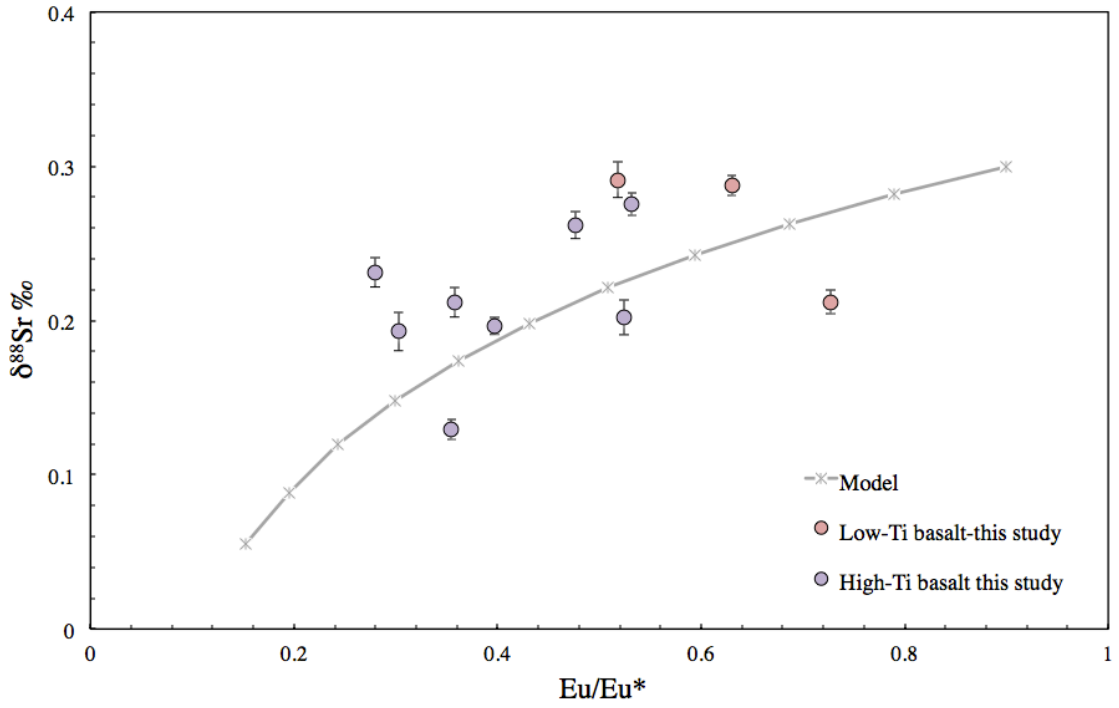

Figure 6.10: δ^{88}Sr and Eu/Eu* data for low and high-Ti basalts from this study along with the best-fit model of δ^{88}Sr fractionation for the lunar basalts.

A tentative positive correlation between δ^{88}Sr and Zr/Hf, shown in Figure 6.11, suggests that the heavier isotopes of Sr may also preferentially partition into clinopyroxene, a major Zr/Hf fractionating phase. A suggestion of a negative trend between the Ti content of the basalts and glasses and their δ^{88}Sr composition (Figure 6.12), also hints at a potential link between fractionation of δ^{88}Sr and Ti bearing mineral phases such as ilmenite or armalcolite. However, these correlations are tenuous and require data for these specific minerals to be confirmed. The degree of partial melting of the basalt sources may also have a control on the extent of δ^{88}Sr fractionation, though this is unlikely as varying degrees of partial melts of terrestrial OIBs show little variability in δ^{88}Sr (Chapter 3). The same holds true for the lunar basalts, reflected in the absence of a correlation between δ^{88}Sr and the Mg# or La/Sm ratio of the basalts

and glasses (Figures 6.13 and 6.14). This suggests that partial melting does not play a major role in fractionating stable Sr isotopes.

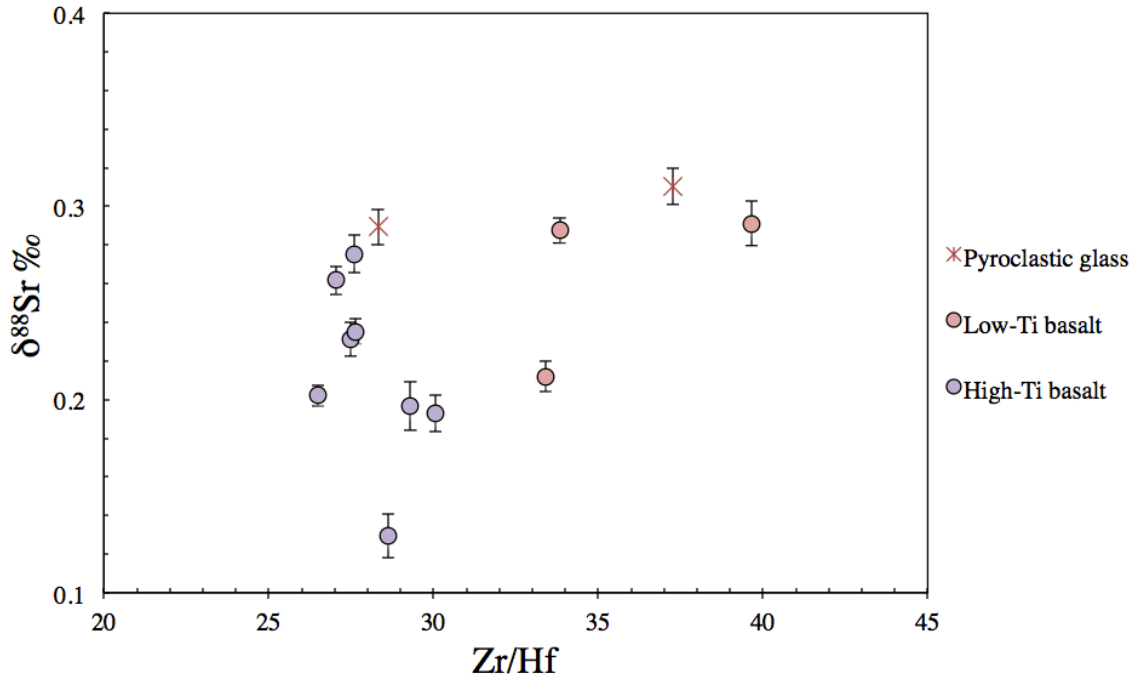

Figure 6.11: δ^{88}Sr of basalts and glasses with Zr/Hf as an index of clinopyroxene fractionation.

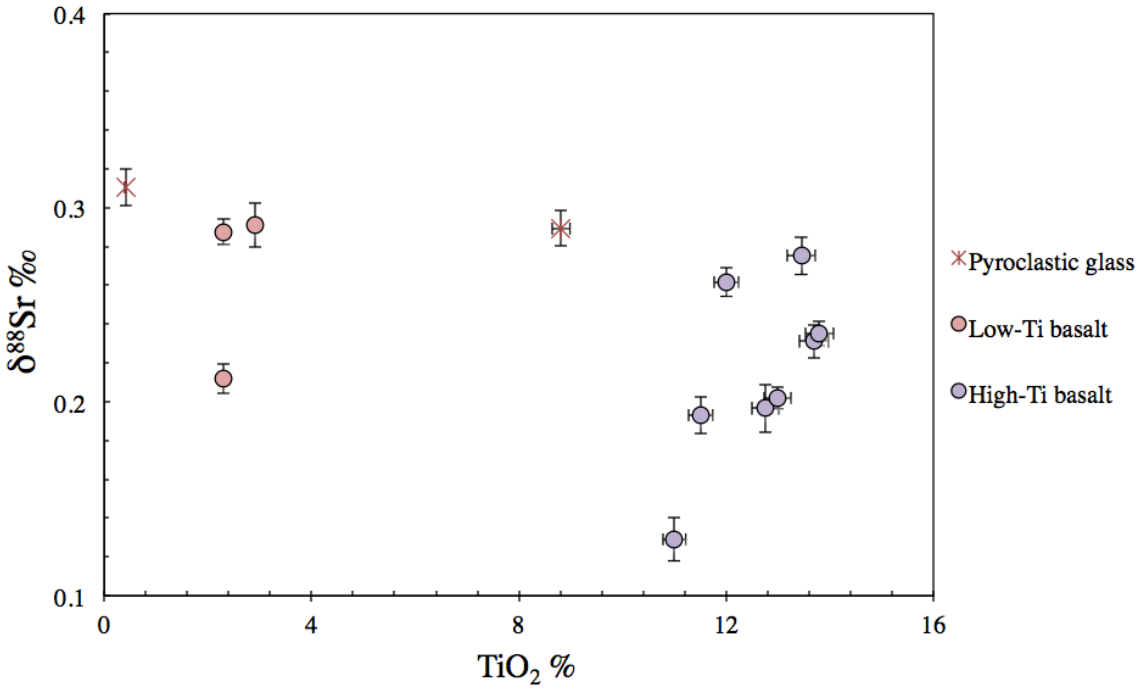

Figure 6.12: TiO_2 % (2% error) contents of the mare basalts and glasses shown with their δ^{88}Sr compositions.

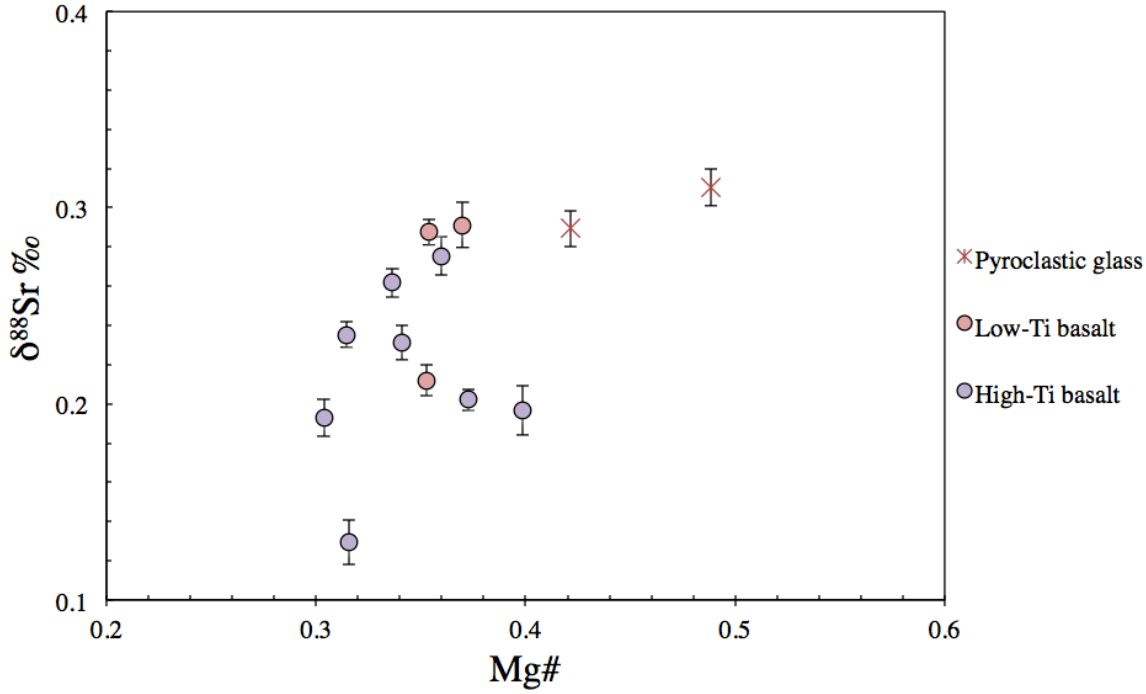

Figure 6.13: Mg# as an index of degree of partial melting in the mare basalts and glasses shows it plays a minimal part, if any, in the determining the $\delta^{88}Sr$ composition of subsequent melts

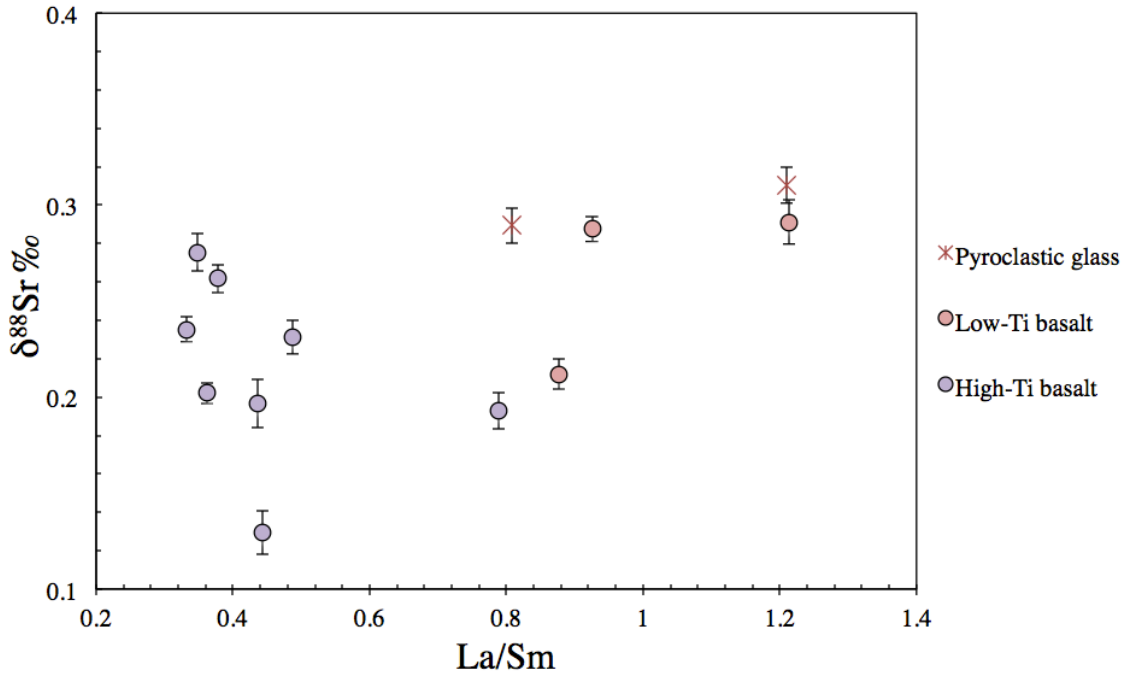

Figure 6.14: La/Sm versus $\delta^{88}Sr$ as an index of degree of partial melting show that for similar sources, the two are not correlated.

Mare basalts have been divided into high and low-Ti basalts based on their Ti concentrations, each of which is thought to reflect distinct source regions in the lunar mantle (Papike et al., 1976). Differences in the stable isotopes of Fe, Li and Mg between high and low-Ti basalts have also been attributed to heterogeneity in the lunar mantle (Liu et al., 2010; Magna et al., 2006; Wiechert and Halliday, 2007). Similarly, the heavier average δ^{88}Sr value of the low-Ti basalts (particularly when sample 15555 is excluded) relative to the lighter high-Ti basalts, in the absence of fractionation during melting, suggests this may be representative of the heterogeneity in the δ^{88}Sr composition of the cumulate sources. This is consistent with magma ocean crystallization models indicating that >78% of the lunar mantle would be dominated by olivine and orthopyroxene, whereas ilmenite-rich cumulates formed after 95% crystallization (Snyder et al., 1992). This also agrees with the hypothesis that plagioclase crystallisation occurred after 75% of crystallisation of the LMO, long after most of the source cumulates of the low-Ti basalts had segregated. The higher average Eu anomalies and heavier δ^{88}Sr compositions of low-Ti basalts relative to high-Ti basalts may reflect a lower degree of plagioclase crystallisation and resulting δ^{88}Sr fractionation to light values. As high-Ti basalts are considered to have formed late and from a small mantle reservoir (Spicuzza et al., 2007), the magnitude of variations in δ^{88}Sr is a testament to the isotopic variability in δ^{88}Sr that must exist in the high-Ti basalt source (cumulate residues) due to extensive and variable plagioclase fractionation. However, it should be noted that the apparent differences in δ^{88}Sr values between the two groups may also be a result of a sampling bias, and further measurements of low-Ti basalts are required to confirm the generally lighter high-Ti compositions.

In summary, the variability in the $\delta^{88}Sr$ compositions of the mare basalts is most likely the result of an amalgamation of processes rather than a single simple process such as plagioclase crystallisation during igneous differentiation as observed for the terrestrial Hekla suite. Firstly, igneous differentiation to create mantle sources variably depleted in plagioclase and fractionated in $\delta^{88}Sr$, and secondly, crystallisation of plagioclase and fractionation of $\delta^{88}Sr$ during melting and crystal settling of these basalts. However, the basalts analysed are relatively primitive, that is, their SiO_2 contents are low, and with an Mg# within the range 0.3 to 0.4, therefore only limited amounts of olivine and/or pyroxene would have crystallised, neither of which will greatly affect $\delta^{88}Sr$. As a result, variability in $\delta^{88}Sr$ is most likely due to a heterogeneity of the basalt sources, as is also the case for Mg, Li and Fe, caused by isotope fractionation of the heavier isotopes of $\delta^{88}Sr$ into the plagioclase rich highland rocks to leave variably plagioclase depleted and $\delta^{88}Sr$ fractionated cumulates.

6.5.2.3. Comparison with high-precision terrestrial data

The lunar rocks possess a wider range of $\delta^{88}Sr$ compositions than the terrestrial samples (including the Hekla data in Chapter 5) due to the extreme plagioclase fractionation that occurred during the differentiation of the LMO, which is not thought to have occurred on Earth. Despite this, the averages of the terrestrial basalts analysed in Chapter 3 and the lunar samples measured here are identical within error (Figure 6.5). These comparable values are consistent with stable isotope data for other refractory heavy elements such Si, Cr, Ti and W (Armytage et al., 2012; Touboul et al., 2007; Zhang et al., 2012; Lugmair and Shukulyokov, 1998), and show no evidence for the loss of lighter isotopes during the Giant Impact, as has been proposed for the stable isotopes

of the volatile element Zn (Paniello et al., 2012). This is to be expected for a heavy refractory element such as Sr.

6.5.3. Rb-Sr model age of the Moon

The anorthosite 60025 is considered by many to be the most pristine sample returned and has been the subject of extensive analyses. A recent combined Pb and Sm-Nd study yielded an age far younger than previously determined for the anorthositic crust, of 4.360 ± 0.003 Ga; 207.1± Myr after the start of the solar system (Borg et al., 2011), much younger than previous analyses for the same sample (Hanan and Tilton, 1987; Carlson and Lugmair, 1988) and other crustal material (Norman et al., 2003). This surprisingly young age has been taken to imply either that either the magma ocean crystallised significantly later than most previous estimates, or that anorthosites are not the by-product flotation cumulates of a magma ocean as is typically thought. In either case, the model age obtained for 60025 in this study of ~65 Myr is in contrast to the age reported previously. If the age determined by Borg et al. (2011) is indicative of the age of the Moon, the only possible cause for discrepancies between this and the value obtained from precise and accurate Rb-Sr data are from the assumptions made in the model age calculations. For example, the assumed $^{87}Rb/^{87}Sr$ ratio of the bulk Earth is poorly constrained and may be inaccurate; this is discussed further in this section. Another possible cause for the discrepancy is that the Sm-Nd ages are likely to reflect closure temperatures rather than crystallisation ages, and may not be representative of the age of formation of the Moon. In such a scenario, the closure of the Sm-Nd isotopic system is extended past the point of crystallisation as a result of prolonged cooling in the warm lunar crust, which has been previously suggested (Warren et al., 1989; Snyder

et al., 2000). Based on the young Sm-Nd and Pb age of 60025 and the widespread range of FAN ages, Borg et al., (2011) suggest that 60025 may have been overturned and thus suffered serial magmatism. This would contest age data for other FANs and dispute their genesis. Another possibility is that 60025 could be a mix of related anorthosites, which might explain why such contrasting ages are derived for the same sample (Ryder, 1982). Should this be the case, the oldest possible age of 60025 could still be indicative of the age of the Moon. Despite the fact that 60025 has the most unradiogenic $^{87}Sr/^{86}Sr$ composition measured, based on the ambiguity as to its mode of origin and crystallisation age, the age of the Moon is based on data for the FAN 60015.

An estimate for the lunar initial $^{87}Sr/^{86}Sr$ value is based on the initial $(^{87}Sr/^{86}Sr)_I$ value of 60015, of 0.699032 ± 0.000013 (2σ), which corresponds to a model age of 4.523 ± 0.013 Ga, equivalent to 44 ± 13 Ma after the start of the solar system. This new limit on the age of the Moon is in good agreement with Hf-W data as it is roughly equivalent with the upper limit provided of 45 Myr (Touboul et al., 2007). Based on Hf-W data, the age of the Moon is considered to be more than 45 Ma after the start of the Solar System, but less than the age of the oldest lunar rock (Touboul et al., 2007). Following this, when the Rb-Sr age of the Moon is combined with limits obtained from Hf-W studies, the age of formation is constrained to between 45 and 57 Myr after the start of the solar system, a range of only 12 Myr. This age is also consistent with a 'late' giant impact and constrains the timescale of crystallisation and initial differentiation of the lunar magma ocean (LMO) to 83-103 Myr after the giant impact assuming the anorthositic crust to have formed 4.42–4.44 Ga (Dasch et al., 1988; Norman et al., 2003), after the solidification of at least 80–85% of the LMO (Nemchin et al., 2009). It should be noted, however, that care should be taken when using 60015 as basis for the

age of the Moon as it is brecciated, and may not necessarily be representative of the initial $^{87}Sr/^{86}Sr$ composition of the Moon.

The Rb–Sr model age for the Moon obtained in this study, based on 60015, is comparable to, but lower than, previous Rb–Sr model ages of 4.468 ± 0.025 Ga determined by Halliday (2008) using the Efremovka initial $^{87}Sr/^{86}Sr$ for the BSSI (Nyquist et al., 2004), the age calculated by Halliday (2008) using the angrite SAH99555 initial $^{87}Sr/^{86}Sr$ of 0.69896 ± 0.00002 at 5 Ma (Markowski et al., 2007) of 4.491 ± 0.026 Ga, and the estimate of 4.47 ± 0.02 Ga by Tera et al. (1973) based on U–Pb chronology. However, when the initial $^{87}Sr/^{86}Sr$ value for the BSSI (Nyquist et al., 2004) is used to calculate the model age using 60015, the age obtained of 4.491 ± 0.019 Ga (76 ± 19 Ma) is consistent with, and within error of, these previous estimates. Using the more recent and precise value for $^{87}Sr/^{86}Sr_{BSSI}$ obtained from accurate analyses of angrites, eucrites and CAIs (Hans et al., 2013) yields younger and more precise ages for all samples, and the model age using 60015 is shifted to lower values, from 76 ± 19 Ma to 44 ± 13 Ma. The precise data result in a smaller uncertainty on the age of the Moon and constrain its formation to between 31 and 57 Ma after the start of the Solar System, an improvement on previous calculations of 45 to 150 Ma after the start of the Solar System (Carlson and Lugmair, 1988; Touboul et al., 2007) and reducing the uncertainty in the age estimate of the Moon by a factor of ~4, from ±53 Ma to ±13 Ma.

However, this age is in contrast to the young crystallisation age of 60025 of ~200 Myr after the start of the solar system (Borg et al., 2011). Should the age determined by Borg et al. (2011) be indicative of the age of the Moon, assuming a short time interval between the formation of the Moon and the crystallisation of 60025, the only possible cause for discrepancies between this and the value obtained from precise and accurate

Rb-Sr data are from the assumptions made in the model age calculations. A possible reason could be the Rb/Sr ratio assumption, which is likely the least constrained variable in the calculation. Following this, the Rb/Sr ratio of the precursor material can be calculated using the young age of the Moon and the $^{87}Sr/^{86}Sr_{LUNI}$ value by rearranging Equation 6.4. Assuming the young age of 60025 to be correct, and representative of the age of the Moon, yields a Rb/Sr ratio of the precursor material of ~0.018, nearly three times lower than previously assumed (e.g. Halliday, 2008). This implies the loss of nearly half Earth's Rb, which could occur, for example, by collisional and impact erosion (e.g. O'Neill and Palme, 2008; Halliday, 2013). Using a Rb/Sr value of the Earth of 0.018 yields an "oldest" model age for 60015 of ~207 Myr after the start of the solar system, close to the new age of 60025 (Borg et al., 2011), although this argument is somewhat circular. Model ages for the Moon calculated using a lower Rb/Sr value of 0.018 are given in Appendix E for all samples.

System	BSSI $^{87}Sr/^{86}Sr$	Reference	Age Ga
Pb, Sm-Nd		Borg et al. (2011)	4.360 ± 0.003
U-Pb		Tera et al. (1973)	4.47 ± 0.02
Sr	0.69893 ± 0.00002	Halliday (2008)	4.468 ± 0.025
Sr	0.69896 ± 0.00002	Halliday (2008)	4.491 ± 0.026
Sr	0.69893 ± 0.00002	This study	4.491 ± 0.019
Sr	0.698975 ± 0.000008	This study	4.523 ± 0.013

Table 6.3: A summary of all age data discussed, along with the BSSI $^{87}Sr/^{86}Sr$ initials used.

6.6. Conclusions

Very high precision strontium isotope measurements are required to determine any differences in nucleosynthetic ^{84}Sr that may exist between the Earth and it's moon. New high-precision $^{84}Sr/^{86}Sr$ data obtained here indicate that there is no distinguishable difference between terrestrial and lunar samples, and all samples from both bodies lie on the same mass dependent fractionation line on a three-isotope Sr plot of $\delta^{88/86}Sr$ against $\delta^{84/86}Sr$. This is in agreement with isotope data for O, Cr, Ti, and Mo (Clayton et al., 1984; Dauphas et al., 2002; Trinquier et al., 2007, 2009). This is also in accord with recent views that the Moon may be predominantly formed of terrestrial material rather than of the impactor (Reufer et al., 2012), and in any event provides evidence for a well-mixed Sr reservoir common to both the proto-Earth and Theia. High precision double-spike analyses are also required to reveal resolvable variations in $\delta^{88}Sr$ between different lunar rock types. A total variation of ~0.32‰ is resolved between heavier highland rocks and lighter mare basalts. This Sr isotope variation among lunar rocks most likely reflects the preferential partitioning of the heavier isotopes of Sr into plagioclase during the magmatic differentiation that formed the lunar magma ocean. The large isotope variability of the high-Ti basalts is thought to be due to melting of residual cumulates variably depleted in plagioclase, and fractionated in $\delta^{88}Sr$, formed after extensive plagioclase crystallisation from the magma ocean. It is unclear as to whether secondary plagioclase fractionation has occurred during melting, as the basalts are primitive, or whether crystallisation of additional minerals results in further isotope fractionation, as the correlation between the Eu anomaly and $\delta^{88}Sr$ composition of the lunar basalts shows considerable scatter. Lastly, combined with ID Rb-Sr data, precise $^{87}Sr/^{86}Sr$ data is used to derive a new Rb-Sr model age of the Moon based on the FAN 60015. This yields an age of formation of 4.523 ± 0.013 Ga, equivalent to 44 ± 13 Ma

after the start of the solar system, which is earlier than, but still consistent with, many previous estimates (Carlson and Lugmair, 1988; Touboul et al., 2007; Halliday, 2008; Tera et al., 1973), and with an early Giant Impact. Alternatively, assuming the young Pb and Sm-Nd age for FAN 60025 (Borg et al., 2011) to be representative of the Moon yields a Rb/Sr ratio (0.018) of the precursor material much lower than previously assumed.

CHAPTER SEVEN

Summary of findings and outlook

Summary

The aim of this thesis was to make high precision Sr isotope measurements on a selection of terrestrial and extra terrestrial materials, in order to further our understanding regarding the degree of variability of stable Sr in the Earth-Moon system and the processes responsible for Sr isotope fractionation. This was achieved through the analyses of a wide range of materials from silicates to shale, terrestrial to extra-terrestrial, and whole rocks to minerals, using thermal ionisation mass spectrometry (TIMS) and a double- spike (DS) technique for the $^{88}Sr/^{86}Sr$, $^{87}Sr/^{86}Sr$ and $^{84}Sr/^{86}Sr$ ratios, measured to external precisions of better than 10 ppm, 7 ppm and 20 ppm, respectively. The combination of DS and TIMS techniques used in the analysis of samples in this thesis and the high precisions obtained allows small variations in high temperature materials to be resolved that otherwise not could not be detected at the precision of previous MC-ICPMS measurements. This opens up potential for variations in stable and radiogenic isotopes to be revealed in material that previously has been presumed to be homogenous in Sr composition, as well as allowing investigations using $^{84}Sr/^{86}Sr$ that must be precise due to the small mass difference between the two isotopes in addition to the relatively low abundance of the ^{84}Sr isotope.

7.1. Stable Sr isotope behaviour in the terrestrial environment

The $\delta^{88}Sr$ compositions of an extensive suite of oceanic basalts were measured to better constrain the composition of the mantle, and to investigate the effect that mantle processes have on the stable Sr composition of mantle melts. Based on data from existing studies, which are limited largely to MORB and geostandards, it was previously thought that mantle melts possessed uniform $\delta^{88}Sr$ compositions (e.g. Moynier et al., 2010; Charlier et al., 2012). This study has shown that MORB vary in composition from $\delta^{88}Sr = +0.312 \pm 0.007$ to $+0.176 \pm 0.010$‰, a relatively large variation ($\delta^{88}Sr$ =~0.14‰) at high temperatures. Importantly, these variations are not strongly correlated with indices of crystal fractionation, as would be expected, and this combined with covariations in $^{87}Sr/^{86}Sr$ suggests that mantle heterogeneity also plays a part in generating such varied compositions. Surprisingly, the size of the variation observed in MORBs relates primarily to samples located on the FAMOUS ridge segment in the Mid-Atlantic. That such a small ridge section (~45km long) can generate melts with such varied $\delta^{88}Sr$ compositions was unexpected, especially as the crystallization of plagioclase does not appear to play the dominant role expected. That mantle heterogeneity can exist at such a small scale contributes to the on-going debate regarding the overturning of the now largely obsolete view that MORB are largely uniform in their isotopic compositions, and that variations are viewed on large scales within the mantle (e.g. Niu et al., 2012).

Prior to this study no $\delta^{88}Sr$ data existed for Ocean Island Basalts, and another unexpected outcome is their comparatively homogenous $\delta^{88}Sr$ compositions particularly when compared to MORB. These basalts are restricted in $\delta^{88}Sr$, from $\delta^{88}Sr = +0.280 \pm 0.008$ to $+0.224 \pm 0.018$‰, and possess a far lower variance (0.0003) than MORB (0.0013), though the averages of both are indistinguishable. The small variations

observed do not correlate with any obvious features such as indices of partial melting or crystal fractionation. As they are so geographically diverse and taken from a number of mantle end-members, which is further evident from the large range in $^{87}Sr/^{86}Sr$ compositions, it would appear that global recycling of crustal material has little affect on the stable Sr composition of mantle melts. A plausible scenario to account for this could be that the average $\delta^{88}Sr$ composition of inputs into the mantle, for example through subduction, is equal to the average $\delta^{88}Sr$ composition of the mantle melts. An alternative view is that some process cancels out or resets any changes in the composition, though it is difficult to speculate on what this process might be. To further investigate this a number of continental samples that could serve as potential inputs to subduction zones, including shale were analysed. When taken with existing data for carbonates, these vary in isotopic composition and are on average posses a lighter Sr stable isotope composition ($\delta^{88}Sr$ = ~0.20‰) than oceanic basalts. Although further measurements are needed, this implies that the average input into the mantle is different to that of oceanic basalts and the difference between their compositions must be accounted for in some another way. This warrants further investigation: the composition of the mantle must be further constrained by way of direct analyses of mantle peridotites and ultra mafic rocks in order to deduce whether there is fractionation occurring during mantle melting and whether this is responsible for the uniform composition of OIB, as well as further constraining the composition of crustal and subducted material.

A study of magmatic minerals was also undertaken in order to deduce the causes of $\delta^{88}Sr$ isotopic fractionation on a mineral scale, which in fact emphasised the fact that such minerals should be carefully selected if their $\delta^{88}Sr$ compositions are to be considered representative of each given mineral family. The $\delta^{88}Sr$ compositions of

plagioclase and clinopyroxene varied widely and inconsistently with mineral type relative to other coexisting minerals and to the melt. Strontium is a mobile element and is thus susceptible to secondary contamination, and plagioclase is often in disequilibrium with the melt, which may have led to $\delta^{88}Sr$ compositions that are not representative of crystallisation alone. However, two plagioclase separates from MORB are heavier in $\delta^{88}Sr$ than their corresponding host glasses, in agreement with the suggestion that the heavy isotopes of Sr preferentially partition into plagioclase by Charlier et al. (2012). Variations in the $^{87}Sr/^{86}Sr$ ratios between all mineral-melt pairs indicate that either the rocks have undergone contamination, or that the two are not in equilibrium. As such, further analyses are required to give reliable fractionation factors between the minerals and the melt.

The fractionation of stable Sr during magmatic evolution has been suggested based on a prior study, but is limited by a poor sample selection and the possibility of crustal contamination (Charlier et al., 2012). A differentiation suite from the volcano Hekla in Iceland was selected to explore the processes causing stable isotope fractionation in the absence of older crustal contamination. In this, variations in $\delta^{88}Sr$ of ~0.13‰ were found from a basalt to rhyolite sequence that correlate strongly with indices of magmatic differentiation. This suggests that magmatic differentiation does indeed cause fractionation by the removal mineral phases into which the lighter isotopes of Sr partition (likely plagioclase +/- clinopyroxene). However, a variation was also observed in radiogenic $^{87}Sr/^{86}Sr$, from $^{87}Sr/^{86}Sr$ = 0.703161 (±2) for a basalt to $^{87}Sr/^{86}Sr$ = 0.703220 (±5) for a rhyolite. These variations were not detected in recent studies of Hekla due to limitations in either sampling (Chekol et al., 2011) or analytical precision (Sigmarsson et al. 1992b). The cause of such contamination is difficult to identify based on Sr alone, though the most likely candidate is either altered basalt with secondary

carbonate present, or older, unaltered, basalt. This is a significant discovery as it may question the validity of any previous stable isotope analysis based solely on Hekla. Such assimilation during fractional crystallisation is also consistent with previous studies and models magma generation at Hekla (e.g. Chekol et al., 2011).

7.2. Stable Sr isotope behaviour in the lunar environment

A variety of lunar samples from highland to mare basalt in lithology were analysed to a high precision in order to resolve variations in $\delta^{88}Sr$ previously observed (Charlier et al., 2012), but for a more extensive sample suite, in order to compare and contrast the processes responsible for stable Sr isotope fractionation in the terrestrial and lunar environment. It was found that variations in $\delta^{88}Sr$ of ~0.3‰ exist with significant fractionation to light compositions in mare basalts relative to heavy highland material. With the exception of FAN 60025, the heaviest lunar composition determined to date, the highland rocks appear to be relatively uniform in their $\delta^{88}Sr$ composition. These variations are associated with fractionation of plagioclase during differentiation of the lunar magma ocean, and are consistent with prior modelling (Charlier et al., 2012).

For the first time a comparison in three-isotope space between high precision $\delta^{84/86}Sr$ and $\delta^{88/86}Sr$ data between the Earth and Moon was made so as to reveal the presence and nature of any nucleosynthetic anomalies in the ^{84}Sr isotope. A comparison of terrestrial and lunar data revealed no offset between the respective mass dependent fractionation lines at the level of precision of this study, in agreement with previous ^{84}Sr data for other isotope systems (Clayton et al., 1984; Dauphas et al., 2002; Trinquier et al., 2007, 2009).

Lastly, high precision $^{87}Rb/^{86}Sr$ and $^{87}Sr/^{86}Sr$ data yielded a precise Rb-Sr model age of the Moon based on Fan 60015 of 4.523 ± 0.019 Ga. Combined with Hf-W data (Touboul et al., 2007), this constrains the formation of the Moon to 45-57 Ma after the start of the solar system, suggesting an old Moon-forming Giant Impact. Alternatively, assuming the young Pb and Sm-Nd age for FAN 60025 (Borg et al., 2011) to be representative of the Moon yields a Rb/Sr ratio (0.018) of the precursor material much lower than previously assumed.

7.3. The Earth-Moon system

This study enables a detailed comparison between the Earth and its Moon. The variations in $\delta^{88}Sr$ observed in both bodies are dominated by the same control-plagioclase crystallisation: the former due to plagioclase removal during igneous evolution of basalt to acidic compositions, and the latter due to separation of an anorthositic crust during differentiation of the lunar magma ocean. Equally, both show large variations due to mantle heterogeneity (Chapters 3 and 6). The results of this thesis show that material from both bodies show similar ranges of $\delta^{88}Sr$ compositions ($\delta^{88}Sr$ = 0.129 ± 0.011‰ to 0.448 ± 0.007‰ for the Moon, $\delta^{88}Sr$ = 0.080 ± 0.011‰ to 0.395 ± 0.007‰ for the Earth) as summarised in Figure 7.1. Previously, based on limited lunar and terrestrial basalt samples it was previously speculated that the Moon is lighter in $\delta^{88}Sr$ than the Earth. From new data in this study, the average $\delta^{88}Sr$ composition of all oceanic basalts analysed in Chapter 3 ($\delta^{88}Sr$ = +0.25 ±0.01‰; 2se, n=34) and average of all lunar samples ($\delta^{88}Sr$ = + 0.26 ± 0.03‰) are identical. However, analyses of peridotites and ultramafic material are required to confirm the mantle compositions to draw more accurate comparisons, as to a certain extent, the majority of the basalts analysed are potentially fractionated due to plagioclase crystallisation.

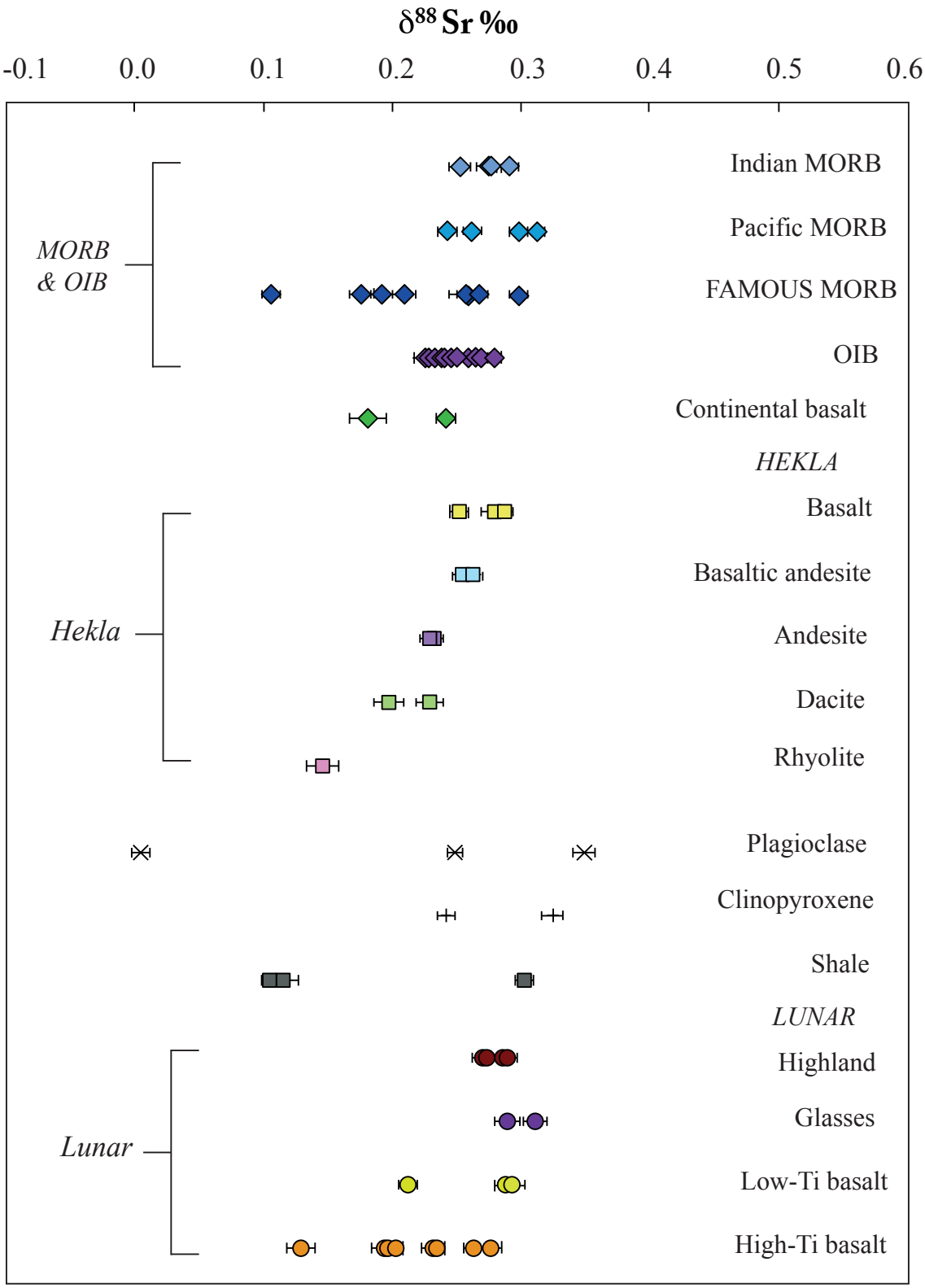

Figure 7.1: Summary of all δ^{88}Sr data measured by DS-TIMS in this study.

7.4. Overview

Overall, this thesis demonstrates that improvements in analytical techniques and the precision of measurements offer new insights into old processes and new information can be gained by revisiting "old" samples. A prime example of this is the detection of variations in radiogenic $^{87}Sr/^{86}Sr$ in the Hekla sample suite, its implications for contamination, and the consequences this may have for past and future isotope (including stable) studies. Another is the detection of variations in the $\delta^{88}Sr$ compositions of oceanic basalts studied in Chapter 3 that were previously thought to be homogenous and heavy in composition. The potential to detect and resolve such small variations in the stable isotopes of an element as heavy as Sr, and the ability to ascribe these to processes and components, opens up a multitude of possibilities and invites further analyses of high temperature systems.

REFERENCES

Albarede F. and Beard B. (2004) Analytical methods for non-traditional isotopes. *Reviews in Mineralogy and Geochemistry* **55**, 113-152.

Allegre C.J., Louvat P., Gaillardet J., Meynadier L., Rad S. and Capmas, F. (2010). The fundamental role of island arc weathering in the oceanic Sr isotope budget. *Earth and Planetary Science Letters* **292**, 51-56.

Amelin Y., Wadhwa M. and Lugmair G. (2006) Pb-isotopic dating of meteorites using 202Pb–205Pb double-spike: comparison with other high-resolution chronometers. *Lunar and Planetary Science Conference Abstracts* **37**, 1970.

Andreasen R. and Sharma M. (2007) Mixing and homogenization in the early solar system: Clues from Sr, Ba, Nd, and Sm isotopes in meteorites. *Astrophysical Journal* **665**, 874-883.

Armytage R. M. G, Georg, R. B., Williams, H. M. and Halliday A. N. (2011) Silicon isotopes in lunar rocks: Implications for the Moon's formation and the early history of the Earth. *Geochimica et Cosmochimica Acta* **77**, 504-514.

Attendorn H.-G. and Bowen R. N. C. (1997) *Radioactive and Stable Isotope Geology*. Chapman and Hall.

Birck, J.L. (2004) An overview of isotopic anomalies in extraterrestrial materials and their nucleosynthetic heritage. *Reviews in Mineralogy & Geochemistry: Geochemistry of Non-Traditional Stable Isotopes* **55**, Mineralogical Society of America.

Bohm F., Eisenhauer A., Tang J., Dietzel M., Krabbenhoft A., Kisakurek B. and Horn, C. (2012) Strontium isotope fractionation of planktic foraminifera and inorganic calcite. *Geochimica et Cosmochimica Acta* **93**, 300–314.

Borg L. E., Connelly J. N., Boyet M. and Carlson R. W (2011) Chronological evidence that the Moon is either young or did not have a global magma ocean. *Nature* **477**, 70–72.

Canup R.M. and Asphaug E. (2001) Origin of the Moon in a giant impact near the end of the Earth's formation. *Nature* **412**, 708-712.

Cameron A. G. W. (1986) The impact theory for origin of the Moon. In: *Origin of the Moon* (W. K. Hartmann, R. J. Phillips, and G. J. Taylor, eds.), 609-616.

Cameron A.G.W. (2000) Higher resolution simulations of the Giant Impact. In: Righter, K., Canup, R. (Eds.), *Origin of the Earth and Moon*. University of Arizona Press, Tucson, AZ, 133–144.

Cameron A.G.W. and Benz W. (1991) The origin of the Moon and the single impact hypothesis-IV. *Icarus* **92**, 204-216.

Carlson R.W. and Lugmair G.W. (1988) The age of ferroan anorthosite-60025 - oldest crust on a young Moon. *Earth and Planetary Science Letters* **90**, 119-130.

Charlier B.L.A., Ginibre C., Morgan D., Nowell G.M., Pearson D.G., Davidson J.P. and Ottley C.J. (2006) Methods for the microsampling and high-precision analysis of strontium and rubidium isotopes at single crystal scale for petrological and geochronological applications. *Chemical Geology* **232**, 114-133.

Charlier B.L.A, Nowell G., Parkinson I.J., Kelley S.P., Pearson D.G. and Burton, K.W. (2012) High temperature strontium stable isotope behaviour in the early solar system and planetary bodies. *Earth and Planetary Science Letters* **329-330**, 31-40.

Chekol T. A., Kobayashi K., Yokoyama T., Sakaguchi C. and Nakamura E. (2011) Timescales of magma differentiation from basalt to andesite beneath Hekla Volcano, Iceland: Constraints from U-series disequilibria in lavas from the last quarter-millennium flows. *Geochimica et Cosmochimica Acta* **75,** 256-283.

Clayton R. N., Onuma N. and Mayeda T. K. (1976) A classification of meteorites based on oxygen isotopes. *Earth and Planetary Science Letters* **30**, 10–18.

Clayton, R. N. and Mayeda (1984) T. K. Genetic relations between the moon and meteorites. *Proceedings of the 6th Lunar and Planetary Science Conference* 1761-1769.

Clift P.D., Schouten H. and Vannucchi P. (2009) Arc-Continent Collisions, Subduction Mass Recycling and the Maintenance of the Continental Crust. In: Cawood P. and Kroener A.(Eds.), *Accretionary Orogens in Space and Time*, **318**. Geological Society, London. 75–103.

Clocchiatti R. and Metrich N. (1984) Temoinages de la contamina-tion dans les produits des eruptions explosives des M.Silvsesti (1892) et Mt. Rossi (1669) (Mt. Etna). *Bulletin of Volcanology* **47**, 909-928

Condie K. C. (1997) *Plate tectonics and crustal evolution.* Butterworth-Heinemann, Boston.

Condomines M., Gronvold K., Hooker P.J., Muehlenbachs K., O'Nions R.K., Oskarsson N. and Oxburgh E.R. (1983) Helium, oxygen, strontium and neodymium isotopic relationships in Icelandic volcanics. *Earth and Planetary Science Letters* **66**, 125–136.

Dasch E.J., Ryder G. and Nyquist L.E. (1988) Age of lunar crust and earliest volcanism. *Chemical Geology* **70**, 7.

Dauphas N., Marty B. and Reisberg L. (2002) Molybdenum evidence for inherited planetary scale isotope heterogeneity of the protosolar nebula. *The Astrophysical Journal* **565**(1), 640–644.

de Souza G.F., Reynolds B.C., Kiczka M. and Bourdon B. (2010) Evidence for mass-dependent isotopic fractionation of strontium in a glaciated granitic watershed. *Geochimica et Cosmochimica Acta* **74**, 2596-2614.

Deniel C. and Pin C. (2001) Single-stage method for the simultaneous isolation of lead and strontium from silicate samples for isotopic measurements. *Analytica Chimica Acta* **426**, 95-103.

DePaolo D. J. (1981) Trace element and isotopic effects of combined wallrock assimilation and fractional crystallization. *Earth and Planetary Science Letters* **53,** 189-202.

Dissanayake C. B. (1976) The geochemistry of bismuth in the Skaergaard intrusion. *Geochemical Journal of Japan* **10**. 71-78.

Dissanayake C. B. and Vincent E.A. (1972) Zinc in rocks and minerals from the Skaergaard intrusion, east Greenland. *Chemical Geology* **9**, 285-297.

Dosso L., Bougault H., Beuzart P., Calvez J.-Y. and Joron J.-L. (1988) The geochemical structure of the South-East Indian ridge. *Earth and Planetary Science Letters* **88**, 47–59.

Dupré B., Lambret B., Rousseau D. and Allègre C. J. (1981) Limitations on the scale of mantle heterogeneities under oceanic ridges. *Nature* **294**, 552-554.

Dupré B. and Allégre C. J. (1983) Pb–Sr isotope variation in Indian Ocean basalts and mixing phenomena. *Nature* **303**, 142–146.

Edmunson J., Borg L.E., Nyquist L.E. and Asmerom Y. (2009) A combined Sm-Nd, Rb-Sr, and U-Pb isotopic study of Mg-suite norite 78238: Further evidence for early differentiation. *Geochimica et Cosmochimica Acta* **73**, 514-527.

Escrig S., Capmas F., Dupré B. and Allègre, C.J., (2004) Os isotopic constraints on the nature of the DUPAL anomaly from Indian Mid-Ocean-Ridge Basalts. *Nature* **431**, 59-63.

Evensen N.M., Murthy V.R. and Coscio M.R. (1973) Taurus-Littrow - Age of mare volcanism - chemical and Rb-Sr isotopic systematics of dark mantle soil. *Transactions of the American Geophysical Union* **54**, 587-588.

Farley K. A., Natland J. H., and Craig H. (1992) Binary mixing of enriched and undegassed (primitive?) mantle components (He, Sr, Nd, Pb) in Samoan lavas. *Earth and Planetary Science Letters* **111**, 183–199.

Faure, G. (1986) *Principles of Isotope Geology*, *2nd ed.* John Wiley & Sons.

Fehlhaber K. and Bird,D. K. (1991) Oxygen-isotope and mineral alteration in gabbros of the Lower Layered Series, Kap Edvard Holm Complex, East Greenland. *Geology* **19**, 819–822.

Fietzke J. and Eisenhauer A. (2006) Determination of temperature-dependent stable strontium isotope (Sr-88/Sr- 86) fractionation via bracketing standard MC-ICP-MS. *Geochemistry Geophysics Geosystems* **7**, (8).

Gale A., Laubier M., Escrig S. and Langmuir C. H. (2013) Constraints on melting processes and plume-ridge interaction from comprehensive study of the FAMOUS and North Famous segments, Mid-Atlantic Ridge. *Earth and Planetary Science Letters* **365**, 209–220.

Galer S.J.G. (1999) Optimal double and triple spiking for high precision lead isotopic measurement. *Chemical Geology* **157**, 255-274.

Gannoun A., Burton K.W., Parkinson I.J., Alard O., Schiano P. and Thomas L.E. (2007) The scale and origin of the osmium isotope variations in mid-ocean ridge basalts. *Earth and Planetary Science Letters* **259**, 541–556.

Gast P. W., Tilton G. R., and Hedge C. (1964) Isotopic composition of lead and strontium from Ascension and Gough Islands. *Science* **145**, 1181–1185.

Geist D. J., White W. M. and McBirney A. R. (1988) Plume asthenosphere mixing beneath the Galápagos Archipeligo. *Nature* **333**, 657-660.

Gerlach D. C., Stormer J. C. and Mueller P. A. (1987) Isotopic geochemistry of Fernando de Noronha. *Earth and Planetary Science Letters* **85**, 129–144.

Grove T. L. and Krawczynski M. J. (2009) Lunar mare volcanism: Where did the magmas come from? *Elements* **5**, 29–34.

Harpp K. S. and W. M. White (2001) Tracing a mantle plume: Isotopic and trace element variations of Galapagos seamounts, *Geochemistry Geophysics Geosystems* **2**, 1042.

Harvey J., Yoshikawa M., Hammond S. J. and Burton K. W. (2012) Deciphering the Trace Element Characteristics in Kilbourne Hole Peridotite Xenoliths: Melt–Rock Interaction and Metasomatism beneath the Rio Grande Rift, SW USA. *Journal of Petrology* **0**, 1-34.

Halicz L., Segal I., Fruchter N., Stein M. and Lazar B. 2008 Strontium stable isotopes fractionate in the soil environments? *Earth and Planetary Science Letters* **272**, 406-411.

Halliday A.N. (2008) A young Moon-forming giant impact at 70-110 million years accompanied by late-stage mixing, core formation and degassing of the Earth. *Philosophical Transactions of the Royal Society* **366**, 4163-4181.

Halliday A.N. (2013) The origins of volatiles in the terrestrial planets. *Geochimica et Cosmochimica Acta* **105**, 146-171.

Halliday A.N. and Porcelli D. (2001) In search of lost planets - the paleocosmochemistry of the inner solar system. *Earth and Planetary Science Letters* **192**, 545-559.

Halliday A., A. Dickin A. Fallick and J. Fitton (1988) Mantle dynamics–A Nd, Sr, Pb and Os isotopic study of the Cameroon Line Volcanic Chain. *Journal of Petrology* 29, 181–211.

Halliday A. N., Davidson J. P., Holden P., DeWolf C., Lee D-C. and Fitton, J. G. (1990) Trace-element fractionation in plumes and the origin of HIMU mantle beneath the Cameroon Line. *Nature* **347**, 523-528.

Halliday A. N., Davies G. R. Lee, D-C., Tommasini S., Paslick C. R. Fitton, J. G. and James D. E. (1992) Lead isotope evidence for young trace element enrichment in the oceanic upper mantle. *Nature* **359**, 623-627.

Hamelin B. and Allegre C. J. (1985) Large-scale regional units in the depleted upper mantle revealed by an isotope study of the South-West Indian Ridge. *Nature* **315,** 196-199.

Hamelin B., Dupré B. and Allegre C. J. (1985) Pb-Sr-Nd isotopic data of Indian Ocean ridges: new evidence of large-scale mapping of mantle heterogeneities. *Earth and Planetary Science Letters* **76**, 288-298.

Hanan B.B and Graham D. (1996) Lead and helium isotope evidence from oceanic basalts for a common deep source of mantle plumes. *Science* **272**, 991–995.

Hanan B.B. and Tilton G.R. (1987) 60025 - Relict of primitive lunar crust. *Earth and Planetary Science Letters* **84**, 15-21.

Hans U., Kleine T. and Bourdon B. (2011) Strontium isotope anomalies in Ca-Al-rich inclusions and the Rb-Sr chronology of volatile depletion revisited. *42nd Lunar and Planetary Science Conference* **1608**, p.2672.

Hans U., Kleine T. and Bourdon B. (2013) Rb–Sr chronology of volatile depletion in differentiated protoplanets: BABI, ADOR and ALL revisited. *Earth and Planetary Science Letters* **374**, 204–214.

Hart S. R. (1971) K, Rb, Cs, Sr, Ba contents and Sr isotope ratios of ocean floor basalts. *Philosophical Transactions of the Royal Society London* **268**, 573–587.

Hart S.R., Schilling J.-G. and Powell J.L. (1973) Basalts from Iceland and along the Reykjanes Ridge: Sr isotope geochemistry. *Nature* **246**, 104–107.

Hart S. R. (1984) A large-scale isotope anomaly in the southern hemisphere mantle. *Nature* **309**, 753–757.

Hart S. R. (1988) Heterogeneous mantle domains: signatures, genesis and mixing chronologies. *Earth and Planetary Science Letters* **90**, 273-296.

Hart S. R. Hauri E. H., Oschmann L. A. and Whitehead J. A. (1992) Mantle plumes and entrainment: isotopic evidence. *Science* **256**, 517–520.

Hartmann W.K. and Davis D.R. (1975) Satellite-sized planetesimals and lunar origin. *Icarus*, **24**, 504-515.

Hedge C. E. and Walthall F. G. (1963) Radiogenic strontium-87 as an index of geological processes. *Science* **140**, 1214.

Hemond C., Condomines M., Fourcade S., Allegre C.J., Oskarsson N. and Javoy M. (1988) Thorium, strontium and oxygen isotopic geochemistry in Recent tholeiites from Iceland: crustal influence on mantle-derived magmas. *Earth and Planetary Science Letters* **87**, 273–285.

Hirschmann M. M., Renne P. and McBirney A. R. (1997) $^{40}Ar/^{39}Ar$ dating of the Skaergaard Intrusion. *Earth and Planetary Science Letters* **146**, 645–658.

Hodell D. A., Mead G. A. and Mueller P. A. (1990) Variation in the strontium isotopic composition of seawater (8 Ma to present): implications for chemical weathering rates and dissolved fluxes to the oceans. *Chemical Geology* **80**, 291–307.

Hofmann A. W. (2003) Sampling mantle heterogeneity through oceanic basalts: isotopes and trace elements. In: *Treatise of Geochemistry* (ed. R. W. Carlson). Elsevier Ltd.

Hofmann A. W. and Hart S. R. (1978) An assessment of local and regional isotopic equilibrium in the mantle. *Earth and Planetary Science Letters* **39**, 44–62.

Horwitz E. P., Chiarizia R. and Dietz M. L. (1992) A Novel Strontium Selective Extraction Chromatographic Resin. *Solvent Extraction and Ion Exchange* **10**, 313-336.

Hoskin P. W. O., Kinny P. D.,Wyborn D. and Chappell B. W. (2000). Identifying accessory mineral saturation during differentiation in granitoids magmas: an integrated approach. *Journal of Petrology* **41**, 1365-1396.

Huang F., Chakraborty P., Lundstrom C. C., Holmden C., Glessner J. J. G., Kieffer S. W. and Lesher C. E. (2010) Isotope fractionation in silicate melts by thermal diffusion. *Nature* **464**, 396-400.

Humayun M. and Clayton R. N. (1995) Potassium isotope geochemistry: Genetic implications of volatile element depletion. *Geochimica et Cosmochimica Acta* **59**, 2131–2148.

Hurley P. M., Hughes H., Faure G., Fairbairn H. W. and Pinson W. H. (1962) Radiogenic strontium-87 model of continent formation. *Journal of Geophysical Research* **67**, 5315–5334.

Jakobsson, S.P. (1979). Petrology of recent basalts of the Eastern Volcanic Zone, Iceland. *Acta Naturalia Islandica* **26**, 1-103.

James D.E. (1981) The combined use of oxygen and radiogenic isotopes as indicators of crustal contamination. *Earth and Planetary Science Letters* **9**, 311–344.

Johnson C. and Beard B. (1999) Correction of instrumentally produced mass fractionation during isotopic analysis of Fe by thermal ionization mass spectrometry, *International Journal of Mass Spectrometry* **193**, 87–99.

Johnson C., Beard B. and Albarède, F. (2004) *Reviews in Mineralogy & Geochemistry: Geochemistry of Non-Traditional Stable Isotopes* **55**, Mineralogical Society of America.

Krabbenhöft A., Eisenhauer A., Bohm F., Vollstaedt H., Fietzke J., Liebetrau V., Augustin N., Peucker- Ehrenbrink B., Muller M.N., Horn C., Hansen B.T., Nolte N. and Wallmann K. (2010) Constraining the marine strontium budget with natural strontium isotope fractionations ((87)Sr/(86)Sr*, delta(88/86)Sr) of carbonates, hydrothermal solutions and river waters. *Geochimica et Cosmochimica Acta* **74**, 4097-4109.

Krabbenhöft A., Fietzke J., Eisenhauer A., Liebetrau V., Bohm F. and Vollstaedt, H. (2009) Determination of radiogenic and stable strontium isotope ratios ((87)Sr/(86)Sr; delta(88/86)Sr) by thermal ionization mass spectrometry applying an (87)Sr/(84)Sr double spike. *Journal of Analytical Atomic Spectrometry* **24**, 1267- 1271.

Kryc K. A., Murray R. W. and Murray D. W (2003) Elemental fractionation of Si, Al, Ti, Fe, Ca, Mn, P, and Ba in five marine sedimentary reference materials: results from sequential extractions. *Earth and Planetary Science Letters* **211**, 125-141.

Kyser T. K., Lesher C. E. and Walker D. (1998) The effects of liquid immiscibility and thermal diffusion on oxygen isotopes in silicate liquids *Contributions to Mineralogy and Petrology* **133**, 373–381.

Lacks D. J., Goel G., Bopp C. J., Van Orman J. A., Lesher C. E.and Lundstrom C. C. (2012) Isotope fractionation by thermal diffusion in silicate melts. *Physical Review Letters* **108**(6):065901.

Langmuir C., Vocke R., Hanson G. and Hart S. (1978) A general mixing equation with applications to Icelandic basalts. *Earth and Planetary Science Letters* **37**, 380-392.

Langmuir C., Humphris S., Fornari D., Van Dover C., Von Damm K., Tivey M., Colodner D., Charlou J.-L., Desonie D., Wilson C., Fouquet Y., Klinkhammer G., Bougault H. (1997) Hydrothermal vents near a mantle hot spot: The Lucky Strike vent field at 37°N on the Mid-Atlantic Ridge. *Earth and Planetary Science Letters* **148**, 69-91.

Laubier M., Gale A. and Langmuir, C.H. (2012) Melting and crustal processes at the FAMOUS segment (Mid-Atlantic Ridge): New insights from olivine- hosted melt inclusions from multiple samples. *Journal of Petrology*, **53**, 665–698.

Lee D-C., Halliday A. N., Fitton J. G. and Poli G. (1994) Isotopic variations with distance and time in the volcanic islands of the Cameroon line: evidence for a mantle plume origin. *Earth and Planetary Science Letters* **123**, 119-138.

le Roex A.P., Erlank A.J. and Needham H.D. (1981) Geochemical and mineralogical evidence for the occurrence of at least three distinct magma types in the 'Famous' region. *Contributions to Mineralogy and Petrology* **77**, 24–37.

le Roex A.P., Frey F.A. and Richardson S.H. (1996). Petrogenesis of lavas from the AMAR Valley and Narrowgate region of the FAMOUS Valley, 361–371 N on the Mid-Atlantic Ridge. *Contributions to Mineralogy and Petrology* **124**, 167–184.

Liang Y-H. (2013) Mass dependent isotopic fractionation of molybdenum in the solar system. PhD Thesis, University of Oxford, United Kingdom.

Liu Y., Spicuzza M. J., Craddock P. R., Day J. M. D., Valley J. W., Dauphas N. and Taylor L. A. (2010) Oxygen and iron isotope constraints on near-surface fractionation effects and the composition of lunar mare basalt source regions. *Geochimica et Cosmochimica Acta* **74**, 6249–6262.

Liu H. C., You C. F., Huang K. F. and Chung C. H. (2012) Precise determination of triple Sr isotopes (δ87Sr and δ88Sr) using MC-ICP-MS. *Talanta* **88**, 338-344.

Lodders K. (2003) Solar system abundances and condensation temperatures of the elements. *Astrophysical Journal* **591**, 1220–1247.

Lugmair, G.W., Scheinin, N.B. & Marti, K., 1975. Sm-Nd age and history of Apollo 17 basalt 75075 - Evidence for early differentiation of the lunar exterior. *Proceedings of the 6th Lunar and Planetary Science Conference* 1419-1429.

Lugmair G. W. and Shukolyukov A. (1998) Early solar systemtimescales according to Mn-53-Cr-53 systematics. *Geochimica et Cosmochimica Acta* **62**, 2863–2886.

Lundstrom C.C. Chaussidon M., Hsui A.T., Kelemen P. and M. Zimmerman (2005) Observations of Li isotopic variations in the Trinity Ophiolite: Evidence for isotopic fractionation by diffusion during mantle melting. *Geochimica et Cosmochimica Acta* **69**, 735-751.

Lundstrom C.C. (2009). Hypothesis for origin of convergent margin granitoids and Earth's continental crust by thermal migration zone refining. *Geochimica et Cosmochimica Acta* **73**, 5709–5729.

Ma JL., Wei G., Liu Y., Ren ZY., Xu YG. and Yang YH. (2013) Precise measurement of stable (δ88/86Sr) and radiogenic (87Sr/86Sr) strontium isotope ratios in geological standard reference materials using MC-ICP-MS. *Chinese Science Bulletin* ISSN: 1001-6538.

Magna T., Wiechert U. and Halliday A. N. (2006) New constraints on the lithium isotope compositions of the moon and terrestrial planets. *Earth and Planetary Science Letters* **243**, 336–353.

Mahoney J. J., Natland J. H., White W. M., Poreda R., Bloomer S. H., Fisher R. L. and Baxter A. N. (1989) Isotopic and geochemical provinces of the western Indian Ocean spreading centers. *Journal of Geophysical Research* **94**, 4033-4050.

Mahoney J., Le Roex A.P., Peng Z., Fisher R.L. and Natland, J.H. (1992) Southwestern limits of Indian Ocean Ridge mantle and the origin of low $^{206}PB/^{204}Pb$ mid-ocean ridge basalt: Isotope systematics of the central Southwest Indian Ridge (17° 50°E). *Journal of Geophysical Research* **97**, 19771–19790.

Markowski A., Quitte G., Kleine T., Halliday A.N., Bizzarro M. and Irving A.J. (2007) Hafnium-tungsten chronometry of angrites and the earliest evolution of planetary objects. *Earth and Planetary Science Letters* **262**, 214-229.

Marques L. S., Ulbrich M. N. C., Ruberti E. and Tassinari C. G. (1999) Petrology, geochemistry and Sr-Nd isotopes of the Trindade and Martin Vaz volcanic rocks (Southern Atlantic Ocean). *Journal of Volcanology and Geothermal Research* **93**, 191-216.

Mata J., Kerrich R., MacRae N.D. and Wu T-U. (1998) Elemental and isotopic (Sr, Nd, and Pb) characteristics of Madeira Island basalts: evidence for a composite HIMU-EM I plume fertilizing lithosphere. *Canadian Journal* of *Earth Sciences* **35**, 980-997.

McArthur J.M, Howarth R. J. and Bailey T. R. (2001) Strontium isotope stratigraphy: LOWESS version 3: Best fit to the marine Sr-isotope curve for 0–509 Ma and accompanying look-up table for deriving numerical age. *Geology*, **109**, 155-170.

McBirney A. R (1975) Differentiation of the Skaergaard Intrusion. *Nature* **253**, 691 – 694.

McBirney A. R. (1996) The Skaergaard Intrusion. In: Cawthorn, R. G. (ed.) *Layered Intrusions*. Amsterdam: Elsevier. 147–180.

McBirney A. R. and Creaser R. A. (2003) The Skaergaard Layered Series, part VII: Sr and Nd isotopes. *Journal of Petrology*. **44,** 757-771.

McDonough W. F. and Sun S.-S. (1995) The composition of the Earth. *Chemical Geology* **120**, 223–253.

Michael P.J and Schilling J-G. (1989) Chlorine in mid-ocean ridge magmas: Evidence for assimilation of seawater-influenced components. *Geochimica et Cosmochimica Acta* **53**, 3131–3143.

Michard A., Montigny R. and Schlich R. (1986) Geochemistry of the mantle beneath the Rodriguez triple junction and the South-East Indian Ridge. *Earth and Planetary Science Letters* **78**, 104-114.

Moynier F., Agranier A., Hezel D.C. and Bouvier A. (2010) Sr stable isotope composition of Earth, the Moon, Mars, Vesta and meteorites. *Earth and Planetary Science Letters* **300**, 359-366.

Moynier F., Day J. M. D., Okui W., Yokoyama T., Bouvier A., Walker R. J. and Podosek F. A. (2012) Planetary scale strontium isotopic heterogeneity and the age of volatile depletion of solar system materials. *Astrophysical Journal* **758** 45-52.

Nakamura N., Tatsumoto M., Nunes P.D., Unruh D.M., Schwab A.P. and Wildeman T.R., (1976) 4 b.y.-old clast in Boulder 7, Apollo 17: A comprehensive chronological study by U-Pb, Rb-Sr and Sm-Nd methods. *Proceedings of the 7th Lunar and Planetary Science Conference* 2309-2333.

Nemchin A., Timms N., Pidgeon R., Geisler T., Reddy S. and Meyer C. (2009) Timing of crystallization of the lunar magma ocean constrained by the oldest zircon. *Nature Geoscience* **2**, 133-136.

Nier A. O. (1938) The isotopic constitution of strontium, barium, bismuth, thallium and mercury. *Physical Reviews* **5**, 275-279.

Niu Y.L., Wilson M., Humphreys E.R. and O'Hara M.J. (2012) A trace element perspective on the source of ocean island basalts (OIB) and fate of subducted ocean crust (SOC) and mantle lithosphere (SML). *Episodes* **35**, 310-317.

Norman M.D., Borg L.E., Nyquist L.E. and Bogard D.D. (2003) Chronology, geochemistry, and petrology of a ferroan noritic anorthosite clast from Descartes breccia 67215: Clues to the age, origin, structure, and impact history of the lunar crust. Meteoritics and Planetary Science **38**, 645-661.

Norman M.D., Shih C.-Y., Nyquist L.E., Bogard D.D. and Taylor L.A. (2007) Early impacts on the Moon: Crystallization ages of Apollo 16 melt breccias, *Proceedings of the 28th Lunar and Planetary Science Conference*, 1991-1992.

Nowell G.M., Charlier B.L.A., Pearson D.G. and Burton, K.W. (2007) Quantification of stable strontium isotope variability in nature by MC-ICP-MS. *Geochimica et Cosmochimica Acta* **71**, A725-A725.

Nyquist L.E., Bansal B.M. and Wiesmann H. (1975) Rb-Sr ages and initial 87Sr/86Sr for Apollo 17 basalts and KREEP basalt 15386. *Proceedings of the 6th Lunar and Planetary Science Conference* 1445-1465.

Nyquist L.E., Bansal B.M. and Wiesmann H. (1976) Sr isotopic constraints on the petrogenesis of Apollo 17 mare basalts. *Proceedings of the 7th Lunar and Planetary Science Conference* 1507-1528.

Nyquist L.E., Bansal B.M., Wiesmann H. and Jahn B.M. (1974). Taurus-Littrow chronology: Some constraints on early lunar crustal development. *Proceedings of the 5th Lunar and Planetary Science Conference* 1515-1539.

Nyquist L.E. and Shih C.-Y. (1992) The Isotopic Record of Lunar Volcanism. *Geochimica et Cosmochimica Acta* **56**, 2213-2234.

Nyquist, L.E., Shih, C.-Y., Wiesmann, H. & Mikouchi, T., 2004, Fossil 26Al and 53Mn in d'Orbigny and Sahara 99555 and the timescale for angrite magmatism. *Proceedings of the 34th Lunar and Planetary Science Conference*, 1388.

O'Hara M. J. (1977) Open system crystal fractionation and incompatible element variation in basalts. *Nature* **268**, 36–38.

O'Hara M. J. and Mathews R. E. (1981) Geochemical evolution in an advancing, periodically replenished, periodically tapped, continuously fractionated magma chamber. *Journal of the Geological Society* **138**, 237–277.

O'Neil J. R (1986) Theoretical and experimental aspects of isotopic fractionation. *Reviews in Mineralogy and Geochemistry* **16**, 1-40.

O'Neill H.St.C. and Palme H. (2008) Collisional erosion and the non-chondritic composition of the terrestrial planets. *The Philosophical Transactions of the Royal Society* **366**, 4205-4238.

O'Nions R.K. and Pankhurst R.J. (1973) Secular variations in the Sr-isotope composition of Icelandic volcanic rocks. *Earth and Planetary Science Letters* **21**, 13-21.

Onions R. K. and Gronvold K. (1973) Petrogenetic relationships of acid and basic Rocks in Iceland -Sr- isotopes and Rare-Earth elements in late and postglacial volcanics. *Earth and Planetary Science Letters* **19**, 397-409.

Ohno T. and Hirata T. (2007) Simultaneous determination of mass-dependent isotopic Fractionation and radiogenic isotope variation of strontium in geochemical samples by multiple collector-ICP-mass spectrometry. *Analytical Sciences* **23**, 1275-1280.

Ohno T., Komiya T., Ueno Y., Hirata T. and Maruyama S. (2008) Determination of Sr-88/Sr-86 mass- dependent isotopic and radiogenic isotope variation of Sr-87/Sr-86 in the Neoproterozoic Doushantuo Formation. *Gondwana Research* **14**, 126-133.

Paces J.B., Nakai S., Neal C.R., Taylor L.A., Halliday A.N. and Lee D.C. (1991) A strontium and neodymium isotopic study of Apollo 17 high-Ti mare basalts: Resolution of ages, evolution of magmas, and origins of source heterogeneities. *Geochimica et Cosmochimica Acta* **55**, 2025-2043.

Pahlevan K. and Stevenson D. J. (2007) Equilibration in the aftermath of the lunar-forming giant impact. *Earth and Planetary Science Letters* **262**, 438-449.

Paniello R. C, Day J. M. D. and Moynier F. (2012) Zinc isotopic evidence for the origin of the Moon. *Nature* **490**, 376.

Papanastassiou D.A. and Wasserburg G.J. (1973) Rb-Sr ages and initial strontium in basalts from Apollo 15. *Earth and Planetary Science Letters* **17**, 324-337.

Papanastassiou D.A. and Wasserburg G.J. (1976) Early lunar differentiates and lunar initial 87Sr/86Sr. *Proceedings of the 7th Lunar and Planetary Science Conference* 665–667.

Papanastassiou D.A. and Wasserburg G.J. (1978) Strontium isotopic anomalies in Allende meteorite. *Geophysical Research Letters* **5**, 595-598.

Papike J. J., Hodges F. N., Bence A. E., Cameron M. and Rhodes J. M. (1976) Mare basalts: Crystal chemistry, mineralogy, and petrology. *Reviews of Geophysics* **14**, 475–540.

Parkinson I.J., Burton K.W. Mokadem F. and Charlier B.L.A. (2007a) High-precision double spike Sr isotope measurements: Applications to geochemistry and geochronology. *EOS, transactions of the American Geophysoical Union* **88**, V41E-07.

Parkinson I. J., Hammond S. J., James R. H. and Rogers, N. W. (2007b) High-temperature lithium isotope fractionation: Insights from lithium isotope diffusion in magmatic systems. *Earth and Planetary Science Letters* **257**, 609–621.

Patchett P.J. (1980a) Sr isotopic fractionation in Allende chondrules - a reflection of Solar nebular processes. *Earth and Planetary Science Letters* **50**, 181-188.

Patchett P.J. (1980b) Sr isotopic fractionation in Ca-Al inclusions from the Allende meteorite. *Nature* **283**, 438-441.

Paton C., Schiller M. and Bizzarro M. (2013) Identification of an 84-Sr depleted carrier in primitive meteorites and implications for thermal processing in the solar protoplanetary disk. *Astrophysical Journal* **763** L40.

Plank T. and Langmuir C. H. (1998) The chemical composition of subducting sediment and its consequences for the crust and mantle. *Chemical Geology* **145**, 325–394.

Podosek , F. A., Prombo C. A., Amari S. and Lewis R. S. (2004) *s*-process Sr isotopic compositions in presolar SiC from the Murchison meteorite. *Astrophysical Journal* **605,** 960-965.

Premo W.R. and Tatsumoto M. (1992) U-Th-Pb, Rb-Sr, and Sm-Nd Isotopic Systematics of Lunar Troctolitic Cumulate-76535 - Implications on the age and origin of this early lunar, deep-seated cumulate. *Proceedings of the 10th Lunar and Planetary Science Conference* 381-397.

Price R. C., Kennedy. A. K., Riggs-Sneeringer M. and Frey F.A (1986) Geochemistry of basalts from the Indian Ocean triple junction: implications for the generation and evolution of Indian Ocean ridge basalts. *Earth and Planetary Science Letters* **78**, 379-396.

Prinzhofer A., Lewin E. and Allegre C. J. (1989) Stochastic melting of the marble cake mantle: evidence from local study of the East Pacific Rise at 12^{o} 50' N *Earth and Planetary Science Letters* **92**, 189-206.

Prowatke S, and Klemme S. (2006) Trace element partitioning between apatite and silicate melts. *Geochimica et Cosmochimica Acta* **70**, 4513-4527.

Prytulak J., Nielsen S. G., Ionov D. A., Halliday A. N., Harvey J., Kelley K. A., Niu Y. L., Peate D.W., Shimizu K., and Sims K. W. W., (2013), The stable vanadium isotope composition of the mantle and mafic lavas. *Earth and Planetary Science Letters* **365**, 177-189.

Rauscher T., Heger A., Hoffman R. D. and Woosley, S. E. (2002) Nucleosynthesis in massive stars with improved nuclear and stellar physics**.** *The Astrophysical Journal* **576**, 323–348.

Rehkamper, M. and Hofmann, A.W. (1997) Recycled ocean crust and sediment in Indian Ocean MORB. *Earth and Planetary Science Letters* **147**, 93-106.

Reufer A., Meier M. M. M., Benz W. and Wieler R., (2012) A hit-and-run Giant Impact scenario. *Icarus* **221**, 296–299.

Richter F. M., Liang Y. and Davis A. M. (1999) Isotope fractionation by diffusion in molten oxides. *Geochimca et Cosmochimica Acta* **63,** 2853-2861.

Richter F. M., Watson E. B., Mendybaev R. A., Teng F-Z. and Janney P. E. (2008) Magnesium isotope fractionation in silicate melts by chemical and thermal diffusion. *Geochimca et Cosmochimica Acta* 72, 206–220.

Richter F. M., Davis A. M., DePaolo D. J. and Watson E. B. (2003) Isotope fractionation by chemical diffusion between molten basalt and rhyolite. *Geochimca et Cosmochimica Acta* **67,** 3905-3923.

Richter F. M., Dauphas N. and Teng F. (2009a) Non-traditional fractionation of non-traditional isotopes: Evaporation, chemical diffusion and Soret diffusion. *Chemical Geoogy* **258**, 92-103.

Richter F. M., Watson E. B., Mendybaev R., Dauphas N., Georg B., Watkins J. and Valley J. (2009b) Isotopic fractionation of the major elements of molten basalt by chemical and thermal diffusion. *Geochimca et Cosmochimica Acta* **73**, 4250-4263.

Rotenberg E., Davis D.W., Amelin Y., Ghosh S., Bergquist B.A. (2012) Determination of the decay-constant of 87Rb by laboratory accumulation of 87Sr. *Geochimica et Cosmochimica Acta* **85**, 41-57.

Rudge J.F., Reynolds B.C. and Bourdon B. (2009) The double spike toolbox. *Chemical Geology* **265**, 420-431.

Ruggeberg A., Fietzke J., Liebetrau V., Eisenhauer A., Dullo W.C. and Freiwald, A. (2008) Stable strontium isotopes (delta Sr-88/86) in cold-water corals - A new proxy for reconstruction of intermediate ocean water temperatures. *Earth and Planetary Science Letters* **269**, 569-574.

Ryder G. (1982) Lunar anorthosite 60025. *Geochimica et Cosmochimica Acta* **46**, 1591-1601.

Savage P. S., Georg R. B., Williams H. M. Burton, K. W. and Halliday, A. N. (2011) Silicon isotope fractionation during magmatic differentiation, *Geochimica et Cosmochimica Acta* **75**, 6124 – 6139.

Schaeffer O.A. and Husain L. (1974) Chronology of lunar basin formation. *Proceedings of the 5th Lunar and Planetary Science Conference* 1541-1555.

Schauble E. A. (2004) Applying stable isotope fractionation theory to new systems. *Reviews in Mineralogy and Geochemistry* **55**, 65–111.

Schiano P., Birck J. and Allegre C. J. (1997) Osmium-strontium-neodymium-lead isotopic covariations in mid-ocean ridge basalt glasses and the heterogeneity of the upper mantle. *Earth and Planetary Science Letters* **150,** 363-379.

Schiano P., Clocchiatti R., Ottolini L. and Busa' T. (2001) Transi-tion of Mount Etna lavas from a mantle-plume to an island-arc magmatic source *Nature* **412,** 900-904.

Schiffman P., Zierenberg R., Chadwick W.W., Clague D.A. and Lowenstern J. (2010) Contamination of basaltic lava by seawater: evidence found in a lava pillar from Axial Seamount, Juan de Fuca Ridge. *Geochemistry, Geophysics, Geosystems* **11**(4) Q04004.

Schilling J.G., Zajac M., Evans R., Johnston T., White W., Devine J. D. and Kingsley R. (1983). Petrologic and geochemical variations along the mid- Atlantic Ridge from 29 degrees N to 73 degrees N. *American Journal of Science* **283**, 510–586.

Schuessler J. A., Schoenberg R. and Sigmarsson O. (2009) Iron and lithium isotope systematics of the Hekla volcano, Iceland - Evidence for Fe isotope fractionation during magma differentiation. *Chemical Geology* **258,** 78-91.

Schwarz E. J., Coleman L. C. and Cattrol H. M. (1979) Paleomagnetic results from the Skaergaard intrusion, East Greenland. *Earth and Planetary Science Letters* **42**, 437-443.

Shearer C. K., Hess P., Wieczorek M. A., Pritchard M. E., Parmentier E., Borg L., Longhi J., Elkins-Tanton L., Neal C. R., Antonenko I., Canup R. M., Halliday A. N., Grove T. L., Hager B. H., Lee D. C. and Wiechert U. (2006) Thermal and magmatic evolution of the Moon. *Reviews in Mineralogy and Geochemistry* **60**, 365– 518.

Shimizu N., Sobolev A. V., Layne G. D., and Tsameryan, O. P. (2003) Large Pb isotope variations in olivine-hosted melt inclusions in a basalt from the Mid-Atlantic Ridge. *Science*

Siebel W., Becchio R., Volker F., Hansen M.A.F., Viramonte J., Trumbull R.B., Haase, G. and Zimmer M. (2000) Trindade and Martin Vaz islands, South Atlantic: isotopic (Sr, Nd, Pb) and trace element constraints on plume related magmatism. *Journal of South American Earth Sciences* **13**, 79-103.

Siebert C., Nägler T. and Kramers J. (2001) Determination of molybdenum isotope fractionation by double-spike multicollector inductively coupled plasma mass spectrometry. *Geochemistry, Geophysics, Geosystems* **2**, 1032.

Sigmarsson O., Condomines M. and Fourcade, S. (1992a). Mantle and crustal contribution in the genesis of Recent basalts from off-rift zones in Iceland: constraints from Th, Sr, and O isotopes. *Earth and Planetary Science Letters* **110**, 149–162.

Sigmarsson O., Condomines M. and Fourcade S. (1992b) A detailed Th, Sr and O isotope study of Hekla: differentiation processes in an Icelandic Volcano. *Contributions to Mineralogy and Petrology* **112,** 20-34.

Sigmarsson O. and Steinthorsson S. (2007) Origin of Icelandic basalts: A review of their petrology and geochemistry. *Journal of Geodynamics* **43**, 87–100.

Snyder G. A., Taylor L. A. and Neal C. R. (1992) A chemical model for generating the sources of mare basalts: Combined equilibrium and fractional crystallization of the lunar magmasphere. *Geochimica et Cosmochimica Acta* **56**(10), 3809–3823.

Sobolev A. V., Hofmann A. W. and Nikogosian I. K. (2000) Recycled oceanic crust observed in 'ghost plagioclase' within the source of Mauna Loa lavas. *Nature* **404**, 986-990.

Spicuzza M., Day J., Taylor L.A., and Vally J.W. (2007) Oxygen isotope constraints on the origin and differentiation of the Moon. *Earth and Planetary Science Letters* **253**, 254-265.

Spooner E. T. C., Chapman H. J and Smewing J. D (1977) Strontium isotopic contamination and oxidation during ocean floor hydrothermal metamorphism of the ophiolitic rocks of the Troodos Complex, Cyprus. *Geochimica et Cosmochimica Acta* **41**, 873-890.

Steiger R. H. and Jager E. (1977) Subcommission on geochronology: convention on the use of decay constants in geo- and cosmo-chronology. *Earth and Planetary Science Letters* **36**, 359-362.

Stettler A., Eberhardt P., Geiss J., Grogler N. and Maurer P. (1973) Ar39-Ar40 ages and Ar37- Ar38 exposure ages of lunar rocks. *Proceedings of the 4th Lunar and Planetary Science Conference* 1865-1888.

Stewart B. W. and DePaolo D. J. (1990) Isotopic studies of processes in mafic magma chambers: II. The Skaergaard Intrusion, East Greenland. *Contributions to Mineralogy and Perology* **104,** 125-141.

Sun S. S. and McDonough W. F. (1989) Chemical and isotopic systematics of oceanic basalts: implications for mantle composition and processes. In: *Magmatism in the ocean basins* Geological Society of London, United Kingdom, 313–345.

Tatsumoto M., Hedge C. E. and Engel A. E. J. (1965) Potassium, rubidium, strontium, thorium, uranium, and the ratio of strontium-87 to strontium-86 in oceanic tholeiitic basalt. *Science* **150**, 886–888.

Taylor S. R. (1980) Refractory and moderately volatile element abundances in the earth, moon and meteorites. *Proceedings of the Apollo 11 Lunar Science Conference* 333–348.

Taylor H. P. and Epstein S. (1962) The relationship between O18/O16 ratios in coexisting minerals of igneous and metamorphic rocks. *Geological Society of America Bulletin* **73**, 461.

Taylor H. P. and Forester R. W. (1979) An oxygen and hydrogen isotope study of the Skaergaard intrusion and its country rocks: A description of a 55 M.Y. old fossil hydrothermal system. *Journal of Petrology.* **20,** 355-419.

Telus M., Dauphas N., Moynier F., Tissot F. L. H., Teng F.-Z., Nabelek P. I., Craddock P. R. and Groat L. A. (2012) Iron, zinc, magnesium and uranium isotopic fractionation during continental crust differentiation: the tale from migmatites, granitoids, and pegmatites. *Geochimica et Cosmochimica Acta* **97**, 247–265.

Teng F.-Z., Dauphas N. and Helz R. T. (2008) Iron isotope fractionation during magmatic differentiation in Kilauea Iki lava lake. *Science* **320**, 1620–1622.

Teng F. Z., Dauphas N., Huang S. and Marty, B. (2013) Iron isotopic systematics of oceanic basalts. *Geochimica et Cosmochimica Acta* **107**, 12-26.

Teng F. Z., McDonough W. F., Rudnick R. L. and Walker R. J. (2006) Diffusion-driven extreme lithium isotopic fractionation in country rocks of the Tin Mountain pegmatite. *Earth and Planetary Science Letters.* **243,** 701-710.

Tera F., Papanastassiou D.A. and Wasserburg G.J. (1973) A lunar cataclysm at ~3.95 AE and the structure of the lunar crust. *Proceedings of the 4th Lunar and Planetary Science Conference*, 723–725.

Thirlwall M. F., Gee M. A. M., Lowry D., Mattey D. P., Murton B. J. and Taylor R. N. (2006) Low delta O-18 in the Icelandic mantle and its origins: Evidence from Reykjanes Ridge and Icelandic lavas. *Geochimica et Cosmochimica Acta* **70**, 993–1019.

Thorarinsson S., and Sigvaldason G.R. (1972) The Hekla eruption of 1970. *Bulletin of Volcanology* **36**, 269-288.

Tonarini S., Armienti P. D'Orazio M. and Innocenti F. (2001) Subduction- like fluids in the genesis of Mt. Etna magmas: evidence from boron isotopes and fluid mobile elements. *Earth and Planetary Science Letters* **192**, 471-483.

Touboul M., Kleine T., Bourdon B., Palme H. and Wieler R. (2007) Late formation and prolonged differentiation of the Moon inferred from W isotopes in lunar metals. *Nature* **450**, 1206-1209.

Travaglio C. Röpke F. K. Gallino R. and Hillebrandt W. (2011) Type Ia Supernovae as Sites of p-process: Two-Dimensional Models Coupled to Nucleosynthesis. *Astrophysical Journal* **739**, 1-19.

Trinquier A., Elliott T., Ulfbeck D., Coath C., Krot A. N. and Bizzarro, M. (2009) Origin of nucleosynthetic isotope heterogeneity in the solar protoplanetary disk. *Science* **324**, 374–376.

Trinquier A., Birck J-L. and Allègre C-J. (2007) Widespread ^{54}Cr Heterogeneity in the Inner Solar System. *The Astrophysical Journal* **655**, 1179-1185.

Turner S., Blundy J., Wood B. and Hole M. (2000) Large 230Th-excess in basalts produced by partial melting of spinel lherzolite,. *Chemical Geology* **162**, 127–136.

Urey H. C. (1947) The Thermodynamic Properties of Isotopic Substances. *Journal of the Chemical Society* 562-581.

Vance D., Teagle D.A.H. and Foster G.L. (2009) Variable Quaternary chemical weathering fluxes and imbalances in marine geochemical budgets. *Nature* **458**, 493-496.

Wager L. R (1960) The major element variation of the Layered Series of the Skaergaard Intrusion and a Re-estimation of the Average Composition of the Hidden Layered Series and of the Successive Residual Magmas. *Journal of Petrology* **1**, 364-398.

Wager L. R. and Deer W. A. (1939) Geological investigations in East Greenland, part III. The petrology of the Skaergaard intrusion, Kangerdlugssuaq, East Greenland. *Meddelelser om Grønland* **105**, 1-352.

Wager L. R. and Brown G. M. (1968) *Layered Igneous Rocks.* Oliver & Boyd. Edinburgh and London.

Wänke H. (1981) Constitution of terrestrial planets. *Philosophical transactions of the Royal Society of London*. **A303**, 287–302.

Warren P.H., Jerde E.A., and Kallemeyn G.W (1989) Lunar meteorites: Siderophile element contents, and implications for the composition and origin of the Moon. *Earth and Planetary Science Letters* **91**, 245-260.

Wasserburg G. J. and Depaolo D. J. (1979) Models of Earth structure inferred from neodymium and strontium isotopic abundances. *Proceedings of the National Academy of Sciences* **76**, 3594 – 3598.

Wei G., Ma J., Liu Y., Xie L., Lu W., Deng W., Ren Z., Zeng Ti. and Yang Y. (2013) Seasonal changes in the radiogenic and stable strontium isotopic composition of Xijiang River water: Implications for chemical weathering. *Chemical Geology* **343**, 67-75.

Weis D., Kieffer B., Maerschalk C., Pretorius W. and Barling J. (2005) High-precision Pb-Sr-Nd-Hf isotopic characterization of USGS BHVO-1 and BHVO-2 reference materials. *Geochemistry Geophysics Geosystems* **5**, (2).

Weyer S. and Seitz H. M. (2012) Coupled lithium- and iron isotope fractionation during magmatic differentiation. *Chemical Geology* **294–295**. 42–50.

Wiechert U. and Halliday A. N. (2007) Non-chondritic magnesium and the origins of the inner terrestrial planets. *Earth and Planetary Science Letters* **256**, 360– 371.

Wiechert U., Halliday A.N. Lee D.C., Snyder G.A., Taylor L.A. and Rumble D. (2001) Oxygen isotopes and the Moon-forming giant impact. *Science* **294**, 345-348.

White W. M. (1979) Geochemistry of basalts from the FAMOUS area: a re-examination. *Carnegie Institution* of *Washington Year Book* **78**, 325–331.

White W. M. (1993) 238U/204Pb in MORB and open system evolution of the depleted mantle. *Earth and Planetary Science Letters* **115**, 211–226.

White W. M. (1995) Geochemical tracers of mantle processes. *Reviews of Geophysics* **33,** 19–24.

White W. M. (2010) Oceanic island basalts and mantle plumes. *The Geochemical Perspective Annual Review of Earth and Planetary Sciences* **38**, 133-160.

White W. M. and Bryan W. B. (1977) Sr-isotope, K, Rb, Cs, Sr, Ba, and rare-earth geochemistry of basalts from the FAMOUS area. *Geological Society of America Bulletin* **88**, 571–576.

White W.M. and Schilling J.-G. (1978) The nature and origin geochemical variation in Mid-Atlantic Ridge basalts from the Central North Atlantic. *Geochimica et Cosmochimica Acta* **42**, 1501–1516.

Yang L., Peter C., Panne U. and Sturgeon R.E. (2008) Use of Zr for mass bias correction in strontium isotope ratio determinations using MC-ICP-MS. *Journal of Analytical Atomic Spectrometry* **23**, 1269-1274.

Young E.D., Galy A. and Nagahara H. (2002) Kinetic and equilibrium mass-dependent isotope fractionation laws in nature and their geochemical and cosmochemical significance. *Geochimica et Cosmochimica Acta* **66**, 1095–1104.

Yu D., Fontignie D. and Schilling J.-G. (1997) Mantle plume-ridge interactions in the central North Atlantic: A Nd isotope study of Mid-Atlantic Ridge basalts. *Earth and Planetary Science Letters* **146**, 259-272.

Zindler A. and Hart S. (1986) Chemical geodynamics. *Annual Review of Earth and Planetary Science* **14**, 493–571.

Zhang J., Dauphas N., Davis A. M. Leya, I. and Fedkin A. (2012) The Proto-Earth as a Significant Source of Lunar Material. *Nature Geoscience* **5**(4), 251-255.

APPENDICES

APPENDIX A:

Pb isotopes in iron meteorites

Supervised by Alex Halliday, Sune Nielsen, Kevin Burton, and Fatima Mokadem

Abstract

Magmatic iron meteorites are considered to sample the metal cores of planetesimals and the U-Pb system can be used to determine the ages of meteorites by analysis of Pb isotope ratios alone (known as the lead-lead dating method). The U-Pb isotopic chronometer can be used to date core formation on planetesimals and measurements of Pb isotopes can be used in conjunction with Hf-W ages of core formation to determine the parent -daughter ratios of the planetesimal, μ ($^{238}U/^{204}Pb$). This would potentially provide insights into our understanding of the processes of planetary formation and volatile depletion as Pb is volatile whilst U is not. Blanks, standard solutions and samples were analysed using various Pb separation techniques. Samples of the group IIAB iron meteorite Navajo were analysed. However, iron meteorites require extensive leaching in order to remove contamination by terrestrial Pb. Additionally, many iron meteorites possess exceptionally low levels of primordial Pb which requires large amounts (up to 10g) of meteorite to be processed. This proportionally increases the procedural blank and the uncertainty of the results. Such low procedural blanks are difficult to achieve due to the comparatively high levels of terrestrial Pb in the environment. The procedural blank for this study varied considerably over time, from a minimum of 0.044ng to a maximum of 3.8ng, despite attempts to reduce and standardize the procedural blank. The persistent large variation prevented reproducible isotopic measurements of iron meteorite samples and rendered any results highly uncertain. Therefore, the project was abandoned.

1. Introduction

Radionuclide systems, such as ^{182}Hf–^{182}W, can be used to understand the differentiation and cooling histories of melted meteorites. The radiogenic isotope compositions of early solar system objects can be used to define time-averaged parent-daughter ratios of precursor materials. Core formation in planets and planetesimals can be dated with the ^{182}Hf–^{182}W decay system (Markowski et al*.,* 2006b; Schersten et al*.,* 2006). Such ^{182}Hf–^{182}W studies show core formation on some planetesimals began within 1 Myr after CAI formation (Markowski et al*.,* 2006a). Planetary accretion and differentiation were synchronous, and W dating shows that both occurred rapidly (Markowski et al*.,* 2006a). Once differentiation had occurred, the core cooled and subsequently solidified by crystallisation. Crystallisation of the core created phases with variable isotopic compositions that allows dating of the metal in planetary cores. Magmatic iron meteorites are considered to sample the metal cores of planetesimals that formed by metal-silicate fractionation followed by fractional crystallisation of the metallic liquid. As such isotopic analyses of iron meteorites can reveal information on processes involving the core such as crystallisation. Core crystallisation chronometers include ^{205}Pb - ^{205}Tl, ^{187}Re-^{187}Os, ^{190}Pt-^{186}Os, ^{53}Mn–^{53}Cr, and ^{107}Pd-^{107}Ag systems. Core crystallisation ages range from 4517±32 to 4558±4.6 Myr and are summarised in Table A1. The most precise ages are those of the ^{107}Pd-^{107}Ag and ^{53}Mn–^{53}Cr systems.

Isotope system	Process dated	Group	Age[a] (Myr)	Age[b] (Myr)	References
^{182}Hf–^{182}W	Core formation	IIAB, IID, IIIAB, IVB	4567±1.2	−0.2±1.2	1 and 2
^{187}Re–^{187}Os	Core crystallisation	IIAB	4530±50	37±50	3
		IIIAB	4517±32	50±32	3
		IVA	4456±25	110±25	4

		IVB	4527±29	40±30	4
^{190}Pt-^{186}Os	Core crystallisation	IIAB	4323±80	244±80	3
		IIIAB	4325 ±26	242±26	3
^{107}Pd-^{107}Ag	Core crystallisation	IIIAB	4554±4.9	13.0±4.9	5
		IAB	4547±24	19.5±24	5
		IVA	4558±4.6	8.5±4.6	5
^{53}Mn–^{53}Cr	Phosphate closure	IIIAB	4563±1	4.1±0.5	6

Table A1: Isotopic chronometers of core formation and crystallisation. [a] Absolute ages for Hf–W and Al–Mg chronometers assume CAI formation at 4567.1±0.16 Myr (Amelin et al., 2002).[b] Age since CAI formation at 4567.1±0.16 Myr (Amelin et al., 2002). References: 1= Markowski et al. 2006a 2= Markowski et al. 2006b 3= Cook et al. (2004) 4= Smoliar et al. (1996) 5= Schönbächler et al. (2008) 6= Sugiura and Hoshino (2003)

However, long-lived chronometers lack the precision required to resolve events occurring within the first tens of millions of years of solar system history, while short-lived chronometers are more precise but can only provide relative ages. The U-Pb chronometer is the only absolute chronometer capable of providing both precise and absolute age constraints on core formation timescales (Halliday and Kleine, 2006). The U-Pb system can be used to determine the ages of meteorites by analysis of Pb isotope ratios alone (known as the Pb-Pb dating method). Lead has four stable isotopes, ^{204}Pb, ^{206}Pb, ^{207}Pb and ^{208}Pb the last three of which are the stable end "daughter" Pb isotopes that result from the complete radioactive decay of uranium and thorium in nature; ^{238}U, ^{235}U and ^{232}Th respectively, while ^{204}Pb is the only non radiogenic isotope. Lead is a siderophile element whereas U and Th are lithophile, thus fractionation between these occurs during core formation on planetesimals as Pb is concentrated in the core and U and Th in the silicate mantle. Differentiation results in the depletion of uranium and thorium in the core of these planetesimals to leave the crust and mantle with higher

U/Pb ratios. The U-Pb fractionation into metal generates an isotopic difference relative to other solar system materials, and the U-Pb isotopic chronometer can be used to date core formation on planetesimals by analyses of magmatic iron meteorites. Since Pb isotopic compositions provide simultaneous constraints on the age of the object and the parent -daughter ratios ($^{238}U/^{204}Pb$ or primary "μ") of the precursor material (Halliday and Kleine, 2006), μ can also be determined as it should remain unchanged over time due to its very low U/Pb ratio (Figure 8.1). The $^{238}U/^{204}Pb$ ratio of the planetesimals can be determined using the known ages of core formation (Table A1), which can provide insights into our understanding of the processes of planetary formation and volatile depletion. In turn, this can help with heat modelling in planets and potentially help understand processes on early planetesimals.

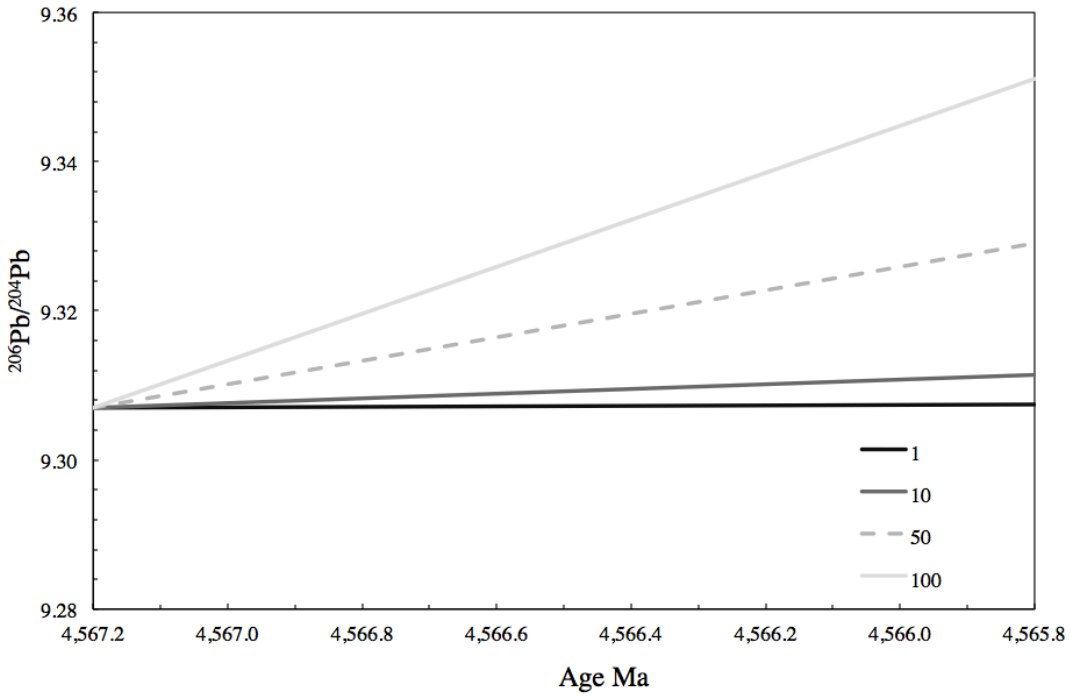

Figure A1: A schematic of the evolution of $^{206}Pb/^{204}Pb$ ratios over time for varying values of μ (μ= 1, 10, 50, 100)

Isotopic analyses of Pb have been carried out for the last 60 years. Patterson et al. (1953) analysed the Pb in a troilite nodule in Canyon Diablo and found an isotopic composition more primitive than any terrestrial Pb. This isotopic composition was considered to define the primordial Pb of the early solar system and remained so until the 1970's at which point improvements in technology allowed a more precise determination of the value. The isotopic composition of primordial Pb was determined by re-analyses of troilite taken from Canyon Diablo: $^{206}Pb/^{204}Pb = 9.307 \pm 0.006$, $^{207}Pb/^{204}Pb = 10.294 \pm 0.006$, $^{208}Pb/^{204}Pb = 29.476 \pm 0.018$ (Tatsumoto et al., 1973). Göpel et al. (1985) confirmed this primordial value and found identical Pb isotopic compositions within 0.2%. Göpel et al. (1985) analysed the metal phases of six non-magmatic iron meteorites of group IA, four of which had been analysed previously, to determine the Pb isotopic composition and U-Pb abundances. The authors circumvented the issue of terrestrial contamination by serial leaching of the meteorites until the isotopic composition of the leachates was consistently the same.

One of the two interrelated analytical difficulties when applying the U-Pb chronometer to iron meteorites is this issue of contamination. Iron meteorites are often highly contaminated with terrestrial Pb depending on how long they have been exposed at the Earth's surface. This requires extensive leaching in order to remove the terrestrial Pb (e.g. Göpel et al., 1985). The other problem is the exceptionally low levels of primordial Pb in many iron meteorites. Such low quantities of Pb require large amounts (up to 10g) of meteorite to be processed which, in turn, proportionally increases the procedural blank and the uncertainty of the results. A low procedural blank is difficult to achieve due to the comparatively high levels of terrestrial Pb in the surrounding environment. A further difficulty when interpreting such U-Pb data concerns the volatility of Pb. Unlike with W we cannot assume that Pb was in chondritic proportions in the planet; indeed

there is clear evidence that material that accreted to form planets was relatively depleted in Pb. Similarly, it is possible that small objects lost volatile Pb during accretion and volcanism. The aims of this study were to analyse a series of magmatic iron meteorites for their Pb composition in order to determine a precise age of core crystallisation. This would allow a determination of the value of μ. In doing so, a key issue is maintaining a low procedural blank during the analyses whilst processing large enough amounts of meteorite to give precise isotope data. A fundamental objective was to achieve procedural blanks in the range of 10-20ρg, but more importantly, to consistently reproduce those blank levels.

2. Methods

Samples ranging in mass from 2-10g were weighed and subjected to a series of acid leachings. For these, 2ml of 2M HBr is added to the sample and left for 24 hours at room temperature. The leachate is removed and the meteorite rinsed with MQ water. This is also extracted and the combination of both is analysed by mass spectrometry. Once the isotopic composition of the leachate is consistent, the sample is assumed to be rid of terrestrial Pb contamination and is dried down and reweighed. The dry sample is then dissolved in 6ml 1M HBr. Following dissolution, known amounts of the ^{207}Pb and ^{208}Pb tracer solutions are added to the sample and allowed to equilibrate for several days at room temperature. These isotopically enriched Pb (spike) solutions are added in order to later determine the concentrations of the isotopes ^{204}Pb and ^{203}Tl. Each sample is processed along with a full procedural blank to quantify the contamination attributed to the experimental process. Purified fractions of Pb were separated from the sample solution by ion exchange chromatography using the basic anion resin AG1X8 (200–400 mesh), which was pre-cleaned through several rinses of 10ml 0.5M HNO_3. The

separation procedure was modelled on the two-stage anion-exchange method developed by Rehkämper and Halliday (1998), which itself is based on a combined optimization of previously developed techniques by Matthews and Riley (1969), de Albuquerque (1972), Batley and Florence (1975), Strelow 1978, Gopel et al. (1985), Galer (1986), and Lugmair and Galer (1992). The steps for this are listed below. The Pb effluent fractions were collected in Teflon beakers, dried down on a hotplate, and 1ml 0.1M HNO_3 was added to all samples.

Step 1: Load resin with 1ml AG1X8.

Step 2: Clean resin with 2+2+10ml 0.5M HNO_3.

Step 3: Equilibrate resin with 2+2+2 ml 0.5M HBr.

Step 4: Load sample: in (0.5-2M HBr).

Step 5: Elute matrix with 1+8 ml 0.2M HBr-0.5M HNO_3.

Step 6: Elute Pb with 2+2+2+2+2+2+2 ml 0.5M HNO_3.

Multiple-collector inductively coupled plasma mass spectrometry (MC-ICPMS) was used to measure the isotope ratios of Pb of the spiked samples, $^{208}Pb/^{206}Pb$, $^{207}Pb/^{206}Pb$, $^{206}Pb/^{204}Pb$, $^{207}Pb/^{204}Pb$ and $^{207}Pb/^{208}Pb$ respectively. A wash of 0.1M HNO_3 was run before and after each sample analysis and a 10ppb Pb- 7ppb Tl standard solution is measured several times to monitor memory retention and variances in flow rate, respectively. Normalisation with $^{205}Tl/^{203}Tl$ was used to correct for mass-dependant isotopic fractionation (Belshaw et al., 1998; Rehkämper and Halliday, 1998).

3. Samples

Aliquots of NBS 981 were processed through column chemistry and analysed. Samples of the group IIAB iron meteorite Navajo were analysed. An aliquot of the Navajo matrix was doped with Pb standard NBS 981 and analysed to ensure chemical separation is possible within an iron meteorite. With every set of columns a procedural blank was run and analysed.

4. Results

Table A2 gives $^{206}Pb/^{204}Pb$ data from repeated analyses of the NBS 981 standard with an average given as the external reproducibility of the measurements. This is illustrated graphically in Figure A2 below, along with the commonly accepted values from Todt et al. (1996) and Baker et al. (2004). $^{208}Pb/^{206}Pb$, $^{207}Pb/^{206}Pb$, $^{206}Pb/^{204}Pb$, $^{207}Pb/^{204}Pb$ and $^{208}Pb/^{204}Pb$ ratios of repeated analyses of Navajo and a single measurement of an aliquot of this spiked with NBS 981 are given in Table A3. Table A4 gives the quantity of Pb procedural blank in ng over time (14 separate procedural blanks), and this is illustrated in Figure A3.

Date	**$^{206}Pb/^{204}Pb \pm 2\sigma$**	**$^{207}Pb/^{204}Pb \pm 2\sigma$**	**$^{208}Pb/^{204}Pb \pm 2\sigma$**
13/01/2010	16.936 ± 0.004	15.489 ± 0.003	36.687 ± 0.008
02/02/2010	16.932 ± 0.006	15.496 ± 0.005	36.725 ± 0.012
23/02/2010	16.938 ± 0.043	15.495 ± 0.048	36.694 ± 0.104
24/02/2010	16.932 ± 0.006	15.496 ± 0.005	36.725 ± 0.012
08/03/2010	16.929 ± 0.004	15.483 ± 0.004	36.673 ± 0.010
09/03/2010	16.928 ± 0.012	15.482 ± 0.011	36.671 ± 0.026
31/03/2010	16.949 ± 0.009	15.505 ± 0.012	36.74 ± 0.027

Average	*16.935 ± 0.006*	*15.492 ± 0.005*	*36.703 ± 0.019*
Todt et al. (1996)	16.9356 ± 0.0022	15.4891 ± 0.0028	36.7006 ± 0.0108
Baker et al. (2004)	16.9416 ± 0.0011	15.4999 ± 0.0011	36.7258 ± 0.0031

Table A2: Tl corrected $^{206}Pb/^{204}Pb$ results of analyses of standard NBS 981. Uncertainty for each analysis is given as 2 standard deviation (2σ) of repeated analyses, unless in italic in which case these values are twice the standard error of the mean (2 se), and are given if only one aliquot of the sample was analysed. Uncertainty for the average is 2 se.

	Navajo with Pb Standard (n=1)	**Navajo (n=3)**
$^{208}Pb/^{206}Pb$	2.16287 ± *0.00004*	2.108 ± 0.002
$^{207}Pb/^{206}Pb$	0.90996 ± *0.00002*	0.871 ± 0.001
$^{206}Pb/^{204}Pb$	16.998 ± *0.001*	17.8 ± 0.4
$^{207}Pb/^{204}Pb$	15.467 ± *0.001*	15.5 ± 0.3
$^{208}Pb/^{204}Pb$	36.764 ± *0.003*	37.6 ± 0.8

Table A3: Number in brackets in header denotes the number of sample analyses. All errors in the table are 2 standard deviations (2σ) unless in italic in which case these values are twice the standard error of the mean (2 se), and are given if only one aliquot of the sample was analysed.

The average of all analyses of NBS 981 gives a value of $^{206}Pb/^{204}Pb$= 16.94 ± 0.02 (2 σ; n=9), which is identical within error to the commonly accepted values in literature of $^{206}Pb/^{204}Pb$= 16.9356 ± 0.0022 (Todt et al., 1996) and $^{206}Pb/^{204}Pb$= 16.9416 ± 0.0011 (Baker et al., 2004), seen in Figure A2. This yields an external reproducibility of ~± 400ppm on $^{206}Pb/^{204}Pb$.

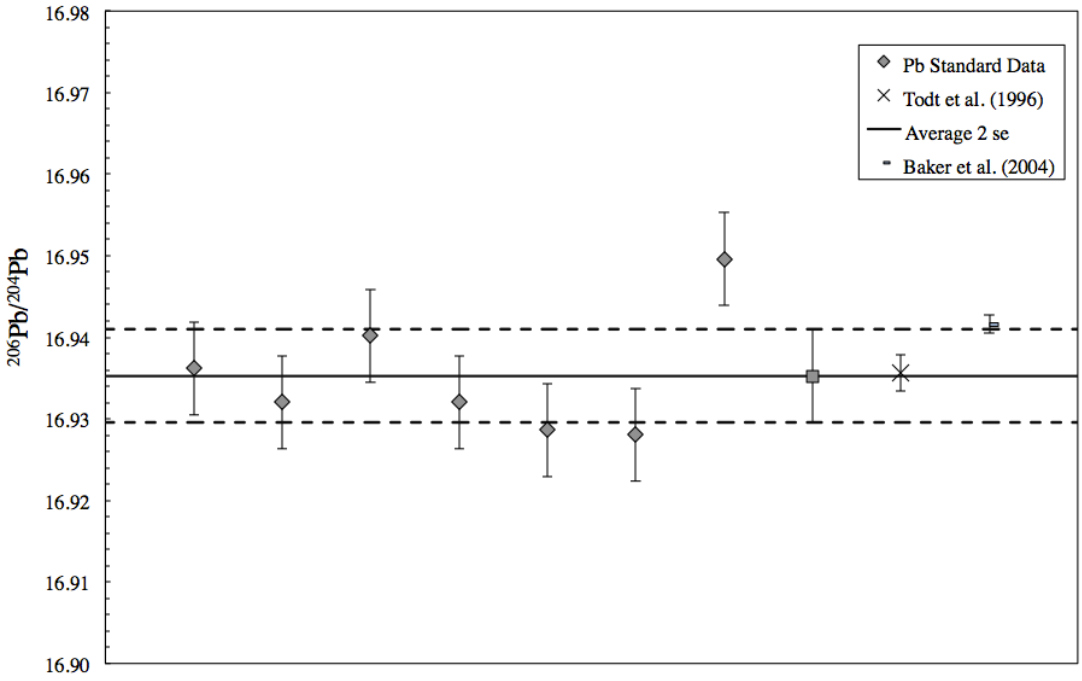

Figure A2: $^{206}Pb/^{204}Pb$ data for NBS 981 with 2 se external error. The solid line represents the average of these measurements and the dotted lines represent 2se of this. The average values from Todt et al. (1996) and Baker et al. (2004) are also shown for comparison.

Date	**Blank 1 (ng)**	**Blank 2 (ng)**	**Blank 3 (ng)**	**Blank 4 (ng)**
22/11/2009	0.04			
11/01/2010	0.44	0.20		
18/02/2010	1.50	3.80		
31/03/2010	1.70	0.18		
14/05/2010	0.48	0.08	0.57	
22/05/2010	0.04	0.21	0.36	0.91
			Average	*0.75 ± 0.55*

Table A4: Procedural Pb blank in ng with date of instrument session. Average uncertainty given to 2 se.

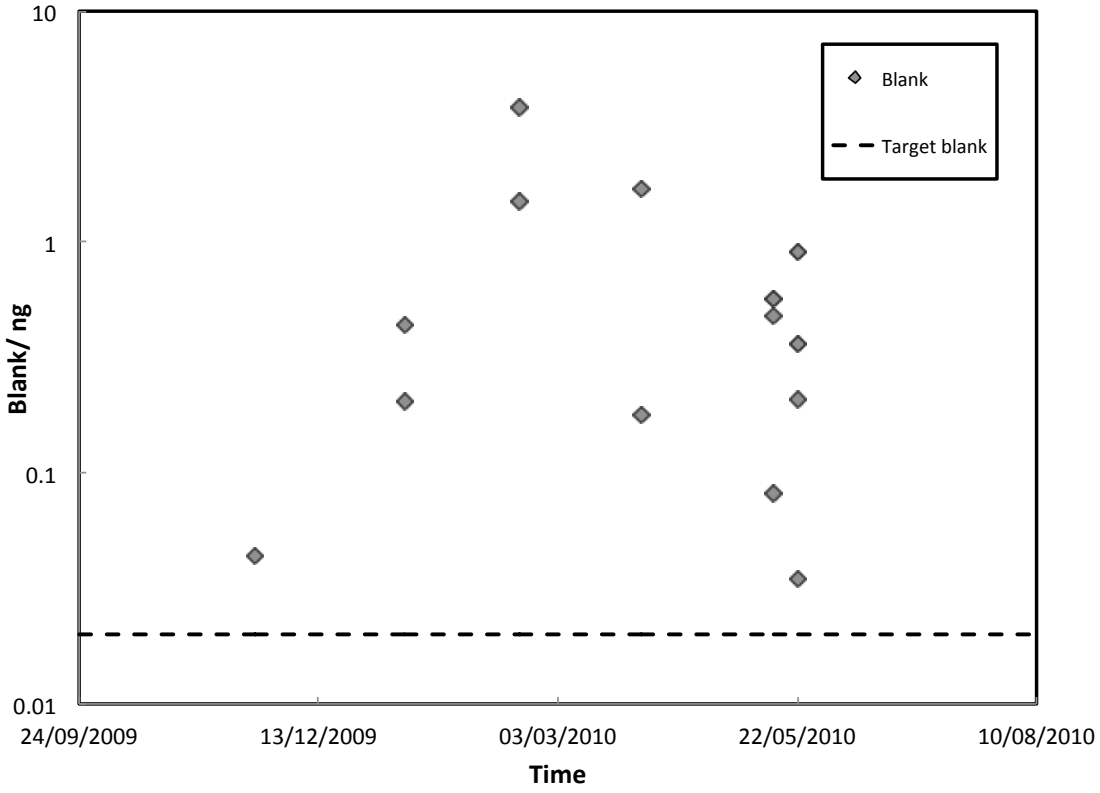

Figure A3: Procedural Pb blank (ng) with date of analysis.

5. Discussion

Analyses of the NBS 981 indicate the measurements are accurate, with an average value identical to that previously reported (Todt et al., 1996), but imprecise with an external reproducibility of ~±400 ppm for $^{206}Pb/^{204}Pb$. Analyses of Navajo, as a preliminary investigation into whether measurements of iron meteorites are feasible using this method, were successful. The isotope compositions of Navajo determined here compare well those obtained by Nielsen et al. (2006), for example, $^{206}Pb/^{204}Pb_{calculated}$ =17.37 ± 0.36 compared to $^{206}Pb/^{204}Pb$= 17.8 ± 0.4 determined here. However, as illustrated by Table 8.4 and Figure 8.3, the procedural blank varied considerably over time, from a minimum of 0.044ng to a maximum of 3.8ng. Several steps were taken to reduce and standardize the procedural blank such that experimental errors during analysis of the iron meteorites would be low. The HNO_3 acid was double distilled, and meticulous care

was taken at each step of chemistry to avoid contamination. However, despite these attempts, the Pb blank variation continued. Although some blanks were near our target value of 10-20ρg, the persistent large variation prevented reproducible isotope measurements of iron meteorite samples and rendered any results highly uncertain. The origin of the blank could not be determined and therefore the project was abandoned.

References:

Amelin Y., Krot A.N., Hutcheon I.D. and Ulyanov A.A. (2002) Lead isotopic ages of chondrules and calcium-aluminum–rich inclusions. *Science* **297**, 1678-1683.

Baker, J., Peate, D., Waight, T. and Meyzen, C. (2004) Pb isotopic analysis of standards and samples using a 207Pb-204Pb double spike and thallium to correct for mass bias with a double-focusing MC-ICP-MS. *Chemical Geology* **211**, 275–303.

Batley G.E. and Florence T.M. (1975) Determination of thallium in natural waters by anodic stripping voltammetry. *Journal of Electroanalytical Chemistry and Interfacial Electrochemistry* **61,** 205–211.

Belshaw N.S., Freedman P.A., O'Nions R.K. and Frank M., Guo Y. (1998) A new variable dispersion double-focussing plasma mass spectrometer with performance illustrated for Pb-isotopes. *International Journal of Mass Spectrometry* **181**, 51–58.

Cook D.L., Walker R.J., Horan M.F., Wasson J.T., and Morgan J.W. (2004) Pt–Re–Os systematics of group IIAB and IIIAB iron meteorites. *Geochimica et Cosmochimica Acta* **68**, 1413–1431.

de Albuquerque C.A.R. (1972) The determination of p.p.b. levels of thallium in silicate rocks by anion exchange-spectrographic analysis. *Chemical Geology* **9**, 167–174.

Galer S. J. G. (1986) Chemical and isotopic studies of crust-mantle differentiation and the generation of mantle heterogeneity. Ph.D. thesis. University of Cambridge.

Göpel C., Manhès G. and Allègre C.J. (1985) U-Pb systematics in iron meteorites: uniformity of primordial lead. *Geochimica et Cosmochimica Acta* **49**, 1681–1695.

Halliday A.N. and Kleine T. (2006) Meteorites and the timing, mechanisms and conditions of terrestrial planet accretion and early differentiation. In: *Meteorites and the Early Solar System II*, eds D. Lauretta, L. Leshin, H. MacSween. 775-801, Univ. Arizona Press.

Lugmair G.W and Galer S.J.G (1992) Age and isotopic relationships among the angrites Lewis Cliff 86010 and Angra dos Reis. *Geochimica et Cosmochimica Acta* **56**, 1673–1694.

Markowski A., Leya I., Quitté G., Ammon K., Halliday A.N., and Wieler R. (2006b) Correlated helium-3 and tungsten isotopes in iron meteorites: Quantitative cosmogenic corrections and planetesimals formation times. *Earth and Planetary Science Letters* **250**, 104–115.

Markowski A., Quitte G., Halliday A.N., and Kleine T. (2006a) Tungsten isotopic compositions of iron meteorites: Chronological constraints vs. cosmogenic effects. *Earth and Planetary Science Letters* **242**, 1 –15.

Matthews A.D and Riley J.P (1969) The determination of thallium in silicate rocks, marine sediments and seawater. *Analytica Chimica Acta* **48,** 25–34.

Nielsen S.G., Rehkämper M., and Halliday A.N. (2006) Large thallium isotopic variations in iron meteorites and evidence for lead-205 in the early solar system. *Geochimica et Cosmochimica Acta* **70**, 2643-2657.

Patterson C., Brown H., Tilton G. and Inghram M., (1953) Concentration of uranium and lead and the isotopic composition of lead in meteoritic material. *Physical Review* **92**, 1234–1236.

Rehkämper, M., and Halliday, A.N., (1998) Accuracy and long-term reproducibility of lead isotopic measurements by MC-ICP-MS using an external method for correction of mass discrimination. *International Journal of Mass Spectrometry and Ion Processes* **58**, 123–133.

Schersten A., Elliott T., Hawkesworth C., Russell S. and Masarik J. (2006) Hf–W evidence for rapid differentiation of iron meteorite parent bodies. *Earth and Planetary Science Letters* **241**, 530–542.

Schönbächler M., Carlson R.W., Horan M.F., Mock, T.D and Hauri E.H. (2008) Silver isotope variations in chondrites: volatile depletion and the initial 107Pd abundance of the solar system. *Geochimica et Cosmochimica Acta* **72**, 5330-5341.

Smoliar M.I., Walker R.J. and Morgan J.W. (1996) Re–Os ages of group IIA, IIIA, IVA, and IVB iron meteorites. *Science* **271**, 1099–1102.

Strelow F.W.E (1978) Distribution coefficients and anion exchange behavior of some elements in hydrobromic-nitric acid mixtures. Analytical Chemistry **50**, 1359–1361.
Sugiura N. and Hoshino H. (2003) Mn-Cr chronology of five IIIAB iron meteorites. *Meteoritics and Planetary Science* **38**, 117-1.

Tatsumoto M., Knight R.J. and Allegre C.J. (1973) Time differences in the formation of meteorites as determined from the ratio of 207Pb-206Pb. *Science* **180**, 1278–1283.

Todt W, Cliff R.A, Hanser A and Hofmann A.W (1996) Evaluation of a ^{202}Pb-^{205}Pb double spike for high-precision lead isotope analysis. In: A.R Basu, S.R Hart (Eds.), *Earth processes: Reading the isotopic code*. American Geophysical Union, 429–437.

APPENDIX B:

Column Calibrations

Representative examples of column calibrations, using BHVO-1:

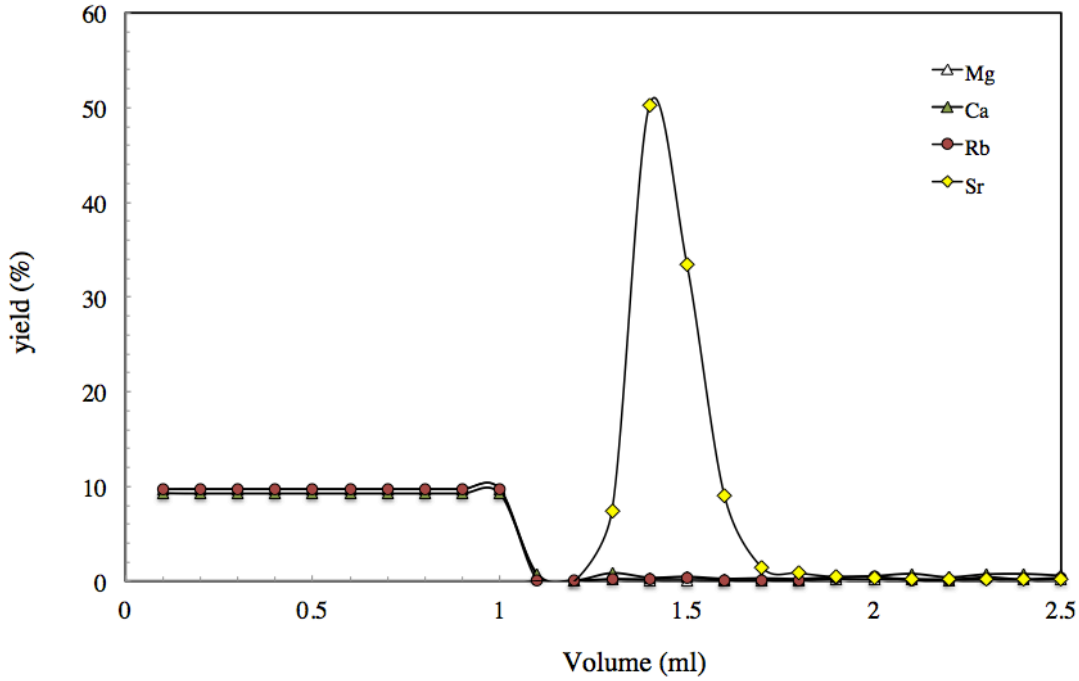

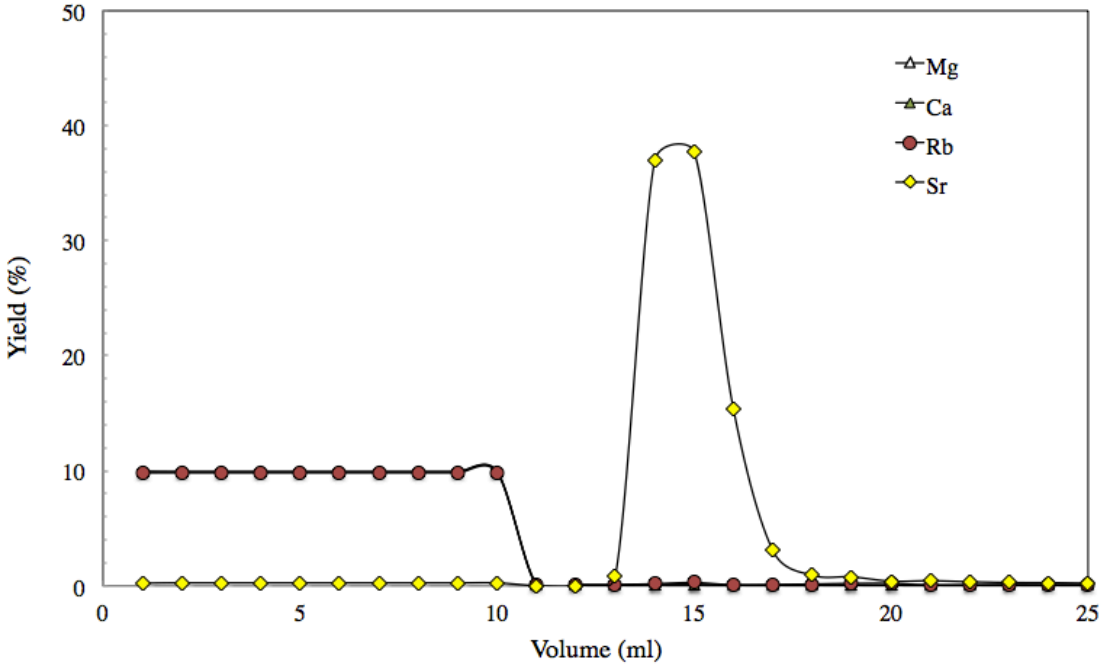

APPENDIX C:

MORB and OIB - trace and rare earth elemental data

Trace element data for MORB and OIB

Sample	Li	P	K	Sc	Ti	Rb	Sr	Y	Zr	Nb	Mo	Ba	Hf	Ta	Pb	Th	U
MORB																	
MD57 D9-1	-	3280	273	-	6899	0.2	115	20.4	38	0.0	0	2	1.6	0.09	0.1	0.04	0.02
MD57 D10-1	6.5	4104	2575	39.2	10535	6.4	166	33.8	99	6.3	1	47	2.9	0.54	0.8	0.74	0.19
MD57 D13-7	6.7	4053	1366	41.4	10128	2.0	133	38.1	114	3.6	1	17	3.4	0.29	0.7	0.32	0.10
MD23 Site 4	5.3	4128	795	33.5	9122	0.4	209	27.8	105	0.7	1	6	2.9	0.15	1.2	0.12	0.05
ARP 74 11-18	4.6			39.7	8124	3.9	110		58	7.8	0	48	1.7	0.52	0.4	0.56	0.17
ARP 74 12-19	6.2			47.1	9948	0.8	81		77	1.7	0	8	2.4	0.12	0.3	0.13	0.04
518 3-1	4.4			42.4	7503	3.7	110	25.6	71	9.4	1	52	2.0	0.57	0.4	0.66	0.16
518 3-2	4.4			41.9	7550	3.8	111	25.9	71	9.6	0	53	2.0	0.55	0.4	0.62	0.16
523-1	3.6			39.9	6885	4.6	118	23.5	67	11.3	0	65	1.9	0.66	0.3	0.76	0.18
519-2-1	3.3			45.8	4666	1.9	64	20.8	37	4.7	0	24	1.1	0.28	0.2	0.29	0.08
522-2-2	3.1			40.9	5290	2.0	70	20.1	43	5.5	0	27	1.3	0.33	0.2	0.37	0.09
525-5-1	3.0			43.4	5143	2.2	77	20.8	46	6.3	0	32	1.2	0.38	0.2	0.41	0.11
525-5-2	3.1			44.1	5221	2.1	78	20.8	47	6.3	0	32	1.3	0.37	0.2	0.39	0.10
521-1-1	3.2			40.3	5288	1.9	71	20.0	42	5.6	0	28	1.3	0.32	0.2	0.35	0.09
525-5-3	3.1			44.2	5186	2.2	78	21.0	47	6.4	0	32	1.4	0.39	0.2	0.41	0.10
SO12 206-1	4.8	3755	660	44.2	9772	0.6	122	30.8	78	1.6	1	7	2.4	0.21	0.4	0.13	0.05
Searise 2 DR07	9.7	4606	1315	46.7	15283	1.0	112	53.3	144	3.0	1	9	4.3	0.31	0.6	0.22	0.08
CY82 18-01	5.9	4380	2228	44.5	11926	2.4	183	33.8	122	4.9	1	26	3.3	0.39	0.8	0.36	0.13
DR7-1 EPR	6.3	5383	7700	39.0	20407	12.5	459	48.7	220	22.5	2	174	5.7	1.29	1.6	1.44	0.50
OIB																	
AZF2		6147	13949	19.5	16047	49.9	758	24.9	286	83.6	6	626	6.0	7.04	3.4	8.38	2.66
AZP8		4170	5473	30.5	10651	13.0	360	14.5	105	22.0	1	168	3.0	2.16	1.7	1.56	0.50
AZFY2		5286	7865	30.7	16505	19.1	532	21.3	152	33.6	2	243	4.1	3.02	1.8	2.32	0.63
PL02 30-1		4022	2636		8008	7.4	212	20.2	77	12.4	1	82	2.2	0.88	0.7	1.07	0.27

PL02 25-1		5608	8066		18022	16.0	566	27.8	203	29.6	2	180	4.9	2.11	1.7	1.87	0.63
MD40		5614	5984	32.4	16115	14.7	536	21.0	156	33.8	3	185	4.0	2.30	1.5	2.51	0.69
MD64		7656	8402	24.6	18094	23.7	822	29.0	279	60.0	2	305	6.3	3.12	2.6	5.16	1.38
FDN25		5397	9938	24.9	21009	28.5	587	21.0	208	37.5	2	223	5.5	2.76	2.8	3.60	0.94
D5-1		4229	4467		15111	10.1	388	20.2	117	16.7	1	134	3.4	1.13	1.5	1.03	0.32
TD4		12828		11.3	25664	60.4	2374	53.2	626	103.2	4	1006			3.8	10.06	3.39
C195						29.0	885	29.0	307	72.0		414			3.0		1.56
FP23		2304		27.7	22332	26.3	698	23.5	285	41.0	2	406			2.4	4.45	1.29
P19						43.0	1153	33.0	320	78.0		2			3.1		1.58
Rock Standards																	
BHVO-1		1380	4246		17325	11.0	389	23.0	152	19.3	3	120	4.2	1.22	2.1	1.20	0.43
BHVO-2		4720	4522		17253	9.0	408	23.7	150	16.6	4	123	4.3	1.24	1.5	1.21	0.43
BCR-2	8	4570	15499		14240	46.0	359	32.4	170	11.5	273	633	4.7	0.85	10.2	5.91	1.73
*2*RSD%*	*2.30*	*1.23*	*1.65*	*2.11*	*2.20*	*1.38*	*1.25*	*0.90*	*0.80*	*1.89*	*2.79*	*2.51*	*2.30*	*3.10*	*2.13*	*1.32*	*3.50*

All values in ppm. Data for PL02 30-1, PL02 25-1, TD4, D5-1 and FP23 are from Liang (2013).

REE data for MORB and OIB

Sample	La	Ce	Pr	Nd	Sm	Eu	Gd	Tb	Dy	Ho	Er	Tm	Yb	Lu
MORB														
MD57 D9-1	1.1	4	0.72	5	2.0	0.93	3	0.58	3.7	0.77	2.2	0.33	1.9	0.30
MD57 D10-1	6.5	17	2.50	13	3.9	1.36	5	0.94	6.1	1.28	3.9	0.55	3.8	0.52
MD57 D13-7	4.7	14	2.39	13	4.2	1.47	6	1.08	6.5	1.48	4.3	0.61	4.2	0.60
MD23 Site 4	4.1	13	2.23	12	3.7	1.42	4	0.83	4.9	1.07	3.1	0.46	2.9	0.41
ARP 74 11-18	5.4	12	1.73	9	2.6	0.94	3	0.59	4.2	0.87	2.5	0.37	2.5	0.37
ARP 74 12-19	2.6	8	1.55	9	3.4	1.21	5	0.83	6.0	1.27	3.7	0.55	3.7	0.55
518 3-1	5.9	13	1.99	10	2.9	1.07	4	0.70	4.7	1.02	2.9	0.41	2.9	0.43
518 3-2	5.8	13	1.98	9	3.0	1.10	4	0.71	4.7	0.99	2.9	0.44	2.8	0.44
523-1	6.7	14	2.10	10	2.9	0.98	4	0.62	4.3	0.93	2.6	0.39	2.7	0.37
519-2-1	2.9	7	1.06	5	1.7	0.73	3	0.48	3.5	0.80	2.5	0.37	2.6	0.39
522-2-2	3.3	8	1.15	6	1.9	0.74	3	0.49	3.4	0.77	2.4	0.36	2.4	0.37
525-5-1	3.8	9	1.28	6	2.0	0.79	3	0.50	3.6	0.81	2.3	0.36	2.5	0.36
525-5-2	3.9	9	1.34	7	2.1	0.78	3	0.50	3.6	0.81	2.4	0.35	2.6	0.38
521-1-1	3.4	8	1.20	6	1.9	0.74	3	0.49	3.5	0.77	2.4	0.36	2.5	0.37
525-5-3	3.9	9	1.29	6	2.0	0.76	3	0.53	3.6	0.80	2.4	0.36	2.6	0.39
SO12 206-1	2.9	10	1.74	9	3.3	1.22	5	0.87	5.4	1.19	3.6	0.50	3.3	0.49
Searise 2	4.8	16	2.77	16	5.4	1.87	8	1.42	9.3	2.02	6.0	0.86	5.6	0.85
DR07														
CY82 18-01	5.6	17	2.79	14	4.3	1.46	5	0.95	5.9	1.25	3.7	0.50	3.6	0.51
DR7-1 EPR	17.1	40	5.61	27	7.5	2.70	9	1.45	9.2	1.86	5.4	0.76	4.8	0.73
OIB														
AZF2	57.3	104	11.47	44	7.7	2.51	7	0.96	5.1	1.00	2.6	0.36	2.2	0.31
AZP8	15.6	34	4.33	18	4.1	1.34	4	0.59	3.0	0.57	1.6	0.19	1.3	0.18
AZFY2	24.0	50	6.31	27	5.9	1.93	6	0.82	4.7	0.85	2.1	0.28	1.8	0.24
PL02 30-1	9.0	20	2.70	12	2.8	1.07	3	0.62	3.6	0.75	2.3	0.34	2.2	0.31
PL02 25-1	22.5	55	7.30	32	7.2	2.40	7	1.08	5.8	1.13	2.9	0.39	2.5	0.35
MD40	26.0	55	6.93	29	6.4	2.13	6	0.87	4.7	0.82	2.2	0.27	1.6	0.23

MD64	48.5	104	12.40	49	9.4	2.94	8	1.17	6.1	1.11	2.9	0.36	2.1	0.29
FDN25	28.6	64	8.19	35	7.3	2.36	7	0.95	4.9	0.83	2.2	0.23	1.5	0.20
D5-1	13.6	31	4.30	20	4.8	1.61	5	0.76	4.3	0.76	2.1	0.28	1.7	0.25
TD4	167.8	356	38.37	140	27.1	7.35	20	2.55	13.1	2.06	4.6	0.57	3.4	0.43
C195	59.0	129				2.02								
FP23	52.1	107	11.70	43	9.5	2.71	8	1.02	5.4	0.94	2.2	0.30	1.9	0.25
P19	71.0	140		58	11.1	2.10								
Rock Standards														
BHVO-1	14.9	36	4.95	23	5.7	1.98	6	0.90	5.1	0.90	2.4	0.30	1.7	0.26
BHVO-2	15.4	36	4.99	24	5.7	2.01	6	0.89	5.2	0.94	2.4	0.32	1.8	0.27
BCR-2	23.7	50	6.25	28	6.3	1.92	6	1.00	6.0	1.22	3.5	0.48	3.1	0.47
*2*RSD%*	*2.31*	*2.08*	*1.07*	*8.30*	*6.78*	*4.28*	*5.57*	*4.46*	*3.36*	*6.46*	*7.68*	*6.14*	*9.02*	*3.72*

All values in ppm. Data for PL02 30-1, PL02 25-1, TD4, D5-1 and FP23 are from Liang (2013).

APPENDIX D:

Hekla - trace and rare earth elemental data

	HEK 06-09	HEK 12-09	HEK 20-09	HEK 14-09	HEK 16-09	HEK 10-09	HEK 15-09	HEK 18-09	HEK 19-09	HEK 03-10	Relative precision (%)
Lithology	*Basalt*	*Basalt*	*Basalt*	*Basaltic andesite*	*Basaltic andesite*	*Andesite*	*Andesite*	*Dacite*	*Dacite*	*Rhyolite*	
La	25	26	5	38	51	41	58	56	63	84	1.79
Ce	58	61	13	88	115	92	128	119	132	174	2.47
Pr	8	8	2	11	15	12	16	14	16	20	2.77
Nd	36	37	10	51	67	52	70	59	65	82	3.22
Sm	8.5	8.6	2.9	11.5	15.1	11.4	15.2	12.4	13.5	16.9	2.98
Eu	2.92	2.97	1.08	3.63	4.75	3.66	4.83	2.98	3.06	3.00	2.61
Gd	8.9	9.1	3.5	11.7	15.3	11.6	15.4	12.0	13.2	16.0	4.00
Tb	1.33	1.36	0.61	1.74	2.33	1.76	2.38	1.90	2.11	2.60	2.88
Dy	8.0	8.2	3.9	10.2	13.9	10.6	14.3	11.6	12.8	15.6	3.19
Ho	1.56	1.59	0.82	1.97	2.64	2.07	2.83	2.35	2.58	3.10	2.53
Er	4.2	4.3	2.3	5.5	7.4	5.7	7.9	6.8	7.4	8.9	2.49
Tm	0.45	0.58	0.33	0.73	0.99	0.79	1.11	0.97	1.04	1.27	2.00
Yb	3.5	3.7	2.2	4.7	6.3	5.1	7.3	6.5	7.0	8.4	1.84
Lu	0.51	0.50	0.32	0.67	0.90	0.75	1.06	0.91	1.01	1.15	2.11

All values in ppm.

APPENDIX E:

Lunar - rare earth elemental data

	14053	75075	70135	78235	15016	71596	60015	76535	74420	10049	15555	70035	74255	67955	60025	77215	15425	71566	77516
Trace element																			
Li	15.2	12.5	10.6	7.1	8.5	10.1	1.8	3.2	14.1	26.8	8.2	11.2	8.4	7.4	1.7	18.0	8.7	10.9	8.5
Sc	41.3	236.0	288.9	1.9	37.1	88.1	0.3	0.4	83.9	81.0	27.7	44.4	91.0	5.3	0.4	18.1	9.4	99.6	39.9
Ti	14640	116900	82921	850	15053	72797	96	168	53776	81616	13582	92491	148291	2349	226	2365	5638	75843	114008
V	109	237	169	52	247	140	10	17	117	75	252	191	193	32	4	100	126	115	151
Cr	2720	6789	4829	1258	5837	3545	57	480	4733	2892	5373	5403	5789	1185	91	3717	2998	3489	3847
Mn	2097	3166	2599	365	2478	2411	90	189	2214	2465	2676	2690	2611	498	76	1758	1731	2226	2447
Co	29.9	26.6	17.3	40.1	57.0	27.3	1.4	17.4	61.8	36.9	67.1	23.7	53.5	27.6	1.9	26.8	62.0	24.1	29.4
Ni	14.8	4.4	1.4	32.2	75.3	4.5	1.8	36.3	80.6	26.1	90.4	3.9	21.8	281.6	15.2	19.4	211.1	2.9	2.7
Cu	10.7	10.5	6.9	1.2	9.4	10.6	0.7	20.9	51.6	12.6	149.7	10.0	17.2	2.8	2.1	4.1	8.9	9.1	13.0
Zn	8.1	29.0	23.1	3.1	5.8	27.2	3.4	6.8	435.7	26.7	6.4	25.0	33.1	12.3	5.7	11.5	29.2	22.8	28.9
Ga	4.58	3.93	3.00	4.17	3.99	4.08	3.59	3.09	23.54	7.49	3.81	3.44	3.97	4.12	4.48	5.03	3.95	4.43	3.61
Rb	2.77	0.62	0.50	0.65	0.95	0.47	0.12	0.33	1.62	8.12	0.65	0.51	2.58	1.23	0.05	2.96	1.90	0.61	0.47
Sr	128	117	93	153	112	150	189	172	218	228	98	116	141	183	246	132	89	185	113
Y	73	121	110	10	34	86	0	2	84	266	27	99	172	20	0	45	27	107	76
Zr	273	316	268	104	115	227	0	8	638	703	77	245	556	113	1	130	105	261	222
Nb	19.8	28.8	25.1	11.4	8.0	21.8	0.0	2.4	16.0	40.9	5.4	25.1	50.7	7.9	0.1	8.9	9.1	24.7	26.6
Mo	0.175	0.185	0.139	0.044	0.099	0.165	0.169	0.058	21.421	0.553	0.188	0.186	0.187	0.097	0.430	0.587	0.099	0.129	0.159
Sn	0.444	0.258	0.251	0.216	0.132	0.751	0.364	0.258	0.420	0.298	0.138	0.255	0.263	0.443	2.015	4.711	0.160	0.269	0.169
Sb	0.011	0.017	0.009	0.008	0.005	0.086	0.009	0.005	0.008	0.010	0.005	0.016	0.014	0.019	0.020	0.025	0.007	0.007	0.011
Cs	0.144	0.021	0.020	0.043	0.041	0.020	0.018	0.053	0.122	0.256	0.030	0.019	0.118	0.156	0.003	0.140	0.088	0.021	0.017
Ba	207	71	61	81	71	78	10	39	102	441	47	67	143	90	17	176	98	86	70
Hf	6.9	11.5	9.7	2.6	3.4	7.9	0.0	0.2	22.5	23.4	2.3	9.2	19.0	3.3	0.0	3.5	2.8	9.7	8.1
Ta	1.06	2.16	1.91	0.59	0.55	1.53	0.01	0.11	1.20	2.85	0.35	1.97	3.85	0.40	0.01	0.41	0.48	1.91	2.19
Pb	3.49	0.42	0.42	1.54	0.61	0.60	0.45	0.56	4.40	4.31	0.41	0.55	1.07	1.83	0.27	2.38	1.91	0.50	0.63
Th	1.95	0.51	0.61	1.25	0.62	0.46	0.00	0.17	1.32	3.86	0.54	0.29	1.15	1.26	0.01	1.67	0.57	0.44	0.29
U	0.67	0.11	0.10	0.72	0.20	0.13	0.00	0.10	0.19	1.29	0.13	0.10	0.31	0.40	0.00	0.47	0.41	0.12	0.13
Rare Earth elements																			
La	17.2	6.0	5.2	6.9	7.3	6.4	0.1	1.7	7.8	39.2	4.6	5.8	13.9	6.3	0.3	10.6	8.4	6.6	6.1
Ce	44.1	21.0	18.4	17.7	19.7	20.9	0.3	4.4	45.3	113.5	12.6	20.0	46.8	15.5	0.7	26.1	20.5	22.5	19.0
Pr	6.3	4.1	3.6	2.4	3.0	3.8	0.0	0.6	4.2	17.5	2.0	3.9	8.7	2.2	0.1	3.6	3.1	4.3	3.4
Nd	28.7	24.7	21.8	10.2	14.9	22.1	0.2	2.7	23.4	88.8	9.7	23.2	50.2	9.5	0.4	16.1	14.1	25.7	19.3
Sm	8.9	10.9	9.9	2.7	4.9	9.1	0.0	0.7	9.2	31.2	3.3	10.0	20.0	2.8	0.1	4.8	4.2	10.9	7.8
Eu	1.61	1.50	1.34	1.13	1.11	1.77	0.75	0.88	2.48	3.17	0.88	1.51	2.22	1.14	1.13	1.40	0.80	2.23	1.41
Gd	10.9	16.3	14.5	2.8	6.3	12.6	0.0	0.7	12.1	41.2	4.4	14.5	26.9	3.3	0.1	6.0	5.1	16.1	11.3

Tb	2.03	3.17	2.81	0.46	1.12	2.38	0.01	0.12	2.18	7.66	0.77	2.77	4.95	0.61	0.02	1.15	0.92	3.03	2.16
Dy	13.2	21.2	19.0	2.7	6.9	15.8	0.0	0.6	13.5	49.6	4.8	18.4	31.6	4.0	0.1	7.8	5.9	19.8	14.3
Ho	2.92	4.65	4.12	0.57	1.42	3.40	0.01	0.11	2.78	10.63	1.00	4.01	6.79	0.90	0.02	1.79	1.28	4.32	3.13
Er	8.4	13.2	11.7	1.6	3.8	9.6	0.0	0.3	7.5	30.2	2.7	11.3	18.9	2.7	0.0	5.5	3.6	12.2	9.1
Yb	7.9	12.6	11.1	1.4	3.2	8.8	0.0	0.2	6.9	27.2	2.3	10.4	16.9	2.6	0.0	5.9	3.2	11.1	8.4
Lu	1.15	1.82	1.62	0.18	0.43	1.26	0.00	0.02	0.96	3.82	0.33	1.52	2.43	0.37	0.01	0.88	0.47	1.61	1.25

Trace element and REE data for lunar rocks, all in ppm. Relative precisions are all ~2%.

Model ages for the Moon calculated for each lunar sample using an alternative Rb/Sr ratio of the proto-Earth of ~0.184

Sample name	**Lithology**	**$^{87}Sr/^{86}Sr$ (2se)**	**$^{87}Rb/^{86}Sr$ (2σ)**	**Age (Ga)$_a$**	**$^{87}Sr/^{86}Sr_I$ (2se)**	**T_M (Ga)**	**T_M ss$_b$**
60015	FAN	0.699170 ±(2)	0.00271 ±(5)	3.55 ± 0.05	0.69903 ±(1)	4.36 ± 0.03	207 ± 29
60025	FAN	0.699078 ±(2)	0.000312 ±(5)	4.360 ± 0.003	0.699059 ±(6)	4.26 ± 0.05	307 ± 50
71596	H-TiB	0.699637 ±(3)	0.0091 ±(1)	3.70 ± 0.07	0.69916 ±(1)	3.90 ± 0.03	662 ± 29
76535	Tr	0.699660 ±(3)	0.00764 ±(3)	4.236 ± 0.015	0.699195 ±(6)	3.76 ± 0.03	806 ± 30
71566	H-TiB	0.699706 ±(2)	0.00979 ±(2)	3.70 ± 0.07	0.69919 ±(1)	3.79 ± 0.03	779 ± 30
77516	H-TiB	0.699754 ±(2)	0.01111 ±(3)	3.79 ± 0.05	0.69915 ±(1)	3.93 ± 0.03	642 ± 29
70035	H-TiB	0.699871 ±(3)	0.01383 ±(2)	3.75 ± 0.07	0.69913 ±(2)	4.01 ± 0.03	560 ± 30
75075	H-TiB	0.699981 ±(2)	0.01478 ±(1)	3.70 ± 0.07	0.69920 ±(2)	3.75 ± 0.03	814 ± 50

Table 6.2: FAN= Ferroan anorthosite, H-TiB= high-Ti basalt and Tr= troctolite. a= values used for age correction taken from Schaeffer and Husain (1974), Borg et al. (2011), Nyquist and Shih (1992), Premo and Tatsumoto (1992), Paces et al. (1991), Stettler et al. (1973), and Lugmair et al. (1975). b: age after the start of solar system, taken as 4.567 Ga from Amelin et al. (2006), in Myr.

When someone seeks," said Siddhartha, "then it easily happens that his eyes see only the thing that he seeks, and he is able to find nothing, to take in nothing because he always thinks only about the thing he is seeking, because he has one goal, because he is obsessed with his goal. Seeking means: having a goal. But finding means: being free, being open, having no goal."

— Hermann Hesse, *Siddhartha*